AD-A113 911 ENVIRONMENTAL RESEARCH INST OF MICHIGAN ANN ARBOR F/G 5/8
FINE RESOLUTION IMAGING OF SPACE OBJECTS.(U)
FEB 82 J R FIENUP F49620-80-C-0006
UNCLASSIFIED ERIM-145400-14-F AFOSR-TR-82-0289 NL

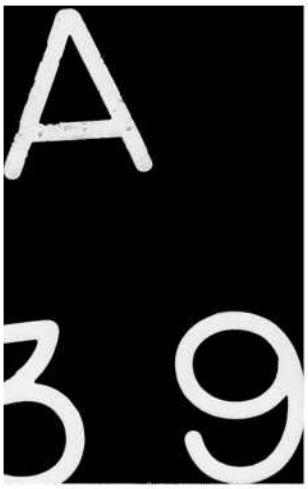
A
39

Final Scientific Report

FINE RESOLUTION IMAGING OF SPACE OBJECTS

Edited by
JAMES R. FIENUP
Radar and Optics Division

FEBRUARY 1982

Director, Physical and Geophysical Sciences
AFOSR/NP, Building 410
Bolling AFB, Washington, DC 20332

ENVIRONMENTAL
RESEARCH INSTITUTE OF MICHIGAN
BOX 8618 • ANN ARBOR • MICHIGAN 48107

UNCLASSIFIED

SECURITY CLASSIFICATION OF THIS PAGE (When Data Entered)

REPORT DOCUMENTATION PAGE	READ INSTRUCTIONS BEFORE COMPLETING FORM
1. REPORT NUMBER AFOSR-TR- 82-0289 GOVT ACCESSION NO AD-A11391	3. RECIPIENT'S CATALOG NUMBER 1
4. TITLE (and Subtitle) FINE RESOLUTION IMAGING OF SPACE OBJECTS	5. TYPE OF REPORT & PERIOD COVERED Final Scientific Report 1 Oct 1979-31 Oct 1981
	6. PERFORMING ORG REPORT NUMBER 145400-14-F
7. AUTHOR(s) Edited by James R. Fienup	8. CONTRACT OR GRANT NUMBER(s) F49620-80-C-0006
9. PERFORMING ORGANIZATION NAME AND ADDRESS Radar and Optics Division Environmental Research Institute of Michigan P.O. Box 8618, Ann Arbor, MI 48107	10. PROGRAM ELEMENT, PROJECT, TASK AREA & WORK UNIT NUMBERS 61102F 2311/A1
11. CONTROLLING OFFICE NAME AND ADDRESS Director, Physical and Geophysical Sciences Air Force Office of Scientific Research/NP Building 410, Bolling AFB, D.C. 20332	12. REPORT DATE February 1982
	13. NUMBER OF PAGES v + 213
14. MONITORING AGENCY NAME AND ADDRESS (if different from Controlling Office)	15. SECURITY CLASS (of this report) Unclassified
	15a. DECLASSIFICATION/DOWNGRADING SCHEDULE N/A

16. DISTRIBUTION STATEMENT (of this Report)
Approved for public release; distribution unlimited.

17. DISTRIBUTION STATEMENT (of the abstract entered in Block 20, if different from Report)

18. SUPPLEMENTARY NOTES

19. KEY WORDS (Continue on reverse side if necessary and identify by block number)
Space object identification
Space object imaging
Speckle interferometry
Phase Retrieval
Image reconstruction

20. ABSTRACT (Continue on reverse side if necessary and identify by block number)
This report describes the results of a two-year research effort to investigate the reconstruction of fine-resolution images of space objects using earth-bound optical telescopes despite the turbulence of the atmosphere. The results of this research are an indication that, using an iterative reconstruction algorithm, it is feasible to reconstruct diffraction-limited images from the Fourier modulus (or autocorrelation) data provided by stellar speckle interferometry.
(over)

DD FORM 1 JAN 73 1473 EDITION OF 1 NOV 65 IS OBSOLETE

UNCLASSIFIED

SECURITY CLASSIFICATION OF THIS PAGE (When Data Entered)

Methods of compensating for systematic errors and noise present in astronomical data were developed and were applied to binary star data, from which a diffraction-limited image was successfully reconstructed. It was analytically shown that the following types of objects are uniquely specified by their Fourier modulus: objects consisting of separated parts satisfying certain disconnection conditions, objects consisting of collections of distinct points, and objects with radial symmetry. Experimental indications are that complicated two-dimensional objects are usually unique. An equivalence of the error-reduction iterative reconstruction algorithm and the steepest-descent gradient search method was shown, and the convergence of this algorithm was proven. However, the input-output iterative algorithm and other gradient search algorithms were found to converge much faster in practice. A survey of other applications of the iterative algorithm was performed, and it was found to be remarkably useful in solving problems for a wide range of applications. A new noniterative method was developed for reconstructing the support of an object from the support of its autocorrelation; and for objects consisting of a collection of distinct points, a new noniterative method was developed for reconstructing the object using a product of three translates of the autocorrelation function.

FOREWORD

This report was prepared by the Radar and Optics Division of the Environmental Research Institute of Michigan. The work was sponsored by the Air Force Office of Scientific Research/AFSC, United States Air Force, under Contract No. F49620-80-C-0006.

This final scientific report covers work performed between 1 October 1979 and 31 October 1981. The contract monitor is Dr. Henry Radoski, Directorate of Physical and Geophysical Sciences, AFOSR/NP, Building 410, Bolling Air Force Base, D.C. 20332. The principal investigator is James R. Fienup. Major contributors of the effort are James R. Fienup and Thomas R. Crimmins. Additional contributors to the effort are Gerald B. Feldkamp, Wlodzimierz Holsztynski, Lawrence S. Joyce, Wayne Lawton, Emmett N. Leith, and Christopher J. Roussi.

SUMMARY

This report describes the results of a two-year research effort to investigate the reconstruction of fine-resolution images of space objects using earth-bound optical telescopes despite the turbulence of the atmosphere. The results of this research are an indication that, using an iterative reconstruction algorithm, it is feasible to reconstruct diffraction-limited images from the Fourier modulus (or autocorrelation) data provided by stellar speckle interferometry.

Methods of compensating for systematic errors and noise present in astronomical data were developed and were applied to binary star data, from which a diffraction-limited image was successfully reconstructed. It was analytically shown that the following types of objects are uniquely specified by their Fourier modulus: objects consisting of separated parts satisfying certain disconnection conditions, objects consisting of collections of distinct points, and objects with radial symmetry. Experimental indications are that complicated two-dimensional objects are usually unique. An equivalence of the error-reduction iterative reconstruction algorithm and the steepest-descent gradient search method was shown, and the convergence of this algorithm was proven. However, the input-output iterative algorithm and other gradient search algorithms were found to converge much faster in practice. A survey of other applications of the iterative algorithm was performed, and it was found to be remarkably useful in solving problems for a wide range of applications. A new noniterative method was developed for reconstructing the support of an object from the support of its autocorrelation; and for objects consisting of a collection of distinct points, a new noniterative method was developed for reconstructing the object using a product of three translates of the autocorrelation function.

TABLE OF CONTENTS

FINE RESOLUTION IMAGING OF SPACE OBJECTS

1
INTRODUCTION AND OBJECTIVES

This report describes the results of a two-year research effort to investigate a method of obtaining high resolution images of space objects using earth-bound optical telescopes.

Atmospheric turbulence severely limits the resolution of large earth-bound optical telescopes. Under good "seeing" conditions, the resolution allowed by the atmosphere is typically one second of arc, compared with 0.02 seconds of arc, the theoretical diffraction-limited resolution of a five-meter diameter telescope. That is, the potential exists for obtaining images having fifty times finer resolution than what one ordinarily can obtain.

Several interferometric methods are capable of providing diffraction-limited information through atmospheric turbulence. The most promising of these interferometric methods is Labeyrie's stellar speckle interferometry. The high-resolution information provided by these methods is the modulus of the Fourier transform of the object; the phase of the Fourier transform is lost. Unfortunately, except for the very special case in which an unresolved star is very near the object of interest, the Fourier modulus can be used to directly compute only the autocorrelation of the object, but not the object itself. The autocorrelation is ordinarily useful only for determining the diameter of the object or the separation of a binary star pair.

We have developed an algorithm for reconstructing the object's spatial (or angular) brightness distribution from its Fourier modulus. The algorithm relies both on the Fourier modulus data measured by stellar speckle interferometry and on the a priori constraint that the object distribution is a nonnegative function. Therefore,

the combination of stellar speckle interferometry with the iterative algorithm can provide fine-resolution diffraction-limited images despite the presence of atmospheric turbulence.

The major goal of this two-year research effort were threefold: (1) to improve the iterative reconstruction algorithm to make it operate reliably in near-real-time on imperfect real-world data; (2) to determine the uniqueness of the solution under various conditions; and (3) to demonstrate the reconstruction technique with real-world interferometer data, thereby providing images with finer resolution than would ordinarily be possible.

2
RESEARCH ACCOMPLISHMENTS

An overview of the problem of image reconstruction for stellar interferometry is given in Appendix A. It serves as a background for the following description of the research accomplishments. It is reprinted from Reference 1.

The research effort can be divided into five major topics:

1. Stellar speckle interferometer data was acquired, evaluated, and processed into imagery; and methods were developed for minimizing the effects of the types of noise and imperfections found in that data[2].
2. Analytical (and to a lesser extent computer) studies of the uniqueness problem were performed[3,4,5].
3. A new method was developed for reconstructing the support of an object; and for objects consisting of a collection of point-like sources, a new noniterative method was developed for reconstructing the object[6,7].
4. A number of variations of the iterative algorithm were studies and compared with gradient search methods[8,9].
5. Numerous other applications of the iterative algorithm were identified[10].

Publications arising from this research effort are listed as References 1-10 at the end of this section.

The results obtained for each of the five topics listed above are summarized in the five respective sections that follow. References 1, 2, and 4-10 are included as Appendices A-I, respectively. For the sake of brevity, Reference 3 is not repeated here; it was included in Appendix B of the Interim Report[11].

2.1 PROCESSING STELLAR SPECKLE INTERFEROMETRY DATA

Processing experiments were performed on data provided by the Steward Observatory Stellar Speckle Interferometry Program (via K. Hege, Steward Observatory). Methods were developed to compensate for errors in the data in order to arrive at a good estimate of the Fourier modulus. It was previously known that it is necessary to compensate the Fourier modulus data for a certain noise bias term due to photon noise. Using the Steward Observatory data, it was found that the detection process resulted in a frequency transfer function, which we call the detection transfer function, which, in addition to being an error itself, prevented the compensation of the noise bias. Methods for determining the detection transfer function from the data and compensating for it were developed. Methods for compensating other systematic errors were also deveoped. These methods were applied to stellar speckle interferometry data of a binary star system, and a diffraction-limited image was successfully reconstructed from the resulting compensated Fourier modulus data. These results are described in detail in Appendix B.

Having gained this experience with single and binary star data, the next step will be to use the same methods on more complicated objects, such as asteroids or Jovian moons.

Data from the Anglo-Australian Telescope (via J.C. Dainty, University of Rochester) in the form of many short-exposure images on 16 mm movie film was also received. The 16 mm film was cut into strips and contact copied, along with grey-scale step wedges, onto 9 x 9 inch sheets of film. The 9-inch sheets of film were digitized at the Image Processing Institute at the University of Southern California using an Optronics digitizer set at 25 micron sample spacing. It will be necessary to develop software for extracting the desired information from the large (4000 x 8000 pixel) digitized arrays. No further work was done on this data because efforts were

concentrated on the Steward Observatory data which was in a much more convenient form. We hope to process this data in the future.

2.2 UNIQUENESS THEORY

The uniqueness of images reconstructed from Fourier modulus information was explored using the theory of analytic functions. As described in Appendix A and in more detail in Appendix B of the Interim Report[11], for the one-dimensional case there are usually many different objects having the same Fourier modulus. Examples of both unique and non-unique cases can be constructed. Most objects consisting of separated parts can be shown to be uniquely specified by their Fourier modulus. However, the separation distance is more stringent than what was previously thought, as shown in Appendix C. It has been shown that a two-dimensional object having radial symmetry is uniquely specified by its Fourier modulus, as discussed in Appendix D. Also, for objects consisting of collections of distinct points, the solution is usually unique, as described in Appendix F.

It was found that when cases were purposely constructed to have two different solutions, then the iterative algorithm would converge to one of the solutions in about half of the trials and converge to the other solution in the other half of the trials, depending on the random number sequence used as the initial input to the algorithm. Therefore, it is believed that in general, if there are multiple solutions, then the iterative algorithm is likely to find any one of them. Our experience with complicated two-dimensional objects has been that the algorithm in almost all cases converged to the original object itself, and not to other solutions. This is a strong indication that, in practice, other solutions usually do not exist in the two-dimensional case.

2.3 NEW NON-ITERATIVE METHODS FOR SUPPORT AND OBJECT RECONSTRUCTION

A new method was developed for reconstructing the support of an object (the set of points at which it is nonzero) from the support of its autocorrelation. In some instances, for example to find the relative locations of a collection of point-like stars, the object's support is the desired information. More generally, once the object's support is known, then the complete reconstruction of the object by the iterative method is simplified. Several methods are shown of finding sets which contain all possible support solutions. Particularly small and informative sets containing the solutions are given by the intersections of two translates of the autocorrelation support. For the special case of convex objects, the intersection of three translates of the autocorrelation support generates a family of solutions to the support of the object. For the special case of an object consisting of a collection of distinct points satisfying certain nonredundancy conditions, the intersection of three translates of the autocorrelation support generates a unique solution. In addition, for these same objects, by taking the product of three translates of the autocorrelation function, one can reconstruct the object itself in addition to reconstructing the support of the object. These results are described in detail in Appendix F (which contains further results and proofs not included in the Interim Report).

2.4 ITERATIVE ALGORITHM VARIATIONS AND GRADIENT SEARCH METHODS

Gradient search methods for solving the image reconstruction (phase retrieval) problem were studied. It was found that the steepest-descent method using an "optimum" step size is exactly equivalent to one version of the iterative algorithm called the error-reduction algorithm. In addition, it was proven that the error-reduction algorithm converges in the sense that after each iteration, the error of the output image is less than or equal to

the error at the previous iteration. However, in practice the error-reduction algorithm converges very slowly for this application, making it impractical. Algorithms that converge much faster than the error-reduction algorithm and that are practical for this application are the input-output family of iterative Fourier transform algorithms and the conjugate gradient method. The algorithm found to converge the fastest is called the hybrid input-output algorithm. A partial reconstruction of the object is available after just a few iterations, and the complete reconstruction takes under one hundred iterations, which, for array sizes of 128 x 128 pixels, takes less than two minutes on a Floating Point Systems AP-120B array processor. The gradient search methods deserve more development; the computation of the gradient can be accomplished rapidly using the method of two Fourier transforms. The problem of phase retrieval from two intensity measurements was also considered in the same context. These results are described in detail in Appendix H.

2.5 ADDITIONAL APPLICATIONS OF THE ITERATIVE ALGORITHM

In addition to the image reconstruction problem for the fine-resolution imaging of space objects through atmospheric turbulence, there are a number of other difficult problems which can be solved by algorithms closely related to the iterative Fourier transform algorithm. Such algorithms can be used to solve problems which can be stated as follows: given a set of constraints on a function (an object, wavefront, or a signal) and another set of constraints on its (Fourier) transform, find a transform pair that satisfies both sets of constraints. Here, the word "constraints" is meant to include both measured data and a priori information. Several applications falling under this general problem statement were identified. They include image reconstruction (phase retrieval problems) in astronomy, electron microscopy, wavefront sensing, X-ray crystallography and computed topography, and the synthesis of pupil functions,

computer-generated holograms, radar signals, digital filters, and other applications. A summary of these applications is given in Appendix I. The family of iterative Fourier transform algorithms appears to be an extremely valuable mathematical tool which can be expected to receive a great deal of attention in the coming years.

2.6 SUMMARY AND CONCLUSIONS

The major conclusion of this research effort is that, for a wide set of objects, the reconstruction of fine-resolution images by the combination of the iterative reconstruction algorithm with stellar speckle interferometry data appears to be feasible. Excellent reconstruction results have been obtained from computer-simulated data of complicated objects and from real telescope data of a simple object. This would make possible a fifty-fold increase in resolution for an optical telescope of five meters diameter. Systematic errors in the collection of the data can be detected and compensated, although further effort is required to demonstrate these techniques on complicated objects. For complicated two-dimensional objects, the Fourier modulus data does appear to uniquely specify the object, although a definitive theory is not available yet. Special cases that have been analyzed, including objects of separated support, objects consisting of collections of discrete points, and radially symmetric objects, were shown to be usually unique. A new noniterative method for support and object reconstruction, particularly useful for objects consisting of collections of discrete points, was invented. A better understanding of the iterative algorithm and its relationship to gradient search methods was developed. Finally, it was shown that algorithms related to the iterative algorithm are applicable to a wide variety of problems and deserve further development for those applications as well.

REFERENCES

1. J.R. Fienup, "Image Reconstruction for Stellar Interferometry," in Current Trends in Optics, ed. F.T. Arecchi and F.R. Aussenegg (Taylor and Francis, London, and Halsted Press, New York, 1981) (Invited Papers from the ICO-12 Meeting in Graz, Austria, September 1981), pp. 95-102.

2. J.R. Fienup and G.B. Feldkamp, "Astronomical Imaging by Processing Stellar Speckle Interferometry Data," in Applications of Speckle Phenomena, Proc. SPIE 243, 95-102 (1980).

3. T.R. Crimmins and J.R. Fienup, "Phase Retrieval for Functions with Disconnected Support," submitted for publication (appears in Appendix B of Reference 11).

4. T.R. Crimmins and J.R. Fienup, "Ambiguity of Phase Retrieval for Functions with Disconnected Support," J. Opt. Soc. Am. 71, 1026-28 (1981).

5. W. Lawton, "Uniqueness Results for the Phase-Retrieval Problem for Radial Functions," J. Opt. Soc. Am. 71, 1519-22 (1981).

6. J.R. Fienup and T.R. Crimmins, "Determining the Support of an Object from the Support of Its Autocorrelation," presented at the 1980 Annual Meeting of the Optical Society of America, Chicago, Ill., 15 October 1980; Abstract: J. Opt. Soc. Am. 70, 1581 (1980).

7. J.R. Fienup, T.R. Crimmins, and W. Holsztynski, "Reconstruction of the Support of an Object from the Support of Its Autocorrelation," to appear in J. Opt. Soc. Am. 72 (April 1982).

8. J.R. Fienup, "Comparison of Phase Retrieval Algorithms," presented at the 1981 Annual Meeting of the Optical Society of America, Kissimmee, Fla., October 1981; Abstract: J. Opt. Soc. Am. 71, 1641 (1981).

9. J.R. Fienup, "Comparison of Phase Retrieval Algorithms," submitted for publication.

10. J.R. Fienup, "Reconstruction and Synthesis Applications of an Iterative Algorithm," to appear in Transformations in Optical Signal Processing, ed. W.T. Rhodes, J.R. Fienup, and B. Saleh (Society of Photo-Optical Instrumentation Engineers, Bellingham, Wa., 1982); and presented at the SPIE Institute, Seattle, Washington, February 1981.

11. J.R. Fienup, "High Resolution Imaging of Space Objects," Interim Scientific Report to AFOSR, ERIM Report No. 145400-7-P (March 1981).

Appendix A

IMAGE RECONSTRUCTION FOR STELLAR INTERFEROMETRY

by

J. R. Fienup

Radar and Optics Division
Environmental Research Institute of Michigan
P.O.Box 8618, Ann Arbor, Michigan 48107 USA

Interferometric methods (Michelson & Pease 1921, Hanbury Brown & Twiss 1956, Labeyrie 1970, Gezari et al. 1972, Currie et al. 1974) are capable of measuring the modulus of the Fourier transform (or equivalently, the autocorrelation) of an astronomical object for resolution out to the diffraction limit of the telescope aperture (0.02 seconds of arc for a 5-meter aperture) although atmospheric turbulence limits the measurement of the Fourier phase to a resolution of about one second of arc. Except for the special cases of objects known to be centro-symmetric or objects having a neighboring unresolved star within the same isoplanatic patch (Liu & Lohmann 1973, Weigelt 1980) it is not possible to directly compute the object from its Fourier modulus.

ITERATIVE RECONSTRUCTION METHOD

Recently an iterative method (Fienup 1978, Fienup 1979) has been successfully used to reconstruct an object from its Fourier modulus (or equivalently, to retrieve the Fourier phase), using the fact that an object's brightness spatial distribution is nonnegative. The method works for any arbitrary object in one or more dimensions. As depicted in Figure 1, the algorithm successively Fourier transforms back and forth between the object domain and the Fourier domain, modifying the estimate according to the known information in each domain. The iterations are usually started with an array of random numbers as the initial estimate of the object. In the Fourier domain, the computed Fourier modulus is replaced by the measured Fourier modulus, and the computed phase is unaltered. In the object domain several different methods for picking a new object estimate have proven successful. The simplest method is to force

Reprinted from Current Trends in Optics, ed. F.T. Arecchi and F.R. Assenegg (Taylor and Francis, London, and Halsted Press, New York, 1981) (Invited Papers from the ICO-12 Meeting in Graz, Austria, September 1981), pp. 95-102.

the object to satisfy the nonnegativity constraint, i.e., set it equal to zero wherever it is negative. One can also set it equal to zero outside of the region of support of the object if that information is known. Although it can be shown that the algorithm converges when using this simple method of picking a new estimate for the object, there are also more sophisticated methods of applying the object-domain constraints which in practice result in much faster convergence of the algorithm (Fienup 1978, Fienup 1979). The algorithm converges to a Fourier transform pair satisfying the constraints in both domains. The image is nonnegative and the modulus of its Fourier transform equals the measured Fourier modulus.

Figure 2 shows a computer experiment testing this reconstruction method on a realistic simulation of the Fourier modulus data provided by stellar speckle interferometry, including the effects of atmospheric turbulence and photon noise (Feldkamp & Fienup 1980). An undegraded object, a digitized photograph of a satellite shown in Figure 2(a), was convolved with 156 different point-spread functions to produce 156 different blurred images. Each of the point-spread functions represented a different realization of the effects of the turbulent atmosphere. The blurred images were then subjected to a Poisson noise process to simulate the effects of photon noise. Two of the resulting 156 degraded images are shown in Figures 2(b) and 2(c). The degraded images were then processed by Labeyrie's (1970) method, as modified by Goodman and Belsher (1976, Dainty & Greenway 1979). The estimate of the modulus of the Fourier transform of the object is given by (Feldkamp & Fienup 1980)

$$|F(u, v)| = W(u, v)\left[\frac{\sum_{k=1}^{M} |I_k(u, v)|^2 - N_c}{\sum_{k=M+1}^{2M} |S_k(u, v)|^2}\right]^{1/2}$$

where $I_k(u,v)$ is the Fourier transform of the k^{th} degraded image, N_c is the total number of photons detected (it is subtracted in order to compensate for a certain noise bias term that arises in the power spectrum due to photon noise)(Goodman & Belsher 1976), $S_k(u, v)$ is the Fourier transform of the k^{th} point-spread function (to provide compensation for the MTF of the speckle interferometry process) and the weighting function $W(u, v)$ is the MTF due to the telescope aperture. The denominator of this expression is obtained by making measurements on a reference star through an atmosphere having the same statistics as that which blurred the images or by using a model of the effects of atmospheric turbulence (Korff et al. 1972). $W(u, v)$ was included in order to restore the natural MTF due to the telescope aperture which was removed by the denominator of the equation above. Figure 2(d) shows the resulting Fourier modulus estimate. In a realistic situation one would also

have to compensate for the MTF of the detection process (Aime et al. 1979, Fienup & Feldkamp 1980). The Fourier modulus estimate was processed by the iterative method, resulting in the reconstructed image shown in Figure 2(e), which agrees very well with the original object. This result was obtained assuming a telescope diameter of 1.2 meters and 300,000 photons per degraded image, which is realistic for extended objects of this type.

UNIQUENESS

Even if one does obtain an image that is nonnegative and has the correct Fourier modulus, the question remains: is the solution unique? For the one-dimensional case it is well known from the theory of analytic functions that there are ordinarily an *enormous* number of different solutions. (Translations and mirror images of the object all have the same Fourier modulus and are not considered to be different solutions.) If the analytic continuation of the Fourier transform off the real line has M non-real zeroes, then there are 2^{M-1} different solutions (Walther 1963, Hofstetter 1964). Imposing the condition of nonnegativity may greatly reduce the number of solutions (Bates 1969), but a theory has not yet been developed that indicates how many nonnegative solutions there would be.

For some special classes of one-dimensional objects the solution is usually unique. One such class is that of objects of separated support, (Greenaway 1977, Bates 1978) providing that the parts of the object are separated by a sufficient distance (Crimmins & Fienup 1981). Another such class is that of objects consisting of collections of discrete points (like stars) randomly distributed within some finite region of space. Unless the spacings of the discrete points satisfy certain redundancy-type conditions, not only is the solution unique, but also there exists a very simple noniterative reconstruction method, which involves the product of three translates of the object's autocorrelation function (Fienup et al. 1981). This reconstruction method also works for the case of two or more dimensions.

The uniqueness situation appears to be much different in two dimensions than in one dimension. Whereas in one dimension uniqueness is unusual, in two (or more) dimensions uniqueness appears to be the rule, and nonuniqueness is unusual. The difference between one and two dimensions can be understood from the results of Bruck and Sodin (1979). They considered the special case of a sampled object, one consisting of a finite array of delta functions (each having a different amplitude) on a rectangular lattice. The Fourier transform of such an object can easily be shown to be a polynomial. It can also be shown that the number of different solutions having the same Fourier modulus is 2^{M-1} where M is the number of irreducible factors into which the polynomial can be factored (not all of these solutions are necessarily nonnegative). Since a one-dimensional polynomial of order M can always be factored into M irreducible factors (the roots of the polynomials can be related to

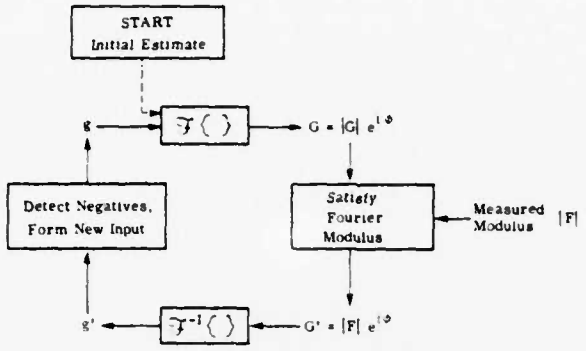

Figure 1. Block Diagram of the Iterative Method for Reconstructing an Object from the Modulus of Its Fourier Transform.

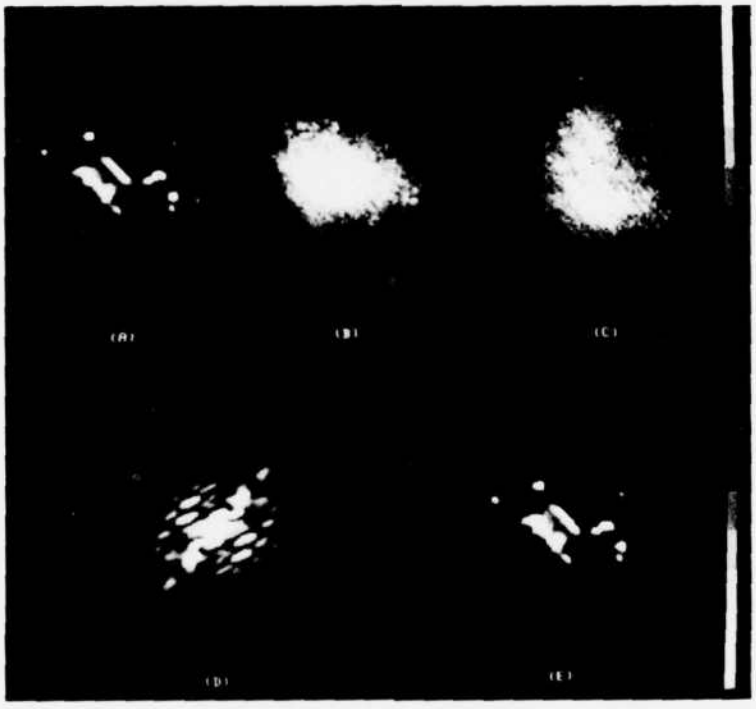

Figure 2. Reconstruction Experiment for Stellar Speckle Interferometry. (A) Undegraded Object; (B), (C) Simulated Images Degraded by Atmospheric Turbulence and Photon Noise; (D) Fourier Modulus Estimate; (E) Image Reconstructed from Fourier Modulus.

the complex zeroes mentioned earlier), the number of possible solutions is 2^{M-1} in the one-dimensional case. On the other hand, two dimensional polynomials having arbitrary coefficients are only rarely factorable. Consequently, the two-dimensional case is usually unique although the one-dimensional case is usually not unique. Efforts have also been made to extend these results to the case of continuous objects (Lawton 1980).

Of course, one can always invent two-dimensional examples that are not unique. One way to do this is to form an object as the convolution of one nonnegative function with a second nonnegative function. In the Fourier domain, one is multiplying the Fourier transforms of the two functions. A second solution is then given by the convolution of the first function with the mirror image of the second function. In the Fourier domain, one has the product of the Fourier transform of the first function with the complex conjugate of the Fourier transform of the second function. Since the complex conjugation does not change the Fourier modulus, both solutions have the same Fourier modulus. Another method of generating cases having multiple solutions is given by Huiser and vanToorn (1980). Despite the fact that nonunique cases can be constructed, it appears to be true that for most two-dimensional objects taken from the real world the solution will be unique. Experimental evidence upholds this view: for a variety of objects reconstructed by the iterative method so far, the two-dimensional reconstructed images usually differ very little from the original object (Fienup 1979). Furthermore, the presence of noise in the Fourier modulus data has had the effect of causing the reconstructed image to be noisy rather than having it converge to an essentially different solution (Feldkamp & Fienup 1980).

In those cases for which there are multiple solutions, however, then the iterative algorithm converges to different members of the set of solutions, depending on the random numbers used to initialize the algorithm. Therefore by multiple trials of the algorithm one can find a number of different solutions if they exist. If there is only one solution, then the algorithm will converge only to that solution.

ALTERNATIVE METHODS

Although the iterative algorithm appears to be the only practical reconstruction method for general two-dimensional objects, there are some other methods which may be useful in certain cases. For collections of point-like stars, the method of using the product of three autocorrelations (Fienup et al. 1981) would usually work well, as would the iterative method of Baldwin and Warner (1978) which is the same as one used in X-ray crystallography. When only a small number of resolvable elements is involved, then an iterative Newton-Raphson method is practical (Frieden & Currie 1976). If the signal-to-noise ratio is high enough, then the Napier and Bates (1974) method of tracking the complex zeroes of projections of the image may be feasible.

If one utilizes all the individual short-exposure images in stellar speckle interferometry, instead of trying to reconstruct the image from the Fourier modulus only, then additional reconstruction methods are possible. By the Knox-Thompson (1974, Stachnik et al. 1977) technique, one averages over phase differences between adjoining points in the Fourier transforms of the short-exposure images, then integrates over the averaged phase differences to arrive at an estimate of the Fourier phase. When the image includes one star that is considerably brighter than the others, then the shift-and-add method of Bates and Cady (1980, Cady & Bates 1980) should work well. When the diameter of the object is only a couple of times the size of a diffraction-limited resolution element, then the shift-and-add method of Worden, Lynds and Harvey (1976) may be useful.

CONCLUSIONS

From both theoretical and experimental viewpoints, it appears that the reconstruction of diffraction-limited images of astronomical objects should be feasible using stellar speckle interferometry combined with the iterative algorithm. The iterative algorithm converges fast enough to make it practical to reconstruct images of complicated two-dimensional objects, and the solution has been found to be usually unique for the two-dimensional case. The reconstruction method is not overly sensitive to noise, making it practical for reconstructing images from real-world telescope data.

ACKNOWLEDGMENT

This work was supported in part by the United States Air Force Office of Scientific Research under Contract F49620-80-C-0006.

REFERENCES

AIME, C. et al., 1979, "Measurement of Stellar Speckle Interferometry Lens-Atmosphere Modulation Transfer Function," Optica Acta, 26, 575-81.

BALDWIN, J.E. & P.J. WARNER, 1978, "Phaseless Aperture Synthesis," Monthly Notices of the Royal Astronomical Society, 182, 417-22.

BATES, R.H.T., 1969, "Contributions to the Theory of Intensity Interferometry," Monthly Notices of the Royal Astronomical Society, 142, 413-28.

BATES, R.H.T., 1978, "Fringe Visibility Intensities May Uniquely Define Brightness Distributions," Astronomy and Astrophysics, 70, L27-L29.

BATES, R.H.T. & F.M. CADY, 1980, "Towards True Imaging by Wideband Speckle Interferometry," Optics Communications, 32, 365-69.

BRUCK, Y.M. & L.G. SODIN, 1979, "On the Ambiguity of the Image Reconstruction Problem," Optics Communications, 30, 304-08.

CADY, F.M. & R.H.T. BATES, 1980, "Speckle Processing Gives Diffraction-Limited True Images from Severely Aberrated Instruments," Optics Letters, 5, 438-40.

CRIMMINS, T.R. & J.R. FIENUP, 1981, "Ambiguity of Phase Retrieval for Functions with Disconnected Support," to appear in Journal of the Optical Society of America, 71, August.

CURRIE, D.G., S.L. KNAPP, & K.M. LIEWER, 1974, "Four Stellar-Diameter Measurements by a New Technique: Amplitude Interferometry," Astrophysical Journal, 187, 131-44.

DAINTY, J.C. & A.H. GREENAWAY, 1979, "Estimation of Spatial Power Spectra in Speckle Interferometry," Journal of the Optical Society of America, 69, 786-90.

FELDKAMP, G.B. & J.R. FIENUP, 1980, "Noise Properties of Images Reconstructed from Fourier Modulus," 1980 International Optical Computing Conference, Proceedings of the Society of Photo-Optical Instrumentation Engineers, 231, 84-93.

FIENUP, J.R., 1978, "Reconstruction of an Object from the Modulus of Its Fourier Transform," Optics Letters, 3, 27-29.

FIENUP, J.R., 1979, "Space Object Imaging through the Turbulent Atmosphere," Optical Engineering, 18, 529-34.

FIENUP, J.R., T.R. CRIMMINS, & W. HOLSZTYNSKI, 1981, "Reconstruction of the Support of an Object from the Support of Its Autocorrelation," submitted for publication.

FIENUP, J.R. & G.B. FELDKAMP, 1980, "Astronomical Imaging by Processing Stellar Speckle Interferometry Data," Applications of Speckle Phenomena, Proceedings of the Society of Photo-Optical Instrumentation Engineers, 243, 95-102.

FRIEDEN, B.R. & D.G. CURRIE, 1976, "On Unfolding the Autocorrelation Function," Journal of the Optical Society of America, 66, 1111 (Abstract).

GEZARI, D.Y., A. LABEYRIE, & R.V. STACHNIK, 1972, "Speckle Interferometry: Diffraction-Limited Measurements of Nine Stars with the 200-inch Telescope," Astrophysical Journal Letters, 173, L1-L5.

GOODMAN, J.W. & J.F. BELSHER, 1976, "Fundamental Limitations in Linearly Invariant Restoration of Atmospherically Degraded Images," Imaging Through the Atmosphere, Proceedings of the Society of Photo-Optical Instrumentation Engineers, 75, 141-54.

GREENAWAY, A.H., 1977, "Proposal for Phase Recovery from a Single Intensity Distribution," Optics Letters, 1, 10-12.

HANBURY BROWN, R. & R.Q. TWISS, 1956, "Correlation Between Photons in Two Coherent Beams of Light," Nature, 177, 27-29.

HOFSTETTER, E.M., 1964, "Construction of Time-Limited Functions with Specified Autocorrelation Functions," IEEE Transactions on Information Theory, IT-10, 119-26.

HUISER, A.M. & P. VANTOORN, 1980, "Ambiguity of the Phase-Reconstruction Problem," Optics Letters, 5, 499-501.

KNOX, K.T. & B.J. THOMPSON, 1974, "Recovery of Images from Atmospherically Degraded Short-Exposure Photographs," Astrophysical Journal Letters, 193, L45-L48.

KORFF, D., G. DRYDEN & M.G. MILLER, 1972, "Information Retrieval from Atmospheric Induced Speckle Patterns," Optics Communications, 5, 187-92.

LABEYRIE, A., 1970, "Attainment of Diffraction Limited Resolution in Large Telescopes by Fourier Analysing Speckle Patterns in Star Images," Astronomy and Astrophysics, 6, 85-87.

LAWTON, W., 1980, "A Numerical Algorithm for 2-D Wavefront Reconstruction from Intensity Measurements in a Single Plane," 1980 International Optical Computing Conference, Proceedings of the Society of Photo-Optical Instrumentation Engineers, 231, 94-98.

LIU, C.Y.C. & A.W. LOHMANN, 1973, "High Resolution Image Formation through the Turbulent Atmosphere," Optics Communications, 8, 372-77.

MICHELSON, A.A. & F.G. PEASE, 1921, "Measurement of the Diameter of Alpha Orionis with the Interferometer," Astrophysical Journal, 53, 249-59.

NAPIER, P.J. & R.H.T. BATES, 1974, "Inferring Phase Information from Modulus Information in Two-Dimensional Aperture Synthesis," Astronomy and Astrophysics Supplement, 15, 427-30.

STACHNIK, R.V., P. NISENSON, et al., 1977, "Speckle Image Reconstruction of Solar Flares," Nature, 266, 149-51.

WALTHER, A., 1963, "The Question of Phase Retrieval in Optics," Optica Acta, 10, 41-49.

WEIGELT, G., 1980, "Stellar Speckle Interferometry and Speckle Holography at Low Light Levels," Applications of Speckle Phenomena, Proceedings of the Society of Photo-Optical Instrumentation Engineers, 243, 103-11.

WORDEN, S.P., C.R. LYNDS, & J.W. HARVEY, 1976, "Reconstructed Images of Alpha Orionis Using Stellar Speckle Interferometry," Journal of the Optical Society of America, 66, 1243-46.

APPENDIX B

ASTRONOMICAL IMAGING BY PROCESSING STELLAR SPECKLE INTERFEROMETRY DATA

by
J.R. Fienup and G.B. Feldkamp

Presented at the 24th Annual Technical Symposium of the SPIE, San Diego, California, 30 July 1980; published in SPIE Proceedings Vol. 243, Applications of Speckle Phenomena (July 1980), p. 95.

Astronomical imaging by processing stellar speckle interferometry data

J.R. Fienup and G.B. Feldkamp

Environmental Research Institute of Michigan
Radar and Optics Division
P.O. Box 8618, Ann Arbor, Michigan 48107

Abstract

Diffraction-limited images, of resolution many times finer than what is ordinarily obtainable through large earth-bound telescopes, can be obtained by first measuring the modulus of the Fourier transform of an object by the method of Labeyrie's stellar speckle interferometry, and then reconstructing the object by an iterative method. Before reconstruction is performed, it is first necessary to compensate for weighting functions and noise in order to arrive at a good estimate of the object's Fourier modulus. A simple alternative to Worden's method of compensation for the MTF of the speckle process is described. Experimental reconstruction results are shown for the binary star system SAO 94163.

Introduction

As discussed in several papers in this session on Stellar Speckle Interferometry, Labeyrie's method[1] of processing many short-exposure images can be used to arrive at a diffraction-limited estimate of the Fourier modulus of an astronomical object despite the presence of atmospheric turbulence. Since the diffraction limit of a large-aperture telescope is many times finer than the resolution ordinarily obtainable through the atmosphere at optical wavelengths, stellar speckle interferometry has the potential for providing images having many times finer detail than what is ordinarily obtainable from earth-bound telescopes. Unfortunately, except for special cases in which an unresolved star is very near the object of interest[2], the Fourier modulus data can be used to directly compute only the autocorrelation of the object and not the object itself. In recent years, it has been shown that this stumbling block can be overcome by an iterative method[3] of computing the object's spatial (or angular) brightness distribution, which uses the Fourier modulus data provided by stellar speckle interferometry combined with the a priori knowledge that the object distribution is nonnegative. This method provides an alternative to other fine-resolution imaging techniques[4,5].

In the remainder of this paper, stellar speckle inteferometry and the iterative reconstruction method are briefly reviewed. Then more detailed discussions of noise terms and MTF factors present in speckle interferometry are given, and methods of obtaining an improved estimate of an astronomical object's Fourier modulus are described. Finally, some recent results obtained with telescope data are shown.

Basic stellar speckle interferometry

Labeyrie's stellar speckle interferometry starts by taking a number of short-exposure images of an astronomical object:

$$d_m(x) = f(x) \ast s_m(x) \tag{1}$$

where $f(x)$ is the spatial or angular brightness distribution of the object and $s_m(x)$ is the point-spread function due to the combined effects of atmosphere and the telescope for the m^{th} exposure. The coordinate x is a two-dimensional vector and $\ast$ denotes convolution. It is assumed that the exposure time is short enough to "freeze" the atmosphere and only a narrow spectral band is used. The Fourier transform of each short-exposure image is computed:

$$D_m(u) = \int_{-\infty}^{\infty} d_m(x) \exp(i2\pi ux)\, dx \tag{2}$$

In this paper, capital letters will denote the complex Fourier transforms of the corresponding lower-case letters, and the coordinate u is referred to as a spatial frequency. The summed squared Fourier modulus (the summed power spectrum) is computed:

$$\sum_{m=1}^{M} |D_m(u)|^2 = \sum_{m=1}^{M} |F(u)S_m(u)|^2 = |F(u)|^2 \sum_{m=1}^{M} |S_m(u)|^2 \tag{3}$$

The factor $\sum|S_m(u)|^2$ can be thought of as the square of the MTF of the speckle interferometry process (the speckle MTF^2) and it can be determined approximately by performing stellar speckle interferometry on an isolated unresolved star through atmospheric conditions having the same statistics as those through which the object imagery is taken. Dividing the summed power spectrum by the speckle MTF^2 yields, according to Eq. (3), $|F(u)|^2$, the squared Fourier modulus of the object.

Since it is simply the Fourier transform of $|F(u)|^2$, the autocorrelation of the object can be obtained by Labeyrie's method. However, the autocorrelation gives only very limited information about the object: its diameter, and the separation for the case of a binary star system. Only for the special cases of (1) an object known to be centro-symmetric and (2) an object having an isolated unresolved star within the same isoplanatic patch[2] (within a few seconds of arc) can the autocorrelation, or equivalently $|F(u)|^2$, be used to directly compute the object.

The iterative method

We have, in addition to the measured Fourier modulus, the a priori knowledge that the object brightness is a real, nonnegative function. The reconstruction problem consists of finding a nonnegative object that is consistent with the measured Fourier modulus data. This problem can be solved by the iterative method depicted in Figure 1. It consists of

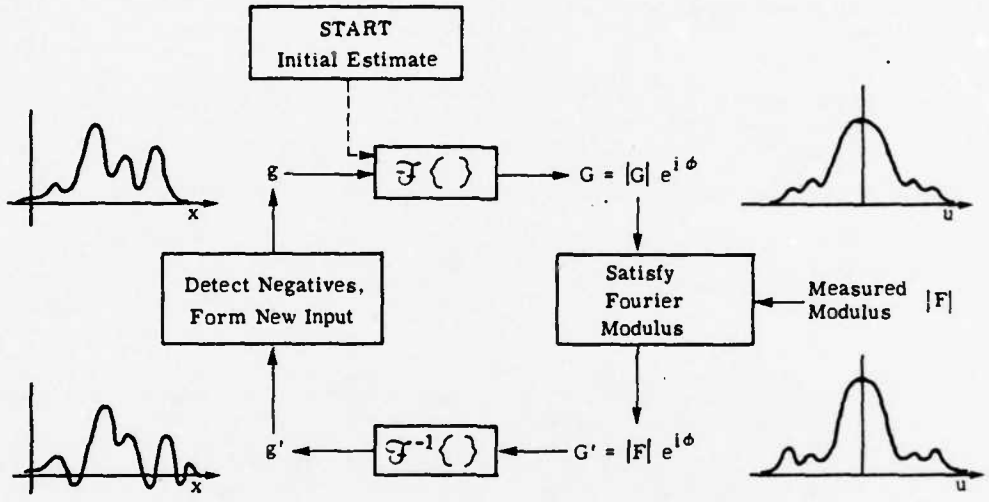

Figure 1. Iterative processing overview.

four steps: (1) an initial estimate of the object, g(x) (which we usually choose to be a field of random numbers), is Fourier transformed; (2) in the Fourier domain, the measured Fourier modulus is substituted for the computed Fourier modulus, and the computed phase is unaltered; (3) the result is inverse Fourier transformed, yielding an image g'(x); and (4) a new g(x) is chosen, based on the violation of the object-domain constraints by g'(x). The four steps are repeated until the mean-squared error is reduced to a small value consistent with the signal-to-noise ratio of the measured Fourier modulus data. The mean-squared error in the image domain is

$$E_o^2 = \frac{\int_\gamma [g'(x)]^2\, dx}{\int_{-\infty}^{\infty} [g'(x)]^2\, dx} \tag{4}$$

where the region γ includes all points at which g'(x) violates the object domain constraints (where it is negative or possibly where it exceeds an a priori known diameter). Several different methods for choosing a new g(x) have proven successful. For the results shown in this paper, we used for most iterations

$$g_{k+1}(x) = \begin{cases} g_k'(x) & , \quad x \notin \gamma \\ g_k(x) - .5g_k'(x), & x \in \gamma \end{cases} \tag{5}$$

interspersing with

$$g_{k+1}(x) = \begin{cases} g'_k(x), & x \notin \gamma \\ 0, & x \in \gamma \end{cases} \qquad (6)$$

every few iterations, where the subscript k refers to the k^{th} iteration and γ is defined as in Eq. (4). More detailed discussions of the iterative method and why it works can be found in References 3 and 6.

For the binary star results shown later, when random numbers were used for the initial input, then over a hundred iterations were required for an array size of 128 x 128 pixels (about the same number of iterations that has been required for complicated two-dimensional objects), taking about two minutes on a Floating Point Systems AP 120B array processor. When a binary star pattern with the correct spacing (which can be determined from the autocorrelation) but the incorrect brightness ratio was used as the initial input, then only a dozen iterations were required for convergence, taking about 10 seconds. It was found that the nonnegativity constraint was sufficient, and the diameter constraint was not needed.

Noise and MTF characteristics and their compensation

The data used for the experiments described here were obtained from the Steward Observatory Speckle Interferometry Program which is described in more detail elsewhere in this proceedings volume[7]. For this "event detection" data, it is assumed that any one short exposure image contains no more than one photon in any one pixel (and most pixels record zero photons). After an image is magnified, intensified, and detected, (among other things) it is thresholded to produce an image consisting of ones (where above the threshold) and zeros. Each image is autocorrelated, and the sum of all the autocorrelations is computed. The summed power spectrum is computed as the Fourier transform of the summed autocorrelation. In addition, each image is centroided (translated to make their centroids coincident) to within the nearest pixel, and the sum of the centroided images is computed.

The telescope diameter is 2.3 meters; and, for 30X magnification of the image, the image scale is approximately 0.02 arc-sec per pixel along each line, and is about 0.017 arc-sec per line (it is stretched by about 13% in that dimension relative to the along-line dimension). For 60X magnification, the scale is half that. The data is digitized in 256 x 256 arrays.

Figure 2 shows an example of a cut through the summed power spectrum of an unresolved star, SAO 36615. This data was taken at 60X magnification (0.01 arc-sec per pixel = 4.7×10^{-8} radians per pixel) at a 30 nm wavelength band centered at 750 nm. The scale in the Fourier domain is 750 nm/(4.7×10^{-8} rad x 256) = 0.062 meters (of telescope aperture) per pixel. For a telescope diameter of 2.3 meters, the highest spatial frequency passed by the telescope aperture is 2.3 m/(0.062 m/pix) = 37 pixels from zero frequency. Ideally (no atmosphere or aberrations and no noise), the summed power spectrum of an unresolved star would be the square of the MTF due to the telescope aperture (that MTF is the autocorrelation of the telescope pupil function). Assuming a circular aperture, a cut through the telescope aperture MTF would have a roughly cone shape[8] and be zero beyond pixel 37. However, the summed power spectrum of the unresolved star shown in Figure 2 is very far from this ideal.

Two effects dominate the shape of the power spectrum. First, the speckle MTF^2, mentioned earlier in connection with Eq. (3), drops very rapidly for the very low spatial frequencies near the atmospheric cut-off. This results in the spike-like behavior of the summed power spectrum for very low spatial frequencies. Beyond the very low spatial-frequency region, the speckle MTF^2 is much better behaved and decreases slowly[9]. Second, photon noise results in, among other things, a noise bias term in the summed power spectrum[10]. This noise bias term dominates in the higher spatial frequencies. Beyond a radius of 37 pixels in the summed power spectrum, no signal energy exists -- it is purely noise. They so dominate the summed power spectrum that little useful information can be obtained unless compensation is made for both of these two effects.

The noise bias term and the detection transfer function

One would ordinarily eliminate the noise bias term simply by subtracting a constant from the summed power spectrum[10,11]. However, as seen from Figure 2, the noise bias term, which is seen by itself beyond pixel 37, is not a constant in this case. This results from the fact that upon detection and thresholding, a single photon sometimes results in more than one pixel recording a one, depending upon the threshold level and the size of the splotch of light exiting from the image intensifier. Table 1 shows the autocorrelations and the individual squared transfer functions of some of the various patterns of ones resulting from a single photon. Each pattern is, in effect, the impulse response of the de-

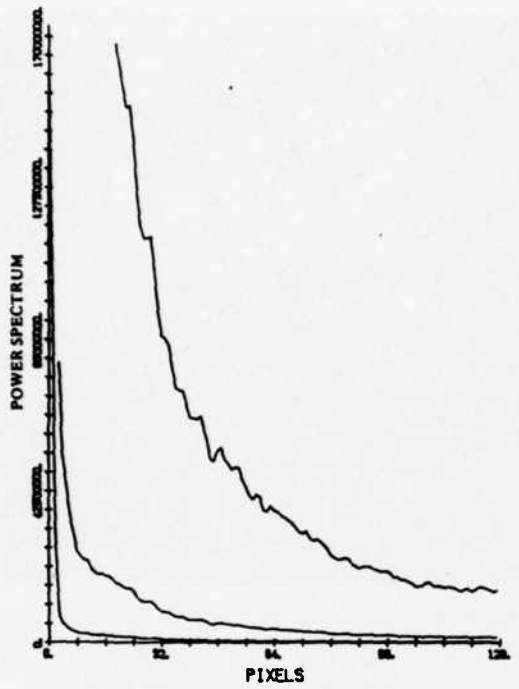

Figure 2. Summed power spectrum of an unresolved star (linear scale). The middle and upper curves are the same as the lower curve, except have 10X and 100X vertical scales, respectively.

Table 1. Event detection data: individual impulse responses, their auto correlations, and their power spectra.

DETECTION IMPULSE RESPONSE	AC OF IMPULSE RESPONSE	DETECTION TRANSFER FUNCTION²
1	1	1
1 1	1 2 1	$2 + 2\cos(2\pi u/N)$
1 / 1	1 / 2 / 1	$2 + 2\cos(2\pi v/N)$
1 1 1	1 2 3 2 1	$3 + 4\cos(2\pi u/N) + 2\cos(4\pi u/N)$
1 / 1 1	1 1 / 1 3 1 / 1 1	$3 + 2\cos(2\pi u/N) + 2\cos(2\pi v/N) + 2\cos[2\pi(u+v)/N]$
⋮	⋮	⋮

tection system; and in any one image, several different patterns may appear. That is, this impulse response may vary from photon to photon within the same image. Assuming a sparse population of photons within each image, it can be shown that the net squared transfer function, due to the ensemble of photon-produced patterns within an image, is given by a weighted sum of the individual squared transfer functions of the individual patterns. We refer to this weighted sum as the detection transfer function squared (DTF^2).

One can compensate for the noise bias term by the following steps[12]. (1) Over the spatial frequencies above the telescope cut-off, perform a two-dimensional least-squares fit of a weighted sum of individual squared transfer functions (some of which are shown in Table 1) to the summed power spectrum. By this, the DTF^2 is determined. (2) Compensate the effects of the DTF^2 by dividing the summed power spectrum by the DTF^2 (for all spatial frequencies). By this, the noise bias term is made a constant. (3) Subtract from the DTF^2-compensated summed power spectrum the constant noise bias term. This DTF^2 and noise bias compensation are demonstrated in Figures 3 and 4 for the binary star system SAO 94163. In this case, the magnification was 30X and the wavelength was 750 nm (10 nm spectral bandwidth) and so the telescope cut-off is at a spatial frequency of 74 pixels. This data set resulted from power-spectrum averaging of 1820 short exposure images containing a total of about 2.4×10^5 photons.

In the autocorrelation domain, the noise bias term results in a spike at the (0, 0) coordinate, and the DTF^2 causes the spike to be spread over a few pixels about (0, 0). Compensation for the DTF^2 causes the spike to collapse to a delta-function at (0, 0). Then the subtraction of the noise bias in the Fourier domain removes the delta-function at (0, 0) in the autocorrelation.

More generally, the functional form of the DTF^2 is heavily dependent on the manner in which the images are detected and should be modified according to the characteristics of the detection hardware used.

The speckle MTF^2

Compenstion for the speckle MTF^2 would ordinarily be accomplished by dividing the summed power spectrum by the summed power spectrum of a reference star[1]. Both power spectra should first be corrected for the DTF^2 and the noise bias term.

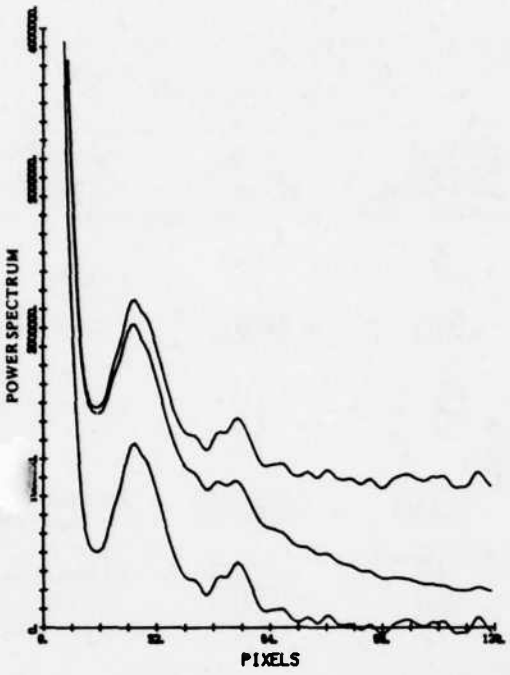

Figure 3. Power spectrum of the binary SAO 94163. (A) Middle curve: raw summed power spectrum; (B) upper curve: summed power spectrum divided by the DTF^2; (C) lower curve: DTF^2 - compensated summed power spectrum with noise bias subtracted.

Figure 4. (A)-(C) Two dimensional view of Figure 3(A)-(C); (D) the Fourier modulus, i.e., the square root of (C). Note: the residual noise beyond the telescope cut-off frequency is visible in this case and not in (C) because the square root operation reduces the dynamic range of the data.

In some instances, there is not available the summed power spectrum of a reference star close enough in both space and time to the observation of the object. In that case, one approach is to approximate the actual speckle MTF^2 by fitting a model[9] of the speckle MTF^2 to the data. Another alternative is the Worden subtract method[13]. There seems to be some controversy over the effectiveness of this method[14]; there is no doubt that it provides a much better estimate of the object's power spectrum than the summed power spectrum, but further investigation is needed to determine whether it is the best available estimate.

The Worden subtract method of compensating for the speckle MTF^2 consists of subtracting from the summed autocorrelation the sum of cross-correlations of different short-exposure images. The short-exposure images must be centroided before being cross-correlated[15]. It is easily shown that subtraction of a properly scaled version of the power spectrum of the sum of the centroided images from the summed power spectrum is exactly equivalent to the Worden subtract method. Figure 5(a) shows a cut through these two functions for very low spatial frequencies for the unresolved star SAO 36615. Both are similar in their spike-like behavior for very low spatial frequencies. However, for spatial frequencies at four pixels from zero frequency and beyond, the power spectrum of the sum of the centroided images is essentially zero. Thus, it would appear that the Worden subtract method could correct only for the very lowest spatial frequencies. This is borne out in Figures 5(b) and 5(c). Furthermore, recalling that the compensated summed power spectrum for an unresolved star should be a constant (weighted by the MTF^2 of the telescope aperture which is nearly unity for these very low spatial frequencies), we see from Figures 5(b) and (c) that the Worden subtract method did not produce the expected result. By getting rid of most of the low-frequency spike in the summed power spectrum, the Worden subtract method did greatly decrease its mean-squared error; however, it did not replace the spike with the correct low-frequency information. It is not presently known whether this apparent inadequacy of the Worden subtract method is due to basic inadequacies of the method itself or due to problems with this particular data set; however, it is consistent with the analysis of Fante[14].

A better speckle MTF^2 compensation than the Worden subtract method in this case would simply be to clip the summed power spectrum at the very low spatial frequencies. That is, assuming that the object's power spectrum is nearly constant for the very low spatial fre-

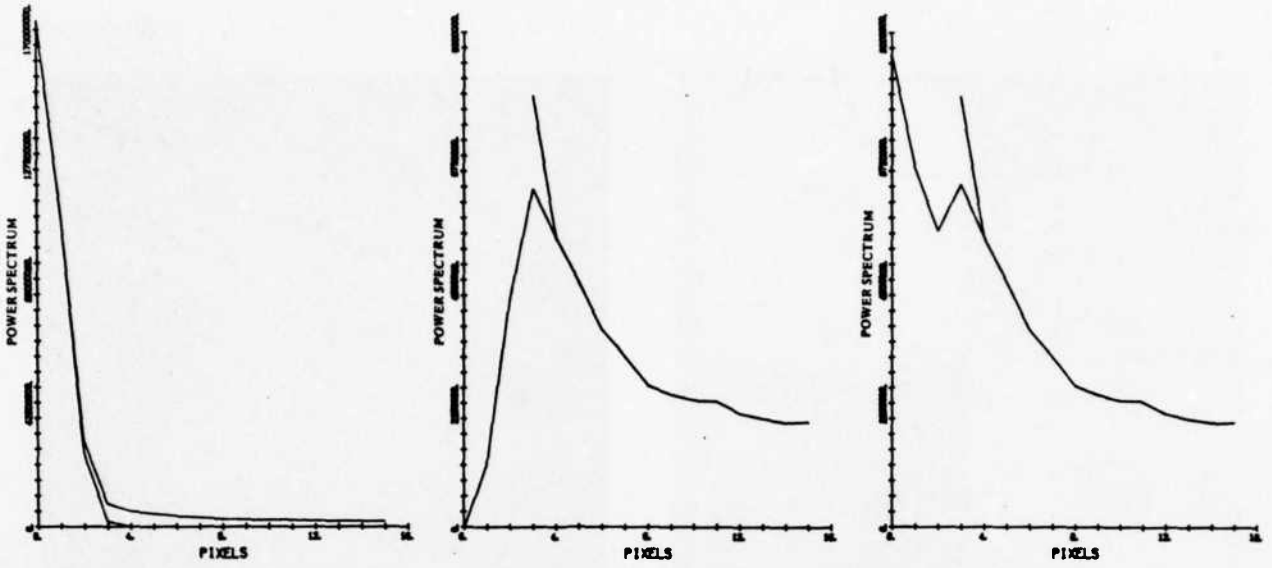

Figure 5. Worden subtract method on an unresolved star (low apatial frequencies). (A) upper curve: summed power apectrum; lower curve: power spectrum of the sum of the centroided images; (B) upper curve: summed power spectrum (note expanded vertical scale); lower curve: summed power spectrum minus the power spectrum of the aum of the centroided images; (C) same aa (B), except a smaller percentage of the power spectrum of the sum of the centroided images was subtracted.

quencies (which would be true for objects of diameter only a small fraction of an arc-sec), we replace the summed power spectrum in that region by a constant. The constant is chosen to be consistent with the value of the summed power spectrum in the region just beyond the very low-frequency spike. As in this case of the Worden subtract method, this method does not correct for the midole-frequency vs. higher-frequency regions of the speckle MTF^2; however, as noted earlier, the speckle MTF^2 is reasonably well behaved for those spatial frequencies, and correcting for the very low spatial frequencies corrects for the greatest part of the error.

The method of clipping the summed power spectrum to correct for the speckle MTF^2 is demonstrated in Figure 6 for the binary SAO 94163 for which reference star data was not available. In order to increase the accuracy of the assumption that the Fourier modulus (or its square, the power spectrum) is constant for very low spatial frequencies, the DTF and noise-bias-corrected Fourier modulus was divided by the MTF due to the telescope aperture (which was approximated by the MTF due to a circular aperture of diameter 2.3 meters). The elliptical shape of the Fourier modulus data is due to the difference in scale factors in the two dimensions as noted earlier. Within the low frequency region, wherever the Fourier modulus exceeded a threshold value, it was clipped to that threshold value. The result was multiplied by the MTF due to the telescope to arrive at our final estimate of the Fourier modulus of SAO 94163 including the telescope MTF. In the process of multiplying back in the telescope MTF, the residual noise beyond the telescope cut-off frequency was set to zero.

Image reconstruction results

The Fourier modulus estimate shown in Figure 6(d) was truncated to a 128 x 128 array, in order to save computation time in the iterative reconstruction. This caused a slight truncation of the highest spatial frequencies along the horizontal dimension of Figure 6(d). SAO 94163 was reconstructed using the iterative method, and the images resulting from two different selections of the initial input to the algorithm are shown in Figures 7(a) and (b), respectively. The rms error E_0 was reduced to about 0.05. For the purpose of display, a $(\sin x)/x$ interpolation was performed on the images of Figure 7 in order to increase the sampling rate across the image. In order to get an indication of the sensitivity of the method to the clipping threshold level described in the previous section, the clipping was done over again using a 33% greater threshold value (which is obviously greater than the optimum threshold). Two images reconstructed from the resulting Fourier modulus estimate are shown in Figure 7(c) and (d). Half the time, the iterative reconstruction algorithm produces an image rotated by 180° due to the inherent 2-fold ambiguity of the Fourier modulus data.

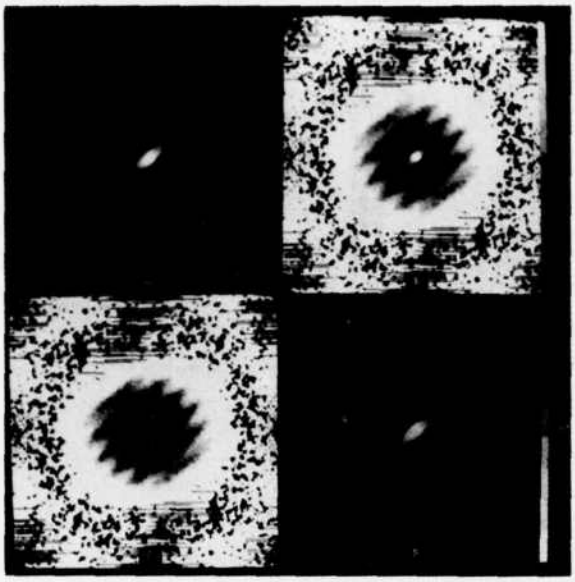

Figure 6. Clipping to compensate for the speckle MTF (for "seeing") for the binary SAO 94163. (A) Fourier modulus, same as Figure 4(D); (B) Fourier modulus compensated for telescope MTF (attempted division by zero is evident for spatial frequencies above the telescope cut-off frequency); (C) clipping of the low spatial frequencies; (D) Fourier modulus estimate obtained by putting back in the telescope MTF.

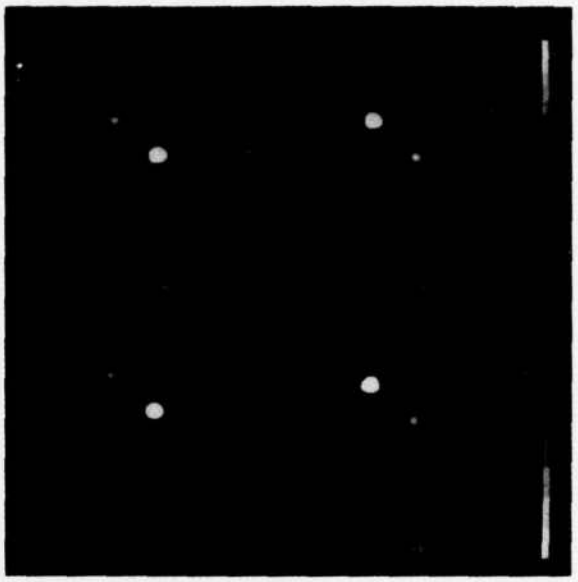

Figure 7. Reconstructed images of SAO 94163 (see text).

The average separation of the reconstructed images is 13.9 pixels = 0.27 arc-sec and the orientation angle is 42.7° (47.3° from the orthogonal axis). The brightness ratios, based on the maximum brightness of each star in the pair, are 4.38, 4.17, 4.14, and 3.96 for Figures 7(a) through (d), respectively, and the corresponding magnitude differences are 1.60, 1.55, 1.54, and 1.49, respectively. Thus, a 33% increase in threshold level caused only a 6% decrease in the computed brightness ratio. The average magnitude difference of the reconstructions of Figures 7(a) and (b) is 1.57.

Conclusions

We have discussed steps necessary to obtain an accurate estimate of an object's Fourier modulus from the raw summed power spectrum: detection transfer function compensation, noise bias subtraction, and speckle MTF compensation. For compensation of the speckle MTF when reference star data is not available, an improvement over the Worden subtract method is the simple method of clipping the Fourier modulus spike at the very low spatial frequencies (for objects much smaller than one arc-sec in diameter). A reconstruction of the binary SAO 94163 using this method resulted in an image having a binary separation of 0.27 arc-sec at an angle of 42.7° (47.3°) and a magnitude difference of 1.57 (brightness ratio of 4.26). The reconstruction of a binary is trivial and does not require the use of the iterative method; however, the iterative method is required for complicated objects, and the data processing steps described here for this simple example can be used in more general circumstances. Based on the success of image reconstruction experiments using summed power spectra of complicated two-dimensional objects computer-simulated to include the effects of atmospheric turbulence and photon noise[11], it is expected that it will be possible to reconstruct fine-resolution images of complicated astronomical objects.

Acknowledgements

We gratefully acknowledge the helpful suggestions of K. Hege and thank him and his colleagues at Steward Observatory for sharing this stellar speckle interferometry data with us. Programming assistance by C. Roussi is also acknowledged. This work was supported by the Air Force Office of Scientific Research under Contract No. F49620-80-C-0006.

References

1. A. Labeyrie, "Attainment of Diffraction Limited Resolution in Large Telescopes by Fourier Analysing Speckle Patterns in Star Images," Astron. and Astrophys. 6, 85 (1970); O.Y. Gezari, A. Labeyrie, and R.V. Stachnik, "Speckle Interferometry: Diffraction-Limited Measurements of Nine Stars with the 200-inch Telescope," Astrophys. J. Lett. 173, L1 (1972).

2. C.Y.C. Liu and A.W. Lohmann, "High Resolution Image Formation through the Turbulent Atmosphere," Opt. Commun. 8, 372 (1973); G.P. Weigelt, "Stellar Speckle Interferometry and Speckle Holography at Low Light Levels," Proc. SPIE 243-17, Applications of Speckle Phenomena (July 1980).

3. J.R. Fienup, "Reconstruction of an Object from the Modulus of Its Fourier Transform," Opt. Lett. 3, 27 (1978); J.R. Fienup, "Space Object Imaging through the Turbulent Atmosphere, Opt. Eng. 18, 529 (1979).

4. K.T. Knox and B.J. Thompson, "Recovery of Images from Atmospherically Degraded Short-Exposure Photographs," Astrophys. J. Lett. 193, L45 (1974); J.W. Sherman, "Speckle Imaging Using the Principal Value Decomposition Method," Proc. SPIE 149 (1978).

5. Special issue on Adaptive Optics, J. Opt. Soc. Am. 67, March 1977; J.W. Hardy, "Active Optics: A New Technology for the Control of Light," Proc. IEEE 66, 651 (1978).

6. J.R. Fienup, "Iterative Method Applied to Image Reconstruction and to Computer-Generated Holograms," Opt. Eng. 19, 297 (1980).

7. P.A. Strittmatter, "The Steward Observatory Speckle Interferometry Program," Proc. SPIE 243-12, Applications of Speckle Phenomena (July 1980).

8. J.W. Goodman, Introduction to Fourier Optics (McGraw-Hill, San Francisco, 1968), p. 119.

9. D. Korff, G. Oryoen, and M.G. Miller, Opt. Commun. 5, 187 (1972).

10. J.W. Goodman and J.F. Belsher, "Fundamental Limitations in Linear Invariant Restoration of Atmospherically Degraded Images," Proc. SPIE 75, Imaging through the Atmosphere (1976), p. 141; J.C. Dainty and A.H. Greenaway, "Estimation of Power Spectra in Speckle Interferometry," J. Opt. Soc. Am. 69, 786 (1979).

11. G.B. Feldkamp and J.R. Fienup, "Noise Properties of Images Reconstructed from Fourier Modulus," Proc. SPIE 231-08, 1980 International Optical Computing Conference (April 1980).

12. C. Aime, S. Kadir, G. Ricort, C. Roddier, and J. Vernin, "Measurements of Stellar Speckle Interferometry Lens-Atmosphere Modulation Transfer Function," Optica Acta 26, 575 (1979).

13. S.P. Worden, M.K. Stein, G.D. Schmidt, and J.R.P. Angel, "The Angular Diameter of Vesta from Speckle Interferometry," Icarus 32, 450 (1977); G. Welter and S.P. Worden, "A Method for Processing Stellar Speckle Data," J. Opt. Soc. Am. 68, 1271 (1978).

14. R.L. Fante, "Comments on a Method for Processing Stellar Speckle Data," J. Opt. Soc. Am. 69, 1394 (1979).

15. S.P. Worden and M.K. Stein, "Angular Diameter of the Asteroids Vesta and Pallas Determined from Speckle Observations," Astronomical J. 84, 140 (1979).

Reprinted from Journal of the Optical Society of America, Vol. 71, page 1026, August, 1981

Appendix C

Ambiguity of phase retrieval for functions with disconnected support

T. R. Crimmins and J. R. Fienup

Radar and Optics Division, Environmental Research Institute of Michigan, P.O. Box 8618, Ann Arbor, Michigan 48107

Received February 2, 1981

Questions are raised concerning the uniqueness of solutions to the phase-retrieval problem for functions with disconnected support. A counterexample is presented showing the importance of considering the flipping of infinite proper subsets of nonreal zeros.

INTRODUCTION

In this Letter, questions are raised concerning some claims by Greenaway[1] and Bates.[2] Their papers are concerned with the question of uniqueness of solutions to the phase-retrieval problem. This problem, in the one-dimensional case, can be stated as follows.

Let f be a complex-valued function on the real line that vanishes outside some finite interval. Let F be its Fourier transform. Given the modulus of F on the real line, i.e., $|F(u)|$ for all real u, the problem is to reconstruct the original function f from this information. The general uniqueness question is: *How many other functions, $g \neq f$, exist that vanish outside some finite interval and whose Fourier transforms satisfy $|G(u)| = |F(u)|$ for all real u?*

GREENAWAY'S PAPER

Greenaway[1] considers a situation in which the unknown function f is known to be zero outside the union of two disjoint intervals (a,c) and (d,b). In other words,

$$f = g + h,$$

where g is zero outside (a,c) and h is zero outside (d,b) (see Fig. 1).

Now let F, G, and H be the Fourier transforms of f, g, and h, respectively, extended by analyticity into the complex plane:

$$F(w) = \int_{-\infty}^{\infty} f(x)e^{-iwx}dx,$$

where $w = u + iv$ and u and v are real. The modulus of F on the real line, i.e., $|F(u)|$, is given.

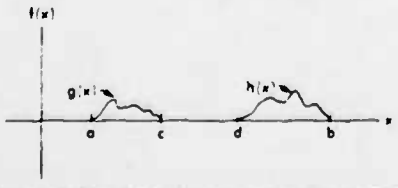

Fig. 1. Member of the class of functions with disconnected support. Note: Although the functions g and h are represented here as positive real functions, they can be complex valued.

The question is: *To what extent do the conditions described above determine the function f?*

The functions

$$e^{i\alpha}f(x + \beta) \quad \text{and} \quad e^{i\alpha}\overline{f(-x + \beta)},$$

where the overbar denotes complex conjugation and α and β are real, have the same Fourier modulus on the real line as does f. If any of these functions are also zero outside the union of the intervals (a,c) and (d,b), then they satisfy all the requirements and qualify as alternative solutions. These solutions will be said to be *associated* with the solution f.

Now the revised question is: *Are there any other solutions not associated with f?*

Let w_0 be a nonreal zero of F, and let

$$F_1(w) = F(w)\frac{w - \overline{w_0}}{w - w_0}.$$

The function F_1 can be viewed as being gotten from F by first removing a zero at w_0 and then adding a zero at $\overline{w_0}$. In other words, the zero at w_0 has been "flipped" about the real line. Now for real w, $w = u$,

$$\left|\frac{u - \overline{w_0}}{u - w_0}\right| = 1,$$

and therefore

$$|F_1(u)| = |F(u)| \qquad \text{for all real } u.$$

Hofstetter[3] and Walther[4] proved that if f_1 is any function that vanishes outside some finite interval and $|F_1(u)| = |F(u)|$ for all real u, then F_1 is gotten from F by flipping various sets of nonreal zeros of F and multiplying by a constant of modulus 1 and by an exponential function. In particular, if F_1 is obtained from F by flipping the set of all its nonreal zeros, then its inverse transform f_1 satisfies

$$f_1(x) = \overline{f(-x)},$$

and thus, if f_1 vanishes outside the union of (a,c) and (d,b), then f_1 is a solution associated with f. (Here, if a zero of F has multiplicity n, it must be flipped n times.)

Now let $Z(F)$ denote the set of all nonreal zeros of F.

Greenaway claims that if F_1 is obtained from F by flipping any *proper* subset S of $Z(F)$ [i.e., $S \neq Z(F)$] and if f_1 vanishes outside the union of (a,c) and (d,b), then all the points in S are zeros of both G and H.

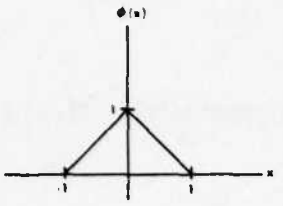

Fig. 2. The function $\phi(x)$.

Thus, if G and H have no zeros in common (which would usually be the case if g and h are gotten more or less randomly from the real world), it would follow that the only solutions are f and its associated solutions. Bates[5] also considers this problem from another point of view.

Greenaway's claim is true in the special case in which F has only a finite number of nonreal zeros. (Actually, Greenaway's proof holds only for the more restricted case in which F has a finite number of nonreal zeros of order 1. However, the case of higher-order zeros can be taken care of by an extension of his argument. See Ref. 6.)

The following counterexample shows that Greenaway's claim is not true in general. In this counterexample, the set $Z(F)$ is infinite and S is an infinite proper subset of $Z(F)$.

Counterexample

Let

$$\phi(x) = \begin{cases} 1 - |x| & \text{for } |x| < 1 \\ 0 & \text{for } |x| \geq 1 \end{cases}.$$

(See Fig. 2.) Then the Fourier transform Φ of ϕ is given by

$$\Phi(w) = \frac{\sin^2(w/2)}{(w/2)^2} = \operatorname{sinc}^2(w/2).$$

Note that Φ has no nonreal zeros.

Now let

$$g(x) = 8\phi(x)$$

and

$$h(x) = 2\phi(x-4) + 3\phi(x-8) + 2\phi(x-12).$$

Then $G = 8\Phi$ has no nonreal zeros, and hence G and H have no nonreal zeros in common. Let

$$f(x) = g(x) + h(x)$$
$$= 8\phi(x) + 2\phi(x-4) + 3\phi(x-8) + 2\phi(x-12)$$

and let

$$a = -1, \quad c = 1, \quad d = 3, \quad b = 13.$$

(See Fig. 3.) Then $a < c < d < b$, the intervals (a,c) and (d,b) are disjoint, and f is zero outside the union of (a,c) and (d,b). The Fourier transform of f is

$$F(w) = (8 + 2e^{-4iw} + 3e^{-8iw} + 2e^{-12iw})\Phi(w)$$
$$= 2(e^{-4iw} + 2)(e^{-8iw} - 0.5e^{-4iw} + 2)\Phi(w). \qquad (1)$$

Now let

$$g_1(x) = 4\phi(x)$$

and

$$h_1(x) = 7\phi(x-4) + 4\phi(x-12).$$

Then $G_1 = 4\Phi$ has no nonreal zeros, and hence G_1 and H_1 have no nonreal zeros in common. Let

$$f_1(x) = g_1(x) + h_1(x)$$
$$= 4\phi(x) + 7\phi(x-4) + 4\phi(x-12).$$

(See Fig. 3.) Then f_1 is also zero outside the union of (a,c) and (d,b). The Fourier transform of f_1 is

$$F_1(w) = (4 + 7e^{-4iw} + 4e^{-12iw})\Phi(w)$$
$$= 2(2e^{-4iw} + 1)(e^{-8iw} - 0.5e^{-4iw} + 2)\Phi(w)$$
$$= 2e^{-4iw}(e^{4iw} + 2)(e^{-8iw} - 0.5e^{-4iw} + 2)\Phi(w). \qquad (2)$$

It follows from Eqs. (1) and (2) that

$$F_1(w) = e^{-4iw}\left(\frac{e^{4iw} + 2}{e^{-4iw} + 2}\right)F(w).$$

Now, for real w, $w = u$,

$$\left|e^{-4iu}\frac{e^{4iu} + 2}{e^{-4iu} + 2}\right| = 1.$$

Therefore

$$|F_1(u)| = |F(u)| \qquad \text{for all real } u.$$

Thus f and f_1 are both solutions, and it is clear that they are not associated.

In order to see which zeros must be flipped to get F_1 from F, let

$$\Gamma_1(w) = e^{-4iw} + 2$$

and

$$\Gamma_2(w) = e^{-8iw} - 0.5e^{-4iw} + 2.$$

Then

$$F(w) = 2\Gamma_1(w)\Gamma_2(w)\Phi(w) \qquad (3)$$

and

$$F_1(w) = 2e^{-4iw}\overline{\Gamma_1(\bar{w})}\Gamma_2(w)\Phi(w). \qquad (4)$$

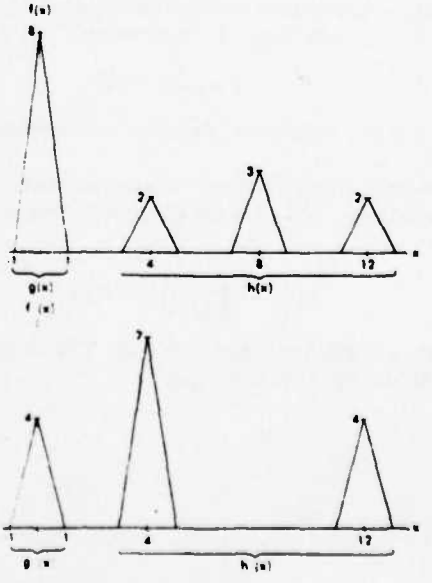

Fig. 3. Functions $f(x)$ (above) and $f_1(x)$ (below) have the same Fourier modulus.

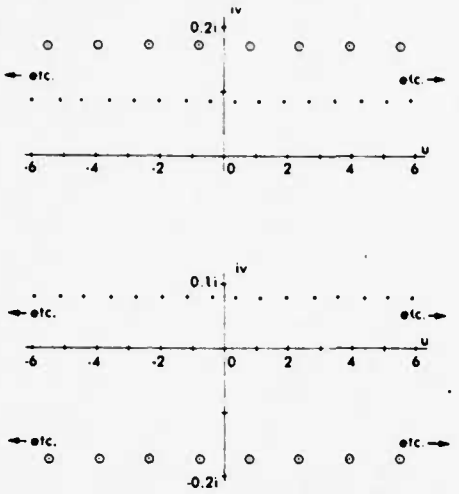

Fig. 4. Above: nonreal zeros of F. Below: nonreal zeros of F_1. The circled zeros are flipped.

Since Φ has no nonreal zeros and e^{-4iw} is never zero, it follows from Eqs. (3) and (4) that

$$Z(F) = Z(\Gamma_1) \cup Z(\Gamma_2)$$

and

$$Z(F_1) = \overline{Z(\Gamma_1)} \cup Z(\Gamma_2),$$

where

$$\overline{Z(\Gamma_1)} = \{\bar{w}: \quad w \in Z(\Gamma_1)\}.$$

Thus the zeros of F that are in $S = Z(\Gamma_1)$ are flipped. The sets $Z(\Gamma_1)$ and $Z(\Gamma_2)$ are given by

$$Z(\Gamma_1) = \left\{\frac{\pi}{4} + \frac{\pi}{2}n + \frac{i}{4}\log 2: \quad n = 0, \pm 1, \pm 2, \ldots\right\}$$

and

$$Z(\Gamma_2) = \left\{\pm\frac{1}{4}\tan^{-1}\sqrt{31} + \frac{\pi}{2}n + i\,\frac{1}{8}\log 2: \quad n = 0, \pm 1, \pm 2, \ldots\right\}.$$

(See Fig. 4.) The flipping of the zeros in S is followed by multiplication by the exponential e^{-4iw}. The latter simply has the effect of translating f_1 into the proper position.

In the above example the function ϕ could be replaced by any function that is zero outside the interval $(-1,1)$ and whose Fourier transform has no nonreal zeros. For example, ϕ could be replaced by

$$\phi_1(x) = (\phi * \phi)(2x),$$

where $*$ denotes convolution, or by

$$\phi_2(x) = \begin{cases} 1 & \text{for } |x| < 1 \\ 0 & \text{for } |x| \geq 1 \end{cases}.$$

BATES'S PAPER

Bates[2] considers the situation in which

$$f(x) = \sum_{n=1}^{N} f_n(x),$$

where each f_n is zero outside an interval I_n and the intervals I_n, $n = 1 \ldots N$, are pairwise disjoint. He claims that if the Fourier transforms F_n have no nonreal zeros common to all of them, then f and its associated solutions are the only functions with compact support and whose Fourier transforms have the same moduli as that of the Fourier transform of f. Thus Bates claims even more than Greenaway does. Therefore the above example is also a counterexample to Bates's claim.

It should be noted that the function f to which Bates is applying this argument is the one-dimensional projection of a function defined on the plane. He concludes from this argument that, in the two-dimensional case, solutions with disconnected support are almost always unique (up to associated solutions). This conclusion regarding two-dimensional uniqueness may well be true for other reasons discussed by Bruck and Sodin.[7]

COMMENTS

We stress that functions with disconnected support whose Fourier transforms have only a finite number of nonreal zeros form a special class of functions. It can be shown (see Ref. 6) that such functions satisfy certain special conditions. Thus it is quite common for functions with disconnected support gotten more or less randomly from the real world to have Fourier transforms with an infinite number of nonreal zeros. The fact that one is able, in practice, to compute only a finite number of them does not change these conclusions. One cannot claim to be making statements about the uniqueness of a solution unless the entire infinity of nonreal zeros of its Fourier transform is properly considered.

Finally, we note that the example presented here does not imply that the attempt to reconstruct functions from the moduli of their Fourier transforms is hopeless. It can be shown[6] that a stronger separation condition on the separate parts of the support of f (i.e., that the parts are separated by certain greater intervals than assumed by Greenaway and Bates) does imply that f and its associated solutions are the only solutions.

This research was supported by the U.S. Air Force Office of Scientific Research under contract no. F49620-80-C-0006.

REFERENCES

1. A. H. Greenaway, "Proposal for phase recovery from a single intensity distribution," Opt. Lett. 1, 10–12 (1977).
2. R. H. T. Bates, "Fringe visibility intensities may uniquely define brightness distributions," Astron. Astrophys. 70, L27–L29 (1978).
3. E. M. Hofstetter, "Construction of time-limited functions with specified autocorrelation functions," IEEE Trans. Inf. Theory IT-10, 119–126 (1964).
4. A. Walther, "The question of phase retrieval in optics," Opt. Acta 10, 41–49 (1963).
5. R. H. T. Bates *et al.*, "Self-consistent deconvolution. I. Theory," Optik (Stuttgart) 44, 183–201 (1976).
6. T. R. Crimmins and J. R. Fienup, "Phase retrieval for functions with disconnected support," in Appendix B of J. R. Fienup, "High resolution imaging of space objects," interim scientific report to Air Force Office of Scientific Research, ERIM Report No. 145400-7-P (Environmental Research Institute of Michigan, Ann Arbor, Mich., March 1981).
7. Yu. M. Bruck and L. G. Sodin, "On the ambiguity of the image reconstruction problem," Opt. Commun. 30, 304–308 (1979).

Appendix D

Uniqueness results for the phase-retrieval problem for radial functions

Wayne Lawton

Radar and Optics Division, Environmental Research Institute of Michigan, P.O. Box 8618, Ann Arbor, Michigan 48107

Received April 3, 1981; revised manuscript received July 24, 1981

A representation theorem for band-limited functions of several variables whose moduli are radial is stated. The proof of this theorem, which is based on techniques from Fourier analysis and the theory of analytic functions of several variables, is outlined in the Appendix. Several uniqueness results concerning the phase-retrieval problem that follow from the representation theorem are derived. References that relate the phase-retrieval problem to the problem of wave-front reconstruction in optics and image reconstruction in speckle interferometry are cited.

INTRODUCTION

The phase-retrieval problem, which consists of determining a function that vanishes outside a bounded region from the modulus of its Fourier transform, arises in several areas of physics and engineering, e.g., wave-front reconstruction in optics and electron microscopy and stellar speckle interferometry.

A major problem that arises concerns the uniqueness of solutions. This problem has been extensively studied for the one-dimensional case (see Refs. 1–6) by using the theory of analytic functions of a complex variable. The main result of these studies indicates that it is not possible, in general, to reconstruct a function of one variable from the modulus of its Fourier transform. This result follows from the fact that if f is a (square-integrable and nonzero) function of one variable that vanishes outside a finite interval of real numbers, then its Fourier transform $\hat{f}$, considered to be extended to a function of a complex variable, admits a particular factorization in which appears the infinite set of complex zeros of $\hat{f}$. Flipping any of the nonreal zeros of $\hat{f}$ (that is, replacing a zero in the factorization of $\hat{f}$ with its complex conjugate) does not change the modulus of $\hat{f}$ or the interval outside which f vanishes. Since, in general, an infinite subset of the set of zeros of $\hat{f}$ will be nonreal, this zero-flipping argument shows that, in general, the one-dimensional phase-retrieval problem admits of an infinite number of distinct solutions.

Although the physical situations in which the phase-retrieval problem arises involve functions of two variables, the corresponding uniqueness problem has not been completely solved. A practical iterative technique for reconstructing f from the modulus of its Fourier transform for the stellar speckle interferometry problem (in this problem f is a real-valued nonnegative function representing the brightness distribution of a star or other space object) is discussed in Refs. 7–10. Empirical results using this technique and the theoretical discussions in Refs. 11–13 indicate that the ambiguity for the phase-retrieval problem in two dimensions (especially when f is a real-valued nonnegative function) is reduced. However, specific examples of nonuniqueness for the two-dimensional phase-retrieval problem can easily be constructed as shown in Ref. 12 and also by the following: Let $g(x, y)$ and $h_1(x, y)$ be (nonzero) real-valued nonnegative and square-integrable functions that vanish outside a bounded region of the plane and such that $h_2(x, y) \neq h_1(-x, -y)$ for all (x, y). Then define $f_1(x, y)$ and $f_2(x, y)$ by

$$f_k(x, y) = \int_{-\infty}^{\infty} \int_{-\infty}^{\infty} g(u, v) h_k(x - u, y - v) \mathrm{d}u \mathrm{d}v$$

for $k = 1, 2$.

Then the functions f_1 and f_2 are distinct, real-valued, nonnegative, and square integrable and vanish outside a bounded region of the plane, and an application of the convolution theorem for Fourier transforms shows that the moduli of their Fourier transforms are identical.

The discussion above suggests some of the distinctive and intriguing aspects of the uniqueness question for the two-dimensional phase-retrieval problem. This paper treats two uniqueness-related questions that arise in the following *special case* of the phase-retrieval problem: Let f be a function (of $N \geq 1$ variables) such that f is square integrable and vanishes outside a bounded set and such that the modulus $|\hat{f}|$ of its Fourier transform is *radially symmetric*.

Question 1. What, if any, symmetry properties concerning f can be deduced?

Question 2. Under what conditions is f determined uniquely from $|\hat{f}|$?

The answers to these questions, together with two physical applications, are stated below.

Answer 1. If $N \geq 3$, then, up to translation, f is a radial function. If $N = 2$, then, up to translation, f is the product of a radial function times the function $\exp(ik\theta)$, where $i = \sqrt{-1}$, k is an integer, and $\theta = \theta(x, y)$ denotes the polar angle of a planar point having rectangular coordinates (x, y). If $N = 1$, no symmetry property for f necessarily holds.

Application 1. Answer 1 implies that if the real (detected) impulse response function of a thin lens (whose thickness and index of refraction are continuous) is radially symmetric, then its aperture function (both phase and apodization) must be

0030-3941/81/121519-04$00.50

radially symmetric and hence its coherent transfer function is radially symmetric.

Answer 2. For N arbitrary, if f is known to be real, then f is uniquely determined by $|\hat{f}|$. Otherwise, in general, there are an infinite number of distinct solutions.

Application 2. Answer 2 implies that the brightness distribution of a space object having a radially symmetric brightness function f (for instance a star with no significant sunspots) can be uniquely reconstructed from $|\hat{f}|$ (where $|\hat{f}|$ is obtained from the stellar speckle interferometry technique of Labeyrie) by using Fienup's iterative technique.

In the following section we introduce mathematical notation that is used to state a representation theorem for band-limited functions. Since the derivation of this theorem is quite elaborate, it is placed in the Appendix. Then three consequent results that are stated as corollaries are derived.

Answer 1 follows directly from Corollary 1 and the example in Eq. (3), whereas Answer 2 follows from Corollaries 2 and 3.

NOTATION AND DERIVATIONS

If N is a positive integer and $z = (z_1, \ldots, z_N), \omega = (\omega_1, \ldots, \omega_N)$ are elements of C^N, where C is the complex plane, define $(z, \omega) = \sum_{k=1}^{N} z_k \omega_k$. Denote by $L_2(R^N)$ the set of complex valued functions on $R^N \subset C^N$ (R is the real line) having integrable squared modulus, and for $f \in L_2(R^N)$ let

$$\hat{f}(x) = \int_{R^N} f(y)\exp(-2\pi i\,(x, y))dy \tag{1}$$

denote the Fourier transform of f.

We define a function $F \in L_2(R^N)$ to be band limited if $\hat{F}$ vanishes identically off some bounded subset of R^N. Let $B(R^N)$ denote the set of band limited functions on R^N. Note that a function is band limited if and only if it is the Fourier transform of a square integrable function that vanishes outside a bounded region. We define a function F on R^N to be radial if $F(x) = F(y)$ whenever $\langle x, x\rangle = (y, y)$. Let $\mathrm{RAD}(R^N)$ denote the set of radial functions of R^N.

Representation Theorem

If $N > 1$ and $F \in B(R^N)$ and $|F| \in \mathrm{RAD}(R^N)$, then F can be extended to an analytic function $F: \mathcal{C}^N \to \mathcal{C}$, which admits the representation

$$F(z) = P(z)\exp(2\pi i\,(x_0, z)) \prod_{k=1}^{\infty}\left[1 - \frac{(z, z)}{\lambda_k{}^2}\right], \tag{2}$$

where

$x_0 \in R^N$,

$|\lambda_k|$ are an infinite sequence of nonzero complex numbers,

$P(z)$ is a polynomial having either the form (a) If $N = 2$, then $P(z_1, z_2) = A(z_1 + iz_2)^{m_1}(z_1 - iz_2)^{m_2}$ for some integers $m_1, m_2 \geq 0$ and some $A \in \mathcal{C}$ or (b) If $N \geq 3$, then $P(z) = A((z, z))^m$ for some integer $m \geq 0$ and some $A \in \mathcal{C}$.

Proof. See Appendix.

The representation in Eq. (2) above is interesting because it is not necessarily true in the one-dimensional situation, as is demonstrated by the following example:

Let $f: R \to \mathcal{C}$ be defined by

$$f(y) = \begin{cases} \exp(-2\pi y) & \text{for } |y| \leq \tfrac{1}{2}, \\ 0 & \text{otherwise} \end{cases} \tag{3}$$

and let

$$F(x) = \hat{f}(x) = \frac{\sin \pi(x - i)}{\pi(x - i)}. \tag{4}$$

Then the analytic continuation $F(z)$ of $F(x)$ admits the factorization

$$F(z) = A \prod_{k=1}^{\infty}\left(1 - \frac{z}{i + k}\right)\left(1 - \frac{z}{i - k}\right), \tag{5}$$

where

$$A = \prod_{k=1}^{\infty}\left(1 + \frac{1}{k^2}\right).$$

Clearly, $F \in B(R)$ and $|F| \in \mathrm{RAD}(R)$; however, the roots $(i \pm k)$ do not occur in negative pairs, as Eq. (2) would imply. This difference is based on the topological property, utilized in the Appendix, that the sphere

$$S^{N-1} = (x \in R^N | (x, x) = 1) \tag{6}$$

is connected if and only if $N > 1$.

Corollary 1. A function F satisfies the hypothesis of the theorem if and only if $F = \hat{f}$, where f is the translation, by $x_0 \in R^N$, of a function $h \in L_2(R^N)$ and that has the form either

(a) For $N = 2$, $h(y_1, y_2) = \exp[i(m_1 - m_2)\theta]\, g(y_1, y_2)$, where $\theta = \arctan(y_2/y_1)$ and g is radial,

or

(b) For $N \geq 3$, h is radial.

Proof. The translation part follows directly from the Fourier inversion theorem, and parts (a) and (b) follow from the facts: (1) the Fourier transform satisfies the following property with respect to rotation: If M is a rotation transformation $M: R^N \to R^N$ and $f \in L_2(R^N)$ and $g(x) = f(Mx)$, then $\hat{f}(My) = \hat{g}(y)$, and (2) for $N \geq 3$, $P(Mz) = P(z)$, and for $N = 2$, $P(Mz) = \exp[i(m_1 - m_2)\theta]\, P(z)$, where θ is the angle of rotation.

Corollary 2. For $N > 1$ the following two conditions are equivalent:

(1) $F, G \in B(R^N)$, $|F| = |G|$, $|F|$ is radial, $\hat{F}$ and $\hat{G}$ are real.

(2) There exists a real radial function $h \in L_2(R^N)$ such that h vanishes off some bounded subset of R^N and both $\hat{F}$ and $\hat{G}$ are translates of h.

Proof. Fact (2) implies that fact (1) follows directly. If $\hat{F}$ and $\hat{G}$ are real, then $\overline{F(x)} = F(-x)$ and $\overline{G(x)} = G(-x)$ for every $x \in R^N$; hence in the representation in Corollary (2) for F and G, the polynomials must have the form given by (b), and the roots of each must occur in the conjugate pairs. Also, since $|F(x)| = |G(x)|$ for all $x \in R^N$, the representations must be identical except for the exponential terms that correspond to translation.

Corollary 3. Let F satisfy the hypothesis of the theorem and let λ_k be any of the roots in Eq. (2). Then the function G, defined by

$$G(x) = F(x)\frac{1 - (x, x)/\lambda_k{}^{-2}}{1 - (x, x)/\lambda_k{}^2}, \tag{7}$$

also satisfies the hypothesis of the theorem. Furthermore, $|G(x)| = |F(x)|$ for every $x \in R^N$.

Proof. The equality is evident, as is the fact that $|G| \in \mathrm{RAD}(R^N)$ and $G \in L_2(R^N)$. We must prove that $\hat{G}$ vanishes identically off a bounded subset of R^N. We need the following result, proved in Ref. 14.

Result

If $N \geq 1$ and $F: R^N \to \mathcal{C}$, then $F \in B(R^N)$ if and only if $F \in L_2(R^N)$ and F extends to an analytic function $F: \mathcal{C}^N \to \mathcal{C}$ of *exponential type* [that is, there exists $A > 0$ and $a > 0$ such that $|F(z)| < A\exp(a|z|)$ for all $z \in \mathcal{C}^N$].

Now, to complete the proof of Corollary 3, let $F(z)$ and $G(z)$ be the analytic continuations of $F(x)$ and $G(x)$. By the *only if* part above, $F(x) \in L_2(R^N)$ and $F(z)$ is of exponential type. Hence it follows from Eq. (7) that $G(x) \in L_2(R^N)$ and that $G(z)$ is of exponential type. The result now follows from the *if* part above.

APPENDIX A:

We will outline a proof of the representation theorem. Define the sphere $S^{N-1} = (x \in R^N | (x, x) = 1)$. Let F satisfy the hypothesis of the theorem, and for any $v \in S^{N-1} \subset R^N$ let $F_v(t)$: $R \to C$ be defined by

$$F_v(t) = F(tv). \tag{9}$$

It can be demonstrated that $F_v \in B(R)$. Therefore $F_v(t)$ can be extended to an analytic function $F_v(\omega)$: $\mathcal{C} \to C$ of exponential type.

By Hadamard's factorization theorem,[15] $F_v(\omega)$ admits the factorization

$$F_v(\omega) = \omega^{L(v)}A(v)\exp[ia(v)\omega]\prod_{k=1}^{\infty}\left[1 - \frac{\omega}{\lambda_k(v)}\right], \tag{10}$$

where, for every $v \in S^{N-1}$, $L(v)$ is a nonnegative integer, $A(v) \in C$, $a(v) \in R$, and $[\lambda_k(v)]$ are the infinite set of zeros of $F_v(\omega)$.

Furthermore, the set (F_v) of functions forms a continuous family of functions (in the topology of uniform convergence on compact subsets) parameterized by the parameter $v \in S^{N-1}$. Hence, by Rouché's theorem,[16] since the zeros $[\lambda_k(v)]$ form a discrete subset of C (they have no limit points), the $\lambda_k(v)$ are continuous functions of v (after a suitable permutation of indices).

Now, let $u = (1,0,0,\ldots,0) \in S^{N-1}$. Since $|F|$ is radial, $|F_v(t)| = |F_u(t)|$, and hence $F_v(\omega)\overline{F_v(\bar{\omega})} = F_u(\omega)\overline{F_u(\bar{\omega})}$. Therefore $L(v) = L(u)$, $|A(v)| = |A(u)|$, and for every k, the function $\lambda_k(v)$: $S^{N-1} \to C$ is continuous and S^{N-1} is connected (since $N > 1$); hence the set $[\lambda_k(v)$: $V \in S^{N-1}]$ is connected. However, for each $v \in S^{N-1}$ it follows from Eq. (10) and the equality $|F_v(t)| = |F_u(t)|$ that

$$\lambda_k(v) \in \lambda_k(u) \cup [\overline{\lambda_k(u)}].$$

Since the latter set is discrete, its only connected subsets are single points; hence each function $\lambda_k(v)$ is a constant λ_k. Hence we can write

$$F_v(\omega) = \omega^L|A|\exp[ia(v)\omega + ib(v)]\prod_{k=1}^{\infty}\left(1 - \frac{\omega}{\lambda_k}\right), \tag{11}$$

where $L = L(u)$, $A = A(u)$, and $b(v) \in R$ and $a(v) \in R$.

Equation (11) implies that if $F_v(\lambda) = 0$ then $F_v(-\lambda) = F(-v\lambda) = F_{-v}(\lambda) = 0$ for $\lambda \in \mathcal{C}$. Therefore, after a suitable relabeling of indices, we may write

$$F_v(\omega) = \omega^L|A|\exp[ia(v)\omega + ib(v)]\prod_{k=1}^{\infty}\left(1 - \frac{\omega^2}{\lambda_k{}^2}\right). \tag{12}$$

From Eq. (12) it follows that the function $F(z)$: $C^N \to C$ admits the factorization

$$F(z) = S(z)\prod_{k=1}^{\infty}\left(1 - \frac{\langle z, z\rangle}{\lambda_k{}^2}\right), \tag{13}$$

where $S(z)$ satisfies the following properties:

(1) $S(z)$ is analytic in a neighborhood of $\langle 0,0,\ldots,0\rangle \in C^N$,

(2) $S(z)\overline{S(\bar{z})} = A^2(z, z)^L$ for $z \in C^N$,

(3) $S(vt) = t^L A\exp[ia(v)t + ib(v)]$ for $v \in S^{N-1}, t \in R$.

We will prove that the properties above imply that $S(z) = P(z)\exp(2\pi i(x_0, z))$ for some $x_0 \in R^N$ and some polynomial $P(z)$ having the form given in either part (a) or part (b) of the conclusion of the theorem.

First, we will need the following results:

Lemma 1. If $N = 2$, the polynomial $\langle z, z\rangle$ factorizes (over C) into irreducible factors as $\langle z, z\rangle = z_1{}^2 + z_2{}^2 = \langle z_1 + iz_2)(z_1 - iz_2)$. If $N \geq 3$, the polynomial (z, z) is irreducible.

Proof. The first part is obvious. If, for $N \geq 3$, $\langle z, z\rangle$ is not irreducible, then it factors as the product of two linear polynomials. Hence, there exist vectors $a, b \in R^N$ such that $\langle z, z\rangle = ((z, a))((z, b)) = za^*bz^*$ (where * denotes transpose). Then $M = 1/2(a^*b + ba^*)$ is a matrix having rank ≤ 2. However, $(z, z) = zMz$ for all $z \in C$ implies that M is the identity matrix that has rank ≥ 3. The contradiction completes the proof.

Let $\mathbf{0}$ denote the set of functions on C^N that are analytic in some neighborhood of $(0,0,\ldots,0) \in C^N$. An element $f \in \mathbf{0}$ is a unit if $(1/f) \in \mathbf{0}$. Clearly, f is a unit if and only if $f(0,0,\ldots,0) \neq 0$. An element $f \in \mathbf{0}$ is reducible over $\mathbf{0}$ is it can be written as $f = g_1g_2$, where neither g_1 nor g_2 is a unit; otherwise it is irreducible.

Lemma 2. Every nonunit element in $\mathbf{0}$ can be written as a finite product of irreducible factors, and such a product is unique up to the order of its factors and units.

Proof. This is a statement of the fact that $\mathbf{0}$ is a unique factorization domain. A proof of this deep result is given in Ref. 17.

Clearly, not every irreducible polynomial is irreducible over $\mathbf{0}$. However, the following particular result is valid.

Lemma 3. The polynomials $z_1 + iz_2$ and $\langle z, z\rangle$ (for $N \geq 3$) are irreducible over $\mathbf{0}$.

Proof. If f and g are nonunits in $\mathbf{0}$, then their Taylor series expansions have no constant term and hence fg has no linear terms. Therefore $fg \neq z_1 \pm iz_2$. Also, the product of the linear terms of f and g yields the quadratic term of fg that, by Lemma 1, can never equal (z, z) for $N \geq 3$.

The proof of the theorem is concluded as follows. From Properties 1 and 2 and Lemmas 2 and 3, it follows that $S(z)$ admits the factorization

$$S(z) = P(z)H(z), \tag{14}$$

where $P(z)$ is a polynomial having the form in part (a) of the theorem with $L = m_1 + m_2$, or in part (b) of the theorem with $L = 2m$, and $H(z)$ is a function that is analytic in some neighborhood of the origin and nonzero at the origin. Hence $H(z)$ admits the representation

$$H(z) = \exp[iG(z)], \tag{15}$$

where $G(z)$ is analytic in some neighborhood of the origin. Since $H(z)\overline{H(\bar{z})} = 1$, it follows that $G(z) = \overline{G(\bar{z})}$; hence the coefficients of the Taylor expansion for G are real. Combining Property 3 and Eqs. (14) and (15) yields either

(a) If $N = 2$,

then

$$G(vt) = a(v)t + b(v) - (m_1 - m_2)\theta, \tag{16}$$

where

$$\theta = \arctan\left(\frac{v_2}{v_1}\right), \qquad v = (v_1, v_2) \in R^2,$$

or

(b) If $N \geq 3$,

then

$$H(vt) = a(v)t + b(v). \tag{17}$$

Examining the Taylor series expansion for G shows that all terms except for the constant and linear terms vanish and that therefore there exist $x_0 \in R^N$ and $b_0 \in R$ such that

$$G(z) = b_0 + \langle x_0, z \rangle \tag{18}$$

in some neighborhood U of the origin in C^N. Therefore

$$F(z) = P(z)\exp(i\langle x_0, z\rangle + ib_0)\prod_{k=1}^{\infty}\left(1 - \frac{(z,z)}{{\lambda_k}^2}\right) \tag{19}$$

for $z \in U$.

Since F is entire on C^N, Eq. (19) holds for all $z \in C^N$. The proof is concluded.

ACKNOWLEDGMENTS

The author wishes to thank Thomas Crimmins and James Fienup, both with Environmental Research Institute of Michigan, for their encouragement and helpful discussions. This research was supported by the U.S. Air Force Office of Scientific Research.

REFERENCES

1. R. E. Burge, M. A. Fiddy, A. H. Greenaway, and G. Ross, "The phase problem," Proc. R. Soc. London Ser. A 350, 191–212 (1976).
2. T. R. Crimmins and J. R. Fienup, "Phase retrieval for functions with disconnected support," Appendix B in "High resolution imaging of space objects." Interim report to U.S. Air Force of Scientific Research, contract no. F49620-80-0006; ERIM Rep. no. 145400-7-P. (Environmental Research Institute of Michigan, Ann Arbor, Mich., March 1981.)
3. B. J. Hoenders, "On the solution of the phase retrieval problem," J. Math. Phys. 16, 1719–1725 (1975).
4. E. M. Hofstetter, "Construction of time-limited functions with specified autocorrelation functions," IEEE Trans. Inf. Theory IT-10, 119–126 (1964).
5. A. S. Marathay and P. Roman, "Analyticity and phase retrieval," Nuovo Cimento, 30, 1452–1464 (1963).
6. A. Walther, "The question of phase retrieval in optics," Opt. Acta 10, 41–49 (1963).
7. J. R. Fienup, "Reconstruction of an object from the modulus of its Fourier transform," Opt. Lett. 3, 27–29 (1978).
8. J. R. Fienup, "Space object imaging through the turbulent atmosphere," Opt. Eng. 18, 529–534 (1979).
9. J. R. Fienup, "Astronomical imaging by processing stellar speckle interferometry data," Proc. Soc. Photo-Opt. Instrumen. Eng. 243, 92–102 (1980).
10. J. R. Fienup, "Iterative method applied to image reconstruction and to computer-generated holograms," Opt. Eng. 19, 297–305 (1980).
11. Yu M. Bruck and L. G. Sodin, "On the ambiguity of the image reconstruction problem," Opt. Commun. 30, 304–308 (1979).
12. A. M. J. Huiser and P. van Toorn, "Ambiguity of the phase reconstruction problem," Opt. Lett. 5, 499–501 (1980).
13. W. Lawton, "A numerical algorithm for 2-D wavefront reconstruction from intensity measurements in a single plane," Proc. Soc. Photo-Opt. Instrum. Eng. 231, 94–98 (1980).
14. L. I. Ronkin, *Introduction to the Theory of Entire Functions of Several Variables*, Translations of Mathematical Monographs, Vol. 44 (American Mathematical Society, Providence, R.I., 1974).
15. R. P. Boas, *Entire Functions* (Academic, New York, 1954), p. 22.
16. L. V. Ahlfors, *Complex Analysis* (McGraw-Hill, New York, 1979), p. 153.

Appendix E

WB6. Determining the Support of an Object from the Support of Its Autocorrelation.* J. R. FIENUP AND T. R. CRIMMINS, *Radar and Optics Division, Environmental Research Institute of Michigan, P.O. Box 8618, Ann Arbor, Michigan 48107.*—In astronomy, x-ray crystallography, and other disciplines, one often wishes to reconstruct an object distribution from its autocorrelation or, equivalently, from the modulus of its Fourier transform (i.e., the phase retrieval problem). It is also useful to be able to reconstruct just the support of the object (i.e., the region on which it is nonzero). In some cases, for example, to find the relative locations of a number of pointlike stars, the object's support is the desired information. In addition, once the object's support is known, the reconstruction of the object distribution by the iterative method[1] is simplified. We show several methods of finding sets which contain the support of an object, based on the support of its autocorrelation. The smaller these sets are, the more information they give about the support of the object. Particularly small sets containing the object's support are given by intersections of its autocorrelation's support with translates of its autocorrelation's support. It will be shown that for special cases this gives rise to a unique reconstruction of the support of the object from the support of its autocorrelation. (13 min.)

* Work support by AFOSR.

[1] J. R. Fienup, Opt. Lett. 3, 27 (1978).

Reprinted from: J. Opt. Soc. Am. 70, 1581 (1980). Presented at the 1980 Annual Meeting of the Optical Society of America, Chicago, IL, October 1980.

Appendix F

RECONSTRUCTION OF THE SUPPORT OF AN OBJECT FROM THE SUPPORT OF ITS AUTOCORRELATION

by

J.R. Fienup, T.R. Crimmins, and W. Holsztynski*

Radar and Optics Division
Environmental Research Institute of Michigan
P.O. Box 8618, Ann Arbor, MI. 48107

ABSTRACT

The phase retrieval problem consists of the reconstruction of an object from the modulus of its Fourier transform, or equivalently from its autocorrelation. This paper describes a number of results relating to the reconstruction of the support of an object from the support of its autocorrelation. Methods for reconstructing the object's support are given for objects whose support is convex and for certain objects consisting of collections of distinct points. The uniqueness of solutions is discussed. In addition, for the objects consisting of collections of points, a simple method is shown for completely reconstructing the object functions.

*Present Address: Martin Marietta Aerospace, Orlando Division, M.P. 304, P.O. Box 5837, Orlando, Florida 32855

To appear in J. Opt. Soc. Am. 72 (April 1982).

1
INTRODUCTION

In astronomy, X-ray crystallography and other disciplines one often wishes to reconstruct an object from its autocorrelation or, equivalently, from the modulus of its Fourier transform (i.e., the phase retrieval problem)[1]. It is also useful to be able to reconstruct just the support of the object (the set of points over which it is nonzero). In some cases, for example, to find the relative locations of a collection of point-like stars, the object's support is the desired information. In addition, once the object's support is known, the reconstruction of the object by the iterative method[2] is simplified. Therefore, we are motivated to find a quick way to determine the support of the object from the support of its autocorrelation.

In the general case there may be many solutions for the object's support given the autocorrelation support. In what follows a method for generating sets containing all possible solutions is given. In addition, for the special case of convex sets a method for generating a family of support solutions is described. For the special case of objects consisting of sets of discrete points, this method is shown to yield a unique support solution unless the vector separations of the points in the object satisfy certain redundancy-type conditions. If instead of manipulating the autocorrelation support one uses the autocorrelation function, then for the same objects one can reconstruct the object itself.

2
DEFINITIONS AND BACKGROUND

The results shown in this paper apply to functions on Euclidean spaces of any number of dimensions except where otherwise noted. For simplicity we consider only objects represented by real, nonnegative functions, $f(x) \geq 0$, where $x \epsilon E^N$ (N-dimensional Euclidian space). The <u>support</u>, S, of a nonnegative function, f(x), is the smallest closed set such that the integral of f(x) over the complement of S in E^N is zero. (Roughly speaking, S is the set on which $f(x) > 0$.) In this paper we consider only functions with compact (i.e., closed and bounded) support. If f(x) is a finite positive linear combination of translates of the delta function, then S is a <u>finite set</u>.

We will be making use of linear operations on sets. Let X and Y be subsets of E^N. Then the addition of two sets and multiplication by scalars is defined by

$$aX + bY \equiv \{ax + by : x \epsilon X \text{ and } y \epsilon Y\} \tag{1a}$$

where a and b are real numbers. Similarly, the addition of a point (which can be though of as a vector) $x \epsilon E^N$ to a set is defined by

$$ax + bY \equiv \{ax + by : y \epsilon Y\} \tag{1b}$$

where again a and b are real numbers. While these linear operations on sets enjoy some of the properties expected from addition and from multiplication by a scalar, other properties do not hold. For example for a real number a and for sets X, Y, and Z, $(X + Y) + Z = X + (Y + Z)$; $a(bX) = (ab)X$; and $a(X + Y) = aX + aY$. However, $(a + b)X$ does not equal $aX + bX$ except for special cases. The role of zero in this case is played by the set $\{0\}$ consisting of the single point $0 = (0, \ldots, 0) \epsilon E^N$. We have $X + \{0\} = X$ and $a\{0\} = \{0\}$. But $X - X$ does not equal $\{0\}$ unless X consists of a single point.

The autocorrelation of f(x) is[3]

$$f \bigstar f(x) = \int_{E^N} f(y)\, f(y + x)\, dy \tag{2a}$$

$$= \int_{E^N} f(y)\, f(y - x)\, dy\ . \tag{2b}$$

The autocorrelation of f(x) is equal to the inverse Fourier transform of the squared modulus of the Fourier transform of f(x). Note that the autocorrelation is (centro-) symmetric: $f \bigstar f(-x) = f \bigstar f(x)$. It is most illuminating to interpret Eq. (2a) as a weighted sum of translated versions of f(x). That is, in the integrand of Eq. (2a), f(y) acts as the weighting factor for f(y + x), which is f(x) translated by -y. If the support, S, of a nonnegative integrable function, f(x), is compact and if A is the support of its autocorrelation function, $f \bigstar f(x)$, then

$$A = \bigcup_{y \in S} (S - y)$$

$$= S - S = \{x - y: x, y \in S\}\ . \tag{3}$$

The proof of Eq. (3) is in Appendix A. Note that A is symmetric:

$$-A = A \tag{4}$$

where $-A = \{-x : x \in A\}$. In addition,

$$0 \in A \tag{5}$$

as long as S is non-empty. To illustrate the interpretation of an autocorrelation support, consider the case of the two-dimensional support S shown in Figure 1(a), having the form of a triangle with vertices at points a, b, and c. The autocorrelation support A can be thought of as being formed by successively translating S so that each point in S is at the origin, and taking the union of all these translates of S. Figure 1(b) shows three such translates, (S - a), (S - b), and (S - c). The rest of A is filled in, as shown in Figure 1(c), by including all (S - y) such that $y \in S$.

We are concerned with the following problem. Given a symmetric set $A \subseteq E^N$ find sets $S \subseteq E^N$ which satisfy $A = S - S$.

Sets S_1 and S_2, which are subsets of E^N, are <u>equivalent</u>,

$$S_1 \sim S_2 \tag{6a}$$

if there exists a vector $v \in E^N$ such that

$$S_2 = v + \beta S_1 = \{v + \beta x : x \in S_1\} \tag{6b}$$

where $\beta = +1$ or -1. From Eq. 3 it is easily seen that if S_1 is a solution to $S - S = A$, and if $S_2 \sim S_1$, then S_2 is also a solution. If S_1 is a solution and all other solutions are equivalent to S_1, then the solution is said to be <u>unique</u> and A is said to be <u>unambiguous</u>; if there exist any nonequivalent solutions, then the solution is <u>nonunique</u> and A is <u>ambiguous</u>. For example, in one dimension the set of points $A = \{-1, 0, 1\}$ is unambiguous, having the unique solution $S = \{0, 1\}$; whereas the set of points $A = \{-3, -2, -1, 0, 1, 2, 3\}$ is ambiguous, having nonequivalent solutions $S_1 = \{0, 1, 3\}$ and $S_2 = \{0, 1, 2, 3\}$.

Not all symmetric sets that contain 0 are necessarily autocorrelation supports, as the following example shows. As shown in Figure 2, let $A = \{(0, 0), (1, 0), (-1, 0), (0, 1), (0, -1)\}$. Because of the point (1, 0), a solution must include two points separated by (1, 0). Similarly because of the point (0, 1), a solution must include two points separated by (0, 1). Therefore, the solution must have at least three distinct noncolinear points. Of the three possible pairings of the three points, one has a separation along (1, 0), a second has a separation along (0, 1), and the third pair of points must have a separation vector which is not on the horizontal or vertical axes. However, all points in A are on the horizontal or vertical axes, and therefore there is no solution for $A = S - S$ in this case.

A set X is <u>convex</u> if for all $x, y \in X$,

$$tx + (1 - t)y \in X \tag{7}$$

for all $t \in [0, 1]$ (that is, if all points on the line segment between x and y are contained in X). The <u>convex hull</u> of a set X, denoted by c.hull(X), is given by the smallest convex subset of E^N containing X. Thus X is convex if and only if $X = \text{c.hull}(X)$. If S is convex, then $A = S - S$ is also convex. More generally,

$$\text{c.hull}(X - X) = \text{c.hull}(X) - \text{c.hull}(X). \tag{8}$$

3
LOCATOR SETS

In many cases A is ambiguous, and so it would be useful to define a set that contains all possible solutions to the equation $A = S - S$. A set $L \subseteq E^N$ is defined as a locator set for A if for every closed set $S \subseteq E^N$ satisfying $A = S - S$, some translate of S is a subset of L, i.e., there exists a vector v such that

$$v + S \subseteq L. \tag{9}$$

There are many ways to generate locator sets. For example, for $v \in S$, $S - v \subseteq S - S = A$, and so A itself is a locator set. The smaller the locator set, the more tightly it bounds the possible solutions, and the more informative it is. Consequently, we wish to find locator sets that are as small as possible. A smaller locator set than A is

$$L = A \cap H \tag{10}$$

where H is any closed half-space of E^N with the origin on its boundary. To see this, choose $v \in S$ such that $S - v \subseteq H$. Then since $S - v \subseteq A$, it follows that $S - v \subseteq L = A \cap H$. A locator set that is often still smaller can be shown to be

$$L = \frac{1}{2} P \tag{11}$$

where P is any N-dimensional parallelepiped (in two dimensions: parallelogram) containing A.

A particularly interesting locator set is given by the following intersection of two autocorrelation supports. If $w \in A$, then

$$L = A \cap (w + A) \tag{12}$$

is a locator set for A. Note that L is symmetric about the point w/2. The proof that this is a locator set is as follows. Suppose S satisfies $A = S - S$. Since $w \in A$, there exist $u, v \in S$ such that $w = u - v$. Consider $z \in S - v$. Then $z = s - v$ where $s \in S$, $z = s - v \in A$, and $z = s - u + (u - v) = s - u + w \in A + w$. Therefore, $z \in A \cap (A + w) = L$ and therefore $S - v \in L$.

Naturally, the most interesting (smallest) locator sets generated by this method of intersecting two autocorrelation supports are obtained by choosing w to be on the boundary of A. By choosing different points $w \in A$, a whole family of locator sets can be generated by this method.

The locator set defined by Eq. (12) can be shown to be a special case of the following more general locator set. Let W be a set contained in some $S' \sim S$ for every set S satisfying $S - S = A$. That is, W is an intersection of translates of all possible solutions. Then

$$L = \bigcap_{w \in W} (w + A) \tag{13}$$

is a locator set for A. The proof is as follows. Suppose that $S - S = A$ and $S \sim S'$ with $W \subseteq S$. Then $S' \sim p \subseteq A$ for every $p \in S'$. Hence

$$S' \subseteq \bigcap_{p \in S'} (p + A) \subseteq \bigcap_{p \in W} (p + A). \tag{14}$$

Although Eq. (13) has the potential for producing particularly small locator sets, its practicality is limited by the fact that W is defined by all possible solutions to $S - S = A$, but that is what is assumed to be unknown. Nevertheless, one can make some use of Eq. (13). For example, if $S \sim S = A$ and $w \in A$, then there exists a translate S' of S such that $w \in S'$ and $0 \in S'$. Hence, we can use $W = \{0, w\}$, which reduces Eq. (13) to Eq. (12).

Example 1.

Consider the set S shown in Figure 3(a), consisting of two balls joined by two thin rods, and its autocorrelation support $A = S - S$ shown in Figure 3(b). An example of a locator set 1/2 P is shown in Figure 3(c); it is very suggestive of the approximate size of S, but not of any of the details of the shape of S. Figure 3(d) shows the generation of the locator set $L = A \cap (w + A)$ for a particular

point $w \in A$. Figure 3(e) and 3(f) show two other members of this family of locator sets generated with two other points $w \in A$. These locator sets generated by intersecting two autocorrelation supports are very suggestive of the shape of the solution (or solutions). This is especially true if one realizes that any solution must be contained within some translate of each of these locator sets. Unfortunately, for the general case it is difficult to narrow down the solution any further: a way to combine the information from two or more of the family of locator sets has not been devised for the general case. However, as will be shown in the sections that follow, for special classes of sets much more can be done.

Example 2

Consider the set A consisting of a circle of radius 1. Figures 4(a)–4(c) show the locator set $A \cap H$, 1/2 P, and $A \cap (w + A)$, respectively. In addition, Figure 4(d) shows still another locator set for A, a circle of radius $1/\sqrt{3}$, which is due to Jung's theorem[4]. The areas of the four locator sets are $\pi/2 \simeq 1.571$ for the half circle, 1.000 for the square (parallelogram) with sides of length one, $2\pi/3 - \sqrt{3}/2 \simeq 1.228$ for the intersection of two circles, and $\pi/3 \simeq 1.047$ for the circle of radius $1/\sqrt{3}$. Consequently, 1/2 P has the smallest area of the locator sets considered in this case. In other cases, such as in Example 1 above, $A \cap (w + A)$ may have a smaller area than 1/2 P. For example, the locator set shown in Figure 3(e) has a smaller area than the locator set shown in Figure 3(c). Furthermore, as mentioned earlier, locators of the form $A \cap (w + A)$ tend to be more suggestive of the shape of the possible solutions.

4
CONVEX SETS

A number of interesting results hold for objects having convex support. In the following, statements are made about the uniqueness of convex solutions to $A = S - S$ for convex sets A, and methods of detemining solutions are given.

All convex symmetric sets A have at least one solution

$$S = \frac{1}{2} A = \{x/2 : x \in A\} \tag{15}$$

The proof is as follows. Let $u, v \in 1/2\ A$. Then $2u \in A$, $2v \in A$ and $-2v \in A$. Therefore, $u - v = 1/2\ (2u) + 1/2\ (-2v) \in A$, since A is convex, and so $(1/2\ A) - (1/2\ A) \subseteq A$. Now let $v \in A$. Then $v/2 \in 1/2\ A$ and $-v/2 \in 1/2\ A$. Therefore $v = (v/2) - (-v/2) \in (1/2\ A) - (1/2\ A)$ and so $A \subseteq (1/2\ A) - (1/2\ A)$. Therefore, for convex A,

$$A = (\tfrac{1}{2}A) - (\tfrac{1}{2}A) \tag{16}$$

For the one-dimensional convex case the result is trivial: the autocorrelation support A is just a line segment, and a unique solution is given by $S = 1/2\ A$, which is just a segment of the line half the length of the line segment A. An equivalent result for the one-dimensional convex case is the solution

$$S = A \cap (w + A) \tag{17}$$

where w is on the boundary of A (at one end of the line segment A), or in symbols $w \in \partial(A)$.

4.1 AUTOCORRELATION TRI-INTERSECTION FOR CONVEX SETS

For the two-dimensional convex case, we have the following result. Let $A \subseteq E^2$ be a closed convex symmetric set ($-A = A$) with non-null interior, and let

$$w_1 \in \partial(A) \text{ and } w_2 \in \partial(A) \cap \partial(w_1 + A). \tag{18}$$

Furthermore, let

$$B = A \cap (w_1 + A) \cap (w_2 + A). \tag{19}$$

Then B is a solution to $A = S - S$, that is,

$$A = B - B. \tag{20}$$

The proof of this result is in Appendix B. Since w_1 can be any point on the boundary of A, Eq. (19) results in a family of solutions.

Example 3

Consider the set S shown in Figure 5(a), which is the convex hull of the set shown in Figure 3(a). Its autocorrelation support $A = S - S$ [which is the convex hull of Figure 3(b)] is shown in Figure 5(b). The parallelogram shown in Figure 3(c) is a locator set for A. A member of the family of locator sets $A \cap (w + A)$ is shown by the intersection of A and $w + A$ in Figure 5(c). A member of the family of solutions B is shown by the intersection of the three sets $A \cap (w_1 + A) \cap (w_2 + A)$ in Figure 5(d). Two other examples of B obtained using different points w_1 and w_2 are shown in Figures 5(e) and 5(f).

4.2 THREE-DIMENSIONAL INTERSECTIONS OF CONVEX SETS

For convex sets, since in one dimension the intersection of two sets, Eq. (17), results in the solution, and since in two dimensions the intersection of three sets, Eq. (19), results in solutions, one might hope that in three dimensions the set

$$C = A \cap (w_1 + A) \cap (w_2 + A) \cap (w_3 + A) \tag{21}$$

would be a solution to $S - S = A$, where $w_1 \in \partial(A)$, $w_2 \in \partial(A) \cap \partial(w_1 + A)$, and $w_3 \in \partial(A) \cap \partial(w_1 + A) \cap \partial(w_2 + A)$. Unfortunately, this is generally not the case.

A counter-example to $C - C = A$ is the following. Consider S equal to a sphere of diameter one, then $A = S - S$ is a sphere of radius one centered at the origin. Figures 6(a) and 6(b) show planar cuts through the centers of S and A, respectively. Figure 6(c) shows a planar cut through $A \cap (w_1 + A) \cap (w_2 + A)$ through the three points, 0, w_1 and w_2. $A \cap (w_1 + A) \cap (w_2 + A)$ has two vertices, one in front of the plane of the page and one behind the plane of the page, both at distance one from the centers of each of the three intersecting spheres. Taking the intersection of this with $(w_3 + A)$, which is centered at one of the two vertices, gives us C, which is similar to a regular tetrahedron (it has the same vertices) but having spherical surfaces of radius one and centers at the opposite vertices in place of the four plane faces of a tetrahedron. Looking for a moment at the tetrahedron T having the same vertices as C (i.e., the convex hull of points 0, w_1, w_2, and w_3 having edges of length one), we see that $T - T$ is a cuboctahedron, which has eight triangular faces and six square faces. Since $T \subseteq C$, $T - T \subseteq C - C$. The surface of $C - C$ can be subdivided into fourteen patches associated with the fourteen faces of the cuboctahedron. It can be shown that the eight patches associated with the triangular faces coincide exactly with the surface of the sphere A of radius one. However, the six patches corresponding to the square faces do not. For example, the distance from the origin to the center of each of those six patches is equal to the distance between the centers of two non-adjacent edges of C. This distance can be shown to be $\sqrt{3} - \sqrt{2}/2 \approx 1.0249$. That is, the radius of $C - C$ is greater than that of the sphere A by about 2.49 percent at those points. Hence, $C - C \neq A$.

4.3 LINEAR COMBINATIONS OF CONVEX SOLUTIONS

Returning to the N-dimensional case, if S_1 and S_2 are solutions to convex A = S - S, then

$$S_t = tS_1 + (1 - t)S_2 \tag{22}$$

is also a solution for $0 \leq t \leq 1$. The proof of this result is as follows

$$\begin{aligned} S_t - S_t &= [tS_1 + (1 - t)S_2] - [tS_1 + (1 - t)S_2] \\ &= tS_1 - tS_1 + (1 - t)S_2 - (1 - t)S_2 \\ &= tA + (1 - t)A \\ &= A \end{aligned} \tag{23}$$

since A is convex.

If S_1 is a solution, then so is $- S_1$. Then using $t = 1/2$ and $S_2 = - S_1$ in Eq. (22), it is seen that

$$S_{1/2} = \frac{1}{2} S_1 - \frac{1}{2} S_1 = \frac{1}{2} A \tag{24}$$

is a solution, as was previously shown by Eq. (16).

Eq. (22) can easily be generalized as follows. If S_1, ..., S_n are solutions for convex A, and if t_1, ..., $t_n \geq 0$ and $t_1 + t_2 + \ldots + t_n = 1$, then

$$S = \sum_{i=1}^{n} t_i S_i \tag{25}$$

is also a solution.

In the two-dimensional case, if B_1 and B_2 are solutions obtained from the tri-intersection method of Eq. (19), then $tB_1 + (1 - t)B_2$ is a solution which usually cannot be generated by the tri-intersection method. Thus, new solutions can be obtained by this method.

Example 4

Consider the two-dimensional convex set S shown in Figure 6(a), consisting of a circle of diameter one. A = S - S, consisting of a circle of radius one is shown in Figure 6(b), and a tri-intersection solution B is shown as the intersection of three circles in Figure 6(c). This solution is analogous to an equilateral triangle but having arcs of circles of radius one with centers at the opposite vertices for each of the three sides. It can easily be seen that all other solutions B generated by Eq. (19) are similar to the one shown in Figure 6(c) except rotated in the plane. The circle of diameter one shown in Figure 6(a) is not of this form, but it is also a solution to A. As shown by Eq. (24), S = 1/2 A in Figure 6(a) can be generated by applying Eq. (22), using $S_1 = -S_2 = B$ and $t = 1/2$. One of a family of additional solutions generated by Eq. (22) is shown in Figure 6(d). It was generated using S_1 = 1/2 A in Figure 6(a), S_2 = B in Figure 6(c), and $t = 1/2$.

4.4 THE AMBIGUITY OF CONVEX SETS

We now consider the question of uniqueness of convex solutions of A = S - S for convex A. As mentioned earlier, S = 1/2 A is a solution. If all convex solutions are equivalent to 1/2 A, then A is said to be convex-unambiguous. It was shown that in two dimensions one can generate a family of solutions by Eq. (19), the member of the family being determined by the choice of w_1. Eq. (22) or (25) can then be used to generate still more solutions. Therefore one would suppose that convex sets A are generally convex-ambiguous. However, it is also possible that all solutions generated by Eq. (19) are equivalent, in which case A would be convex-unambiguous.

In what follows it is shown that in two dimensions if A is a parallelogram then A is convex-unambiguous. Let A be a

parallelogram having vertices w_1, $-w_1$, w_2, and $-w_2$. By Eq. (12) a locator set for A is $L = A \cap (w_1 + A)$ since $w_1 \in A$. It is easily seen that $L = 1/2\ w_1 + 1/2\ A$, and so $L' = 1/2\ A$, which has vertices $1/2\ w_1$, $-1/2\ w_1$, $1/2\ w_2$, $-1/2\ w_2$ is a locator set for A. Suppose $A = S - S$ where S is convex. Then some translate of S, call it S', is contained in L'. Since $w_1 \in A$ there exist $u, v \in S'$ such that $w_1 = u - v$. Since $S' \subseteq L'$, then $u, v \in L'$. It follows that $u = 1/2\ w_1$ and $v = -1/2\ w_1$. Therefore, $1/2\ w_1 \in S'$ and $-1/2\ w_1 \in S'$. Similarly $1/2\ w_2 \in S'$ and $-1/2\ w_2 \in S'$. Then, since S' is convex,

$$L' = \text{c.hull}\left[\left\{\frac{1}{2}w_1, -\frac{1}{2}w_1, \frac{1}{2}w_2, -\frac{1}{2}w_2\right\}\right] \subseteq S' \subseteq L'. \quad (26)$$

Therefore, $S' = L' = 1/2\ A$, and so S is unique among convex solutions.

It can also be shown that parallelograms are the <u>only</u> two-dimensional convex-unambiguous sets, and convex symmetric sets $A \subseteq E^2$ that are not parallelograms can be shown to have infinitely many nonequivalent solutions to $A = S - S$. The lengthy proof of this last result is omitted here for the sake of brevity.

AUTOCORRELATION TRI-INTERSECTION FOR COLLECTIONS OF POINTS

For the special case of certain finite sets consisting of a collection of distinct points, the solution can be generated by a method similar to the one for convex sets. For example, the function

$$f(x) = \sum_{m=1}^{M} f_m \, \delta(x - x_m) \tag{27}$$

consisting of M delta functions having amplitudes $f_m > 0$, at the distinct points $x_m \in E^N$, $m = 1, \ldots, M$, would have support

$$S = \{x_m : m = 1, \ldots, M\}. \tag{28}$$

Let S be a set consisting of a collection of distinct points and let $A = S - S$. Define the following three conditions on the set S, which are needed for the results that follow.

Condition 1:

Whenever

$$x_1, x_2, y_1, y_2, z_1, z_2 \in S, \; x_1 \neq x_2, \text{ and}$$

$$x_1 - x_2 + y_1 - y_2 + z_1 - z_2 = 0, \tag{29}$$

then

$$x_1 = y_2 \text{ or } z_2, \quad \text{and} \quad x_2 = y_1 \text{ or } z_1.$$

Condition 2:

Whenever the set $G \subseteq A$ consists of three distinct points, and $0 \in G$, and $G - G \subseteq A$, then G is equivalent to a subset of S.

Condition 3:

Whenever $x_1, x_2, y_1, y_2 \in S$, $x_1 \neq x_2$, and $x_1 - x_2 = y_1 - y_2$; then $x_1 = y_1$.

The meaning of Conditions 1 and 3 are discussed in Section 7. Condition 3 is equivalent to saying that no two vector spacings between any distinct pairs of points in S are equal.

Now define the set B as follows. Let $w_1 \in A$ and $w_2 \in A \cap (w_1 + A)$, with $0 \neq w_1 \neq w_2 \neq 0$, and let

$$B = A \cap (w_1 + A) \cap (w_2 + A). \tag{30}$$

We have the following three results, which hold for any number of dimensions.

1. If S satisfies Condition 1, then

$$S \sim B \tag{31}$$

That is, B is the unique solution to $A = S - S$.

2. If S satisfies Condition 2, then S is equivalent to a subset of B.

3. If S satisfies Conditions 2 and 3, then again $S \sim B$. In fact, S satisfies Conditions 2 and 3 if and only if it satisfies Condition 1.

The proofs of these three results are in Appendix C. Since it requires a special relationship between the points in S in order to violate Condition 1, it is probable that for S comprised of randomly located points, B is the unique solution to $A = S - S$. More will be said about this later.

Example 5

Consider the set S consisting of the collection of 9 points shown in Figure 7(a). $A = S - S$ shown in Figure 7(b) has $9^2 - 9 + 1 = 73$ points. Intersecting A with a translate of itself using Eq. (12),

a number of different locator sets, L, for A can be formed, two of which are shown in Figures 7(c) and 7(d). (Each locator set must contain some translate of any solution to A = S - S.) Taking the intersection of L in either Figure 7(c) or 7(d) with a translate of A centered on any point within L yields, according to Eq. (29), the solution B, which is found to be equivalent to S in Figure 7(a). For this example, for all allowable values of w_1 and w_2, B is found to be equivalent to S, which is shown in Figure 7(a); that is, the solution B is unique.

Example 6

Consider the set S consisting of the collection of nine points shown in Figure 8(a). The positions of eight of the points in S are identical to eight of the points of the set shown in Figure 7(a). The ninth point in S (in the lower center) was moved in such a way as to make equal the vector spacing between two pairs of four distinct points. That is, there are four distinct points, x_1, x_2, y_1, y_2, in S satisfying $x_1 - x_2 = y_1 - y_2$. This violates Condition 3 and hence also Condition 1. Therefore, B - B is not necessarily equal to A, where B is given by Eq. (30). A = S - S shown in Figure 8(b) has only 69 points, compared with 73 for the previous example. The redundancy of the vector spacings (the differences) in S results in a two-fold redundancy in four of the points of A (at $x_1 - x_2 = y_1 - y_2$, $x_2 - x_1 = y_2 - y_1$, $x_1 - y_1 = x_2 - y_2$, and $y_1 - x_1 = y_2 - x_2$). Figures 8(c), 8(d) and 8(e) show three of the locator sets for A that are formed using Eq. (12). Once again, each locator set must contain some translate of any solution of A = S - S. Therefore, for any solution there must exist a point v such that a translate of the solution is a subset of $L_1 \cap (v + L_2)$ where L_1 and L_2 are locator sets for A. In addition, S must contain at least 9 points, since if it contained only 8 points, then A could contain at most $8^2 - 8 + 1 = 57$ points. Trying all possible translations of the locator set shown in Figure 8(d), only two of its intersections with the locator

set shown in Figure 8(c) have at least nine points: the set S_1 shown in Figure 8(f), and a translate of $-S_1$. Any solution therefore must be equivalent to S_1 or a subset of S_1. $S_1 - S_1$ is found to have more than the 69 points in A, and $A \subset S_1 - S_1$. Therefore, since S_1 has ten points and any solution must have at least nine points, it follows that any solution must have exactly nine points. Trying other pairs of locator sets for A, depending on the pair of locator sets chosen, we often get intersections containing ten points, but the tenth point will be different, such as in the set shown in Figure 8(g). The only possible solution is obviously S in Figure 8(a) (that is, the solution is unique), since it is the only nine-point set that is equivalent to subsets of both the sets shown in Figures 8(f) and 8(g). Furthermore, if one takes intersections of translates of the two particular locator sets shown in Figures 8(c) and 8(e), then the only resulting set of nine or more points is S in Figure 8(a); that is, by the lucky choice of which two locator sets to intersect, the solution can be found immediately. Equivalently, it can be shown that there are values of w_1 and w_2 such that $B \sim S$, although that is not true for most values of w_1 and w_2.

Therefore, even when Condition 1 is not satisfied it is sometimes possible to find solutions (and the solution may even be unique as it was in Example 6) by intersecting three or more translates of A. However, when Condition 1 is not satisfied, then there is no guarantee that the solution is unique, and finding solutions is considerably more complicated than simply evaluating B by Eq. (30). Unfortunately, given A it is not possible to immediately determine whether Condition 1 is satisfied. A necessary condition that Condition 1 (or Condition 3) be satisfied is that the number of points in A can be expressed as $M^2 - M + 1$ where $M \geq 1$ is an integer.

6
RECONSTRUCTION OF OBJECTS CONSISTING OF COLLECTIONS OF POINTS

By a simple modification of the method described in the previous section for reconstructing the support of an object consisting of a collection of distinct points, it is often possible to reconstruct the object itself. The method is analogous to using Eq. (30) to compute B. Recall that in computing B one takes the intersection of three translates of the autocorrelation support. If one takes the product of three translates of the autocorrelation function of f(x), using the same translations as used to compute B, then the support of that product will be B. And if, as described earlier, Condition 1 is satisfied, then B is a solution to A = S - S; and therefore the support of that product is equivalent to the support of f(x). In what follows it is shown that when Condition 1 is satisfied, f(x) can be reconstructed from that product in a very simple way [using Eqs. (38) to (40)].

Suppose that the object is given by Eq. (27), consisting of M delta functions located at the distinct points x_m having amplitudes f_m, m = 1, 2, ..., M. The positions x_m are vectors in any number of dimensions. The autocorrelation is

$$f \bigstar f(x) = \int_{E^N} f(y)\, f(y + x)\, dy$$

$$= \sum_{n=1}^{M} \sum_{m=1}^{M} f_n f_m \delta(x - x_m + x_n) \qquad (32a)$$

which can be expressed as

$$f \bigstar f(x) = \sum_{n=1}^{M} f_n^2\, \delta(x) + \sum_{n=1}^{M} \sum_{m \neq n} f_n f_m \delta(x - x_m + x_n) \qquad (32b)$$

which has M^2 terms located at positions $x = x_m - x_n$, M of which are at x = 0. That is, it has up to $M^2 - M + 1$ distinct terms. For this type of object, the fact that the support of the autocorrelation is given by A = S - S is obvious from Eq. (32).

At this point we would like to take the product of two such autocorrelation functions; however, the product of two delta functions is not well defined. Several approaches to overcome this difficulty are possible. For simplicity we define the product of two delta functions as follows:

$$[a\delta(x - x_1)][b\delta(x - x_2)] = \begin{cases} ab\,\delta(x - x_1), & x_2 = x_1 \\ 0, & x_2 \neq x_1 \end{cases} \tag{33}$$

It is intuitively helpful to think of f(x) in Eq. (27) as a digitized array of sampled values, with the values f_m at addresses x_m, m = 1, 2, ..., M. Then the delta functions in this section can be thought of as Kronecker delta functions.

As a first step toward forming a product analogous to B of Eq. (30), we consider the product of $f \bigstar f(x)$ and $f \bigstar f(x - w)$, where $w \in A$, and we choose $w \neq 0$. From Eq. (32) it is evident that $w \in A$ is of the form $x_j - x_k$ where $x_j, x_k \in S$. Therefore, we are taking the product of $f \bigstar f(x)$ and $f \bigstar f(x - x_j + x_k)$, where $x_j - x_k \neq 0$ lies within the support of $f \bigstar f(x)$. The center of the translated autocorrelation lies within the support of the untranslated autocorrelation. Using Eq. (32b), the autocorrelation product is (all summations are from 1 to M unless otherwise noted)

$$\begin{aligned} AP_{jk}(x) &= [f \bigstar f(x)][f \bigstar f(x - x_j + x_k)] \\ &= \left[\left(\sum_n f_n^2\right)\delta(x) + \sum_n \sum_{m \neq n} f_n f_m \delta(x - x_m + x_n)\right] \\ &\quad \cdot \left[\left(\sum_n f_n^2\right)\delta(x - x_j + x_k) \right. \\ &\quad \left. + \sum_{n'} \sum_{m' \neq n'} f_{n'} f_{m'} \delta(x - x_{m'} + x_{n'} - x_j + x_k)\right] \end{aligned} \tag{34a}$$

$$= \left(\sum_n f_n^2\right) f_j f_k \delta(x) + \left(\sum_n f_n^2\right) f_j f_k \delta(x - x_j + x_k)$$

$$+ f_j f_k \sum_{m \neq k,j} f_m^2 \delta(x - x_m + x_k)$$

$$+ f_j f_k \sum_{n \neq k,j} f_n^2 \delta(x - x_j + x_n) + (O.T.) \qquad (34b)$$

where (O.T.) denotes "other terms" as will be described later. [As an example of how Eq. (34b) follows from Eq. (34a), the fourth term in Eq. (34b) arises from the product of the second term of the first autocorrelation with the second term of the second autocorrelation, with $m = j$, $n' = n$, and $m' = k$.] Using Eq. (32a), another way of expressing Eq. (34) is

$$AP_{jk}(x) = \sum_n \sum_m \sum_{n'} \sum_{m'} f_n f_m f_{n'} f_{m'} \delta(x - x_m + x_n)$$

$$\cdot \delta(x - x_{m'} + x_{n'} - x_j + x_k) \qquad (34c)$$

from which it is seen that terms survive at points x where

$$x = x_m - x_n = x_{m'} - x_{n'} + x_j - x_k \qquad (35)$$

The terms shown in Eq. (34b) all necessarily appear. In addition, other terms may appear, as indicated by "+ (O.T.)". The existence of other terms depends on the presence of special relationships between the coordinates x_n allowing Eq. (35) to be satisfied "by chance". There being no additional terms is equivalent to Condition 1 (described in the previous section) being satisfied. If the x_m were independent random variables, then the chance of having additional surviving terms would be small, and we would have (O.T.) = 0.

Combining Eq. (27) with (34b), the autocorrelation product can be expressed as

$$AP_{jk}(x) = f_j f_k \left[f^2(x + x_k) + f^2(-x + x_j) \right] + \left(\sum_{n \neq k,j} f_n^2 \right) f_j f_k [\delta(x) + \delta(x - x_j + x_k)] + (O.T.) \quad (36)$$

Therefore, there are translates of the supports of both $f(x)$ and $f(-x)$ which are contained within the support of $AP_{jk}(x)$. This can also be seen from the fact that by Eq. (12) the support of $AP_{jk}(x)$ is a locator set.

Now consider the second step toward forming a product analogous to B of Eq. (30): we take the product of $AP_{jk}(x)$ with a third autocorrelation $f \bigstar f(x - w')$ where w' is within the support of $AP_{jk}(x)$. Suppose that $(O.T.) = 0$. Then from Eq. (34b) it is seen that the support of $AP_{jk}(x)$ consists of the points $x_n - x_k$ and $x_j - x_n$, $n = 1, 2, \ldots, M$. We first take the case where w' is of the form $x_n - x_k$ and treat the case of $w' = x_j - x_n$ later. Suppose that the specific point chosen is for $n = j' \neq j, k$ (i.e., $w' = x_{j'} - x_k \neq 0$ and $w' \neq w = x_j - x_k$). Then the product of the three autocorrelations is

$$\begin{aligned} AP_{jkj'k}(x) &= [f \bigstar f(x)] \, [f \bigstar f(x - x_j + x_k)] \, [f \bigstar f(x - x_{j'} + x_k)] \\ &= AP_{jk}(x) \, [f \bigstar f(x - x_{j'} + x_k)] \\ &= f_j f_k \left[\left(\sum_n f_n^2 \right) \delta(x) + \left(\sum_n f_n^2 \right) \delta(x - x_j + x_k) \right. \\ &\quad \left. + \sum_{n \neq k,j} f_n^2 \delta(x - x_n + x_k) + \sum_{n \neq k,j} f_n^2 \delta(x - x_j + x_n) \right] \\ &\quad \cdot \left[\left(\sum_n f_n^2 \right) \delta(x - x_{j'} + x_k) \right. \\ &\quad \left. + \sum_{n'} \sum_{m' \neq n'} f_{n'} f_{m'} \, \delta(x - x_{m'} + x_{n'} - x_{j'} + x_k) \right] \end{aligned}$$

(equation continued)

$$= f_k f_j f_{j'} \left\{ \sum_{n \neq k,j,j'} f_n^3 \delta(x - x_n + x_k) \right.$$

$$\left. + \left(\sum_n f_n^2 \right) [f_k \delta(x) + f_j \delta(x - x_j + x_k) + f_{j'} \delta(x - x_{j'} + x_k)] \right\} \tag{37a}$$

$$= f_k f_j f_{j'} \left[f^3(x + x_k) + \left(\sum_{n \neq k} f_n^2 \right) f_k \delta(x) \right.$$

$$\left. + \left(\sum_{n \neq j} f_n^2 \right) f_j \delta(x - x_j + x_k) + \left(\sum_{n \neq j'} f_n^2 \right) f_j \delta(x - x_{j'} + x_k) \right] \tag{37b}$$

That is, the product of three autocorrelations has the same support as $f(x + x_k)$, as was shown earlier in connection with Eq. (30), since B is just the support of the product of three such autocorrelation functions. Furthermore, except at the three points $x = 0$, $x_j - x_k$, and $x_{j'} - x_k$ the product is proportional to the cube of $f(x + x_k)$.

The values at all points can be determined as follows: First,

$$D \equiv \sum_n f_n^2 = f \bigstar f(0) \tag{38}$$

is known, so that factor can be divided out from the last three terms of Eq. (37a). Second, let the coefficients of those three terms in Eq. (37a) be (with $\sum f_n^2$ divided out)

$$A = D^{-1} \, AP_{jkj'k}(0) = f_k^2 \, f_j \, f_{j'} \tag{39a}$$

$$B = D^{-1} \, AP_{jkj'k}(x_j - x_k) = f_k \, f_j^2 \, f_{j'} \tag{39b}$$

$$C = D^{-1} \, AP_{jkj'k}(x_{j'} - x_k) = f_k \, f_j \, f_{j'}^2 \tag{39c}$$

Solving, we get

$$f_k = \left(\frac{A^3}{BC}\right)^{1/4} \tag{40a}$$

$$f_j = \left(\frac{B^3}{AC}\right)^{1/4} \tag{40b}$$

$$f_{j'} = \left(\frac{C^3}{AB}\right)^{1/4} \tag{40c}$$

and

$$f_k f_j f_{j'} = (ABC)^{1/4} \tag{40d}$$

The remaining values of f_m, for $m \neq k, j, j'$ can then be computed by dividing Eq. (37a) by $f_k f_j f_{j'}$ and then taking the cube root:

$$f_m = \left[\frac{AP_{jkj'k}(x_m - x_k)}{f_k\, f_j\, f_{j'}}\right]^{1/3} \tag{40e}$$

By this method f(x) is reconstructed exactly to within a translation, as long as (O.T.) = 0.

In performing these calculations, had we chosen a second translation of the form $(x_j - x_{k'})$, $k' \neq k,j$ instead of $(x_{j'} - x_k)$, then the result would have been similar, except a translate of f(-x) would have been reconstructed instead of a translate of f(x). If (O.T.) $\neq$ 0, that is, if Condition 1 is not satisfied, then additional terms appear that make the analysis much more complicated and may prevent the reconstruction of f(x).

Various modifications to this reconstruction method are possible. For example, the product of two autocorrelation products $AP_{jk}(x)$ $AP_{j'k}(x)$ is proportional to $f^4(x + x_k)$ except at three points. Another example is to define the autocorrelation support function as

$$A(x) = \delta(x) + \sum_{n=1}^{M} \sum_{m \neq n} \delta(x - x_m + x_n) \qquad (41)$$

which is just a binary-valued version of Eq. (32b). Then the product of the autocorrelation function with two properly translated autocorrelation support functions is proportional to a translate of $f(x)$, except at a single point which can be determined by a few extra simple steps.

7
THE OTHER TERMS

In arriving at Eq. (37), it was assumed that the other terms (O.T.) = 0, or equivalently that Condition 1 be satisfied. The terms included in Eqs. (34b) and (37) are those that necessarily arise by satisfying

$$x_m - x_n = x_{m'} - x_{n'} + x_j - x_k \tag{42}$$

trivially, for example, for $m = n$, $m' = k$, and $n' = j$. The other terms are those that satisfy Eq. (42) by chance, that is, those that arise in addition to those that (trivially) arise necessarily. The trivial solutions are the ones mentioned in connection with Condition 1 in Section 5. These other terms require a special relationship between the points in S, and would not be expected to occur if the points in S are randomly distributed in some region of E^N.

Figure 9 shows in two dimensions some relationships between points in S that would cause Eq. (42) to be satisfied "by chance", that is to say, in a nontrivial way. (S may contain additional points that are not shown.) For example, if the chords between three pairs of six distinct points in S as shown in Figure 9(a) can be translated to form a triangle as shown in Figure 9(b), then Eq. (42) is satisfied nontrivially. A similar result holds if some of the endpoints of the three chords are the same points, except for the trivial case of three points already in the form of a triangle defining the three chords. Note that when $m' = j$ and $n' = k$, then Eq. (42) reduces to $x_m - x_n = 2(x_j - x_k)$. That is, another nontrivial case is the existence of a vector separation between one pair of points equaling twice the vector separation between another pair of points, as shown in Figure 9(c). Also note that when, say, $m' = n'$, then Eq. (42) reduces to $x_m - x_n = x_j - x_k$. That is, another nontrivial case is the existence of a vector separation between one

pair of points equaling the vector separation between a different pair of points, as shown in Figure 9(d). This last case is also a violation of Condition 3 [see the discussion in the paragraph following Eq. (31)], and an example of that case was shown in Example 6 depicted in Figure 8.

As mentioned earlier, if the points x_m, $m = 1, 2, \ldots, N$, are randomly distributed, then it would be unlikely that any of these special relationships exist, and so one would expect that (O.T.) would equal zero and Condition 1 would be satisfied.

These results, with some modifications, can also be extended to the case of an object having support on a number of disjoint islands having diameters small compared with their separations (as opposed to the support consisting of isolated mathematical points). However, as the number of islands increases and as the ratio of the diameters of the islands to their separations increases, the probability of satisfying a condition analogous to Condition 1 decreases.

8
SUMMARY

We have described a number of new results relating to the reconstruction of the support of an object function from the support of its autocorrelation. Locator sets that contain all possible solutions were described, the most interesting of which is the intersection of the autocorrelation support with a translate of itself. For the special case of convex sets in two dimensions, it was shown that the intersection of three translates of the autocorrelation support is a solution. These solutions can usually be combined to form still more solutions. Among convex sets in two dimensions, only parallelograms have unique solutions. For the case of objects consisting of collections of distinct points it was shown that unless a special relationship exists between the points in the object, the intersection of three translates of the autocorrelation support yields the solution, and it is unique. If instead of intersecting autocorrelation supports one takes the product of translated autocorrelation functions, then for the same objects consisting of collections of points one can easily reconstruct the object function itself.

Some of the results on objects consisting of collections of distinct points are also described in Reference 5. These results were first presented[6] at the Annual Meeting of the Optical Society of America in Chicago, October 1980.

ACKNOWLEDGMENTS

This research was supported by the Air Force Office of Scientific Research under Contract No. F49620-80-C-0006.

REFERENCES

1. see, for example, H.P. Baltes, ed., Inverse Source Problems in Optics, (Springer-Verlag, New York, 1978).
2. J.R. Fienup, "Reconstruction of an Object from the Modulus of Its Fourier Transform," Opt. Lett. 3, 27-29 (1978); J.R. Fienup, "Space Object Imaging through the Turbulent Atmosphere," Opt. Eng. 18, 529-34 (1979).
3. R.N. Bracewell, The Fourier Transform and Its Applications, 2nd Edition (McGraw-Hill, New York, 1978).
4. H.W.E. Jung, "Uber die kleinste Kugel, die eine raumliche Figur einschliesst," J. reine agnew. Math. 123, 241 (1901).
5. J. Christou, "Imaging of Star Clusters from Speckle Interferometry," Opt. Commun. 37, 331-34 (1981).
6. J.R. Fienup and T.R. Crimmins, "Determining of Support of an Object from the Support of Its Autocorrelation," J. Opt. Soc. Am. 70, 1581 (1980) (Abstract).

APPENDIX A

If the support of $f(x)$ is S, then the support of $f(y + x)$ is $S - y$. Then the interpretation of Eq. (1) as the weighted sum of $f(y + x)$ with weights $f(y)$ leads intuitively to the fact that A, the support of $f \bigstar f(x)$, is given by

$$A = \bigcup_{y \in S} (S - y) = S - S .$$

A rigorous proof for compact sets S is as follows.

Define

$$B(x, r) = \{y \in E^N : |x - y| \leq r\},$$

and

$$f_r(x) = \int_{B(x,r)} f(y)dy .$$

Then $x \in S$ if and only if $f_r(x) > 0$ for all $r > 0$. Also, if $|x - y| < r$, then $f_{2r}(y) \geq f_r(x)$.

Part I: $S - S \subseteq A$.

Let $x, y \in S$ and let $r > 0$. Then

$$(f \bigstar f)_{2r}(x - y) = \int_{B(x-y,2r)} f \bigstar f(p)dp$$

$$= \int_{B(0,2r)} \int_{E^N} f(w)f(w + p + x - y)dw\, dp$$

$$= \int_{E^N} f(w)\, f_{2r}(w + x - y)dw$$

$$= \int_{E^N} f(w + y)\, f_{2r}(w + x)dw$$

$$\geq \int_{B(0,r)} f(w + y)\, f_{2r}(w + x)dw$$

$$\geq f_r(x) \int_{B(0,r)} f(w + y)dw = f_r(x)\, f_r(y) > 0.$$

Therefore, since $r > 0$ was arbitrary, $x - y \in A$, and so $S - S \subseteq A$.

Part II: $A \subseteq S - S$

First, note that since S is compact, $S - S$ is a closed set. Let $x \in A$ and let $r > 0$. Then

$$\begin{aligned} 0 < (f \bigstar f)_r(x) &= (f \bigstar f)_r(-x) \\ &= \int_{B(-x,r)} f \bigstar f(p)dp \\ &= \int_{B(0,r)} \int_{E^N} f(y)\, f(y + p - x)\, dy\, dp \\ &= \int_{B(0,r)} \int_{E^N} f(y + p)\, f(y + x)\, dy\, dp \\ &= \int_{E^N} f_r(y)\, f(y + x)\, dy. \end{aligned}$$

Therefore, there exists $z \in E^N$ such that

$$\begin{aligned} 0 < \int_{B(z,r)} f_r(y)\, f(y + x)\, dy &< f_{2r}(z) \int_{B(z,r)} f(y + x)\, dy \\ &= f_{2r}(z)\, f_r(z + x). \end{aligned}$$

Therefore, $f_{2r}(z) > 0$ and $f_r(z + x) > 0$. Hence $S \cap B(z, 2r) \neq \phi$ and $S \cap B(y, r) \neq \phi$, where $y = z + x$. Choose $z' \in S \cap B(z, 2r)$ and $y' \in S \cap B(y, r)$. Then $|y' - y| < r$ and $|z' - z| < 2r$. Then

$$\begin{aligned} |(y' - z') - x| &= |(y' - y) - (z' - z)| \\ &\leq |y' - y| + |z' - z| < 3r . \end{aligned}$$

Since $r \geq 0$ was arbitrary, $S - S$ is closed, and $y' - z' \in S - S$, it follows that $x \in S - S$, and hence $A \subseteq S - S$ and hence $A = S - S$.

APPENDIX B
PROOF THAT A = B - B FOR CONVEX SETS

The proof that $A = B - B$ will be divided into two parts. First, it will be shown that $A \subseteq B - B$ and then it will be shown that $A \supseteq B - B$.

Part 1: $A \subseteq B - B$.

It can be shown that, because A has *non-null* interior, the points, 0, w_1, and w_2 are not colinear. Let

$$B_1 = \text{c.hull } \{0, w_1, w_2\} .$$

Since B is the intersection of three convex sets, B is convex. Therefore, $B_1 \subseteq B$. Let $A_1 = B_1 - B_1$.

Claim 1: $A_1 \subseteq A$

As can be seen from Figure B1, we have

$$A_1 = \text{c.hull } \{w_1, -w_1, w_2, -w_2, w_1 - w_2, w_2 - w_1\}.$$

Furthermore, since A is convex and

$$w_1, -w_1, w_2, -w_2, w_1 - w_2, w_2 - w_1 \in A ,$$

it follows that $A_1 \subseteq A$. This completes the proof of Claim 1.

Now let

$$A_2 = A_1 \cup (B_1 - w_1 - w_2) \cup (B_1 + w_2 - w_1) \cup (B_1 + w_1 - w_2)$$

$$\cup (w_1 + w_2 - B_1) \cup (w_1 - w_2 - B_1) \cup (w_2 - w_1 - B_1).$$

See Figure B2.

Claim 2: $A \subseteq A_2$.

Let

$$C = \{w_2 + \lambda_1 w_1 + \lambda_2 (w_2 - w_1): \lambda_1 > 0 \text{ and } \lambda_2 > 0\}.$$

See Figure B3. Note that C is an open set. We will show that $A \cap C = \phi$. Suppose not. Then let $p \in A \cap C$ and let $D = c.hull \{p, w_1, w_2 - w_1\}$. See Figure B4. Then $D \subseteq A$ and $w_2 \in int(D) \subseteq int(A)$. This contradicts the assumption that $w_2 \in \partial(A)$. Therefore, $A \cap C = \phi$.

Similar arguments apply to the other "notches" in A_2. Therefore, $A \subseteq A_2$. This completes the proof of Claim 2.

Summarizing, we have $B_1 \subseteq B$ and $A_1 \subseteq A \subseteq A_2$.

Let $p \in A$. We want to show that $p \in B - B$. We have

$$A \subseteq A_2 = [B_1 \cup (w_1 + w_2 - B_1)] \cup [(-B_1) \cup (B_1 - w_1 - w_2)]$$
$$\cup [(B_1 - w_1) \cup (w_2 - w_1 - B_1)] \cup [(w_1 - B_1) \cup (B_1 + w_1 - w_2)]$$
$$\cup [(B_1 - w_2) \cup (w_1 - w_2 - B_1)] \cup [(w_2 - B_1) \cup (B_1 + w_2 - w_1)].$$

Case 1: $p \in B_1 \cup (w_1 + w_2 - B_1)$

We have

$$p - w_1 \in (B_1 - w_1) \cup (w_2 - B_1) \subseteq A_1 \subseteq A.$$

Therefore $p \in w_1 + A$. Also, $p - w_2 \in (B_1 - w_2) \cup (w_1 - B_1) \subseteq A_1 \subseteq A$. Therefore $p \in w_2 + A$. Since, by assumption, $p \in A$, it follows that $p \in B$. We also have $0 \in B$. Therefore, $p = p - 0 \in B - B$.

Case 2: $p \in (-B_1) \cup (B_1 - w_1 - w_2)$

We have $-p \in B_1 \cup (w_1 + w_2 - B_1)$. Therefore, by Case 1, $-p \in B - B$, and since $B - B$ is a symmetric set, $p \in B - B$.

In the four other cases, i.e., $p \in (B_1 - w_1) \cup (w_2 - w_1 - B_1)$, etc., we find that $p \in B - B$ by similar arguments. This completes the proof of Part 1.

Part 2: $A \supseteq B - B$

Let ℓ_1, ℓ_2, ℓ_3 be lines tangent to A at points w_1, w_2 and $w_1 - w_2$, respectively. See Figure B5. Then, since A is symmetric, the lines $-\ell_1$, $-\ell_2$, and $-\ell_3$ are tangent to A at points $-w_1$, $-w_2$, and $w_2 - w_1$, respectively.

It follows that $w_1 - \ell_1$ is tangent to $w_1 + A$ at 0. Therefore, $w_1 - \ell_1$ is tangent to B at 0. See Figure B6. Similarly, $w_2 - \ell_2$ is tangent to $w_2 + A$ at 0. Hence, $w_2 - \ell_2$ is tangent to B at 0. Also, $w_2 + \ell_3$ is tangent to $w_2 + A$ at w_1. Therefore, $w_2 + \ell_3$ is tangent to B at w_1. Finally, $w_1 - \ell_3$ is tangent to $w_1 + A$ at w_2. Therefore, $w_1 - \ell_3$ is tangent to B at w_2. It follows that B lies between lines ℓ_1 and $w_1 - \ell_1$ and between ℓ_2 and $w_2 - \ell_2$ and between $w_2 + \ell_3$ and $w_1 - \ell_3$.

Now let C_0 be the closed positive cone spanned by w_1 and w_2. That is,

$$C_0 = \{ \lambda_1 w_1 + \lambda_2 w_2 : \lambda_1 \geq 0 \text{ and } \lambda_2 \geq 0 \}.$$

See Figure B7. Let C_1 be the closed cone spanned by $-w_1$ and $w_2 - w_1$. Finally, let C_2 be the closed positive cone spanned by $-w_2$ and $w_1 - w_2$. Then

$$E^2 = C_0 \cup (-C_0) \cup C_1 \cup (-C_1) \cup C_2 \cup (-C_2).$$

Next, let

$$s_0 = C_0 \cap \partial(B)$$

$$s_1 = (w_1 + C_1) \cap \partial(B)$$

$$s_2 = (w_2 + C_2) \cap \partial(B)$$

Then $\partial(B) = s_0 \cup s_1 \cup s_2$. See Figure B8.

Now, let $p_1, p_2 \in B$. We want to show that $p_1 - p_2 \in A$.

Case 1: $p_1 - p_2 \in C_2$.

First, if $p_1 = p_2$ then $p_1 - p_2 = 0 \in A$.

Now assume $p_1 \neq p_2$. Let ℓ be the (infinite) line passing through p_1 and p_2. See Figure B9. The line ℓ must intersect either s_0 or s_1.

Subcase 1-a: ℓ intersects s_0.

See Figure B9. Let ℓ'_2 be the line parallel to ℓ_2 and passing through p_1. Let ℓ''_2 be the line parallel to ℓ_2 and passing through p_2.

Now, lines ℓ'_2 and ℓ''_2 lie between ℓ_2 and $w_2 - \ell_2$. Also, 0 is on $w_2 - \ell_2$ and w_2 is on ℓ_2. It follows that ℓ'_2 and ℓ''_2 must intersect the line segment $[0, w_2]$. Let r_1 be the point at which ℓ'_2 intersects $[0, w_2]$ and let r_2 be the point at which ℓ''_2 intersects $[0, w_2]$. Then, since $0, w_2 \in B$ and B is convex, $r_1 \in B$ and $r_2 \in B$.

Now let ℓ' be the line parallel to ℓ and passing through w_2. Since $p_1 - p_2 \in C_2$, ℓ cannot be parallel to ℓ_2. Therefore ℓ' is not parallel to ℓ'_2 or ℓ''_2. It follows that ℓ' intersects ℓ'_2 and ℓ''_2. Let q_1 be the point of intersection of ℓ' and ℓ'_2 and let q_2 be the point of intersection of ℓ' and ℓ''_2.

Since ℓ intersects s_0, it follows that $q_1 \in [p_1, r_1]$ and $q_2 \in [p_2, r_2]$. Since $p_1, p_2, r_1, r_2 \in B$ and B is convex, it follows that $q_1 \in B$ and $q_2 \in B$.

Now, since $p_1 - p_2 \in C_2$, we must have $q_2 \in [q_1, w_2]$. That is, there exists λ, $0 \leq \lambda \leq 1$, such that $q_2 = \lambda q_1 + (1 - \lambda) w_2$ or $q_2 - w_2 = \lambda(q_1 - w_2)$.

Now $q_1 \in B \subseteq w_2 + A$. Therefore, $q_1 - w_2 \in A$. Furthermore, since $0 \leq 1 - \lambda \leq 1$, it follows that $(1 - \lambda)(q_1 - w_2) \in A$.

Finally, we have

$$\begin{aligned} p_1 - p_2 &= q_1 - q_2 \\ &= (q_1 - w_2) - (q_2 - w_2) \\ &= (1 - \lambda)(q_1 - w_2) \in A . \end{aligned}$$

This completes the proof of Subcase 1-a.

Subcase 1-b: ℓ intersects s_1.

See Figure B10. An argument similar to the above is indicated in Figure B10. This completes the proof of Case 1.

Case 2: $p_1 - p_2 \in -C_2$.

We have $p_2 - p_1 \in C_2$. Therefore, by Case 1, $p_2 - p_1 \in A$ and hence $p_1 - p_2 \in A$.

Similar arguments apply when $p_1 - p_2 \in C_0$, $-C_0$, C_1 and $-C_1$. This completes Part 2 of the proof that $A = B - B$ for convex sets.

APPENDIX C
PROOF THAT B ~ S FOR CERTAIN POINT-LIKE SETS

In this appendix we take the approach of first proving

Theorem 1.

If S satisfies Condition 2, then S is equivalent to a subset of B.

Then we prove

Theorem 2.

If S satisfies Conditions 2 and 3, then S is equivalent to B.

Finally we prove

Theorem 3.

Condition 1 is satisfied if and only if both Conditions 2 and 3 are satisfied.

It then follows from Theorems 2 and 3 that if S satisfies Condition 1 then S is equivalent to B.

Proof of Theorem 1

Let $G = \{0, w_1, w_2\}$. We have $0, w_1, w_2 \in A$. Since A is symmetric, we also have $-w_1, -w_2 \in A$. Furthermore, since $w_2 \in w_1 + A$, we have $w_2 - w_1 \in A$ and $w_1 - w_2 \in A$. Therefore,

$$G - G = \{0, w_1, -w_1, w_2, -w_2, w_1 - w_2, w_2 - w_1\} \subseteq A$$

Also, G has three members. Therefore, by Condition 2, there exists $v \in E^N$ such that $v + \beta G \subseteq S$ where $\beta = \pm 1$. It follows that $G \subseteq \beta(S - v)$. Let $S_1 = \beta(S - v)$. Then $G \subseteq S_1$. Also, $S \sim S_1$, and therefore, $A = S_1 - S_1$. We want to show that $S_1 \subseteq B$.

Let $x \in S_1$. We have $0 \in G \subseteq S_1$. Therefore

$$x = x - 0 \in S_1 - S_1 = A. \qquad (C\text{-}1)$$

Also, $w_1 \in G \subseteq S_1$. Therefore, $x - w_1 \in S_1 - S_1 = A$, and

$$x \in w_1 + A. \tag{C-2}$$

Similarly,

$$x \in w_2 + A. \tag{C-3}$$

From (C-1), (C-2), and (C-3), it follows that $x \in B$. Since x was an arbitrary element of S_1, it follows that $S_1 \subseteq B$.

Proof of Theorem 2

Let v, β and S_1 be defined as in the proof of Theorem 1. Then, by that same proof, $S_1 \subseteq B$. We want to show that $B \subseteq S_1$. Let $x \in B$. We want to show that $x \in S_1$.

First, suppose that $x \in G$. Then, since $G \subseteq S_1$, $x \in S_1$ and we are done. Now assume x G. Let

$$G_i = \{0, x, w_i\}, \; i = 1, 2 .$$

Since $x \in B$, it follows that $x \in A$ and $-x \in A$. We also have $w_i \in A$ and $-w_i \in A$. Furthermore, since $x \in w_i + A$, $x - w_i \in A$ and $w_i - x \in A$. Therefore,

$$G_i - G_i = \{0, x, -x, w_i, -w_i, x - w_i, w_i - x\} \subseteq A.$$

Also, G_i has three members. Therefore by Condition 2, there exists $v_i \in E^N$ such that $v_i + \beta_i G_i \subseteq S$ where $\beta_i = \pm 1$.

Claim: There exists $j \in \{1, 2\}$ such that $\beta_j = \beta$.

Suppose not. Then $\beta_1 = \beta_2 = -\beta$. We have

$$\{v, v + \beta w_1, v + \beta w_2\} = v + \beta G \subseteq S$$

and

$$\{v_i, v_i + \beta_i x, v_i + \beta_i w_i\} = v_i + \beta_i G_i \subseteq S, \quad i = 1, 2.$$

Also, since $\beta_1 = \beta_2 = -\beta$,

$$(v + \beta w_i) - v = v_i - (v_i + \beta_i w_i), \quad i = 1, 2.$$

Now, applying Condition 3 with

$$x_1 = v + \beta w_i, \quad x_2 = v, \quad y_1 = v_i, \quad y_2 = v_i + \beta_i w_i,$$

we conclude that

$$v_i = v + \beta w_i, \quad i = 1, 2. \tag{C-4}$$

Furthermore,

$$v_1 - (v_1 + \beta_1 x) = v_2 - (v_2 + \beta_2 x).$$

It therefore follows from Condition 3 that

$$v_1 = v_2. \tag{C-5}$$

From (C-4) and (C-5) it follows that $w_1 = w_2$. This contradicts the assumption that $w_1 \neq w_2$ and proves the Claim that there exists $j \in \{1, 2\}$ such that $\beta_j = \beta$.

Now, we have

$$(v_j + \beta_j w_j) - v_j = (v + \beta w_j) - v.$$

By Condition 3, $v_j = v$. Therefore,

$$v + \beta x = v_j + \beta_j x \in v_j + \beta_j G_j \subseteq S$$

and

$$x \in \beta(S - v) = S_1.$$

Proof of Theorem 3

Part I: $1 \rightarrow 2$.

Let G have three elements, $0 \in G \subseteq A$, and $G - G \in A$. We want to show that G is equivalent to a subset of S. That is we want to show that there exists $v \in E^N$ such that $v + \beta G \in S$ where $\beta = \pm 1$.

Let $G = \{0, g_1, g_2\}$. Then $0 \neq g_1 \neq g_2 \neq 0$ and

$$\{0, g_1, -g_1, g_2, -g_2, g_1 - g_2, g_2 - g_1\} = G - G \subseteq A.$$

Since $A = S - S$, there exists $x_1, x_2, y_1, y_2, z_1, z_2, \in S$ such that $g_1 = x_1 - x_2$, $g_2 - g_1 = y_1 - y_2$, and $-g_2 = z_1 - z_2$. Then $x_1 \neq x_2$ and

$$x_1 - x_2 + y_1 - y_2 + z_1 - z_2 = 0. \qquad \text{(C-6)}$$

Therefore, by Condition 1,

$$x_1 = y_2 \text{ or } z_2, \quad \text{and} \quad x_2 = y_1 \text{ or } z_1.$$

Claim 1: Cannot have $x_1 = y_2$ and $x_2 = y_1$.

If this were the case, then it would follow from (C-6) that $z_1 - z_2 = 0$. But $z_1 - z_2 = -g_2 \neq 0$. This proves Claim 1.

Claim 2: Cannot have $x_1 = z_2$ and $x_2 = z_1$.

If this were the case, then it would follow from (C-6) that $y_1 - y_2 = 0$. But $y_1 - y_2 = g_2 - g_1 \neq 0$. This proves Claim 2.

Therefore either $x_1 = y_2$ and $x_2 = z_1$, or $x_1 = z_2$ and $x_2 = y_1$.

Case 1: $x_1 = y_2$ and $x_2 = z_1$.

We have

$$y_1 - x_2 = x_1 - x_2 + y_1 \quad y_2 = g_1 + g_2 - g_1 = g_2$$

and $x_1 - x_2 = g_1$. Rewriting these equations, we have $x_2 + g_2 = y_1$ and $x_2 + g_1 = x_1$. Therefore,

$$x_2 + G = \{x_2, x_2 + g_1, x_2 + g_2\} = \{x_2, x_1, y_1\} \subseteq S.$$

Letting $v = x_2$ and $\beta = 1$, we have $v + \beta G \subseteq S$.

Case 2: $x_1 = z_2$ and $x_2 = y_1$.

We have

$$z_1 - x_2 = x_1 - x_2 + z_1 - z_2 = g_1 - g_2$$

and $x_1 - x_2 = g_1$. This yields $z_1 = x_2 + g_1 - g_2$ and $x_1 = x_2 + g_1$. Therefore,

$$x_2 + g_1 - G = \{x_2 + g_1, x_2, x_2 + g_1 - g_2\} = \{x_1, x_2, z_1\} \subseteq S.$$

Letting $v = x_2 + g_1$ and $\beta = -1$, we have $v + \beta G \subseteq S$.

Part II: $1 \rightarrow 3$.

Let $u_1, u_2, v_1, v_2 \in S$, with $u_1 \neq u_2$ and $u_1 - u_2 = v_1 - v_2$. We want to show that $u_1 = v_1$. Let

$$x_1 = v_2, \quad x_2 = v_1, \quad y_1 = v_1, \quad y_2 = u_2, \quad z_1 = u_1, \quad z_2 = v_1.$$

Then $x_1 \neq x_2$ and

$$x_1 - x_2 + y_1 - y_2 + z_1 - z_2 = 0 . \qquad \text{(C-7)}$$

Therefore, by Condition 1, $x_1 = y_2$ or z_2, and $x_2 = y_1$ or z_1. Now

$$z_2 - x_1 = v_1 - v_2 = u_1 - u_2 \neq 0.$$

Therefore, $x_1 \neq z_2$ and, hence, $x_1 = y_2$, or $v_2 = u_2$. Since, by assumption, $u_1 - u_2 = v_1 - v_2$, it follows that $u_1 = v_1$. This completes Part II of the proof.

Part III: 2 and $3 \rightarrow 1$

Let $x_1, x_2, y_1, y_2, z_1, z_2 \in S$ with $x_1 \neq x_2$ and

$$x_1 - x_2 + y_1 - y_2 + z_1 - z_2 = 0. \qquad \text{(C-8)}$$

We want to show that $x_1 = y_2$ or z_2, and $x_2 = y_1$ or z_1.

Case 1: $y_1 = y_2$.

In this case, it follows from (C-8) that

$$x_1 - x_2 = z_2 - z_1 . \tag{C-9}$$

Therefore, by Condition 3, $x_1 = z_2$ and it follows from (C-9) that $x_2 = z_1$.

Case 2: $z_1 = z_2$.

Here, it follows from (C-8) that

$$x_1 - x_2 = y_2 - y_1. \tag{C-10}$$

Then by Condition 3, $x_1 = y_2$ and it follows from (C-10) that $x_2 = y_1$.

Case 3: $y_1 \neq y_2$ and $z_1 \neq z_2$.

Let $g_1 = x_1 - x_2$ and $g_2 = y_2 - y_1$, and let $G = \{0, g_1, g_2\}$. Now, $g_1, g_2 \in S - S = A$ and hence, also $-g_1, -g_2 \in A$. Furthermore,

$$g_1 - g_2 = x_1 - x_2 + y_1 - y_2 = z_2 - z_1 \in S - S = A$$

and hence, also $g_2 - g_1 \in A$. Thus we have $0 \in G \subseteq A$ and $G - G \subseteq A$. We also have $g_1 = x_1 - x_2 \neq 0$, $g_2 = y_2 - y_1 \neq 0$, and $g_1 - g_2 = z_2 - z_1 \neq 0$. Therefore, G has three members. Hence, by Condition 2, there exists $v \in E^N$ such that $v + \beta G \subseteq S$, where $\beta = \pm 1$.

Subcase 3-a: $\beta = 1$.

We have

$$\{v, v + g_1, v + g_2\} = v + \beta G \subseteq S. \tag{C-11}$$

Now, $(v + g_1) - v = g_1 = x_1 - x_2$. Therefore, by Condition 3, $v = x_2$, and hence, by (C-11), $x_2 + g_1 \in S$ and $x_2 + g_2 \in S$.
Now $(x_2 + g_2) - x_2 = g_2 = y_2 - y_1$. Therefore, by Condition 3, $x_2 + g_2 = y_2$ and $x_2 = y_1$. Also

$$(x_2 + g_1) - (x_2 + g_2) = g_1 - g_2 = z_2 - z_1 .$$

Therefore, by Condition 3, $x_2 + g_1 = z_2$. But $x_2 + g_1 = x_1$.
Therefore $x_1 = z_2$.

Subcase 3-b: $\beta = -1$

We have

$$\{v, v - g_1, v - g_2\} = v + \beta G \subseteq S . \qquad \text{(C-12)}$$

Now, $v - (v - g_1) = g_1 = x_1 - x_2$. Therefore, by Condition 3, $v = x_1$, and hence, by (C-12), $x_1 - g_1 \in S$ and $x_1 - g_2 \in S$. Now, $x_1 - (x_1 - g_2) = g_2 = y_2 - y_1$. Therefore, by Condition 3, $x_1 = y_2$. Also,

$$(x_1 - g_1) - (x_1 - g_2) = g_2 - g_1 = z_1 - z_2.$$

Therefore, by Condition 3, $x_1 - g_1 = z_1$. But $x_1 - g_1 = x_2$.
Therefore, $x_2 = z_1$.

FIGURE CAPTIONS

1. (a) Set S; (b) three of the translates of S that make up A; (c) autocorrelation support $A = S - S$.
2. A symmetric set that is not an autocorrelation support.
3. Locator Sets. (a) Set S; (b) $A = S - S$; (c) locator set $L = 1/2\ P$; (d) formation of $L = A \cap (w + A)$; (e) and (f) two other members of the family of locator sets.
4. Locator sets (shaded areas) for the circle. (a) $A \cap H$; (b) the square $1/2\ P$; (c) $A \cap (w + A)$, (d) circle of radius $1/\sqrt{3}$.
5. Autocorrelation tri-intersection solution for convex sets. (a) Set S; (b) $A = S - S$; (c) formation of locator set $L = A \cap (w + A)$; (d) formation of solution $B = A \cap (w_1 + A) \cap (w_2 + A)$; (e) and (f) two other solutions of the form B.
6. Sphere/circle example. (a) Set S; (b) $A = S - S$; (c) $B = A \cap (w_1 + A) \cap (w_2 + A)$; (d) another solution for the circle combining the solutions (a) and (c).
7. Autocorrelation tri-intersection for sets consisting of a collection of distinct points. (a) Set S; (b) $A = S - S$; (c) and (d) locators of the form $L = A \cap (w + A)$. Intersecting (c) or (d) with (b) yields the unique solution (a).
8. Autocorrelation intersection for redundant case. (a) Set S; (b) $A = S - S$; (c), (d), and (e) locators of the form $L = A \cap (w + A)$; (f) intersection of (c) with (d); (g) another intersection of three translates of A.
9. Redundancy-type relationships within S that would violate Condition 1. (a) and (b) Three vector separations add to zero; (c) one vector separation is twice another; (d) two vector separations are equal.

B1-B10 (see Text)

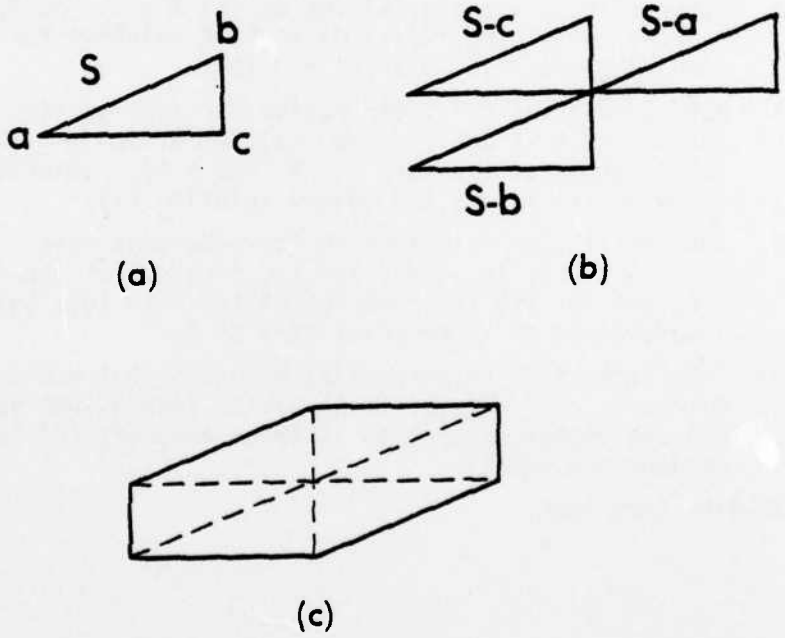

Figure I. (a) Set S; (b) three of the translates of S that make up A; (c) autocorrelation support A = S - S.

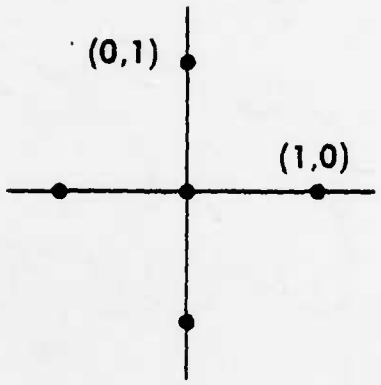

Figure 2. A symmetric set that is not an autocorrelation support.

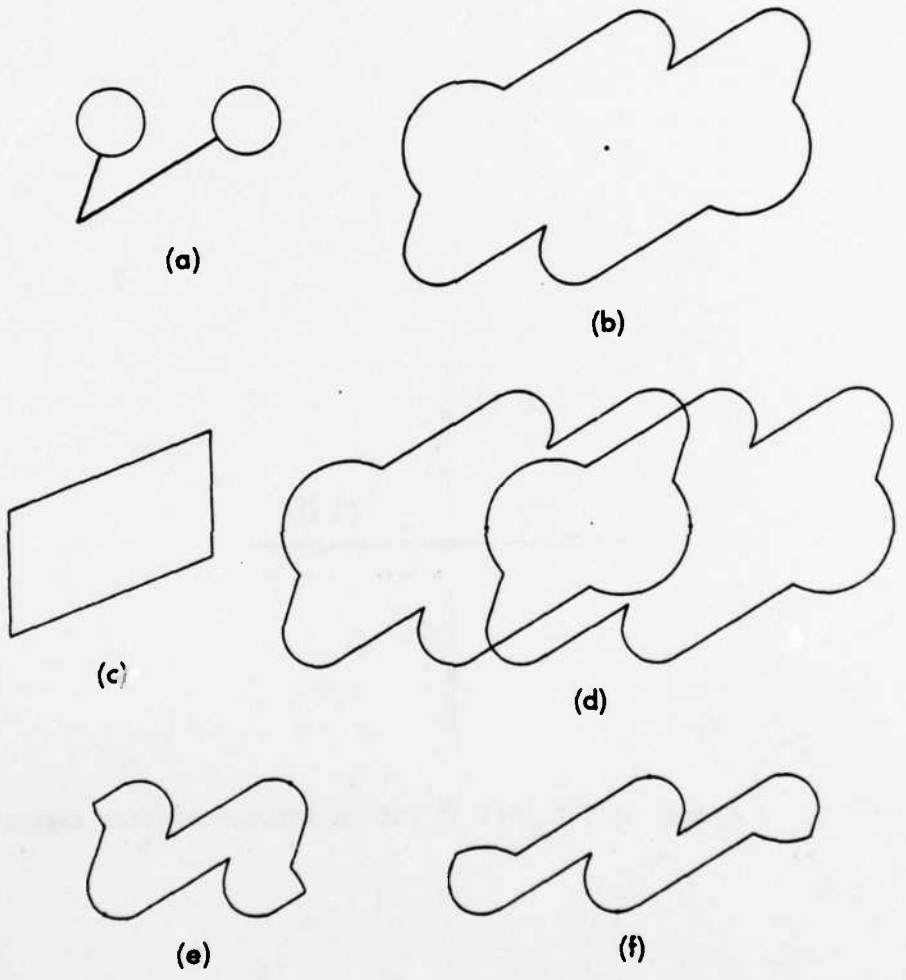

Figure 3. Locator Sets. (a) Set S; (b) $A = S - S$; (c) locator set $L = 1/2\ P$; (d) formation of $L = A \cap (w + A)$; (e) and (f) two other members of the family of locator sets.

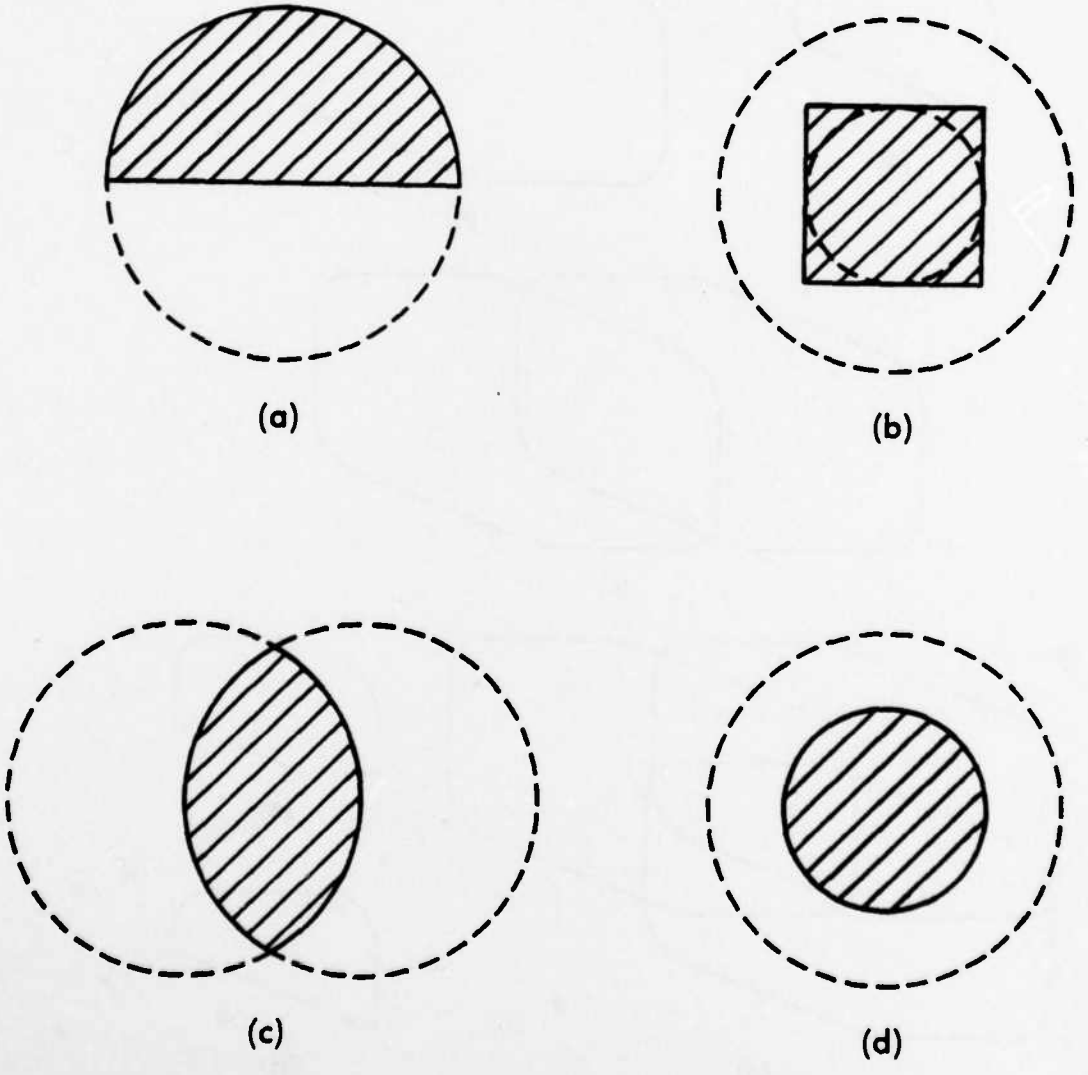

Figure 4. Locator sets (shaded areas) for the circle. (a) $A \cap H$; (b) the square 1/2 P; (c) $A \cap (w + A)$, (d) circle of radius $1/\sqrt{3}$.

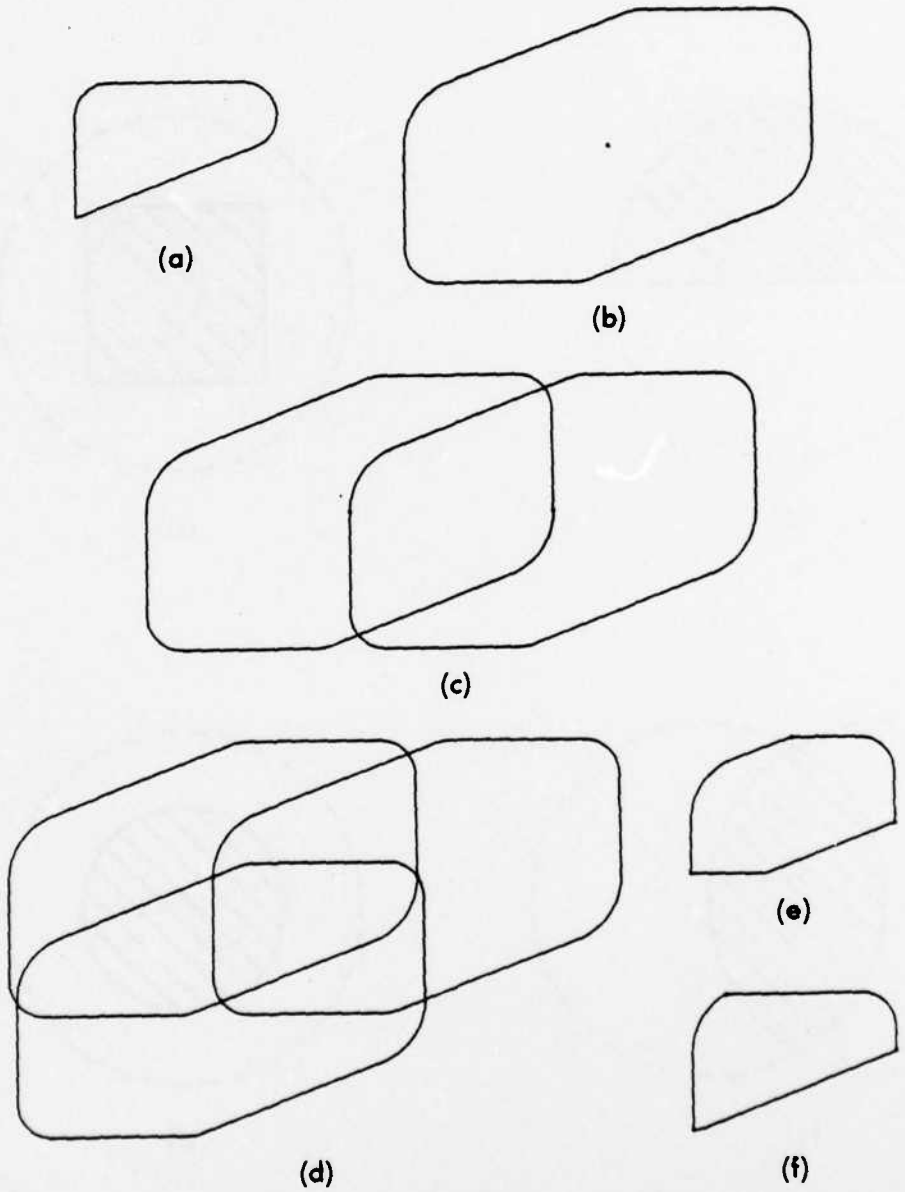

Figure 5. Autocorrelation tri-intersection solution for convex sets. (a) Set S; (b) $A = S - S$; (c) formation of locator set $L = A \cap (w + A)$; (d) formation of solution $B = A \cap (w_1 + A) \cap (w_2 + A)$; (e) and (f) two other solutions of the form B.

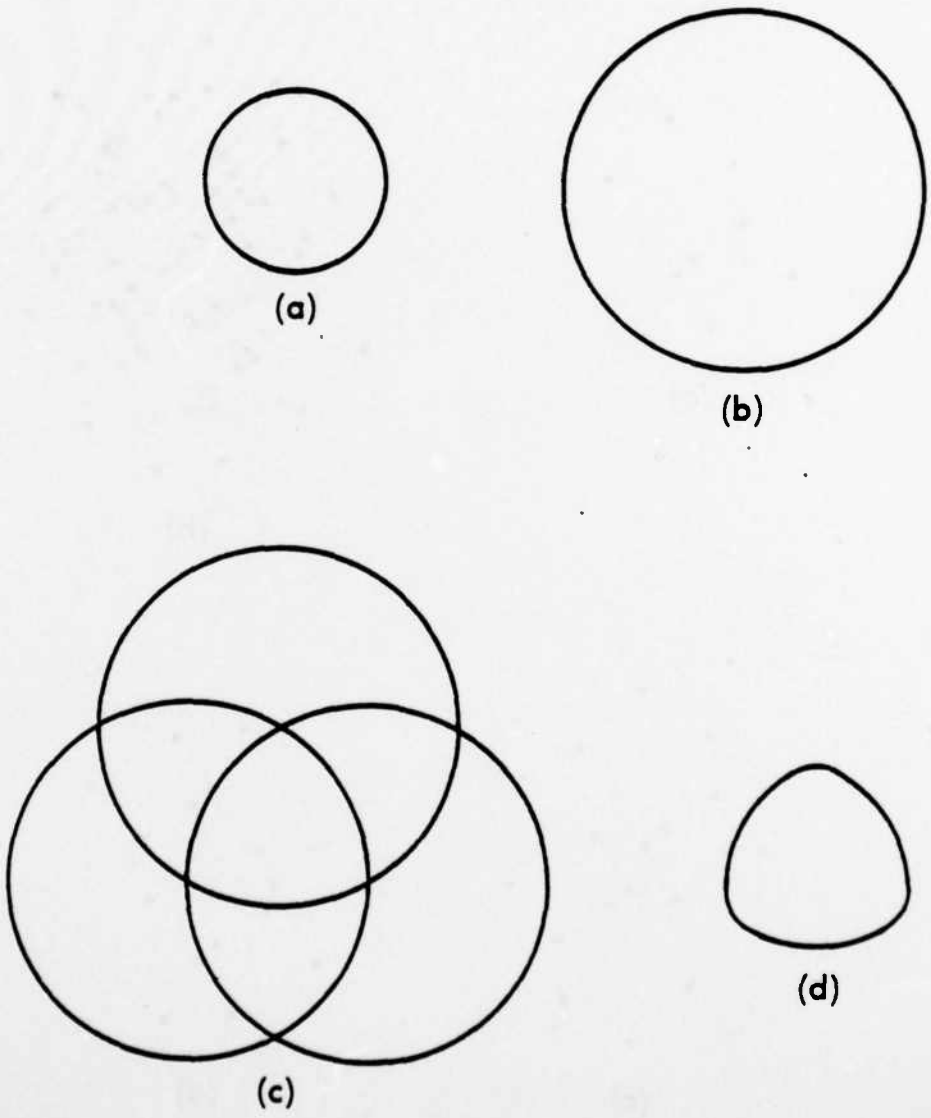

Figure 6. Sphere/circle example. (a) Set S; (b) $A = S - S$; (c) $B = A \cap (w_1 + A) \cap (w_2 + A)$; (d) another solution for the circle combining the solutions (a) and (c).

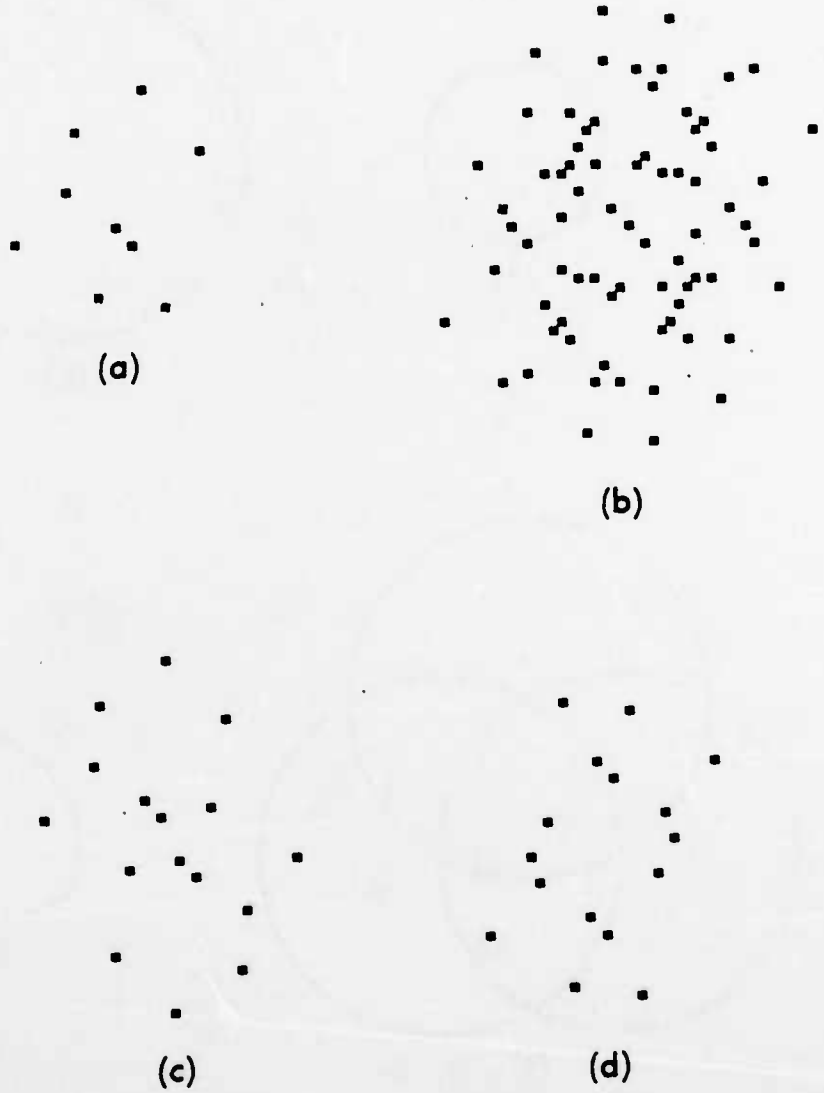

Figure 7. Autocorrelation tri-intersection for sets consisting of a collection of distinct points. (a) Set S; (b) $A = S - S$; (c) and (d) locators of the form $L = A \cap (w + A)$. Intersecting (c) or (d) with (b) yields the unique solution (a).

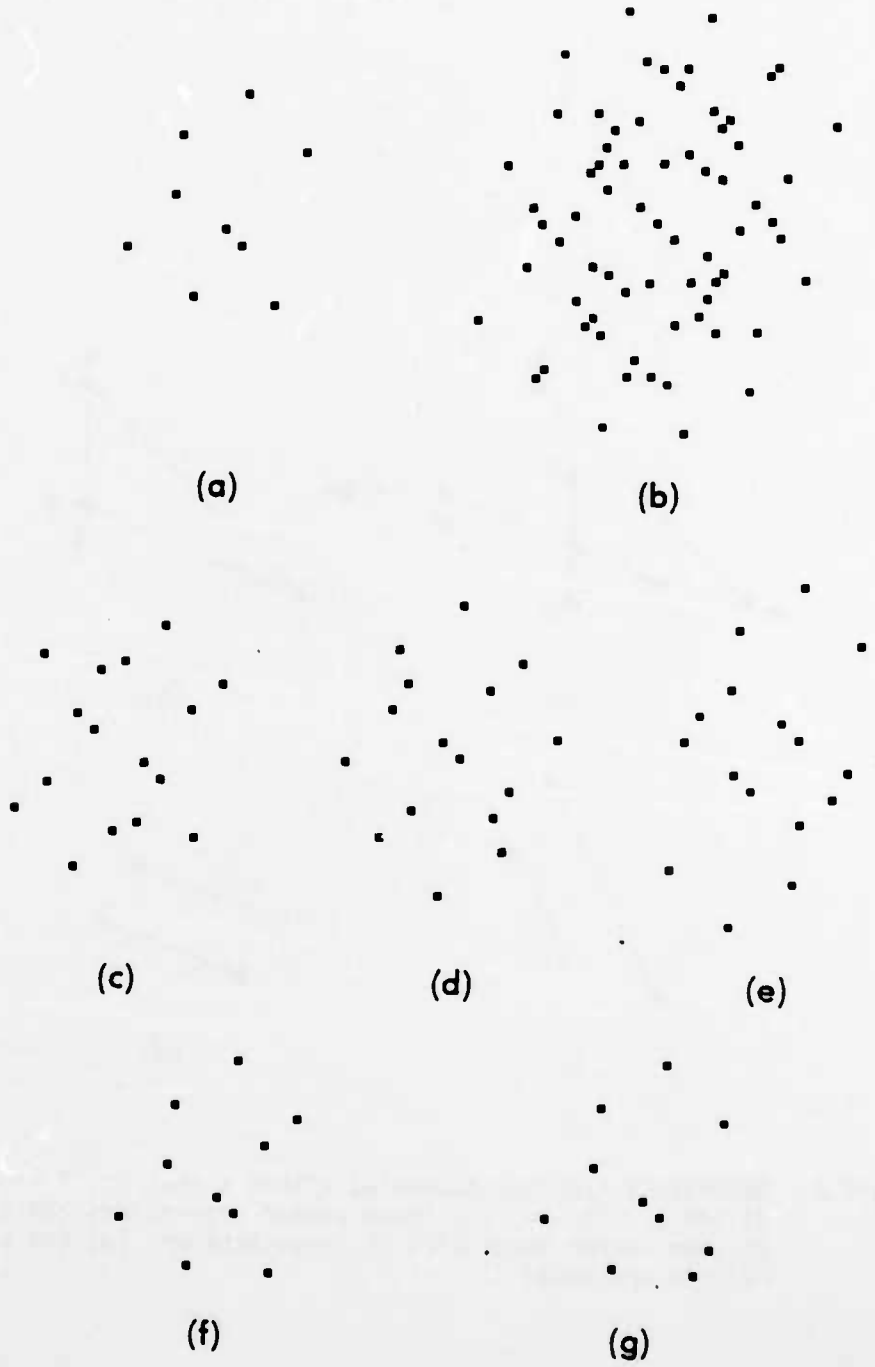

Figure 8. Autocorrelation intersection for redundant case. (a) Set S; (b) $A = S - S$; (c), (d), and (e) locators of the form $L = A \cap (w + A)$; (f) intersection of (c) with (d); (g) another intersection of three translates of A.

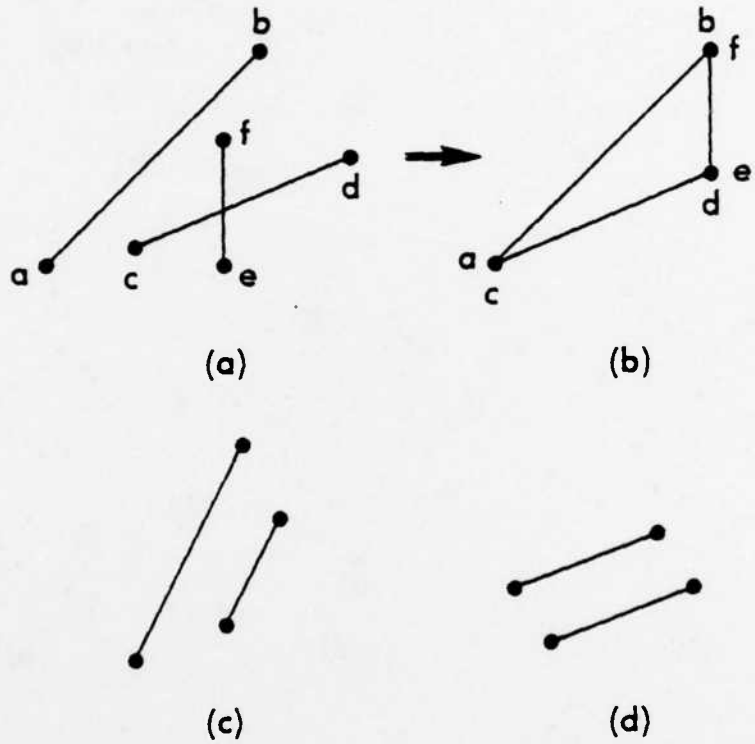

Figure 9. Redundancy-type relationships within S that would violate Condition 1. (a) and (b) Three vector separations add to zero; (c) one vector separation is twice another; (d) two vector separations are equal.

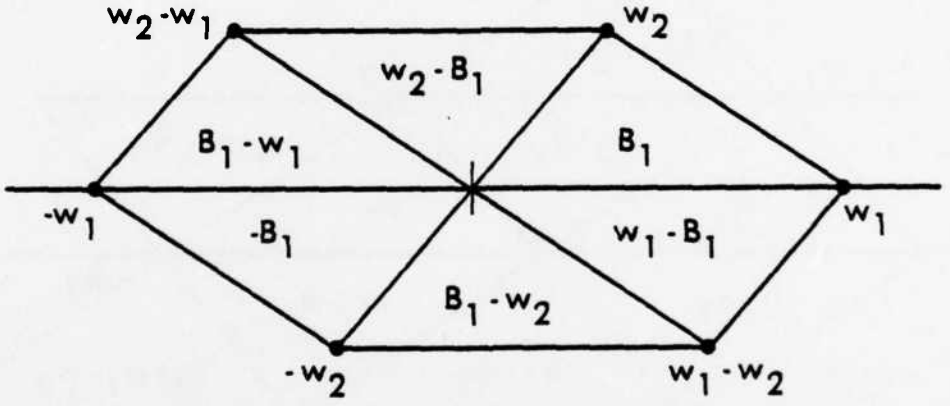

$$A_1 = B_1 - B_1$$

Figure B1

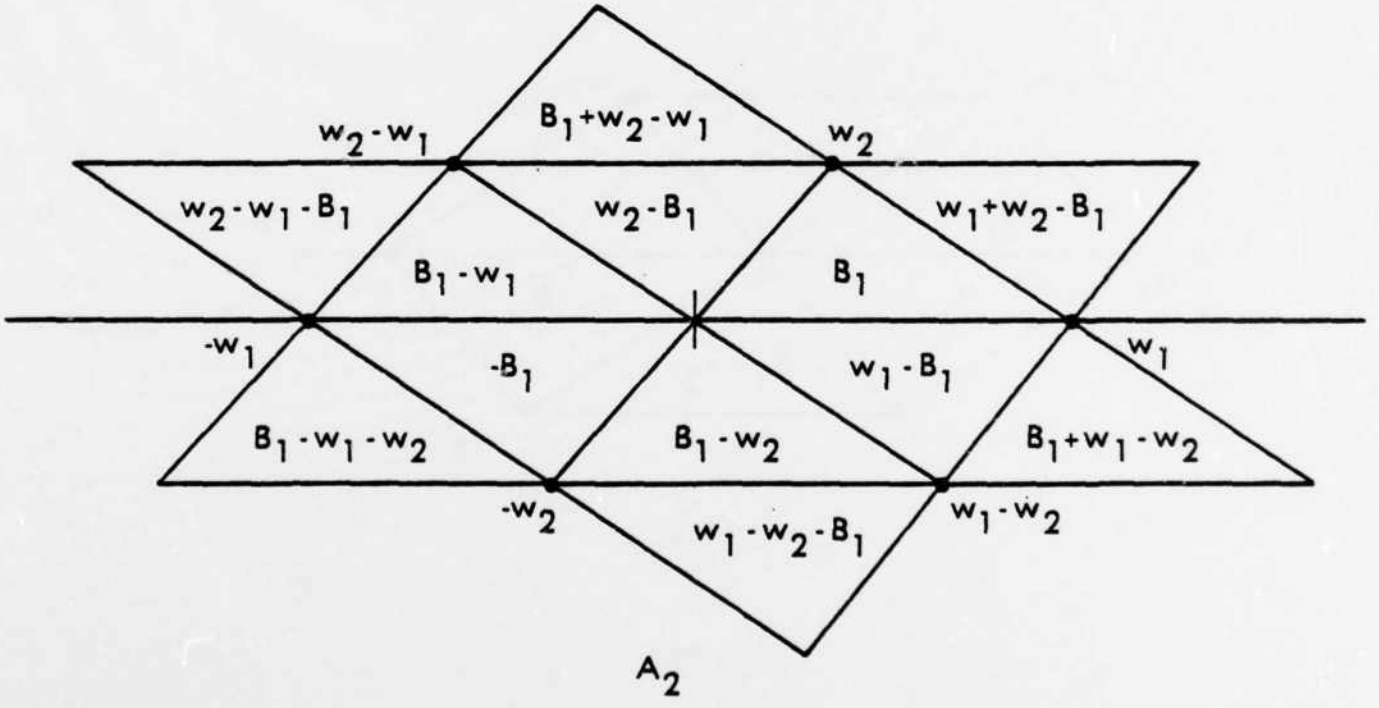
$w_2 - w_1$
$B_1 + w_2 - w_1$
w_2
$w_2 - w_1 - B_1$
$w_2 - B_1$
$w_1 + w_2 - B_1$
$B_1 - w_1$
B_1
$-w_1$
$-B_1$
$w_1 - B_1$
w_1
$B_1 - w_1 - w_2$
$B_1 - w_2$
$B_1 + w_1 - w_2$
$-w_2$
$w_1 - w_2 - B_1$
$w_1 - w_2$
A_2

Figure B2

AD-A113 911 ENVIRONMENTAL RESEARCH INST OF MICHIGAN ANN ARBOR F/G 5/8
FINE RESOLUTION IMAGING OF SPACE OBJECTS.(U)
FEB 82 J R FIENUP F49620-80-C-0006
UNCLASSIFIED ERIM-145400-14-F AFOSR-TR-82-0289 NL

2 OF 3
AD A
113911

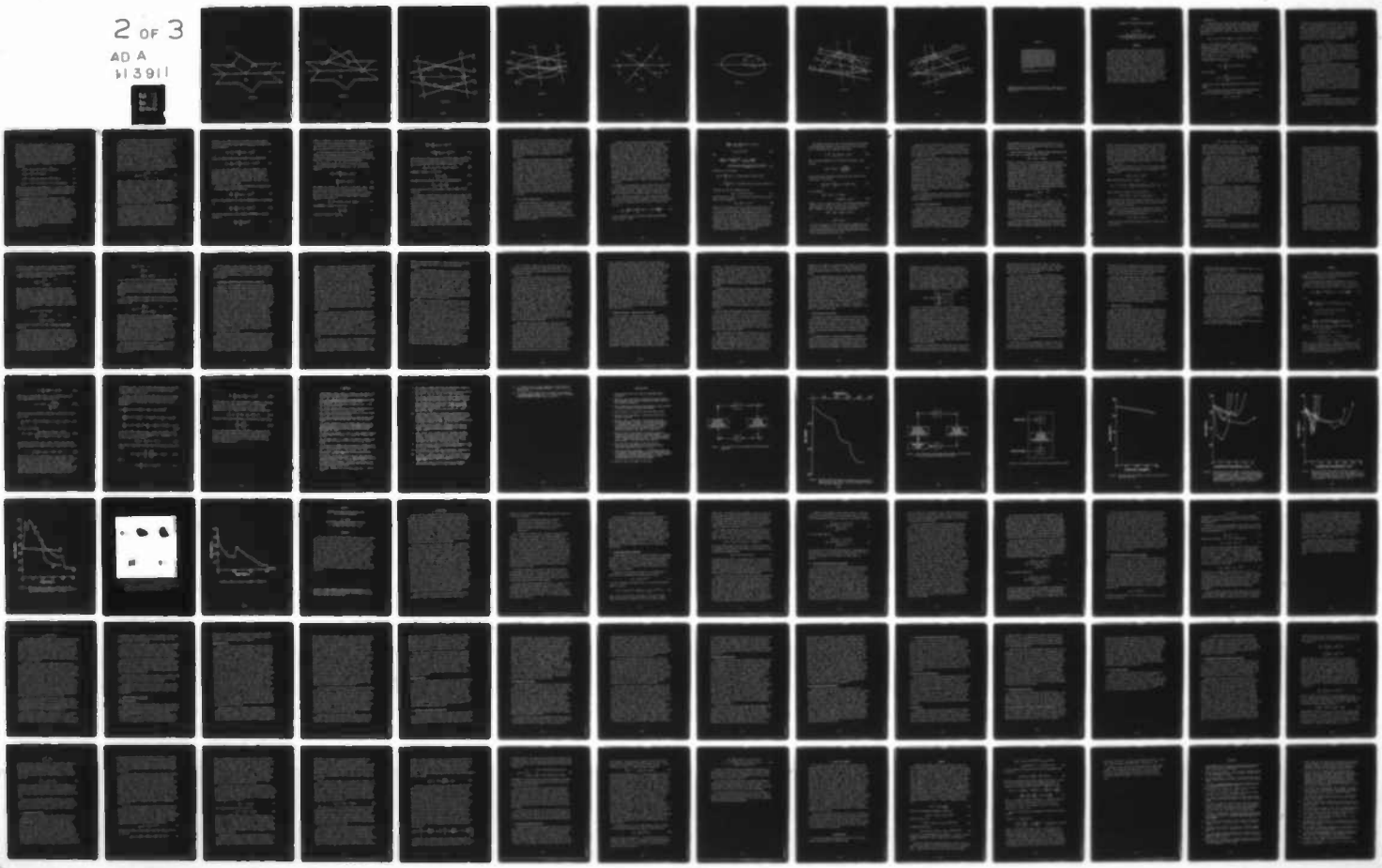

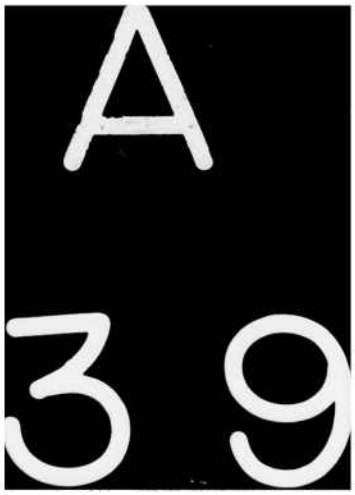
A
39

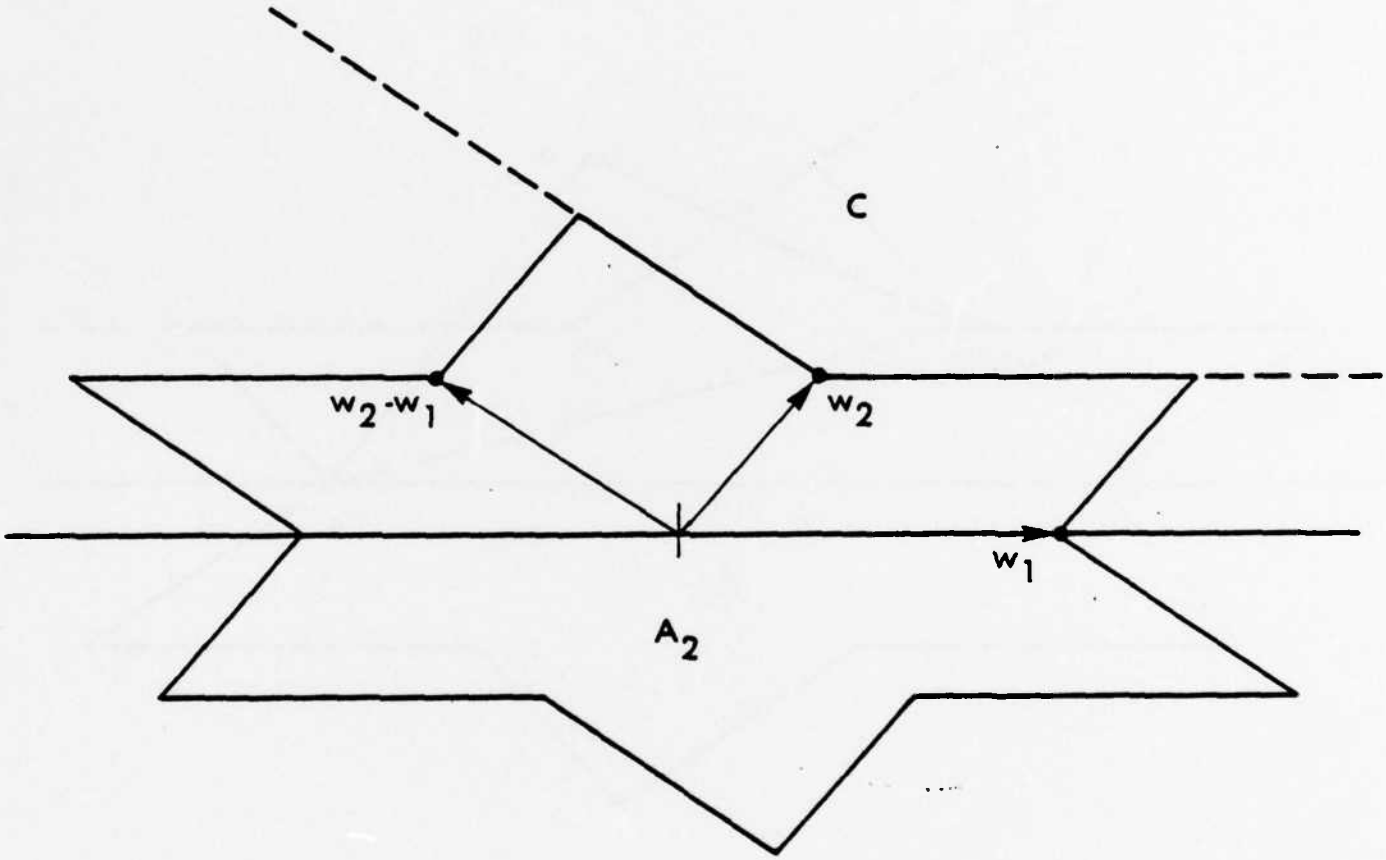

Figure B3

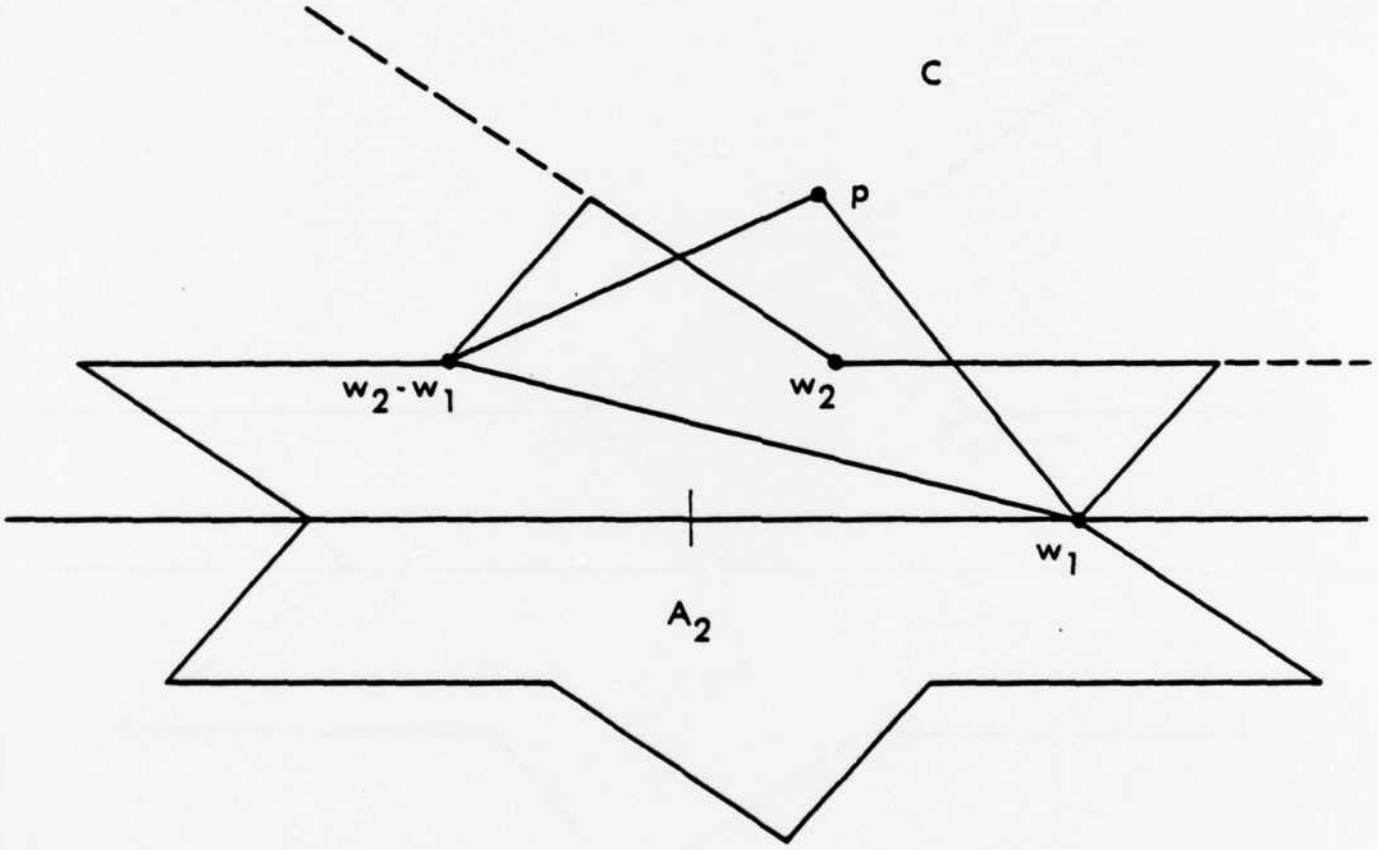

Figure B4

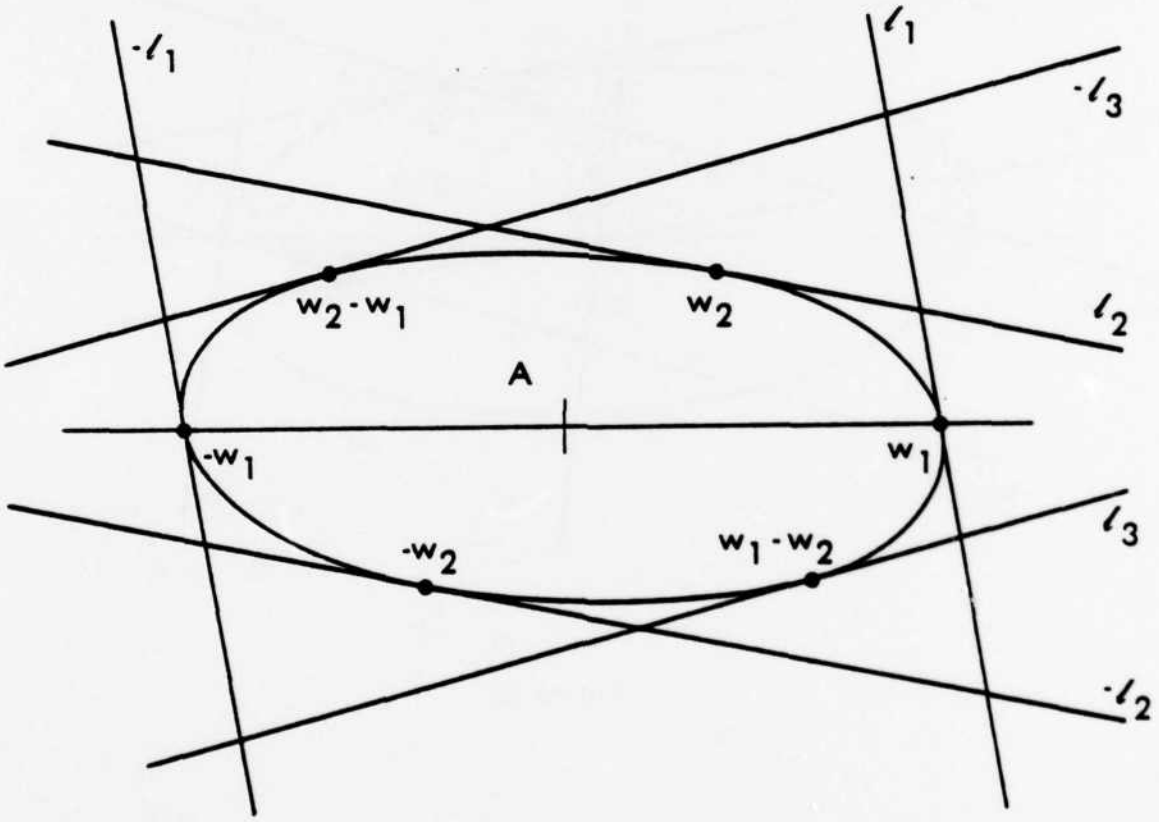

Figure B5

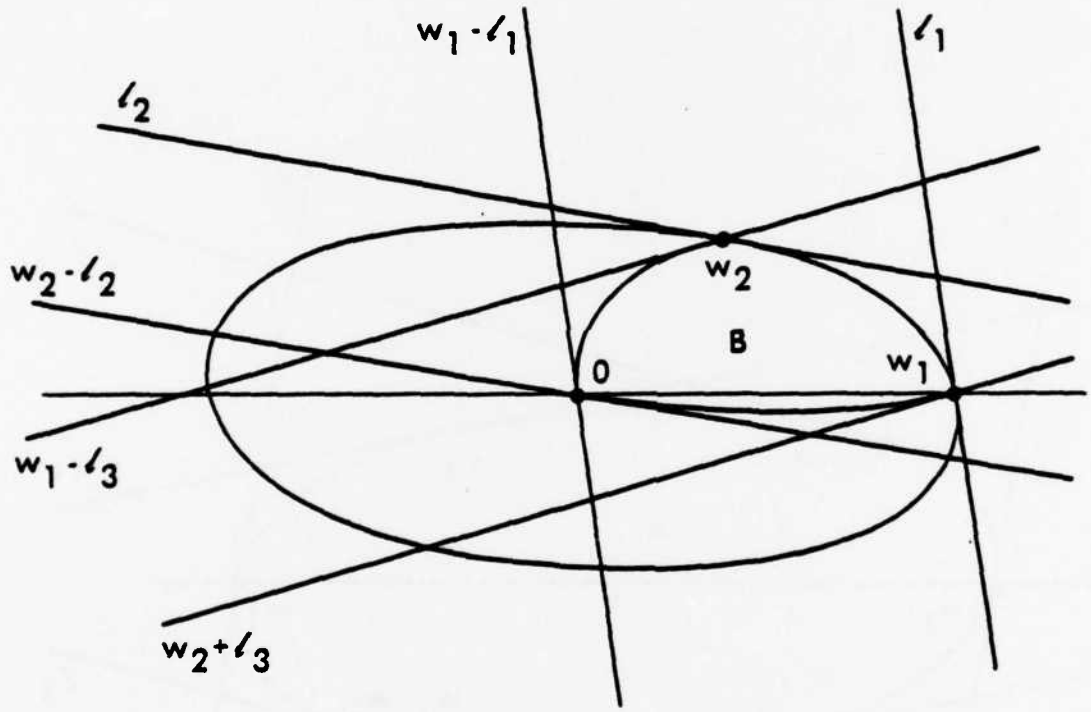

Figure B6

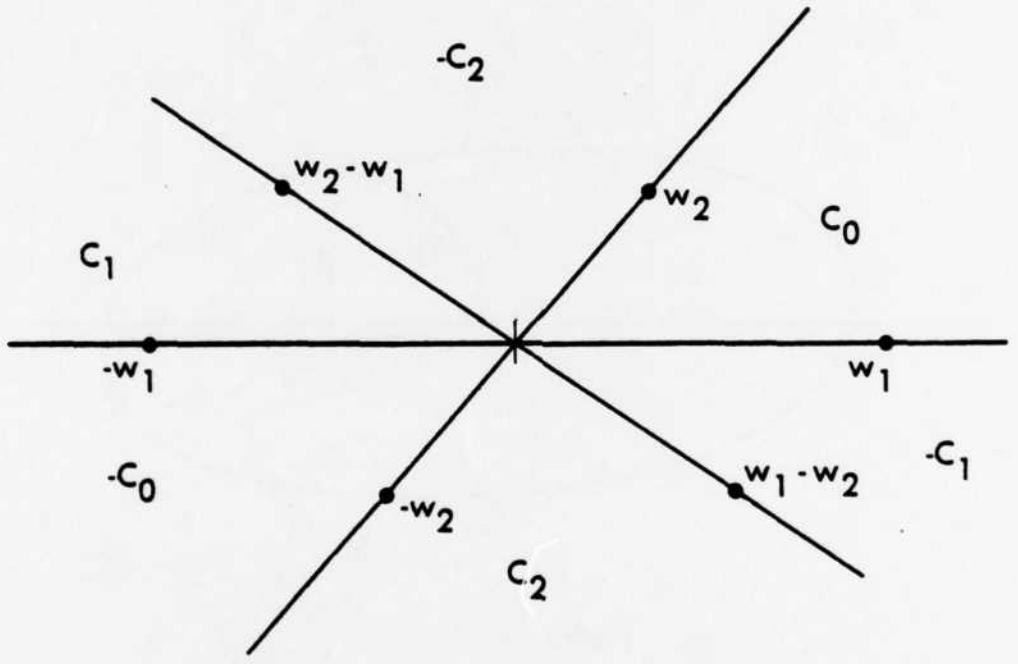

Figure B7

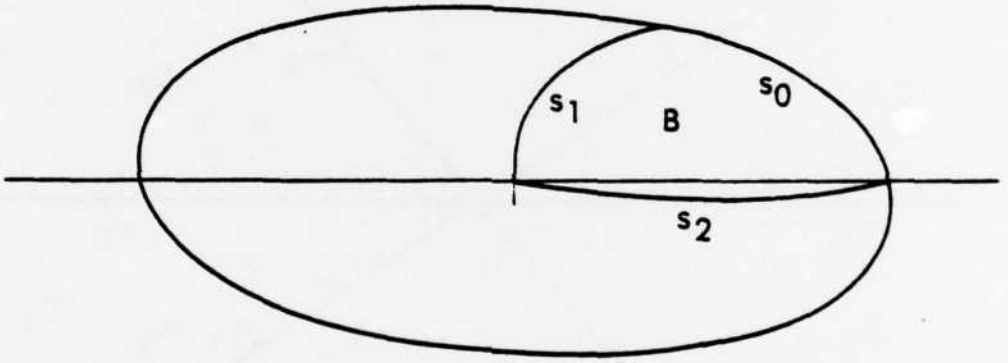

Figure B8

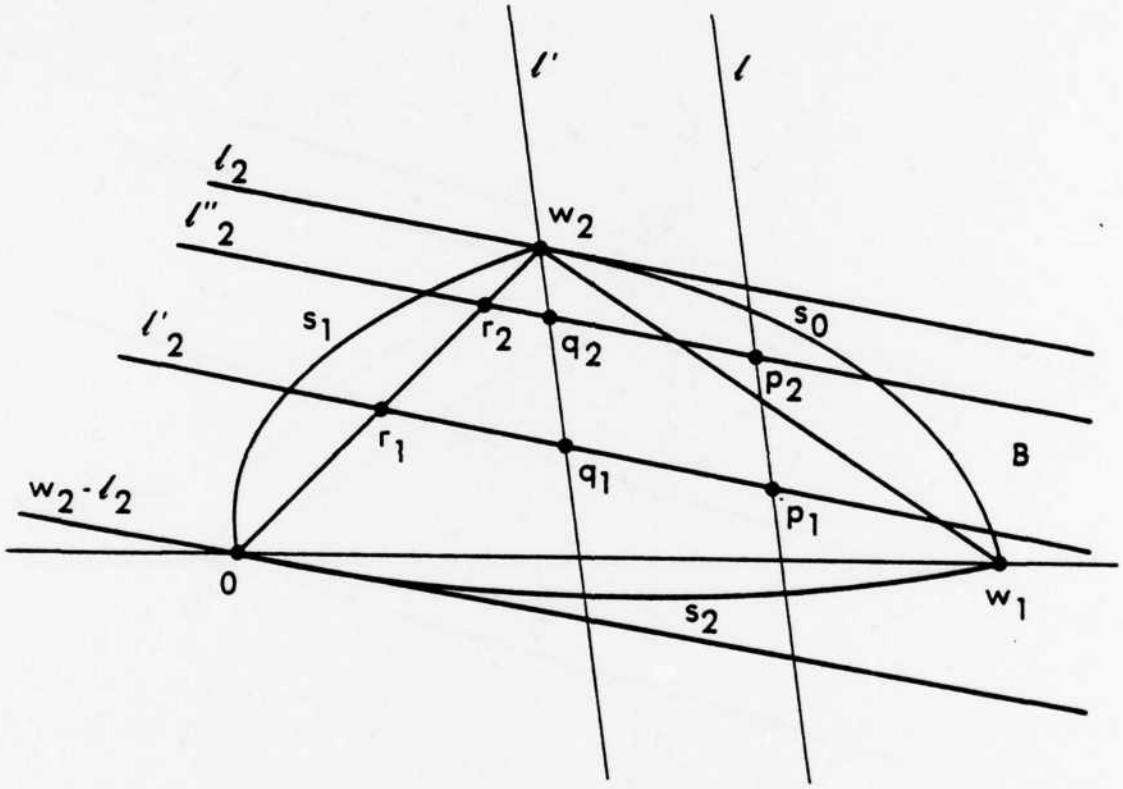

Figure B9

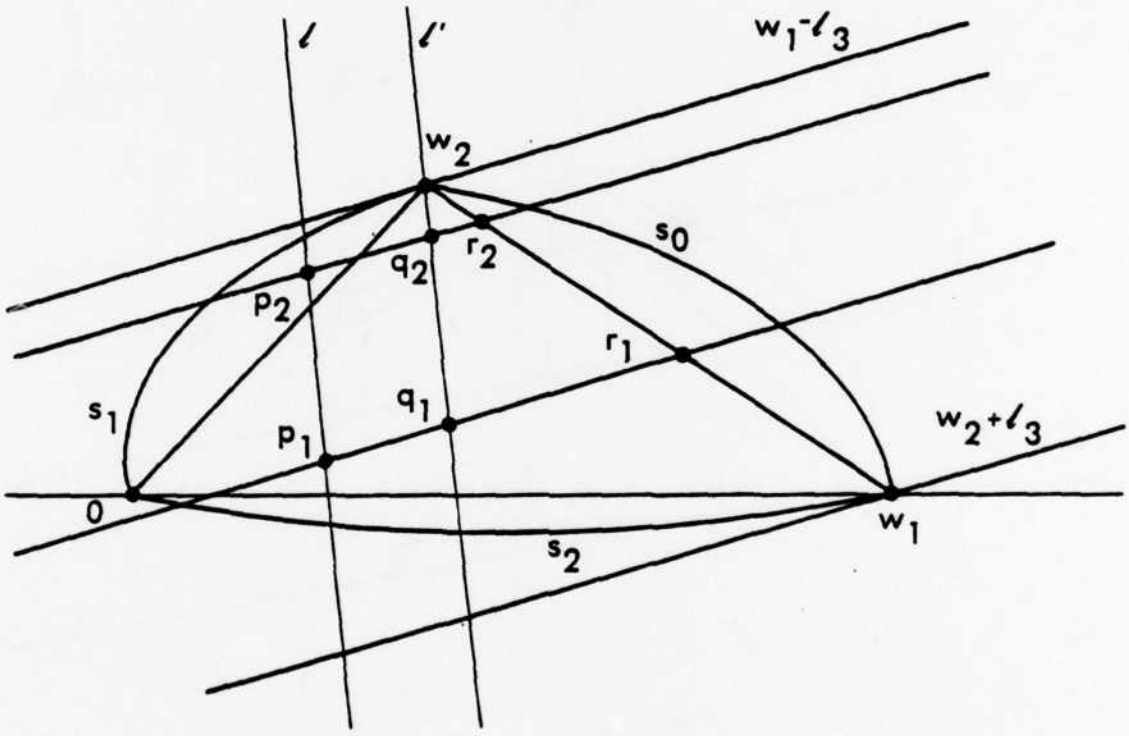

Figure B10

Appendix G

FO3. Comparison of Phase Retrievial Algorithms.* J. R. FIENUP, *Radar and Optics Division, Environmental Research Institute of Michigan, P.O. Box 8618, Ann Arbor, Mich. 48107* —Different versions of the iterative Fourier transform method[1] of reconstructing an object from the modulus of its Fourier transform (solving the phase retrieval problem) are compared. A proof of convergence of the error reduction algorithm is given. The input–output algorithms, although not guaranteed to converge, in practice converge faster than the error reduction algorithm. Other algorithms having accelerated convergence are also discussed. The steepest descent method is shown to be closely related to the iterative Fourier transform method. Application of these methods to complicated two-dimensional objects has in practice usually resulted in unique reconstructions. (13 min.)

* Research supported by the U.S. Air Force Office of Scientific Research.

[1] J. R. Fienup, Opt. Lett. 3, 27 (1978).

Reprinted from: J. Opt. Soc. Am. 71, 1641 (1981). Presented at the 1981 Annual Meeting of the Optical Society of America, Kissimmee, FL, October 1981.

Appendix H

COMPARISON OF PHASE RETRIEVAL ALGORITHMS

by

J.R. Fienup

Radar and Optics Division
Environmental Research Institute of Michigan
P.O. Box 8618, Ann Arbor, MI 48107

Abstract

Iterative algorithms for phase retrieval from intensity data are compared with gradient search methods. Both the problem of phase retrieval from two intensity measurements (in electron microscopy or wavefront sensing) and the problem of phase retrieval from a single intensity measurement plus a nonnegativity constraint (in astronomy) are considered, with emphasis on the latter. It is shown that both the error-reduction algorithm for the problem of a single intensity measurement and the Gerchberg-Saxton algorithm for the problem of two intensity measurements "converge." The error-reduction algorithm is also shown to be closely related to the steepest descent method. Other algorithms, including the input-output algorithm and the conjugate gradient method are shown to converge in practice much faster than the error-reduction algorithm. Examples are shown.

1. INTRODUCTION

In electron microscopy, wavefront sensing, astronomy, crystallography, and other fields, one often wishes to recover phase although only intensity measurements are made. One is usually interested in determining an object, $f(x)$, which is related to its Fourier transform, $F(u)$, by

$$F(u) = |F(u)|\, e^{i\psi(u)} = \mathcal{F}[f(x)] = \int_{-\infty}^{\infty} f(x)\, e^{-i2\pi u \cdot x}\, dx \qquad (1)$$

where x is an M-dimensional spatial coordinate and u is an M-dimensional spatial frequency coordinate. For the majority of interesting problems, $M = 2$. In practice, one deals with sampled data in the computer where, for the two-dimensional case, assuming square arrays, $u = (u_1, u_2)$ and $x = (x_1, x_2)$, where u_1, u_2, x_1, and $x_2 = 0, 1, 2, \ldots, N - 1$. Then one uses the discrete Fourier transform (DFT)

$$F(u) = \sum_{x=0}^{N-1} f(x) \exp\,(-i2\pi u \cdot x/N) \qquad (2)$$

and its inverse

$$f(x) = N^{-2} \sum_{u=0}^{N-1} F(u) \exp\,(i2\pi u \cdot x/N) \qquad (3)$$

which are, of course, computed using the fast Fourier transform (FFT) method.

For the problem of recovering phase from two intensity measurements, as in electron microscopy and in wavefront sensing,

$$f(x) = |f(x)|\, e^{i\eta(x)} \qquad (4)$$

is complex valued and one wishes to recover $\psi(u)$, or equivalently recover $n(x)$ from measurements of both $|F(u)|$ and $|f(x)|$. For the problem of recovering phase from a single intensity measurement, as in image recovery from speckle interferometry data in astronomy and from structure factors in crystallography, one wishes to recover $\psi(u)$, or equivalently recover $f(x)$, given a measurement of $|F(u)|$ and the constraint that $f(x)$ be real and nonnegative,

$$f(x) \geq 0 \ . \tag{5}$$

A particularly successful approach to solving these problems is the use of the Gerchberg-Saxton algorithm[1,2] and related algorithms[3-7]. Reference 7 lists a large number of different problems which have been solved by these algorithms. These algorithms involve iterative Fourier transformation back and forth between the object domain and the Fourier domain, and application of the measured data or known constraints in each domain.

In what follows, a generalized Gerchberg-Saxton algorithm, referred to as the error-reduction algorithm, and its convergence properties are reviewed (Section 2), and it is shown to be equivalent to the steepest-descent gradient search method (Section 3). Alternative gradient search methods (Section 4) and iterative Fourier transform algorithms (Section 5) are described, and are shown to converge much faster than the error-reduction algorithm for the problem of a single intensity measurement (Section 6). Some practical considerations are discussed in Section 7. A typical reconstruction experiment is shown in Section 8, and the major conclusions are summarized in Section 9.

2. THE ERROR-REDUCTION ALGORITHM

The Gerchberg-Saxton algorithm was originally invented in connection with the problem of reconstructing phase from two intensity measurements[1,2] (and for synthesizing phase codes given intensity

constraints in each of two domains[8,9]). The algorithm consists of the following four simple steps: (1) Fourier transform an estimate of the object, (2) replace the modulus of the resulting computed Fourier transform with the measured Fourier modulus to form an estimate of the Fourier transform, (3) inverse Fourier transform the estimate of the Fourier transform and (4) replace the modulus of the resulting computed image with the measured object modulus to form a new estimate of the object. In equations, this is, for the k^{th} iteration,

$$G_k(u) = |G_k(u)| \exp [i\phi_k(u)] = \mathcal{F}[g_k(x)] \tag{6}$$

$$G_k'(u) = |F(u)| \exp [i\phi_k(u)] \tag{7}$$

$$g_k'(x) = |g_k'(x)| \exp [i\theta_k'(x)] = \mathcal{F}^{-1}[G_k'(u)] \tag{8}$$

$$g_{k+1}(x) = |f(x)| \exp [i\theta_{k+1}(x)] = |f(x)| \exp [i\theta_k'(x)] \tag{9}$$

where g_k, θ_k, G_k' and ϕ_k are estimates of f, η, F and ψ, respectively. Here and throughout this paper, functions represented by upper-case letters are the Fourier transforms of the functions represented by the corresponding lower-case letters.

The Gerchberg-Saxton algorithm, as depicted in Figure 1, is easily generalized to a large class of problems[6,7]. The generalized Gerchberg-Saxton algorithm can be used for any problem in which partial constraints (in the form of measured data or information known a priori) are known in each of two domains, usually the object (or image) domain and the Fourier domain. One simply transforms back and forth between the two domains, satisfying the constraints in each domain before returning to the other domain. This generalization of the Gerchberg-Saxton algorithm will be referred to as the error-reduction algorithm, since, as will be shown below, the error decreases at each iteration.

For the most general problem, the error-reduction algorithm consists of the following four steps: (1) Fourier transform $g_k(x)$, an estimate of $f(x)$; (2) make the minimum changes in $G_k(u)$, the resulting computed Fourier transform, which allow it to satisfy the Fourier-domain constraints, to form $G'_k(u)$, an estimate of $F(u)$; (3) inverse Fourier transform $G'_k(u)$; and (4) make the minimum changes in $g'_k(x)$, the resulting computed image, which allow it to satisfy the object-domain constraints, to form $g_{k+1}(x)$, a new estimate of the object. In particular, for the problem of a single intensity measurement (as in astronomy), the first three steps are identical to the first three steps of the Gerchberg-Saxton algorithm, Eqs. (6), (7) and (8); and the fourth step is given by

$$g_{k+1}(x) = \begin{cases} g'_k(x), & x \notin \gamma \\ 0, & x \in \gamma \end{cases} \tag{10}$$

where γ is the set of points at which $g'_k(x)$ violates the object-domain constraints, i.e., wherever $g'_k(x)$ is negative or (optionally) where it exceeds the known diameter of the object. The diameter of the object can be computed, since it is just half the diameter of the autocorrelation function, which is the inverse Fourier transform of the squared Fourier modulus. (However, in two dimensions, the exact support of the object cannot in general be determined uniquely from the support of its autocorrelation[10], and so the diameter constraint cannot be applied very tightly.)

The iterations continue until the computed Fourier transform satisfies the Fourier-domain constraints or the computed image satisfies the object-domain constraints; then one has found a solution, a Fourier transform pair that satisfies all the constraints in both domains. The convergence of the algorithm can be monitored by computing the squared error. In the Fourier domain, the squared error is the sum of the squares of the amounts by which $G_k(u)$, the computed Fourier transform, violates the Fourier-domain constraints.

Since $G_k'(u)$ was formed from $G_k(u)$ by making the minimum changes in order to satisfy the Fourier-domain constraints, the squared error can be expressed as

$$B_k = E_{Fk}^2 = N^{-2} \sum_u |G_k(u) - G_k'(u)|^2 \tag{11}$$

which, for both problems being considered, can be expressed as

$$B_k = E_{Fk}^2 = N^{-2} \sum_u [|G_k(u)| - |F(u)|]^2 \tag{12}$$

In this section, the symbol E_{Fk}^2 is used to distinguish it from the object-domain error, E_{Ok}^2, described below. For economy of notation in the section of this paper dealing with the gradient methods, the symbol B_k is used instead of E_{Fk}^2. The symbol B (with the subscript k deleted) is given by Eq. (11) with G and G' replacing G_k and G_k', respectively.

Similarly, for the error-reduction algorithm, the squared error in the object domain can be expressed as

$$E_{Ok}^2 = \sum_x |g_{k+1}(x) - g_k'(x)|^2 \tag{13}$$

which, for the problem of two intensity measurements can be expressed as

$$E_{Ok}^2 = \sum_x [|f(x)| - |g_k'(x)|]^2 \tag{14}$$

and for the problem of a single intensity measurement can be expressed as

$$E_{Ok}^2 = \sum_{x \epsilon \gamma} [g_k'(x)]^2 \tag{15}$$

where γ is defined as in Eq. (10). The asymmetry in the use of the N^{-2} factor above was chosen because of the similar asymmetry in the definition of the discrete Fourier transform in Eqs. (2) and (3). When the squared error is zero, then a solution has been found.

In the following, the error-reduction algorithm is shown to converge, and this convergence property holds for all the applications of the error-reduction algorithm (not just the problems of recovering phase from a single or from two intensity measurements).

For the general problem, at the k^{th} iteration, the squared error in the Fourier domain is given by Eq. (11). By Parseval's theorem[11],

$$E_{Fk}^2 = N^{-2} \sum_u |G_k(u) - G_k'(u)|^2$$

$$= \sum_x |g_k(x) - g_k'(x)|^2 \ . \qquad (16)$$

Now compare this with Eq. (13), the error in the object domain. Both $g_k(x)$ and $g_{k+1}(x)$ by definition satisfy the object-domain constraints. Also, at any point x, by definition $g_{k+1}(x)$ is the nearest value to $g_k'(x)$ that satisfies the object-domain constraints. Therefore, at all points x,

$$|g_{k+1}(x) - g_k'(x)| \leq |g_k(x) - g_k'(x)| \qquad (17)$$

and therefore, from Eqs. (13) and (16),

$$E_{Ok}^2 \leq E_{Fk}^2 \ . \qquad (18)$$

Similarly, by Parseval's theorem,

$$E_{0k}^2 = \sum_x |g_{k+1}(x) - g_k'(x)|^2$$

$$= N^{-2} \sum_u |G_{k+1}(u) - G_k'(x)|^2 \ . \qquad (19)$$

Since both $G_k'(u)$ and $G_{k+1}'(u)$ satisfy the Fourier domain constraints, and at any point u, by definition $G_{k+1}'(u)$ is the nearest value to $G_{k+1}(u)$ that satisfies the Fourier-domain constraints, then

$$|G_{k+1}(u) - G_{k+1}'(u)| \leq |G_{k+1}(u) - G_k'(u)| \ . \qquad (20)$$

Therefore, from Eqs. (11) and (19),

$$E_{F,k+1}^2 \leq E_{0k}^2 \qquad (21)$$

and combining this with Eq.. (18) gives the desired result

$$E_{F,k+1}^2 \leq E_{0k}^2 \leq E_{Fk}^2 \ . \qquad (22)$$

That is, the error can only decrease (or stay the same) at each iteration.

In practice, the error-reduction algorithm usually decreases the error rapidly for the first few iterations, but then much more slowly for later iterations[1,2,9,12]. The speed of convergence also depends on the type of constraints imposed. Convergence seems to be reasonably fast for the problem of two intensity measurements, but painfully slow for the problem of a single intensity measurement. Figure 2 shows an example of the error as a function of the number of interations of the error-reduction algorithm for the problem of a single intensity measurement. Shown is the normalized rms error, i.e., the square root of E_{Fk}^2 divided by $\sum_u |F(u)|^2$. Both the error and the iteration number are shown on logarithmic scales. The error decreases rapidly during the first 30 iterations, but then

reaches a plateau at a level of 0.16, decreasing very slowly. After 70 iterations, the error again starts to decrease until it reaches a second plateau at the level of 0.02, at which point the error decreases extremely slowly. After 2,000 iterations, the error once again starts to decrease until it reaches a third plateau at the level of 0.003, at which point the decrease in the error is negligible.

The occurrences of plateaus during which convergence is extremely slow seems to occur more often than not for both applications[1,9,12], and it has in the past been observed that with persistence, one can go beyond the plateau region and again make rapid progress toward a solution[1,12]. However, as shown in the example of Figure 2 for the problem of a single intensity measurement, the number of iterations required for convergence of the error-reduction algorithm can be extremely large, making that algorithm unsatisfactory for that application. Fortunately, as will be shown in later sections, other related algorithms converge much faster, reconstructing a recognizable image in 20 or 30 iterations, and completing the reconstruction in under one hundred iterations, which takes less than two minutes on a Floating Point System AP-120B array processor for array sizes of 128 x 128.

3. THE STEEPEST DESCENT METHOD

An alternative approach to solving the phase retrieval problems is to employ one of the gradient search methods. In this section, it is shown that one such method, the steepest descent method, is closely related to the error reduction algorithm for the problem of reconstructing phase from a single intensity measurement. The relationship between the steepest descent method and the Gerchberg-Saxton algorithm is also discussed.

An example of how a gradient search method would be used for this problem is the following. One can define $B = E_F^2$, the squared error in the Fourier domain given by Eq. (12), as the error metric which one seeks to minimize by varying a set of parameters. Here, the N^2 values of $g(x)$, the estimate of $f(x)$, are treated as N^2 independent parameters. Starting at a given point, $g_k(x)$, in the N^2-dimensional parameter space, one would reduce the error by computing the partial derivatives of B with respect to each of the points $g(x)$ (N^2 partial derivatives), forming the gradient, and then move from $g_k(x)$ in a direction opposite that of the gradient to a new point $g_k''(x)$. One would then form a new estimate, $g_{k+1}(x)$, from $g_k''(x)$ by forcing the object-domain constraints to be satisfied. This would be done iteratively until a minimum (hopefully a global minimum) is found. That is, one minimizes the error, B, as a function of the N^2 parameters, $g(x)$, subject to the object-domain constraints.

Ordinarily, the computation of the N^2 partial derivatives would be a very lengthy task since each evaluation of B involves an N x N discrete Fourier transform. However, for the problems considered here, the computation can be greatly reduced, as described below.

First, consider the problem of a single intensity measurement. The partial derivative of B with respect to a value at a given point, $g(x)$, is [$g(x)$ is assumed to be real since $f(x)$ is real], using Eq. (12),

$$\partial_g B \equiv \frac{\partial B}{\partial g(x)} = 2N^{-2} \sum_u [|G(u)| - |F(u)|] \frac{\partial |G(u)|}{\partial g(x)} . \qquad (23)$$

Later, the notation $\partial_g B_k$ will be used to denote $\partial_g B$ evaluated at $g(x) = g_k(x)$. Since

$$\frac{\partial G(u)}{\partial g(x)} = \frac{\partial}{\partial g(x)} \sum_y g(y) \exp\,[-i2\pi u \cdot y/N]$$

$$= \exp\,[-i2\pi u \cdot x/N]\ , \tag{24}$$

then

$$\frac{\partial |G(u)|}{\partial g(x)} = \frac{\partial [|G(u)|^2]^{1/2}}{\partial g(x)} = \frac{1}{2|G(u)|} \frac{\partial |G(u)|^2}{\partial g(x)}$$

$$= \frac{G(u) \exp\,[i2\pi u \cdot x/N] + G^*(u) \exp\,[-i2\pi u \cdot x/N]}{2|G(u)|}\ . \tag{25}$$

Therefore, Eq. (23) becomes

$$\partial_g B = N^{-2} \sum_u [G(u) - |F(u)|G(u)/|G(u)|] \exp\,[i2\pi u \cdot x/N]$$

$$+ N^{-2} \sum_u [G^*(u) - |F(u)|G^*(u)/|G(u)|] \exp\,[-i2\pi u \cdot x/N]\ . \tag{26}$$

Using Eqs. (6) and (7) to define G'(u) as

$$G'(u) = |F(u)|G(u)/|G(u)|\ , \tag{27}$$

and noting that Eq. (26) is in the form of a discrete Fourier transform, it can be reduced to

$$\partial_g B = 2[g(x) - g'(x)] \tag{28}$$

where g'(x) is defined by Eq. (8), and the fact that g(x) and g'(x) are real valued has been used. [Note that since $\partial g'(y)/\partial g(x) \neq 0$, it is not true that Eq. (28) follows immediately from Eq. (16).] From Eq. (28), it is evident that the entire gradient, consisting of the N^2 partial derivatives, can be computed very simply by Fourier transforming g(x), applying Eq. (27), inverse Fourier transforming to arrive at g'(x), subtracting g'(x) from g(x) and multiplying by a constant. In fact, the computation of g'(x) is identical to the first three steps of the error-reduction algorithm.

The "optimum" step size to take in the direction of the gradient can be determined by forming a first-order Taylor series expansion of B as a function of g(x), about the point $g_k(x)$,

$$B \simeq B_k + \sum_x \partial_g B_k [g(x) - g_k(x)] \ . \tag{29}$$

This first-order expansion of B is equal to zero at $g(x) = g_k''(x)$ given by

$$g_k''(x) - g_k(x) = - \frac{B_k \partial_g B_k}{\sum_y (\partial_g B_k)^2} \ . \tag{30}$$

which can be easily verified by inserting Eq. (30) into Eq. (29). Since by Eqs. (28) and (16)

$$\sum_y (\partial_g B_k)^2 = 4 \sum_y [g_k(y) - g_k'(y)]^2 = 4B_k \ , \tag{31}$$

Eq. (30) becomes

$$\begin{aligned} g_k''(x) - g_k(x) &= -(1/4)\partial_g B_k \\ &= (1/2)[g_k'(x) - g_k(x)] \ . \end{aligned} \tag{32}$$

However, since B is quadratic in g(x), the linear approximation above can be expected to predict a step size half as large as the optimum[2]. Therefore, one should use the double-length step,

$$g_k''(x) - g_k(x) = [g_k'(x) - g_k(x)]$$

or

$$g_k''(x) = g_k'(x) \ . \tag{33}$$

In fact, since $|G_k'(u)| = |F(u)|$, moving to $g_k'(x)$ reduces the error, Eq. (12), to zero exactly. As a final step in one iteration, the new estimate should be made to satisfy the object-domain constraints, which is accomplished by using Eq. (10).

Comparing this new estimate to that of the error-reduction algorithm described in Section 2, it is seen that they are identical. That is, the error-reduction iterative Fourier transform algorithm can be looked on as a rapid method of implementing a double-length step steepest descent method.

Although the steepest descent method is identical to the error-reduction algorithm for the problem of a single intensity measurement, the connection is not so close for the problem of two intensity measurements, as explored in Appendix A. In that case, the error is minimized with respect to the phase estimate $\theta(x)$, and the derivative of the error does move one in a direction approximately towards the Gerchberg-Saxton phase, $\theta'(x)$, of Eq. (9). However, the direction, according to Eq. (A-4), is somewhat different than that of the Gerchberg-Saxton algorithm; and the step size, according to Eqs. (A-12) and (A-16) is considerably larger than that of the Gerchberg-Saxton algorithm. Experimental results using the steepest descent method for the problem of two intensity measurements are shown in Reference 2.

The relationship between a gradient search method and the error-reduction algorithm for a problem in digital filter design is discussed in Reference 13.

4. OTHER GRADIENT SEARCH METHODS

As shown in Section 3 for the phase problem of a single intensity measurement, the steepest descent method is equivalent to the error-reduction algorithm. And as described in Section 2, although there is a convergence proof for the error-reduction algorithm, it in practice converges very slowly for the problem of a single intensity measurement. Slow convergence of the steepest descent (also known as the optimum gradient) method has also been observed for other applications as well[14]. In this section, some other gradient

search methods are briefly described, and in Section 6 it will be shown that in practice they converge much faster than the steepest descent method for this problem.

Recall from Eq. (30) that the steepest descent method moves from the point $g_k(x)$ in parameter space to the point

$$g_k''(x) = g_k(x) - h_k \partial_g B_k \tag{34}$$

where h_k, the step size, is a positive constant and the gradient is given by Eq. (28). For many applications, one would search along the direction of $-\partial_g B_k$, evaluating B repeatedly until the value of h_k that minimizes B is found; then from that point, one would recompute the gradient and go off in a new direction. For this application, however, since an N x N Fourier transform is required to evaluate B and only one more Fourier transform is required to recompute the gradient, one may as well recompute the gradient at each step. After each step of this or the other gradient methods described later, one must then satisfy the object-domain constraints to form the new estimate as was done in Eq. (10),

$$g_{k+1}(x) = \begin{cases} g_k''(x), & x \notin \gamma \\ 0, & x \in \gamma \end{cases} \tag{35}$$

where the set γ is defined as in Eq. (10). In Section 3, the "optimum" double-length step value of h_k was shown to be unity, for which the steepest descent method is equivalent to the error-reduction algorithm. In fact, $h_k = 1$ leads to a point $g_k''(x) = g_k'(x)$ at which $B = 0$. This is not a solution, however, unless $g_k'(x)$ satisfies the object-domain constraints. With this in mind, other values of h_k are in practice better, as will be shown in Section 6.

A useful block diagram representation of this and other gradient methods is shown in Figure 3, which emphasizes the similarity of gradient methods to the error-reduction algorithm. The first three

steps of the error-reduction algorithm, resulting in the computation of $g'(x)$, does most of the work of computing the gradient. The final step of satisfying the object-domain constraints is common to gradient methods and the error-reduction algorithm. Therefore, one can think of the error-reduction algorithm as a special case of a more general class of gradient methods. For the error-reduction algorithm (or the double-length step steepest descent method), it just happens that $g_k''(x) = g_k'(x)$.

A gradient search method that is superior to the steepest descent method is the conjugate gradient method. For that method, Eq. (34) is replaced by[14]

$$g_k''(x) = g_k(x) + h_k D_k(x) \tag{36}$$

where the direction, $D_k(x)$, is given by

$$D_k(x) = -(1/2)a_g B_k + \left[\sum_y (a_g B_k)^2 \Big/ \sum_y (a_g B_{k-1})^2 \right] D_{k-1}(x) \ . \tag{37}$$

which, using Eqs. (28) and (31) can be written as

$$D_k(x) = g_k'(x) - g_k(x) + (B_k/B_{k-1})D_{k-1}(x) \tag{38}$$

where one would start the first iteration with $D_1(x) = g_1'(x) - g_1(x)$. After using Eq. (36), one would employ Eq. (35) to form the new estimate, as indicated in Figure 3.

Numerous variations on these gradient methods are possible. For example, one could argue that from one iteration to the next, the solution is going in the following direction,

$$D_k(x) = g_k'(x) - g_{k-1}'(x) \tag{39}$$

Since the step in that direction may be too small, a better point to go to would be

$$g_k''(x) = g_k'(x) + h_k[g_k'(x) - g_{k-1}'(x)] \qquad (40)$$

where the parameter h_k controls the step size. In Eq. (40), one jumps from the point $g_k'(x)$ rather than from $g_k(x)$ since presumably $g_k'(x)$ is closer to the solution than $g_k(x)$. After using Eq. (40), one would employ Eq. (35) to form the new estimate.

A method that does not seem as practical for this problem is that of (damped) least squares (or Newton-Raphson)[14-16]. Since each iteration of a least-squares method involves the inversion of N^2 by N^2 matrix, a large number of iterations of one of the gradient methods or of one of the iterative Fourier transform methods described in the next section could be performed in the same time it takes to do a single iteration of least squares. Furthermore, as has been discussed above, one can readily find a point $g_k''(x) = g_k'(x)$ at which the error B is equal to zero, and so a more sophisticated (and more difficult) method, such as least squares, of finding such a point is not warranted.

The problem here is that one is constantly running into the object-domain constraints on g(x). An approach that would be superior to the ones considered here would be one that minimizes the Fourier-domain error while inherently satisfying the object-domain constraints, or one that minimizes an error metric that combines the Fourier-domain constraints and the object-domain constraints. An example of the former is the use of a gradient search method for the problem of two intensity measurements; by searching over $\theta(x)$, one automatically satisfies the object-domain constraint that it have a given modulus, $|f(x)|$. Something along these lines would be very useful for the problem of a single intensity measurement; clearly, more could be done in this area.

5. INPUT-OUTPUT ALGORITHMS

A solution to the problem of the slow convergence of the error-reduction algorithm has been the input-output algorithm, which has

proven to converge faster for both the problem of two intensity measurements [6,17] and the problem of a single intensity measurement[4,5]. The input-output algorithm differs from the error-reduction algorithm only in the object-domain operation. The first three operations -- Fourier transforming g(x), satisfying the Fourier domain constraints, and inverse Fourier transforming the result -- are the same for both algorithms. Those three operations, if grouped together as indicated in Figure 4, can be thought of as a nonlinear system having an input g(x) and an output g'(x). The useful property of this system is that its output is always an image having a Fourier transform that satisfies the Fourier-domain constraints. Therefore, if the output also satisfies the object-domain constraints, then it is a solution to the problem. Unlike the error-reduction algorithm and the gradient methods, the input g(x) no longer must be thought of as the current best estimate of the object; instead, it can be thought of as the driving function for the next output, g'(x). The input g(x) does not necessarily satisfy the object-domain constraints. This viewpoint allows one a great deal of flexibility and inventiveness in selecting the next input, and allows for the invention of algorithms that converge more rapidly to a solution. The input-output algorithm, then, is actually a class of algorithms, as will be described below.

As described elsewhere[6,7,17], it has been found that a small change of the input result in a change of the output in the same general direction as the change of the input. More precisely, for a small change of the input, the expected value of the corresponding change of the output is a constant, α, times the change of the input. Since additional nonlinear terms also appear in the output, the change of the output due to a particular change of the input cannot be predicted exactly. Nevertheless, by appropriate changes of the input, the output can be pushed in the general direction that is desired. If a change $\Delta g(x)$ is desired in the output, then a logical

choice of the change of the input to achieve that change of the output would be $\beta\Delta g(x)$, where β is a constant ideally equal to α^{-1}.

For the problem of phase retrieval from a single intensity measurement, the desired change of the output is

$$\Delta g_k(x) = \begin{cases} 0, & x \notin \gamma \\ -g_k'(x), & x \in \gamma \end{cases} \tag{41}$$

where γ is the set of points at which $g_k'(x)$ violates the object-domain constraints. That is, where the constraints are satisfied, one does not require a change of the output; but where the constraints are violated, the desired change of the output, in order to have it satisfy the object-domain constraints, is one that drives it to a value of zero (and therefore, the desired change is the negative of the output at those points). Therefore, a logical choice for the next input is

$$\begin{aligned} g_{k+1}(x) &= g_k(x) + \beta\Delta g_k(x) \\ &= \begin{cases} g_k(x), & x \notin \gamma \\ g_k(x) - \beta g_k'(x), & x \in \gamma \end{cases} \end{aligned} \tag{42}$$

We will refer to the use of Eq. (42) as the basic input-output algorithm.

An interesting property of the nonlinear system (consisting of the set of three steps mentioned above) is that if an output g' is used as an input, then its output will be itself. Since the Fourier transform of g' already satisfies the Fourier-domain constraints, g' is unaffected as it goes through the system. Therefore, irrespective of what input actually resulted in the output g', the output g' can be considered to have resulted from itself as an input. From this point of view, another logical choice for the next input is

$$g_{k+1}(x) = g'_k(x) + \beta \Delta g_k(x)$$

$$= \begin{cases} g'_k(x), & x \notin \gamma \\ g'_k(x) - \beta g'_k(x), & x \in \gamma \end{cases} \tag{43}$$

We will refer to the use of Eq. (43) as the output-output algorithm.

Note that if $\beta = 1$ in Eq. (43), then the output-output algorithm reduces to the error-reduction algorithm of Eq. (10). Since the optimum value of β is usually not unity, the error-reduction algorithm can be looked on as a sub-optimal version of a more general approach.

Still another method of choosing the next input which was investigated is a combination of the upper line of Eq. (43) with the lower line of Eq. (42):

$$g_{k+1}(x) = \begin{cases} g'_k(x), & x \notin \gamma \\ g_k(x) - \beta g'_k(x), & x \in \gamma \end{cases} \tag{44}$$

We will refer to the use of Eq. (44) as the hybrid input-output algorithm. The hybrid input-output algorithm is an attempt to avoid a stagnation problem that tends to occur with the output-output algorithm. The output-output algorithm often works itself into a situation in which the output on successive iterations does not change, despite being far from a solution. For the hybrid input-output algorithm, on the other hand, if at a given value of x, the output remains negative for more than one iteration, then the corresponding point in the input continues to grow larger and larger until eventually that output value must go nonnegative.

For the input-output algorithms, the error E_F is usually meaningless since the input $g_k(x)$ is no longer an estimate of the object. Then the meaningful error is the object-domain error, E_o, given by Eq. (15).

For the problem of phase retrieval from two intensity measurements, the desired change of the output takes a different form, and it is described elsewhere[6,7,17] in the context of a computer holography synthesis problem involving intensity constraints in each of the two domains.

6. EXPERIMENTAL COMPARISON OF PHASE RETRIEVAL ALGORITHMS

In this section the gradient search and input-output algorithms are compared for the problem of phase retrieval from a single intensity measurement, by using them all on the same Fourier modulus data and with the same starting input. For each approach, several different values of the algorithm parameter (h or β) were tried. The principal problem with the error-reduction algorithm is that it tends to stagnate after a few iterations. For this reason, the starting point for the iterations was chosen to be a partially reconstructed image on which the error-reduction algorithm was making slow progress. Figure 5 shows a plot of E_0, the rms error, versus the number of iterations beyond this starting point, using the error-reduction algorithm. Starting at 0.071275, E_0 decreased slowly but steadily to 0.067470 after ten iterations and 0.063373 after 19 iterations. In this paper, all values of E_0 are normalized by dividing by the square root of $\sum[g'(x)]^2$, the total image energy. The object for the experiment described in this section is a digitized photograph of a satellite in a field of view of 128 x 128 pixels, and its Fourier modulus is noise-free.

The algorithms were compared by performing ten iterations of each algorithm, followed by nine iterations of the error-reduction algorithm (a total of 19 iterations) using the same starting input for each. During the first ten iterations, the value of the algorithm parameter β or h was held constant. The reason that each algorithm was followed by nine iterations of the error-reduction algorithm is as follows. In many cases, it has been observed that definite

progress (i.e., improved visual quality of the output image) is being made with an input-output algorithm even though E_0 decreases very little or even increases with each iteration. The relationship between E_0 and the visual image quality is not fully understood, although, of course, one would expect a high degree of correlation between the two. For those cases for which the visual quality improves while E_0 does not, it was found that if one then performs a few (say five or ten) iterations of the error-reduction algorithm, then the visual quality of the output image changes very little, but E_0 decreases rapidly until it becomes more consistent with the visual image quality. Therefore, in order to gauge the true progress of an input-output algorithm using the value of E_0, a few iterations of the error-reduction algorithm are performed after the iterations of the input-output algorithm. For this reason, for all cases the ten iterations of the algorithm being tested were followed by nine iterations of the error-reduction algorithm in order to make a fair comparison.

Plots of E_0 after the set of 19 iterations described above (ten iterations followed by nine iterations of the error-reduction algorithm) are shown in Figure 6 as a function of the algorithm parameter for the various algorithms. Note that both the steepest descent method with $h = 1.0$ and the output-output algorithm with $\beta = 1.0$ are equivalent to the error-reduction algorithm, at $E_0 = 0.063373$, both circled in Figure 6. Comparing these plots, it is seen that the algorithm which most reduced the error after the set of 19 iterations is the hybrid input-output algorithm with a value of β equal to about unity.

For each algorithm, the use of a small algorithm parameter (β or h) leads to a steady but slow decline of E_0. Increasing the value of the parameter increases the speed at which E_0 decreases, until one reaches a point where the parameter is too large and the algorithm becomes unstable. The instability of the algorithm for larger

values of the algorithm parameter is what makes possible more than one local minimum in the plots of E_o versus the algorithm parameter.

For all of the algorithms, keeping h or β fixed for all iterations is not the best possible strategy, particularly for the gradient methods. At the point at which the error-reduction algorithm is converging slowly, the gradient is small, and one must then use a large value of h in order to make rapid progress. However, after using a large value of h for a few iterations, one moves to a point where the gradient is much larger. Then one should use a smaller value of h in order to avoid algorithm instability. If a method for adaptively choosing h at each iteration were devised, then one would expect the gradient methods to perform considerably better than the results shown here using a fixed value of h.

Examples of an alternative to using a fixed value of h and β are shown in Figure 7. For the first ten iterations of each algorithm, the indicated value of h or β was used for iterations k = 1, 3, 5, 7, and 9, and the error-reduction algorithm (h = 1 for the steepest descent and conjugate gradient) was used for iterations k = 2, 4, 6, 8, and 10. The iterations using the error-reduction algorithm help to stabilize the algorithm by moving toward a point where the gradient is smaller. Comparing Figures 6 and 7, it is seen that with this alternative strategy, the optimum value of each algorithm parameter is considerably larger than the optimum value when the parameter is kept constant. At the optimum value of the algorithm parameter, the alternative strategy gave better results (a lower value of E_o at the end of the sequence of 19 iterations) than those shown in Figure 6 for the basic input-output and for the output-output algorithms; the two strategies were comparable for the steepest descent method; and for the hybrid input-output algorithm, the alternative strategy gave poorer results than those shown in Figure 6.

Curve E in Figure 7 shows the result using the algorithm of Eq. (40), using the alternative strategy described above. This and numerous other variations on these algorithms can be used with varying degrees of success.

The results shown in Figures 6 and 7 were for a particular set of Fourier modulus data for a particular stage of reconstruction, and for a particular number of iterations; and the results in other circumstances could be significantly different. At the optimum values of the algorithm parameter in each case, the algorithm parameter was large enough to make the algorithm somewhat unstable, and so substantially different results could be obtained if relatively small changes in starting point, algorithm parameter, or number of iterations were made. In general, slower but steadier progress is made if an algorithm parameter is used that is somewhat smaller than the optimum according to Figures 6 and 7. These results do serve to show trends that can be expected to apply in a wider range of circumstances. Further development is needed to determine the best approach for the general case. As of this writing, the most successful strategy has been to alternate between several (10 to 30) iterations of the hybrid input-output algorithm and a few (5 to 10) iterations of the error-reduction algorithm.

Figure 8 shows E_0 versus the number of iterations past the starting point for the hybrid input-output algorithm with $\beta = 1$ (curve B) and for the error-reduction algorithm (curve A, repeated from Figure 5). Curve B1 shows the results for the set of nineteen iterations described above (ten iterations of the hybrid input-output algorithm followed by nine iterations of the error-reduction algorithm). Curve B2 shows the results of twenty iterations of the hybrid input-output algorithm followed by a few iterations of the error-reduction algorithm. The instability of the hybrid input-output algorithm is seen in Curve B, in which E_0 increases from 0.071275 to 0.137707 during the first four iterations. By the end

of ten iterations E_0 decreases to 0.091176, still worse than the starting point, although the appearance of the image is improved from the starting point. At the eleventh iteration of Curve B1, the first iteration of the error-reduction algorithm, E_0 drops sharply to a value of 0.047244, although the appearance of the output image changes little from that of the tenth iteration. If after the tenth iteration the hybrid input-output iterations are continued for ten more iterations (Curve B2), then E_0 continues to decrease to well below the level of E_0 for the error-reduction algorithm alone (Curve A). Similar to the case of B1, after the twentieth iteration of the hybrid input-output algorithm (Curve B2), when a few iterations of the error-reduction algorithm were performed, again E_0 fell rapidly to a level consistent with the improved image quality that was present. This is the characteristic of the input-output algorithms that mandated the use of a few iterations of the error-reduction algorithm to make a fair comparison. For the input-output algorithms, the image quality is often better than what one would infer from the value of E_0.

7. DIAMETER CONSTRAINT, STARTING INPUT, AND STRIPES

A side issue which is pertinent to all algorithms is how one defines the diameter of the object for the purpose of applying the diameter constraint in the object domain. For the problem of phase retrieval from a single intensity measurement, the object is usually of finite extent and on a dark (zero value) background. Then bounds on the support of the object (the set of points over which the object is nonzero) can be determined from the support of the autocorrelation, which, being the inverse Fourier transform of the square of the Fourier modulus, can be computed from the given data. As shown in Reference 10, for extended objects the support of the autocorrelation usually does not uniquely define the support of the object. Nevertheless, reasonably tight bounds can be made on the support of

the object. Locator sets[10] can be defined that contain all possible solutions. One can therefore define a region (a "mask") outside of which the output image is constrained to be zero. That is, the set γ defined in Eq. (10) includes all points outside the mask for which $g'_k(x) \neq 0$. One need not use this information in order for the algorithm to converge, but it is desirable to do so, since using this additional information speeds up the convergence of the algorithm.

A problem often occurs with the diameter constraint even though the mask region is correctly defined. If the partially reconstructed image, $g'_k(x)$, is not centered in the mask region, then in applying the diameter constraint, one might be inadvertently trying to "chop off" (truncate) one part of the object, which usually results in stagnation of the algorithm. For this reason, it is usually advantageous to define the mask as being somewhat larger than the extent of the object.

We have found a good strategy for choosing the mask, as follows. For the first several iterations, define a smaller mask which very tightly constrains the object. This helps to speed up the convergence of the algorithm initially, but slows it down for later iterations when the problem mentioned above becomes more significant. Then for later iterations, use a larger mask which insures that none of the solution is being truncated by the mask. Logical choices for masks are any of the locator sets[10].

Faster convergence can be expected if the starting input, $g_1(x)$, is closer to the solution. A good starting input is formed as follows. Compute the autocorrelation function, and then demagnify it by a factor of two (save only every other pixel in both dimensions). Then threshold the demagnified autocorrelation at a value which is a small fraction of its peak, setting it equal to zero wherever it is below the threshold value. Finally, replace each value above the

threshold with a sample of a random variable uniformly distributed between zero and unity. The result is a random (unbiased) starting input having approximately the same size and shape as the original object.

A curious phenomenon often occurs for the problem of phase retrieval from a single intensity measurement. The phase retrieval algorithm often stagnates at a local minimum characterized by a pattern of stripes across the image[18,19]. In most cases, the stripes are barely noticeable and are of low contrast, superimposed on an otherwise excellent reconstructed image. In some cases, the stripes are of high enough contrast to be objectionable, although they still permit the object to be recognized. The cause of this phenomenon is not well understood, but it is thought that it is an algorithm convergence problem rather than a uniqueness problem[19] (it is at a local, not a global, minimum of E_0). A method of avoiding this phenomenon is presently being sought, although it fortunately is not much of a problem in most cases.

8. IMAGE RECONSTRUCTION EXAMPLE

An example of a computer experiment using the iterative reconstruction algorithm for the problem of phase retrieval from a single intensity measurement is shown in Figure 9. In this example, a realistic simulation was performed to arrive at the kind of noisy Fourier modulus data that would be provided by stellar speckle interferometry[20], including the effects of atmospheric turbulence and photon noise[18].

An undegraded object, a digitized photograph of a satellite, shown in Figure 9(a), was convolved with 156 different point-spread functions to produce 156 different blurred images. Each of the point-spread functions represented a different realization of the effects of the turbulent atmosphere. The blurred images were then

subjected to a Poisson noise process to simulate the effects of photon noise. For this example, there were approximately 300,000 photons per degraded image (or on the order of 100 photons per pixel over the extent of the object), which is realistic for objects of this type when imaged through a telescope of diameter 1.2 meters. Two of the resulting 156 degraded images are shown in Figures 9(b) and 9(c). The degraded images were then processed by Labeyrie's[20] method, as modified by Goodman and Belsher[21]. The estimate of the modulus of the Fourier transform of the object is given by[18]

$$|\hat{F}(u)| = W(u)\left[\frac{\sum_{m=1}^{M} |I_m(u)|^2 - N_p}{\sum_{m=M+1}^{2M} |S_m(u)|^2}\right]^{1/2} \qquad (45)$$

where $I_m(u)$ is the Fourier transform of the m^{th} degraded image, N_p is the total number of photons detected (it is subtracted in order to compensate for a certain noise bias term that arises in the power spectrum due to photon noise[21]), $S_m(u)$ is the Fourier transform of the m^{th} point-spread function (to provide compensation for the MTF of the speckle interferometry process) and the weighting factor $W(u)$ is the MTF due to the telescope aperture. In practice, the denominator of this expression would be obtained by making measurements on a reference star through an atmosphere having the same statistics as that which blurred the images or by using a model of the effects of atmospheric turbulence. $W(u)$ was included in order to restore the natural MTF due to the telescope aperture which was removed by the denominator of the equation above. Figure 9(d) shows the resulting Fourier modulus estimate.

The object was reconstructed (or equivalently, the Fourier phase was retrieved) using the hybrid input-output algorithm alternately with the error-reduction algorithm. The result, shown in Figure 9(e),

agrees very well with the original object shown in Figure 9(a), despite the noise present in the Fourier modulus data. Good reconstructed images were also obtained when only one tenth as many photons were assumed to be available[18].

Figure 10 shows E_o versus the number of iterations for this reconstruction. The starting input used was the randomized demagnified autocorrelation described in the previous section, using a threshold value of 0.004 times the peak of the autocorrelation. For the first ten iterations, the error-reduction algorithm was used, and the mask defining the diameter constraint was chosen to be the region over which the autocorrelation function, spatially demagnified by a factor of two, exceeded 0.004 of its maximum value (providing a fairly tight diameter constraint). For iterations 11 to 20, the error-reduction algorithm was used, and the mask for these and the remaining iterations was chosen to be a square of length 64 pixels, which is larger than the actual object extent of about 60 by 40 pixels (imbedded in an array of 128 by 128 pixels). The error decreased suddenly at the tenth iteration since some positive-valued points that were inside the second mask but outside the first mask were no longer counted as contributing to E_o. By the twentieth iteration, the error-reduction algorithm was converging very slowly. For iterations 21 to 60, the hybrid input-output algorithm, with β equal to one, was used. At first, E_o increased sharply (although the output image appeared no worse than at iteration 20), but then decreased fairly rapidly until stagnating at $E_o \approx 0.05$ at about iteration 55. For iterations 61 to 70, the error-reduction algorithm was used, for which E_o dropped suddenly from 0.05 to 0.02, although the visual appearance of the reconstructed image remained the same as for iteration number 60.

This final value of E_o is comparable to 0.03, the normalized rms error of the Fourier modulus estimate itself[18]. It is impossible to reduce E_o to zero since the noise in the Fourier modulus

estimate results in an inconsistency of the nonnegativity constraint and the Fourier modulus estimate. This inconsistency can be seen from the fact that the autocorrelation estimate computed from the Fourier modulus estimate has areas of negative value.

Reconstruction experiments do not always proceed as smoothly as the one described above. When stagnation occurs before E_0 is reduced to a level consistent with the error in the Fourier modulus data, often the best strategy is to restart the algorithm using a different set of random numbers as the initial input. One must also be careful in the way one chooses the mask as discussed in Section 7. Finally, it is always advisable to reconstruct the image two or three times from the same Fourier modulus data using different starting inputs each time. If the same image is reconstructed each time, then one would have confidence that the solution is unique.

9. COMMENTS AND CONCLUSIONS

For the problem of phase retrieval from a single intensity measurement, it has been shown that the error-reduction algorithm (the Gerchberg-Saxton algorithm applied to this problem) is equivalent to the steepest descent method with a double-length step. Furthermore, it was shown that the error-reduction algorithm converges in the sense that the error monotonically decreases. However, in practice the error-reduction algorithm converges very slowly; and several other algorithms, including other gradient search algorithms which utilize the method of Fourier transforms for rapidly computing the gradient of the error, and the input-output family of iterative Fourier transform algorithms, converge much faster. Of the algorithms investigated so far, the hybrid input-output algorithm has converged the fastest. Nevertheless, the gradient search algorithms also converge reasonably fast, and they deserve further development. The performance of any given algorithm can vary depending on the stage of reconstruction and on what is being reconstructed. Although

a practical phase retrieval algorithm is in hand, there is still an element of trial-and-error involved.

For the problem of a phase retrieval from two intensity measurements, the steepest descent method and the Gerchberg-Saxton algorithm were compared and were found to share some similarities. When manipulating just the object's phase, the object-domain constraint, that the object's modulus equal the measured modulus, is automatically satisfied. Therefore, the gradient search methods seem to be inherently better suited to the problem of two intensity measurements than to the problem of a single intensity measurement.

Not considered here has been the question of the uniqueness of solutions to either of the two phase retrieval problems. There has been considerable controversy surrounding this question, both for the problem of two intensity measurements[2,22,23] and for the problem of a single intensity measurement[24-28]. For the latter problem, the experimental reconstruction results shown here and elsewhere[4,5,10,19] suggest that for complicated two-dimensional objects, the solution is usually unique in practice, even when the Fourier modulus data is corrupted by a considerable amount of noise[19].

This research was supported by the Air Force Office of Scientific Research under Contract No. F49620-80-C-0006.

APPENDIX A

In this appendix, the relationship between the steepest descent method for the problem of two intensity measurements and the Gerchberg-Saxton algorithm is explored.

For the problem of two intensity measurements, the error B is minimized with respect to the phase estimates $\theta(x)$. The partial derivative of B with respect to the value of a given phase, $\theta(x)$, is

$$\partial_\theta B = \frac{\partial B}{\partial \theta(x)} = 2N^{-2} \sum_u [\,|G(u)| - |F(u)|\,] \frac{\partial |G(u)|}{\partial \theta(x)} . \qquad \text{(A-1)}$$

Since

$$\frac{\partial G(u)}{\partial \theta(x)} = \frac{\partial}{\partial \theta(x)} \sum_y |f(y)| \exp [i\theta(y)] \exp [-i2\pi u \cdot y/N]$$

$$= i|f(x)| \exp [i\theta(x)] \exp [-i2\pi u \cdot x/N]$$

$$= ig(x) \exp [-i2\pi u \cdot x/N] , \qquad \text{(A-2)}$$

then

$$\frac{\partial |G(u)|}{\partial \theta(x)} = \frac{G(u)(-i)g^*(x) \exp [i2\pi u \cdot x/N] + \text{c.c.}}{2|G(u)|} \qquad \text{(A-3)}$$

where c.c. indicates the complex conjugate of what precedes it. Using Eq. (27), Eq. (A-1) becomes[2]

$$\partial_\theta B = ig^*(x)[g'(x) - g(x)] + \text{c.c.}$$

$$= ig^*(x)g'(x) + \text{c.c.} = -2 \text{ Im } [g^*(x)g'(x)]$$

$$= -2 |f(x)||g'(x)| \sin [\theta'(x) - \theta(x)] \qquad \text{(A-4)}$$

where $\theta'(x)$ is the phase of $g'(x)$. Therefore, the gradient can be easily computed using two Fourier transforms (the first three steps of the Gerchberg-Saxton algorithm) plus evaluating Eq. (A-4). Analogous to the linear approximation of Eq. (29) is

$$B \approx B_k + \sum_x \partial_\theta B_k [\theta(x) - \theta_k(x)] \qquad \text{(A-5)}$$

where $\partial_\theta B_k$ is $\partial_\theta B$ evaluated at $\theta(x) = \theta_k(x)$, the phase of $g_k(x)$. This linear expansion of B is equal to zero for

$$\theta(x) - \theta_k(x) = - \frac{B_k \partial_\theta B_k}{\sum_y (\partial_\theta B_k)^2} . \qquad \text{(A-6)}$$

which can be easily verified by inserting Eq. (A-6) into Eq. (A-5). By Eq. (A-4),

$$\sum_y (\partial_\theta B_k)^2 = 4 \sum_y |f(y)|^2 |g_k'(y)|^2 \sin^2 [\theta_k'(y) - \theta_k(y)] , \qquad \text{(A-7)}$$

and so Eq. (A-6) becomes

$$\theta(x) - \theta_k(x) = \frac{B_k |f(x) g_k'(x)| \sin [\theta_k'(x) - \theta_k(x)]}{2 \sum_y |f(y)|^2 |g_k'(y)|^2 \sin^2 [\theta_k'(y) - \theta_k(y)]} . \qquad \text{(A-8)}$$

Now consider the situation after several iterations have been performed, and the error is decreasing slowly. Then for most values of x,

$$\sin [\theta_k'(x) - \theta_k(x)] \approx \theta_k'(x) - \theta_k(x) . \qquad \text{(A-9)}$$

Then from Eq. (A-8), it is seen that $\theta(x) - \theta_k(x)$, which is the change of $\theta_k(x)$ indicated by the steepest descent method, is approximately proportional to $\theta_k'(x) - \theta_k(x)$. Recall from Eq. (9) that $\theta_k'(x)$ is new phase that would be given by the Gerchberg-Saxton algorithm. Thus, for the problem of two intensity measurements, the steepest descent method gives a new phase that is going in the same general direction as the Gerchberg-Saxton algorithm, but uses a

different step size. For the steepest descent method, the direction differs somewhat from $\theta'_k(x) - \theta_k(x)$ due to the weighting factor $|f(x)g'_k(x)|$ which varies with x.

In order to obtain some notion of the step size for the steepest descent method, continue to consider the situation where the sum is decreasing and Eq. (A-9) applies. Then using Eq. (16), one can approximate

$$B_k = \sum_x \left| |f(x)| \exp [i\theta_k(x)] - |g'_k(x)| \exp [i\theta'_k(x)] \right|^2$$

$$= \sum_x \left\{ |f(x)|^2 + |g'_k(x)|^2 - 2|f(x)g'_k(x)| \cos [\theta'_k(x) - \theta_k(x)] \right\}$$

$$= \sum_x [\,|f(x)| - |g'_k(x)|\,]^2 + \sum_x |f(x)g'_k(x)| \sin^2 [\theta'_k(x) - \theta_k(x)] \tag{A-10}$$

In order to further simplify things, consider the special case for which $f(x) = f_a$, a constant independent of x. Furthermore, if B is small, then for most values of x,

$$\left| |f(x)| - |g'_k(x)| \right| \ll |f(x)| \,. \tag{A-11}$$

Under these circumstances, inserting Eqs. (A-9) and (A-10) into (A-8) yields

$$\theta(x) - \theta_k(x) \approx \frac{1}{2} \left[1 + \frac{B_k^r}{B_k^t} \right] [\theta'_k(x) - \theta_k(x)] \tag{A-12}$$

where

$$B_k^r = \sum_x [\,|f(x)| - |g'_k(x)|\,]^2 \tag{A-13}$$

and

$$B_k^t = \sum_x |g_k'(x)|^2 [\theta_k'(x) - \theta_k(x)]^2 \qquad \text{(A-14)}$$

are the respective "radial" and "tangential" components of the error $B_k = B_k^r + B_k^t$. The radial component, B^r, is the object-domain squared error of the modulus of $|g_k'(x)|$ and is equal to E_{Ok}^2 according to Eq. (14). When the error is decreasing slowly, then

$$B_k^t \simeq B_k - B_k^r = E_{Fk}^2 - E_{Ok}^2 << E_{Ok}^2 = B_k^r \qquad \text{(A-15)}$$

Therefore, under these circumstances, the coefficient of Eq. (A-12),

$$\frac{1}{2}\left[1 + \frac{B_k^r}{B_k^t}\right] >> 1 \qquad \text{(A-16)}$$

That is, when the Gerchberg-Saxton algorithm is converging slowly, the steepest descent method indicates that a much larger step size be used. Note that if one uses the double-length step steepest descent method, then the factor of 1/2 in Eqs. (A-8), (A-12) and (A-16) is replaced by unity.

REFERENCES

1. R.W. Gerchberg and W.O. Saxton, "A Practical Algorithm for the Determination of Phase from Image and Diffraction Plane Pictures," Optik 35, 237-46 (1972).

2. W.O. Saxton, Computer Techniques for Image Processing in Electron Microscopy (Academic Press, New York, 1978).

3. R.A. Gonsalves, "Phase Retrieval from Modulus Data," J. Opt. Soc. Am. 66, 961-64 (1976).

4. J.R. Fienup, "Reconstruction of an Object from the Modulus of Its Fourier Transform," Opt. Lett. 3, 27-29 (1978).

5. J.R. Fienup, "Space Object Imaging Through the Turbulent Atmosphere," Opt. Eng. 18, 529-34 (1979).

6. J.R. Fienup, "Iterative Method Applied to Image Reconstruction and to Computer-Generated Holograms," Opt. Eng. 19, 297-305 (1980).

7. J.R. Fienup, "Reconstruction and Synthesis Applications of an Iterative Algorithm," to appear in Transformations in Optical Signal Processing, ed. W.T. Rhodes, J.R. Fienup, and B.E.A. Saleh (Society of Photo-Optical Instrumentation Engineers, Bellingham, WA, 1982).

8. P.M. Hirsch, J.A. Jordan, Jr., and L.B. Lesem, "Method of Making an Object-Dependent Diffuser," U.S. Patent No. 3,619,022 (Nov. 9, 1971).

9. N.C. Gallagher and B. Liu, "Method for Computing Kinoforms that Reduces Image Reconstruction Error," Appl. Opt. 12, 2328-35 (1973).

10. J.R. Fienup, T.R. Crimmins, and W. Holsztynski, "Reconstruction of the Support of an Object from the Support of Its Autocorrelation," to be published in J. Opt. Soc. Am., April 1982.

11. R.N. Bracewell, The Fourier Transform and Its Applications (McGraw-Hill, New York, 1965).

12. R.H. Boucher, "Convergence of Algorithms for Phase Retrieval from Two Intensity Distributions," in 1980 International Optical Computing Conference, Proc. SPIE 231, 130-141 (1980).

13. M.T. Manry and J.K. Aggarwal, "The Design of Multidimensional FIR Digital Filters by Phase Correction," IEEE Trans. Circuits and Systems CAS-23, 185-99 (1976).

14. D.P. Feder, "Automatic Optical Design," Appl. Opt. 2, 1209-26 (1963).

15. D.R. Buchele, "Damping Factor for the Least-Squares Method of Optical Design," Appl. Opt. 7, 2433-35 (1968).

16. B.R. Frieden and D.G. Currie, "On Unfolding the Autocorrelation Function," J. Opt. Soc. Am. 66, 1111 (1976) (Abstract).

17. J.R. Fienup, "Improved Synthesis and Computational Methods for Computer-Generated Holograms," Ph.D. Thesis, Stanford University, May 1975 (University Microfilms No. 75-25523), Chapter 5.

18. G.B. Feldkamp and J.R. Fienup, "Noise Properties of Images Reconstructed from Fourier Modulus," in 1980 International Optical Computing Conference, Proc. SPIE 231, 84-93 (1980).

19. J.R. Fienup, "Fourier Modulus Image Construction," Report RADC-TR-81-63 (1981).

20. A. Labeyrie, "Attainment of Diffraction-Limited Resolution in Large Telescopes by Fourier Analysing Speckle Patterns in Star Images," Astron. and Astrophys. 6, 85-87 (1970); D.Y. Gezari, A. Labeyrie, and R.V. Stachnik, "Speckle Interferometry: Diffraction-Limited Measurements of Nine Stars with the 200-inch Telescope," Astrophys. J. Lett. 173, L1-L5 (1972).

21. J.W. Goodman and J.F. Belsher, "Fundamental Limitations in Linearly Invariant Restoration of Atmospherically Degraded Images," in Imaging Through the Atmosphere, Proc. SPIE 75, 141-54 (1976).

22. A.M.J. Huiser, A.J.J. Drenth, and H.A. Ferwerda, "On Phase Retrieval in Electron Microscopy from Image and Diffraction Pattern," Optik 45, 303-316 (1976); A.M.J. Huiser and H.A. Ferwerda, "On the Problem of Phase Retrieval in Electron Microscopy from Image and Diffraction Pattern II: On the Uniqueness and Stability," Optik 46, 407-20 (1976).

23. A.J. Devaney and R. Chidlaw, "On the Uniqueness Question in the Problem of Phase Retrieval from Intensity Measurements," J. Opt. Soc. Am. 68, 1352-54 (1978).

24. Yu.M. Bruck and L.G. Sodin, "On the Ambiguity of the Image Reconstruction Problem," Opt. Commun. 30, 304-08 (1979).

25. W. Lawton, "A Numerical Algorithm for 2-D Wavefront Reconstruction from Intensity Measurements in a Single Plane," in 1980 International Optical Computing Conference, Proc. SPIE 231, 94-98 (1980).

26. A.M.J. Huiser and P. Van Toorn, "Ambiguity of the Phase-Reconstruction Problem," Opt. Lett. 5, 499-501 (1980).

27. T.R. Crimmins and J.R. Fienup, "Ambiguity of Phase Retrieval for Functions with Disconnected Support," J. Opt. Soc. Am. 71, 1026-29 (1981).

28. J.R. Fienup, "Image Reconstruction for Stellar Interferometry," in Current Trends in Optics, ed. F.T. Arecchi and F.R. Aussenegg (Taylor and Francis, London, 1981), pp. 95-102.

FIGURE CAPTIONS

1. Block diagram of the error-reduction (Gerchberg-Saxton) algorithm.

2. RMS error versus the number of iterations for the problem of phase retrieval from a single intensity measurement using the error-reduction algorithm.

3. Block diagram for the gradient search methods, using the method of Fourier transforms to compute the gradient.

4. Block diagram of the system for the input-output concept.

5. RMS error versus the number of iterations using the error-reduction algorithm.

6. RMS error after a fixed number of iterations versus the algorithm parameter. Curve A: steepest descent method (o); B: conjugate gradient method (•); C: basic input-output algorithm (Δ); D: output-output algorithm (▲); E: hybrid input-output algorithm (□). The result using the error-reduction algorithm is indicated by a large circle.

7. RMS error after a fixed number of iterations (using the alternative strategy) versus the algorithm parameter. Curve A: steepest-descent method (o); B: basic input-output algorithm (•); C: output-output algorithm (Δ); D: hybrid input-output algorithm (▲); E: the algorithm of Eq. (40) (□).

8. RMS error versus the number of iterations for the error-reduction algorithm (Curve A), and for the hybrid input-output algorithm (Curve B -- see text).

9. Image reconstruction experiments. (a) Undegraded object; (b), (c) examples of degraded images simulated to include the effects of atmospheric turbulence and photon noise; (d) Fourier modulus estimate computed from the degraded images; (e) image reconstructed using the iterative algorithm.

10. RMS error versus the number of iterations.

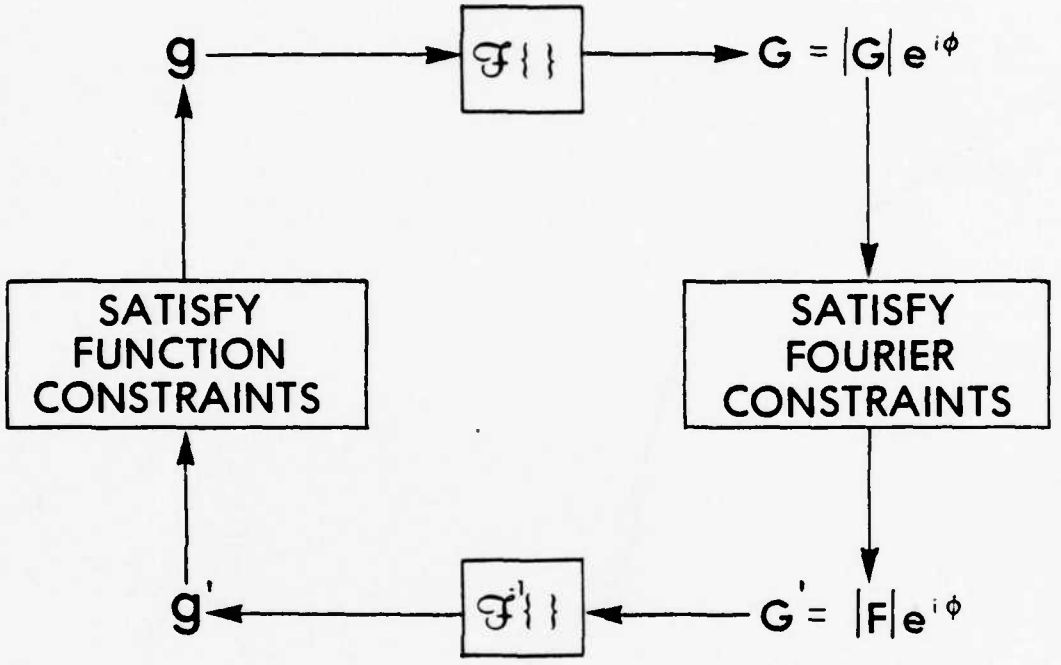

Figure 1. Block diagram of the error-reduction (Gerchberg-Saxton) algorithm.

Figure 2. RMS error versus the number of iterations for the problem of phase retrieval from a single intensity measurement using the error-reduction algorithm.

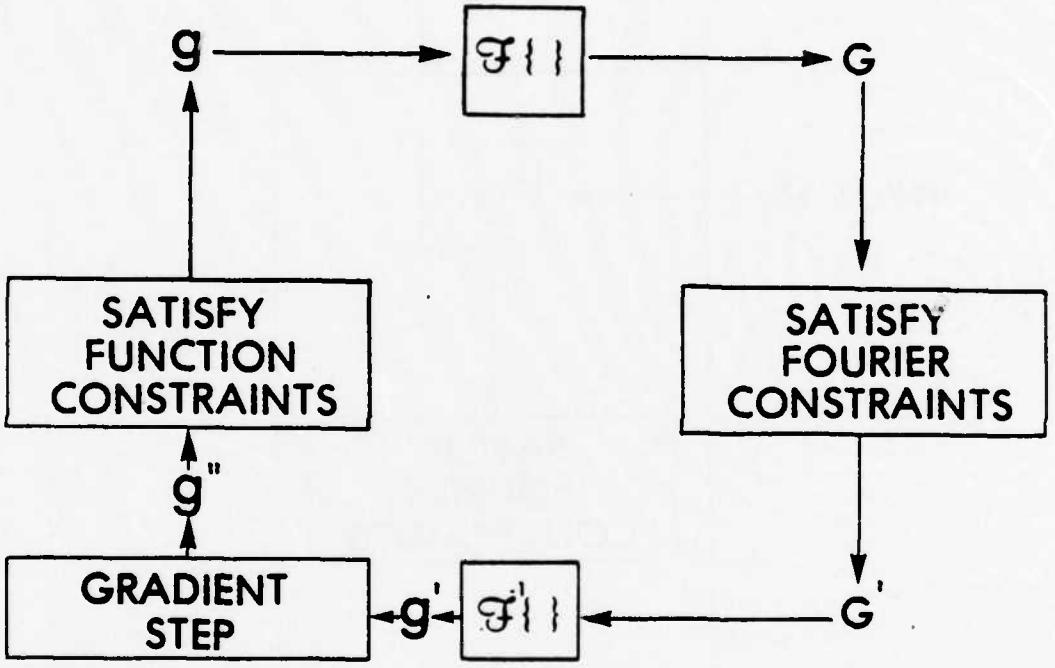

Figure 3. Block diagram for the gradient search methods, using the method of Fourier transforms to compute the gradient.

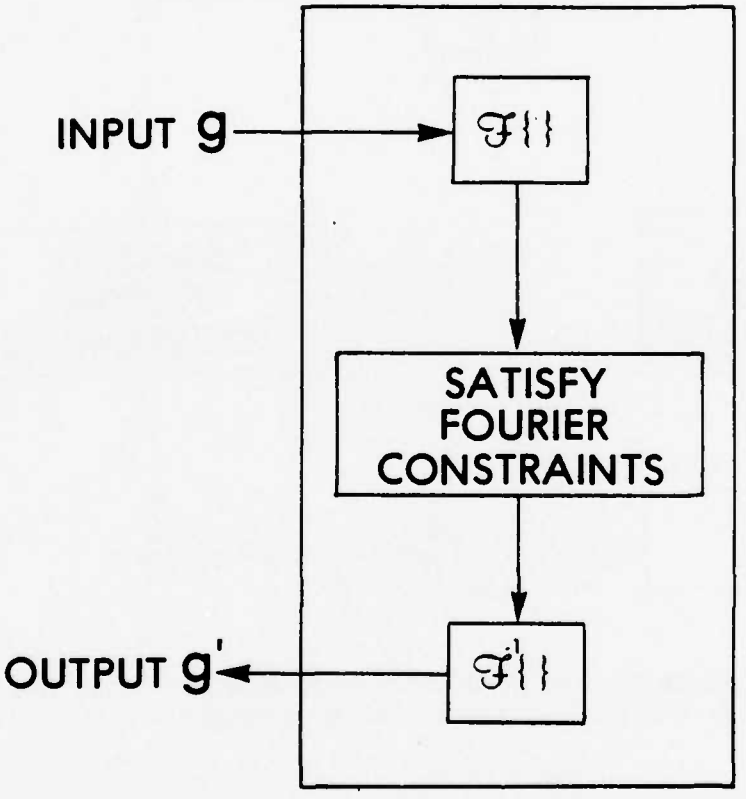

Figure 4. Block diagram of the system for the input-output concept.

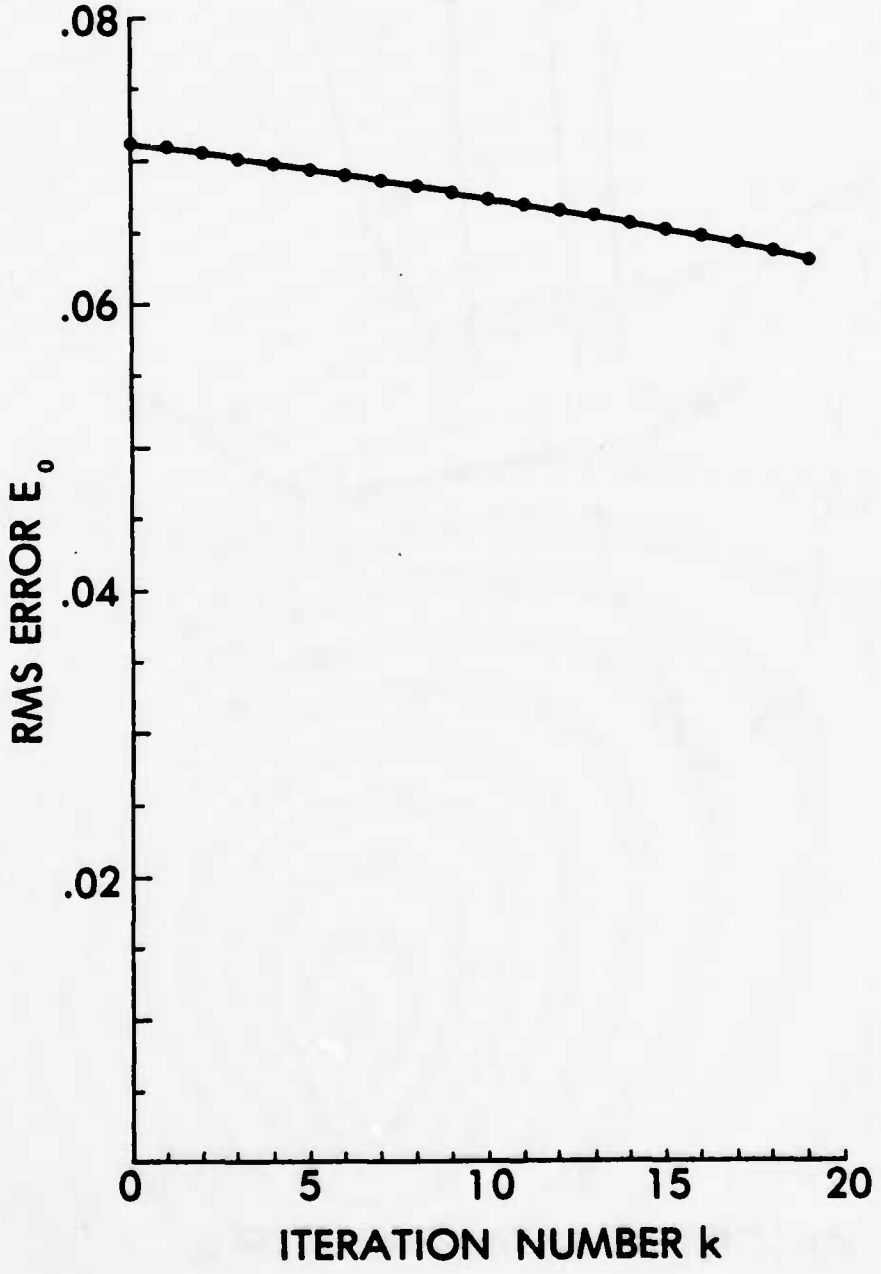

Figure 5. RMS error versus the number of iterations using the error-reduction algorithm.

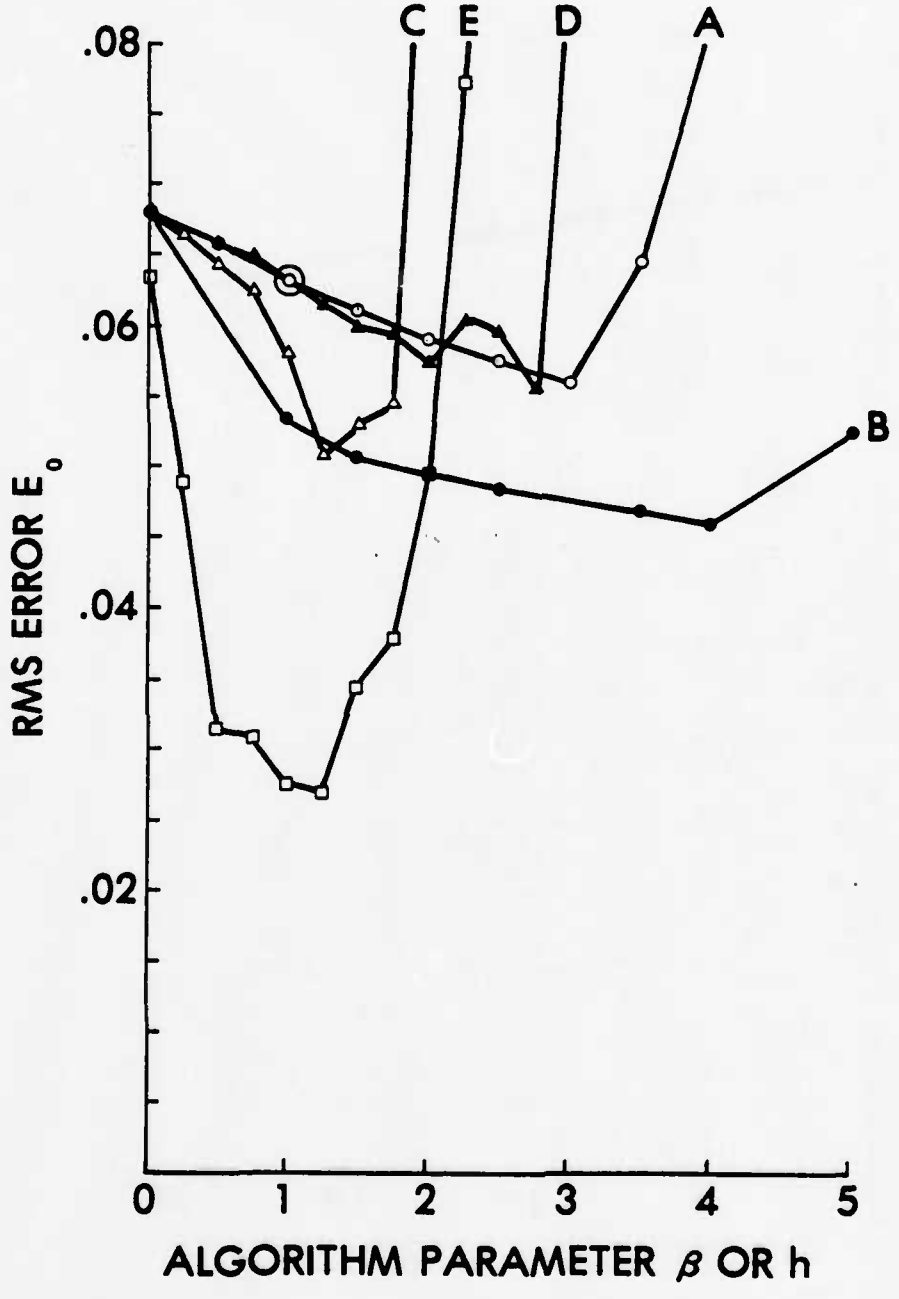

Figure 6. RMS error after a fixed number of iterations versus the algorithm parameter. Curve A: steepest descent method (o); B: conjugate gradient method (•); C: basic input-output algorithm (Δ); D: output-output algorithm (▲); E: hybrid input-output algorithm (□). The result using the error-reduction algorithm is indicated by a large circle.

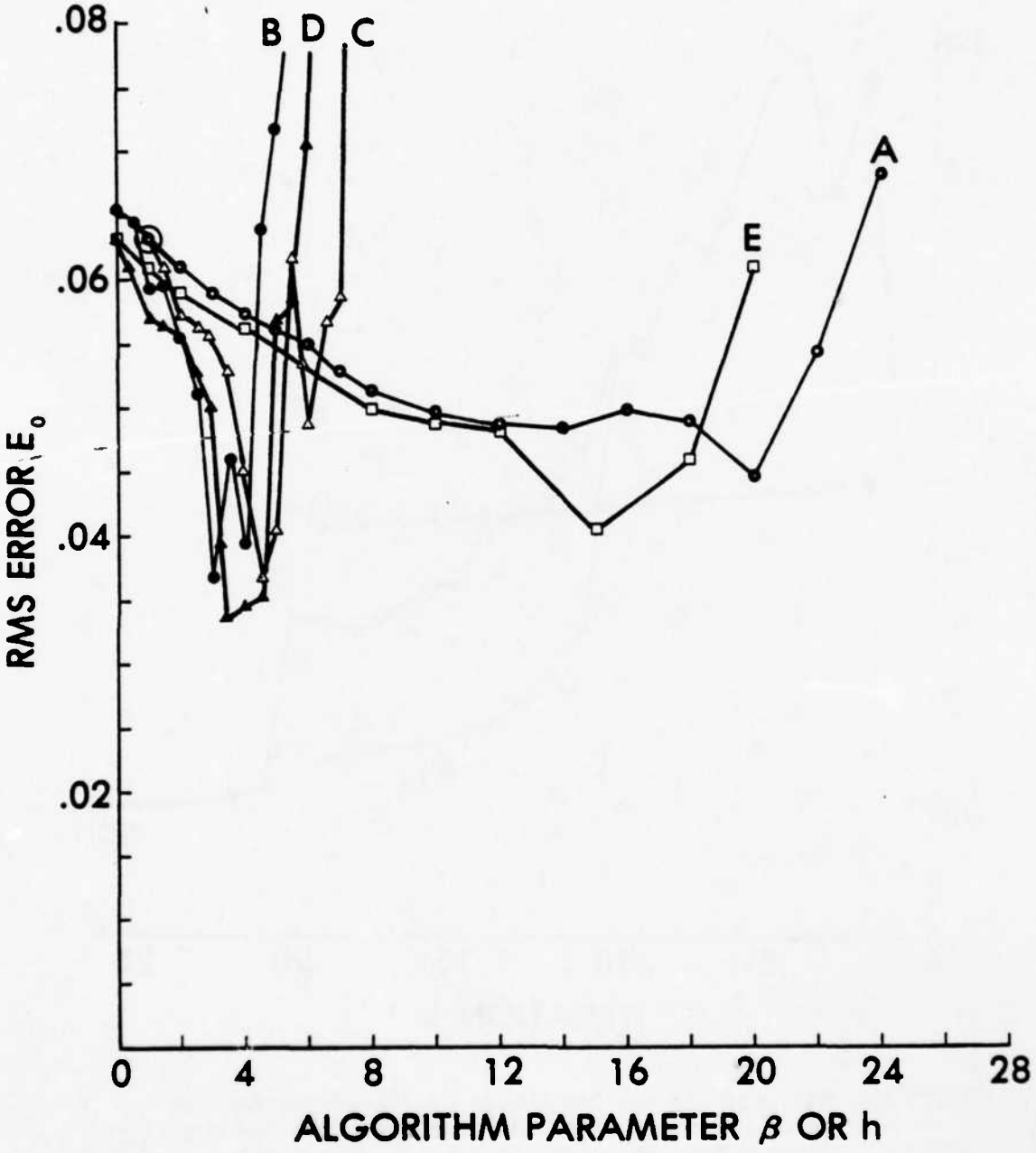

Figure 7. RMS error after a fixed number of iterations (using the alternative strategy) versus the algorithm parameter. Curve A: steepest-descent method (o); B: basic input-output algorithm (•); C: output-output algorithm (Δ); D: hybrid input-output algorithm (▲); E: the algorithm of Eq. (40) (□).

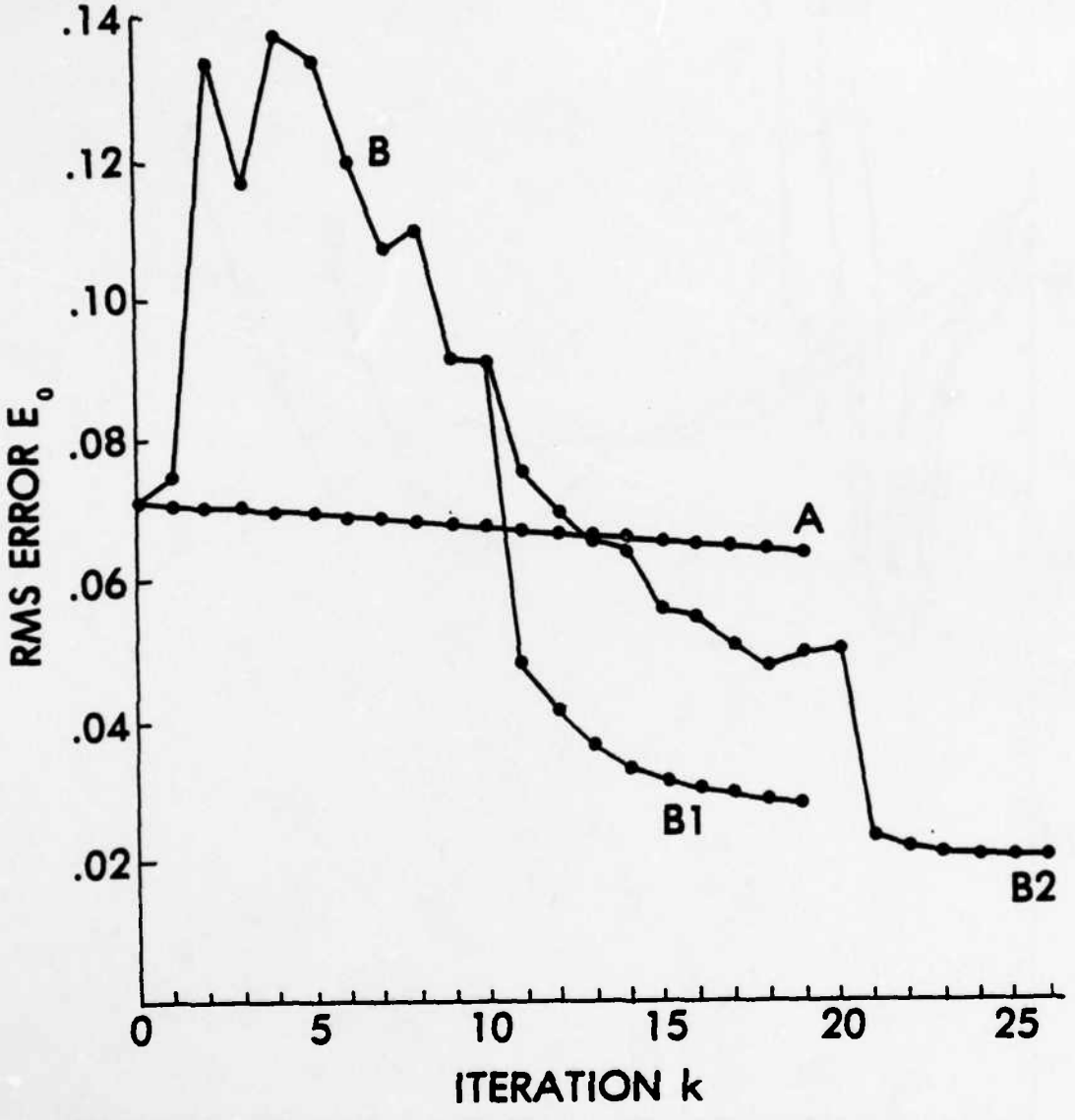

Figure 8. RMS error versus the number of iterations for the error-reduction algorithm (Curve A), and for the hybrid input-output algorithm (Curve B -- see text).

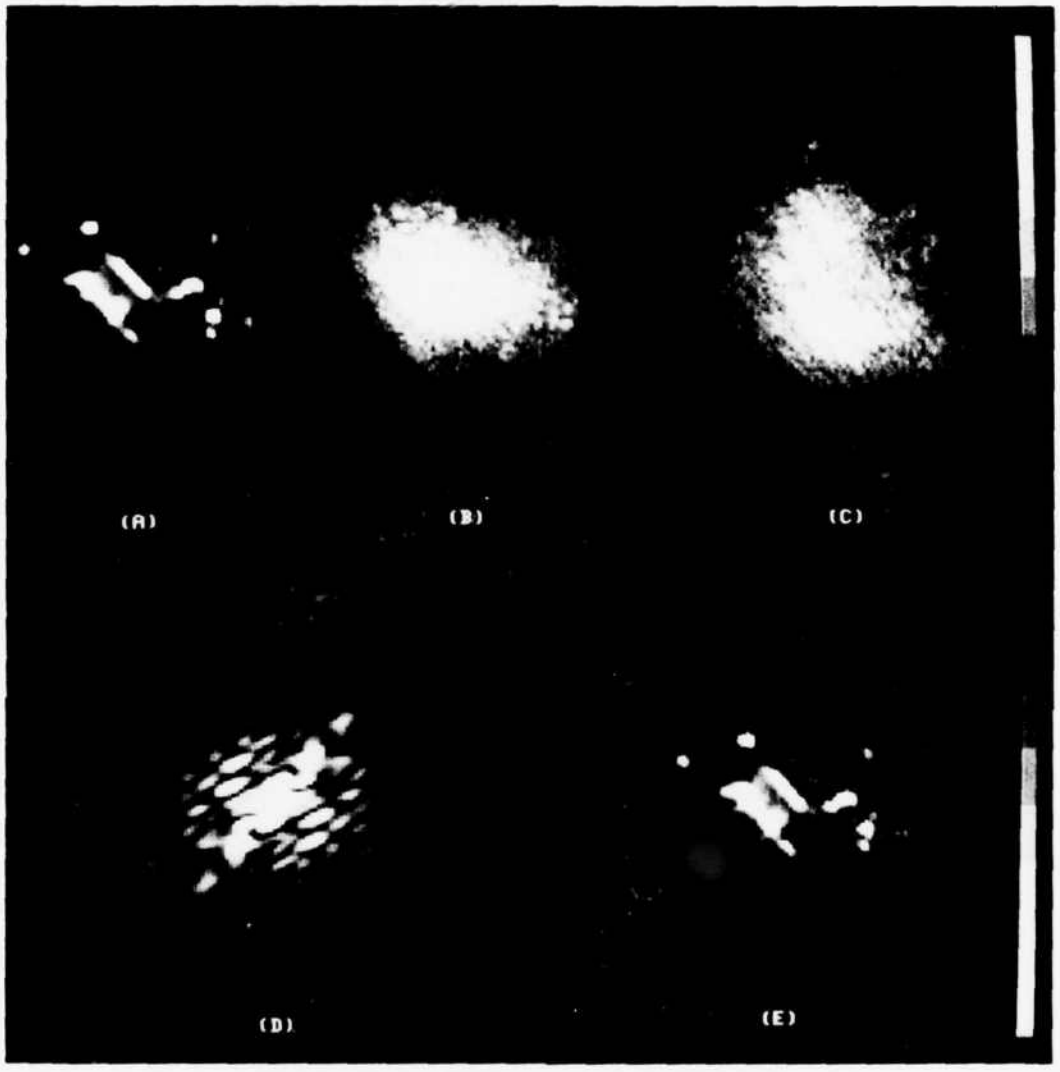

Figure 9. Image reconstruction experiments. (a) Undegraded object; (b), (c) examples of degraded images simulated to include the effects of atmospheric turbulence and photon noise; (d) Fourier modulus estimate computed from the degraded images; (e) image reconstructed using the iterative algorithm.

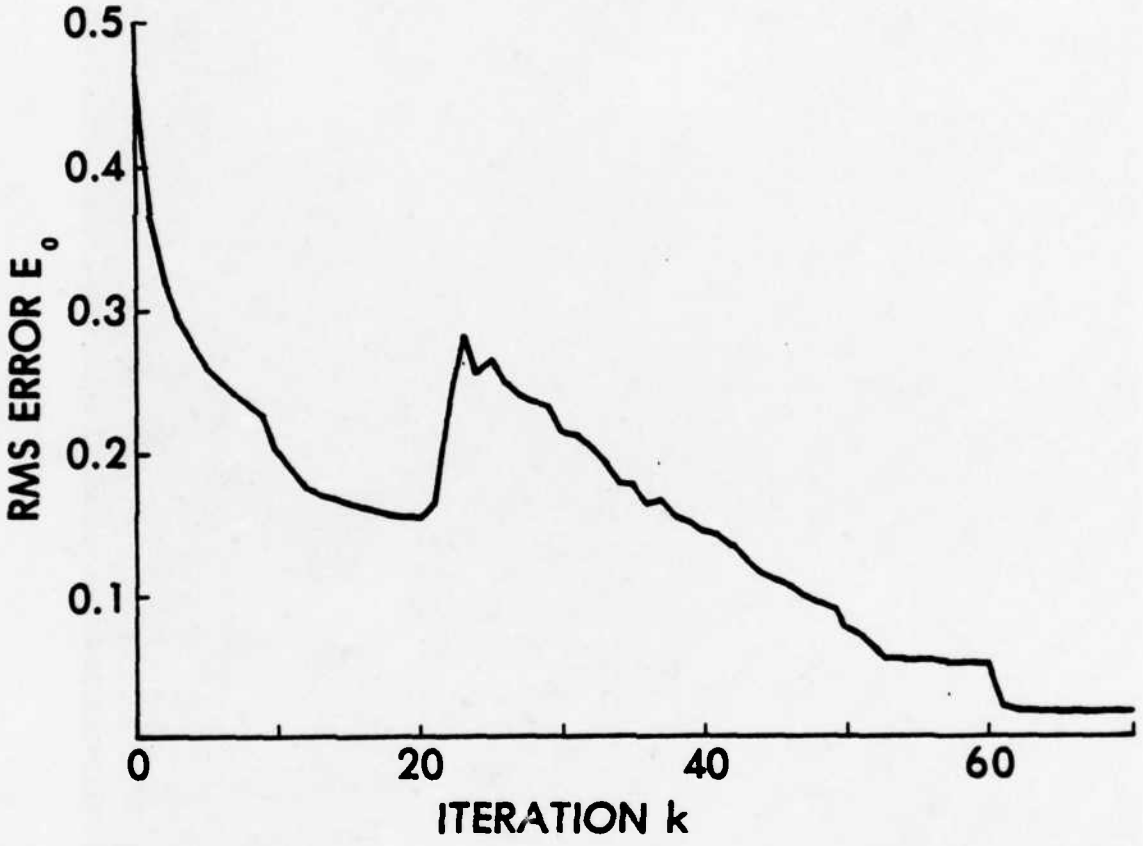

Figure 10. RMS error versus the number of iterations.

Appendix I

RECONSTRUCTION AND SYNTHESIS APPLICATIONS OF AN ITERATIVE ALGORITHM

J.R. Fienup
Environmental Research Institute of Michigan
Radar and Optics Division
P.O. Box 8618, Ann Arbor, Mich. 48107

ABSTRACT

This paper reviews the Gerchberg-Saxton algorithm and variations thereof that have been used to solve a number of difficult reconstruction and synthesis problems in optics and related fields. It can be used on any problem in which only partial information (including both measurements and constraints) of the wavefront or signal is available in one domain and other partial information is available in another domain (usually the Fourier domain). The algorithm combines the information in both domains to arrive at the complete description of the wavefront or signal. Various applications are reviewed, including synthesis of Fourier transform pairs having desirable properties as well as reconstruction problems. Variations of the algorithm and the convergence properties of the algorithm are discussed.

To appear in Transformations in Optical Signal Processing, ed. W.T. Rhodes, J.R. Fienup, and B. Saleh (Society of Photo-Optical Instrumentation Engineers, Bellingham, WA, 1982); and presented at the SPIE Institute, Seattle, WA, February 1981.

1. INTRODUCTION

There exist many problems that are very difficult to solve in astronomy, X-ray crystallography, electron microscopy, spectroscopy, wavefront sensing, holography, particle scattering, superresolution, radar signal and antenna synthesis, filter design, and other disciplines which share an important feature. These are problems which involve the reconstruction or synthesis of a wavefront (or an object or a signal, etc.) when partial information or constraints exists in each of two different domains. The second domain is usually the Fourier transform domain. This paper describes a method of combining all the available information in the two domains to arrive at a complete description and thereby solving the problems.

The problems fall into two general categories: (1) reconstruct the entire information about a function (an image, wavefront, signal, etc.) when only partial information is available in each of two domains; and (2) synthesize a (Fourier) transform pair having desirable properties in both domains. A reconstruction problem arises when only partial information is measured in one domain, and in the other domain, either partial information is measured or certain constraints are known a priori. The information available in any one domain is insufficient to reconstruct the function or its transform. A synthesis problem typically arises when one wants the transform of a function to have certain desirable properties (such as uniform spectrum, low sidelobes, etc.) while the function itself must satisfy certain constraints or have certain desirable properties. Because arbitrary sets of properties and constraints can be contradictory, there may not exist a transform pair that is completely desirable and satisfies all the constraints. Nevertheless, one seeks a transform pair that comes as close as possible to having the desirable properties and satisfying the constraints in both domains.

Both the reconstruction and the synthesis problems can be expressed as follows, if the meaning of the word "constraints" is

broadened to include any kind of measured data, desirable properties, or a priori conditions:

> Given a set of constraints placed on a function and another set of constraints placed on its transform, find a transform pair (i.e., a function and its transform) that satisfies both sets of constraints.

Once a solution is found to such a problem, the question often remains: is the solution unique? For synthesis problems, the uniqueness is usually unimportant — one is satisfied with any solution that satisfies all the constraints; often a more important problem is whether there exists any solution that satisfies what may be arbitrary and conflicting constraints. For reconstruction problems, the uniqueness properties of the solution are of central importance. If many different functions satisfying the constraints could give rise to the same measured data, then a solution that is found could not be guaranteed to be the correct solution. The question of uniqueness must be studied for each problem. Fortunately, as will be described later, for some important reconstruction problems the solution usually is unique.

An effective approach to solving the large class of problems described above is the use of iterative algorithms related to the Gerchberg-Saxton algorithm[1]. The algorithms involve the iterative transformation back and forth between the two domains, repetitively applying the known constraints in each domain.

The basic algorithm is presented in Section 2. A number of different applications having different types of constraints are described, and examples are shown in Section 3. In Section 4 the convergence properties of the algorithm are discussed, and improved versions of the algorithm are reviewed. A brief summary and comments are included in Section 5.

2. THE BASIC ITERATIVE ALGORITHM

The first published account of the iterative algorithm was its use by Gerchberg and Saxton[1] to solve the electron microscopy problem in which both the modulus of a complex-valued image and the modulus of its Fourier transform are measured, and the goal is to reconstruct the phase in both domains. Apparently unknown to them, it was invented somewhat earlier by Hirsch, Jordan, and Lesem[2] to solve a synthesis problem for computer-generated holograms which has a similar set of constraints. (This will be described later in more detail.) The method was again reinvented for a similar problem in computer holography by Gallagher and Liu[3]. The fact that the algorithm was invented repeatedly testifies to its simplicity and effectiveness.

2.1 The Gerchberg-Saxton Algorithm

In what immediately follows, the iterative algorithm is described in terms of its application to the electron microscopy reconstruction problem. An excellent treatment of the electron microscopy phase problem and its solution by this and other methods can be found in Reference 4. Later it is shown how to apply the same principles to a large class of problems.

Suppose that the electron wave function in an image plane is described by the two-dimensional complex-valued function

$$f(x) = |f(x)|\, e^{i\psi(x)} \tag{1}$$

Its Fourier transform, the wave function in a far-field diffraction plane, is given by

$$F(u) = |F(u)|\, e^{i\theta(u)} = \mathcal{F}[f(x)] = \int_{-\infty}^{\infty} f(x)\, e^{-i2\pi u \cdot x}\, dx \tag{2}$$

where x and u are the vector coordinates in the spatial (image) domain and the spatial frequency (far-field diffraction) domain,

respectively. The notation used throughout this paper is that functions represented by capital letters are the Fourier transforms of the functions represented by the corresponding lower-case letters. It is assumed that the intensity spatial distributions are measured in each domain, but the phase information is lost. Therefore one wishes to reconstruct $\psi(x)$ and $\theta(x)$ from $|f(x)|$ and $|F(u)|$.

The iterative algorithm for solving this problem is depicted in Figure 1. One iteration (the k^{th} iteration) of the algorithm proceeds as follows. A trial solution for the wave function (an estimate of the wave function), $g_k(x)$, is Fourier transformed yielding

$$G_k(u) = |G_k(u)| \exp [i\phi_k(u)] = \mathcal{F}[g_k(x)] \tag{3}$$

Then a new Fourier-domain function, $G'_k(u)$, is formed by replacing the computed Fourier modulus by the measured Fourier modulus, $|F(u)|$, and keeping the computed phase:

$$G'_k(u) = |F(u)| \exp [i\phi_k(u)] \tag{4}$$

The resulting $G'_k(u)$, which is in agreement with all the known measurements and constraints in the Fourier domain, is inverse Fourier transformed yielding the wave function $g'_k(x)$. Then the iteration is completed by forming a new estimate for the wave function, $g_{k+1}(x)$, which is obtained by replacing the computed modulus of $g_k(x)$ with the measured modulus $|f(x)|$, and keeping the computed phase.

The algorithm consists of no more than enforcing what information is available on the wave function, Fourier transforming, imposing what information is available on the wave function's Fourier transform, inverse transforming; and repeating these simple operations for a number of iterations. What makes the algorithm practical is the existence of a fast Fourier transform[5] (FFT), so that the number of computations per iteration goes only as N log N, where N is the number of samples of the function computed. This compares very favorably with some other iterative methods, such as Newton-Raphson[4], for which the number of computations per iteration goes as N^3.

A measure of the progress of the iterations, and a criterion by which one can determine when a solution has been found, is the normalized mean-squared error, which is defined in the Fourier domain by

$$E_F^2 = \frac{\int_{-\infty}^{\infty} [|G_k(u)| - |F(u)|]^2 \, du}{\int_{-\infty}^{\infty} |F(u)|^2 \, du} \tag{5}$$

or in the image domain by

$$E_0^2 = \frac{\int_{-\infty}^{\infty} [|g_k'(x)| - |f(x)|]^2 \, dx}{\int_{-\infty}^{\infty} |f(x)|^2 \, dx} \tag{6}$$

It has been shown that the algorithm converges in the sense that the mean-squared error can only decrease at each iteration.[1,4,6] The issue of convergence will be discussed in greater detail in Section 4.

2.2 The Error-Reduction Iterative Algorithm

It is now known that with slight modifications this same algorithm can be applied to many different problems having a variety of available constraints or measurements[7]. Let the function $f(x)$ represent a wave front, an object, a signal, an antenna array, a spectral density function, an electron density function, etc., where x is an N-dimensional vector (spatial, angular, time, etc.) coordinate. Depending on the problem, $f(x)$ may be complex valued or real valued, and, if real, may or may not be nonnegative. Its Fourier transform, $F(u)$, is given by Eq. (2), and is complex valued for most problems. The N-dimensional vector u is a (spatial, angular, time, etc.) frequency coordinate. One can instead consider another transformation of $f(x)$, such as the Fresnel transform, which has been done for more than one problem.[2,8,9] For simplicity of discussion, the

Fourier transform will be assumed, but the reader should keep in mind that what is said also applies to a number of other transformations as well (although the method becomes less attractive if a fast transform algorithm is not available).

With only slight modifications, the Gerchberg-Saxton algorithm can be used to solve the wide class of problems described in Section 1. Referring again to the block diagram of the algorithm in Figure 1, all that is required is to impose constraints in each domain that are pertinent to the problem of interest. Just as for the electron microscopy problem, at the k^{th} iteration, $g_k(x)$, an estimate of $f(x)$, is Fourier transformed, yielding $G_k(u)$ given by Eq. (3). Then a new Fourier-domain function $G_k'(u)$ is formed from $G_k(u)$ by making the smallest possible changes in $G_k(u)$ that allow it to satisfy the Fourier-domain constraints. For example, if the Fourier domain constraint is that the Fourier modulus equals $|F(u)|$ over some region of the Fourier domain, then $|F(u)|$ is substituted for $|G_k(u)|$ in that region of the Fourier domain. The new Fourier-domain function $G_k'(u)$, which satisfies the Fourier-domain constraints, is inverse Fourier transformed to yield $g_k'(x)$. To complete one iteration, a new estimate $g_{k+1}(x)$ is formed from $g_k'(x)$ by making the smallest possible changes in $g_k(x)$ that allow it to satisfy the function-domain constraints. One example is that if the function is complex valued and it is constrained to have a modulus equal to $|f(x)|$ over some region of space, then $|f(x)|$is substituted for $|g_k(x)|$ in that region. A special case of this is when the function is to be zero outside a certain interval (then the Fourier function is bandlimited). Another example is that if the function is constrained to be nonnegative, then $g_{k+1}(x)$ is set equal to $g_k'(x)$ for those x where $g_k'(x) \geq 0$, and $g_{k+1}(x)$ is set equal to zero for those x where $g_k'(x) < 0$. In summary, one transforms back and forth between the two domains, forcing the function to satisfy the constraints in each domain.

For reconstruction problems, whatever characteristics of the actual $F(u)$ and $f(x)$ that are measured or are known a priori are imposed on $G_k(u)$ and $g_k'(x)$, respectively. For synthesis problems, one imposes on $G_k(u)$ and $g_k'(x)$ whatever characteristics one might desire $F(u)$ and $f(x)$, respectively, to have. Once the constraints are defined, the algorithm proceeds the same for synthesis problems as for reconstruction problems. In fact, there are some synthesis problems that are mathematically indistinguishable from some reconstruction problems, and are handled identically by the algorithm.

The first iteration of the algorithm can be started in a number of ways, for example, by setting $g_1(x)$ or $\phi_1(x)$ equal to an array of random numbers. The iterations continue until a Fourier transform pair is found that satisfies all the constraints in both domains to within the desired accuracy (or, if convergence is too slow, until one loses interest or the money runs out). The mean-squared error can generally be defined in the Fourier domain by

$$E_F^2 = \frac{\int_{-\infty}^{\infty} |G_k(u) - G_k'(u)|^2 \, du}{\int_{-\infty}^{\infty} |G_k'(u)|^2 \, du} \tag{7}$$

or in the function domain by

$$E_0^2 = \frac{\int_{-\infty}^{\infty} |g_{k+1}(x) - g_k'(x)|^2 \, dx}{\int_{-\infty}^{\infty} |g_k'(x)|^2 \, dx} \tag{8}$$

In each of these two expressions, the integrand in the numerator is the squared modulus of the amount by which the computed function violates the constraints in that domain. It is easily seen that these expressions reduce to Eqs. (5) and (6), respectively, for the electron microscopy problem.

Just as in the electron microscopy problem, for problems having other sets of constraints it will be shown in Section 4 that the algorithm converges, that is, the error decreases at each successive iteration. The algorithm depicted in Figure 1 may be referred to as the "error reduction" algorithm for that reason, as well as to distinguish it from algorithms described in Section 4 which are related to it but converge faster. Typically, the error is reduced very rapidly for the first few iterations of the error-reduction algorithm, but more slowly for later iterations. For some applications, the error-reduction algorithm has been very successful in finding solutions using a reasonable number of iterations. However, for some other applications, the mean-squared error decreases very slowly with each iteration, requiring an impractically large number of iterations for convergence. The improved algorithms described in Section 4 do much to alleviate this problem.

2.3 Alternative Descriptions of the Algorithm

Once a solution (i.e., a Fourier transform pair satisfying all the constraints in both domains) is found, the error-reduction algorithm ceases to make changes to the estimate, and the algorithm locks onto the solution. The operations of enforcing the constraints in each domain would then leave the function estimate and its Fourier transform unaltered since they already satisfy the constraints. Now let us define the operation $S[g(x)]$ as the successive Fourier transformation of $g(x)$, followed by the imposition of the Fourier domain constraints, followed by inverse Fourier transformation, followed by imposition of the object domain constraints. That is, the operation S is just the performance of one iteration of the error-reduction approach, and

$$g_{k+1}(x) = S[g_k(x)]. \tag{9}$$

From the discussion above, it is evident that any solution $f(x)$ must satisfy the relation

$$f(x) = S[f(x)]. \tag{10}$$

When presented in this form, it is seen that the error-reduction approach is a particular implementation of the method of successive approximations.[10]

The method of successive approximations can be more easily understood from the following simple example. Suppose one wishes to solve the following equation for y:

$$4y^4 - 4y + 1 = 0 \tag{11}$$

Based on the relation $y = y^4 + 1/4$, one could write

$$y_{k+1} = S_1(y_k) = y_k^4 + 1/4 \tag{12}$$

Using the method of successive approximations to find the solution, one would pick an initial estimate, say $y_0 = 0.1$, and, employing Eq. (12) compute $y_1 = 0.2501$, $y_2 = 0.2539$, etc., and rapidly converge to the solution $y' = 0.2541737...$. However, it converges to y' only for $y_0 < y'' = 0.8967902...$. For $y_0 > y''$, Eq. (12) diverges, and for $y_0 = y''$, it stays at y", the second solution. On the other hand, one could just as logically have chosen

$$y_{k+1} = S_2(y_k) = (y_k - 1/4)^{1/4} \tag{13}$$

This second form converges to the second solution y" for $y_0 > y'$, diverges for $y_0 < y'$, an stays at y' for $y_0 = y'$. Figure 2, a graphical representation of Eq. (12), shows the two solutions, y' and y". The irregular staircase between the two curves y and $y^4 + 1/4$ indicates how the estimate y_k approaches the two solutions. Criteria on the derivative of S(y) determine whether the algorithm converges.[11]

The error-reduction algorithm, as described by Eqs. (9) and (10), is analogous to the example of successive approximations described above, except that instead of operating on a scalar y, it operates

on a function g(x). As seen from the example, the method of successive approximations may or may not converge, depending on the particular form chosen and on the initial estimate. Fortunately, as will be discussed further in Section 4, the error-reduction approach never diverges. It may, however, stagnate. A simple example of stagnation is shown by the following. In solving $x = 2 - x$ (which has the obvious solution $x = 1$) by the method of successive approximations, starting with the initial estimate x_0, one obtains $x_1 = 2 - x_0$, $x_2 = 2 - (2 - x_0) = x_0$, ..., $x_{2k-1} = 2 - x_0$, $x_{2k} = x_0$, etc., and no progress is made toward the solution.

Another way of understanding the error-reduction algorithm, applicable for certain sets of constraints, is the alternating projection of the function onto specified subspaces in a Hilbert space.[12] This, along with the possibility of closed-form solutions,[13] is discussed in the chapter of this book by Marks and Smith.

3. APPLICATIONS

A large number of important problems in optics and related fields fit the problem description in Section 1 and can be solved by the iterative algorithm (by the error-reduction algorithm described in Section 2 and the related algorithms described in Section 4). One particular application, that of spectral extrapolation or superresolution, is discussed in detail in the chapter in this book by Marks and Smith. In this section, several classes of applications are listed, followed by more detailed discussions of some of the applications, including examples.

In Section 1, a distinction was made between reconstruction problems and synthesis problems. Another useful way to classify such problems is according to the type of information available. For one set of problems, the modulus (magnitude or amplitude) of a complex-valued function and the modulus of its Fourier transform are measured (or are given), and one wishes to know the phase of the Fourier transform pair in both domains. These include the phase retrieval problem in electron microscopy, the phase retrieval problem in wavefront sensing, the design optimization of radar signals and antenna arrays having desirable properties, and phase coding and spectrum shaping problems for computer-generated holograms and other applications. These applications often involve the Fresnel transform for the near-field case instead of the Fourier transform.

For another set of problems, the function is known to be real and nonnegative and the modulus of its Fourier transform is measured. These include the phase problems of X-ray crystallography, Fourier transform spectroscopy, imaging through atmospheric turbulence using interferometer data, and pupil function determination.

For another set of problems, a low-resolution (i.e., a low-pass filtered) version of a function is measured (i.e., its complex Fourier transform is measured only over a certain interval), and the function is known to have a finite extent (i.e., it is zero outside

of some known region of support). This is the spectral extrapolation or superresolution problem for band-limited time signals or for imaging of objects of finite extent.

For another set of problems, the function is known to be nonnegative and of finite extent and its complex Fourier transform is measured only over a partially filled aperture. These include the interpolation of the complex visibility function for long baseline radio intrferometry and the missing-cone problem in X-ray tomography.

For still another set of problems, the modulus of a complex-valued function is given, and one wishes to find an associated phase function which results in a Fourier transform whose complex values fall on a prescribed set of quantized complex values. These include the reduction of quantization noise in computer-generated holograms and in coded signal transmission.

Another problem is to reconstruct the modulus of a complex-valued function from the phase of the function, given the fact that the Fourier transform of the function has finite support.

The number of types of problems solvable by the iterative algorithm appears to be limited only by one's ingenuity in defining different combinations of information that might be available in each of two domains.

3.1 Modulus--Modulus Constraints

Electron Microscopy

Among the applications for which the modulus is given in each of two domains, the electron microscopy phase retrieval problem was one of the earliest applications of the error-reduction algorithm; the electron microscopy problem has also been the most heavily investigated[1,4,8,14,15]. The initial discussion of the algorithm in Section 2 was in terms of the electron microscopy problem and so it will not be repeated here. The error-reduction algorithm has

been shown to perform very successfully for this problem, and the solution is usually unique.[15] The reader is referred to a book by Saxton[4] for a thorough review of this problem.

Spectrum Shaping

A second application for which the modulus is given in each of two domains is the spectrum shaping problems. Spectrum shaping is a synthesis problem that can be stated as follows: given the modulus (magnitude) $|f(x)|$ of a complex-valued wavefront, $g(x) = |f(x)| \exp[i\theta(x)]$, find a phase function $\theta(x)$ such that $|\mathcal{F}[g(x)]|$ is equal to a given spectrum $|F(u)|$. Such a problem is the one suggested by the Escher engraving shown in Figure 3, in which a bird transforms into a fish. One wishes to find a function with modulus being a picture of a fish, which has a Fourier transform with modulus being a picture of a bird. Or, in terms of computer holography, find a phase function to assign to the image of a fish so that the hologram will look like an image of a bird. Figure 4(a) shows the actual "bird" and "fish" binary patterns used for our experiment. For the first iteration, the fish object was random phase coded, Fourier transformed, and the modulus of the Fourier transform was replaced with the modulus of the bird pattern shown in Figure 4(a). The result was inverse Fourier transformed, yielding the very noisy output image shown in Figure 4(b). The iterative algorithm was then used for seven iterations, resulting in the improved image shown in Figure 4(c). For this example, increasing the number of iterations resulted in a further improvement of the quality of the image; that is, a Fourier transform pair was found that more closely satisfied the constraints in both domains.

Spectrum shaping is also important in computer holography for reducing quantization noise. The objective of computer holography[16] is to synthesize a transparency that can modulate a wavefront according to a calculated wavefront, often corresponding to Fourier coefficients (or samples of the Fourier transform of an image) computed by

the discrete Fourier transform. Let $F = \mathcal{F}[f]$ be the desired wavefront modulation and f be the complex-valued function describing the desired image. Due to the limitations of the display devices and materials used to synthesize computer holograms, it is often not possible to exactly represent any arbitrary complex Fourier coefficient. An extreme example of this is the kinoform[17] which allows nearly continuous phase control which is accomplished by varying the thickness of the recording medium, but quantizes the modulus to a single level. (If a gray-level display device, or recorder, used to synthesize a kinoform has a finite number of gray levels, then the phase is quantized as well.) The desired coefficient F is only approximated by the quantized value $F/|F|$. Since only the squared modulus (the intensity) of the image is observed, one is free to choose the phase of the object (phase code the object) in such a way as to reduce the variance (dynamic range) of $|F|$, which reduces the quantization noise in kinoforms and, to a lesser extent, in other types of computer-generated holograms. Random phase and various deterministic phase codes[18] cause a considerable reduction in the variance of $|F|$, but substantial errors remain.[19]

It was for the kinoform application that the iterative algorithm was first invented.[2,3] Figure 5 shows an example of its use for this synthesis problem. Figure 5(a) shows the image resulting when the input image was random phase coded, encoded as a kinoform in the Fourier plane, and reconstructed by inverse Fourier transformation. The ideal image would be the binary (=0 or 1) block letters SU. Figure 5(b) shows the improved result after eight iterations of the iterative algorithm.[7] In this case, the image-domain constraint is that the modulus equal the SU pattern, and the Fourier-domain constraint is that the modulus equal a constant.

A problem very similar to the kinoform problem is that of synthesizing a quasi-random radar signal having good autocorrelation properties. Specifically, one would like to synthesize a radar

signal f(t) which is a pure phase function, i.e., $|f(t)| = 1$, over some interval of time and which has an autocorrelation function which approaches a delta-function (an impulse), and therefore its Fourier spectrum $|F(\nu)|^2$ is constant over the bandwidth of interest. From the examples shown above, it is obvious that the iterative method would be an effective tool for synthesizing such radar signals.

Another spectrum-shaping application is the phasing of elements of an array of antennas in order to achieve a far-field pattern having desirable properties. For example, one might wish to phase the antenna elements in such a way as to minimize the maximum sidelobe of the far-field pattern, or to place nulls of the antenna pattern at several different prescribed locations simultaneously. A related application for which the iterative method has been used is the transformation of a Gaussian laser beam into a beam having a more rectangular profile.[20]

Wavefront Sensing

The wavefront sensing application is very similar to the electron microscopy problem. Suppose that one measures the image $|f(x)|^2$ of a point source using an aberrated optical system, where the aberrations may be due to atmospheric turbulence or due to the optical system itself. Assuming that the aberration is a pure phase function, then F(u), the Fourier transform of f(x), has modulus $|F(u)|$ equal to the aperture function of the optical system. The problem is to reconstruct the phase of F(u) given $|F(u)|$ and $|f(x)|$. Several investigators[9,21,22] have applied the error-reduction algorithm to this problem with generally good results.

3.2 Nonnegativity—Modulus Constraints

For some reconstruction problems, the physical quantity of interest can be represented as a nonnegative function, and one is able to measure only the modulus of its Fourier transform (or at least the measured modulus information has a much higher signal-to-noise ratio

than the measured phase). From the Fourier modulus, one wishes to reconstruct (or retrieve) the Fourier phase or, equivalently, the function itself. Since the autocorrelation of the function is available as the inverse Fourier transform of the squared Fourier modulus,[23] this problem is equivalent to reconstructing the function from its autocorrelation. This problem, referred to as the phase retrieval problem of optical coherence theory, arises in spectroscopy,[24] a one-dimensional problem; in astronomy, a two-dimensional problem; and in X-ray crystallography,[25] a three-dimensional problem. In spectroscopy, the nonnegative spectral density, $g(\nu)$, is the Fourier transform of the complex degree of temporal coherence, $\gamma(\tau)$, of which $|\gamma(\tau)|$ is most easily measured. In X-ray crystallography, the nonnegative electron density function, $\rho(x, y, z)$, which is periodic, is the Fourier transform of the structure factor F_{hkl}, of which $|F_{hkl}|$ is measured by a diffractometer. The astronomy problem will be described in more detail later.

The Uniqueness of Solutions

For the one-dimensional problem, use of the iterative algorithm (or any other method) to reconstruct the function from its Fourier modulus is of limited interest since the solution in the general case is usually not unique.[26,27] The uniqueness of the solution for the one-dimensional problem can be analyzed using the theory of analytic functions, from which one finds that additional solutions can be generated by "flipping zeros" of the Fourier transform analytically extended over the complex plane.[26,27] The additional "solutions" have the same support as the original function, but are not guaranteed to be nonnegative; therefore one could reduce the degree of ambiguity by generating all possible "solutions" and then keeping only the nonnegative ones.[28]

For certain special types of one-dimensional functions, there is a high probability that the solution is unique. For a function having two separated intervals of support, being separated by an

interval over which the function is zero, the solution usually is unique,[29,30] but only if the two intervals of support are sufficiently separated.[31] Another special type of function for which the solution is usually unique is one consisting of a summation of a number of delta-functions randomly distributed in space; for such functions, one does not need the iterative method—they can be reconstructed by a simple noniterative method involving the product of three translates of the autocorrelation function.[32]

In the event that multiple solutions do exist, it would not appear that the algorithm would be biased toward one over another, and one would expect the algorithm to converge to different solutions, depending on the initial input to the algorithm. For example, Figure 6 shows two functions having the same Fourier modulus. In a computer experiment using the iterative reconstruction algorithm on the functions' Fourier modulus, it converged to one of the solutions in about half of the trials and converged to the other solution in the other half of the trials, depending on the random number sequences used as the initial input to the algorithm.

For the problem in two or more dimensions, it appears that the solution is usually unique. Considering sampled functions defined on a rectangular grid of points, Bruck and Sodin[33] showed that the existence of additional solutions is equivalent to the factorability of a polynomial representation of the Fourier transform. Since a polynomial of one variable of degree M can always be factored into M prime factors, there are 2^{M-1} solutions in the one-dimensional case. Once again, only some of the "solutions" may be nonnegative. On the other hand, polynomials of two or more variables having arbitrary coefficients are only rarely factorable; consequently, the two-dimensional problem is usually unique. Attempts have also been made to extend this concept to continuous, as opposed to discrete, functions.[34] Although it is always possible to make up examples in two dimensions that are not unique,[35] it appears to be true that

for two-dimensional functions drawn from the real world, the solution is usually unique. The general uniqueness of the two-dimensional case is indicated by experimental reconstruction results using the iterative algorithm.[36] Furthermore, noise in the Fourier modulus data has had the effect of adding noise to the reconstructed function rather than causing the algorithm to converge to a radically different solution.[37]

Astronomical Reconstruction

The problem of reconstructing a two-dimensional nonnegative function from the modulus of its Fourier transform arises in astronomy. Due to atmospheric turbulence, the resolution attainable from large optical telescopes on earth is only about one second of arc, many times worse than the diffraction limit imposed by the diameter of the telescope aperture. For a five-meter telescope aperture, the diffraction-limited resolution would be about 0.02 seconds of arc—fifty times finer. Despite atmospheric turbulence, it is possible to measure the modulus of the Fourier transform of a space object out to the diffraction limit of the telescope using interferometric techniques.[38-41] The autocorrelation of the object can be computed from the Fourier modulus, allowing the diameter of the object to be determined. However, unless the Fourier transform phase is also measured, it was previously not possible to determine the object itself, except for some special cases. Previous attempts to solve this problem had not proven to be practical for complicated two-dimensional objects.

The problem of reconstructing an object from interferometer data can be solved by the iterative method.[42,36] The Fourier-domain constraint is that the Fourier modulus equal the Fourier modulus measured by an interferometer, and the function-domain constraint is that the object function be nonnegative. Figure 7 shows an example. Figure 7(a) shows a computer-synthesized object used for the experiment—a sun-like disk having "solar flares" and bright and

dark "sunspots." The modulus of its Fourier transform is shown in Figure 7(b). Figure 7(c) shows a square of random numbers used as the initial input for the iterative algorithm. Figures 7(d), 7(e) and 7(f) show the reconstruction results after 20, 230, and 600 iterations, respectively. Figure 7(g) shows the initial input for a second trial, and the reconstruction results after 2 and 215 iterations are shown in Figure 7(h) and 7(i), respectively. Comparing Figures 7(f) and 7(i) with the original object in Figure 7(a), one sees that for both trials, the reconstructed images match the original object very closely. Note that inverted solutions such as Figure 7(f) are permitted for this problem since the modulus of the Fourier transform of $f(-x)$ equals the modulus of the Fourier transform of $f(x)$. Other successful reconstruction experiments have been performed on data simulated to have the types of noise present in stellar speckle interferometry,[39] and it appears that under realistic levels of photon noise for fairly bright objects, diffraction-limited images can be reconstructed.[37] Initial experiments have also been carried out on data from telescopes.[43]

Pupil Reconstruction and Synthesis

Another case in which one may want to reconstruct a two-dimensional nonnegative function from its Fourier modulus is in pupil function determination. In a diffraction-limited optical system, the point-spread function is the squared Fourier modulus of the system's pupil function. Equivalently, the optical transfer function is the autocorrelation of the pupil function.[44] Given the point-spread function at a given location in an image plane, one could use the interative algorithm to retrieve the corresponding pupil function, in a way which is mathematically equivalent to the astronomy problem. Turning this problem around, one could use the iterative algorithm to synthesize (design) a pupil function which would yield a given, desired point-spread function while possibly satisfying other desirable constraits as well.

3.3 Finite Extent—Measurement Over Part of an Aperture

In a number of reconstruction problems, there is a function of known finite extent (or support) and one wishes to reconstruct the function with resolution appropriate to an aperture in the Fourier domain more complete than the one over which measurements were actually taken. In some cases, the desired aperture is simply larger than the aperture over which measurements were taken, and so one wishes to extrapolate the function's Fourier transform, or equivalently, to obtain superresolution of the function. In other cases, one has made measurements over a partially filled aperture, in which case one wishes to interpolate the Fourier transform of the function, or, equivalently, to obtain an improved impulse response in the function domain.

Extrapolation or Superresolution

The error-reduction algorithm was first applied to the extrapolation (or superresolution) problem by Gerchberg.[45] Much has been written about the iterative algorithm, specifically the error-reduction algorithm, as it relates to this problem, including various ways of understanding the algorithm (see the end of Section 2) and proofs of convergence.[10,12,13,46-48] For this particular problem, the nature of the constraints makes it possible to implement the algorithm by a feedback optical processor[49,50] taking on the order of 10^{-9} seconds per iteration even for the two-dimensional case. The chapter in this book by Marks and Smith describes these matters in detail.

Interpolation

In tomographic imaging systems, many projections of the object are measured, each projection yielding information about a slice through the Fourier transform of the object. When measurements over only a limited cone of angles are made, the effective aperture in the Fourier domain has gaps, and the impulse response of the system

is highly irregular. In applying the iterative algorithm to this problem[51,52], the function-domain constraint is the finite extent and nonnegativity of the object, and the Fourier domain constraint is that the Fourier transform equal the measured Fourier transform over the measurement aperture.

A problem very similar to the tomography problem arises in radio astronomy. The radio sky brightness map is a two-dimensional real, nonnegative function which is the Fourier transform of the complex visibility function. The visibility function is measured by radio interferometry, and in the case of long-baseline interferometry, the visibility function is measured only over a limited set of "tracks" in the visibility plane, resulting in a partially filled effective aperture. The error-reduction algorithm has been used to obtain improved maps by, in effect, interpolating the visibility function to fill in the area between the tracks.[53] For this problem, the constraints on the brightness map are that it be nonnegative and be zero outside the known field of view. In the visibility plane, the constraint is that the complex visibility function equal the measured value within the area of the tracks.

3.4 Modulus—Quantized Values

As mentioned earlier in connection with spectrum shaping, in computer holography one may wish to encode the Fourier transform of an image as a computer-generated hologram, but some types of computer-generated holograms can encode only certain quantized complex values. The kinoform example discussed earlier is a special type of quantization. A more general example is the Lohmann hologram,[54] for which the modulus and phase of a complex sample are determined by the area and relative position, respectively, of an aperture within a sampling cell. The number of allowable quantized values is determined by the number of resolution elements, of the recording device used to fabricate the hologram, used to form one cell. For this synthesis

problem, the function-domain constraint is that the modulus of the function equal the desired image modulus and the Fourier-domain constraint is that the complex Fourier coefficients fall on a prescribed set of quantized values. Experiments have shown that synthesizing such a Fourier transform pair is possible using the iterative algorithm.[55] For example, Figure 8a shows a simulation of an image produced by a Lohmann hologram having only four modulus and four phase quantization levels when the image was random phase coded. Figure 8b shows the image after 13 iterations, a considerable improvement. This problem is one of a more general class of problems regarding the transmission of coded data.

3.5 Finite Extent—Phase

Finally, the iterative algorithm has been used to reconstruct the modulus of a band-limited signal from its phase.[56,57] Or, looking at it in another way, given that a function has finite extent and given the phase of its Fourier transform, reconstruct the modulus of its Fourier transform. For this application, it has been shown that for a wide class of conditions the solution is unique.[56] This application will be discussed further in Section 4.

4. ALGORITHM CONVERGENCE AND ACCELERATED ALGORITHMS

As mentioned in Section 2, the basic interative algorithm depicted in Figure 1, referred to as the error-reduction algorithm, has been shown to converge for some applications. In this section, the convergence is proven for all appliations. In addition, modified algorithms which in practice often converge much faster than the error-reduction algorithm are discussed.

4.1 Convergence of the Error-Reduction Algorithm

The mean-squared error can be defined in general by Eqs. (7) or (8). It is a normalized version of the integral over the square of the amount by which the computed function (or the computed Fourier transform) violates the constraints in the appropriate domain. When the mean-squared error is zero, then a Fourier transform pair has been found that satisfies all the constraints in both domains.

Consider again the steps in the error-reduction algorithm described in Section 2. The k^{th} iteration starts with an estimate $g_k(x)$ for the function which satisfies the function-domain constraints. Figure 9(a) depicts a phasor diagram for the complex-valued $g_k(x)$ at a particular coordinate x. A dot, at which the phasor is pointing in Figure 9(a), was included as an indication that $g_k(x)$ is a complex value that satisfies the function-domain constraints. The function estimate $g_k(x)$ is Fourier transformed, yielding $G_k(u)$, which, for a particular coordinate u, is depicted by the phasor diagram in Figure 9(b). The next step in the algorithm is to change $G_k(u)$ by the smallest possible amount that allows it to satisfy the Fourier-domain constraints, thereby forming $G'_k(u)$. Again a dot is included in Figure 9(b) at $G'_k(u)$ as an indication that it is a complex value at which the Fourier-domain constraints are satisfied. $G'_k(u)$ is the inverse Fourier transformed, yielding $g'_k(x)$ in the function domain [see Figure 9(a)]. Now consider the

unnormalized squared error, given by the numerators in Eqs. (7) and (8). In the Fourier domain, the unnormalized squared error at the k^{th} iteration is

$$e_{Fk}^2 = \int_{-\infty}^{\infty} |G_k(u) - G_k'(u)|^2 \, du$$
$$= \int_{-\infty}^{\infty} |g_k(x) - g_k'(x)|^2 \, dx \tag{14}$$

where the second line in this equation results from Parseval's theorem. Referring to Figure 9(a), at a particular coordinate x, $g_k(x)$ violates the function-domain constraints by an amount no greater than $|g_k(x) - g_k(x)|$. The complex values that g(x) can have that satisfy the function-domain constraints form some set of points in phasor space. For example, if the modulus must equal $|f(x)|$, then the set of such points is a circle of radius $|f(x)|$ in phasor space; if the function must be nonnegative, then the set of such points is the half line on the positive real axis. The unnormalized squared error in the function domain at the k^{th} iteration is given by

$$e_{Ok}^2 = \int_{-\infty}^{\infty} |g_{k+1}(x) - g_k'(x)|^2 \, dx \tag{15}$$

where the complex value $g_{k+1}(x)$ for a given coordinate x is the point in phasor space satisfying the function-domain constraints that is closest to $g_k'(x)$. Since also $g_k(x)$ is a point in phasor space satisfying the function-domain constraints,

$$|g_{k+1}(x) - g_k'(x)| \leq |g_k(x) - g_k'(x)| \tag{16}$$

where equality holds only if $g_k(x)$ is just as close in phasor space to $g_k'(x)$ as $g_{k+1}(x)$ is. When there is a point in phasor space satisfying the constraints that is closer to $g_k'(x)$ than $g_k(x)$ is, then the left-hand side of the expression above is strictly less than the right-hand side. Therefore, combining Eqs. (14) - (16),

$$e_{0k}^2 \leq e_{Fk}^2 \tag{17}$$

for the first half a given iteration. From the perfect symmetry of the error-reduction algorithm, as seen from Figure 1, a similar result holds when one completes the iteration by satisfying the function-domain constraints, thereby forming $g_{k+1}(x)$, and continuing the next iteration by Fourier transforming $g_{k+1}(x)$. One then finds that

$$e_{F,k+1}^2 \leq e_{0k}^2 \leq e_{Fk}^2 \tag{18}$$

Therefore, the unnormalized squared error can only decrease (or at least not increase) at each iteration. Since the normalized mean-squared error is simply proportional to the unnormalized squared error, a similar result holds for the errors defined by Eqs. (7) and (8).

While the error-reduction algorithm converges to a solution sufficiently fast for some applications, it is unbearably slow for others. In most cases, the error is reduced rapidly for the first few iterations, and then much more slowly for later iterations.

4.2 Input-Output Algorithms

Resulting from an investigation into the problem of the slow convergence of the error-reduction algorithm, a new and faster-converging algorithm was developed, the input-output algorithm.[55,7,36,42] The input-output algorithm differs from the error-reduction algorithm only in the function-domain operation. The first three operations--Fourier tranforming g(x), satisfying Fourier domain constraints, and inverse Fourier transforming the result--are the same for both algorithms. Those three operation, if grouped together as shown in Figure 10, can be considered as a nonlinear system with an input g(x) and an output g'(x). A property of this system is that its output is always a function having a Fourier

transform that satisfies the Fourier-domain constraints. Therefore, if the output also satisfies the function-domain constraints, then all the constraints are satisfied and it is a solution to the problem. Then it is necessary to determine how to manipulate the input in such a way as to force the output to satisfy the function domain constraints.

For the error-reduction algorithm, the next input g(x) is chosen to be the current best estimate of the function, satisfying the function-domain constraints. However, for the input-output algorithm, the input is not necessarily an estimate of the function or a modification of the output, nor does it have to satisfy the constraints; instead, it is viewed as the driving function for the next output. This viewpoint allows one a great deal of flexibility and inventiveness in selecting the next input, and allows the invention of an algorithm that converges more rapidly to a solution. As will be seen later, the "input-output algorithm" actually comprises a few different algorithms, all of which are based on the input-output point-of-view.

How the input should be changed in order to drive the output to satisfy the constraints depends on the particular problem at hand. The analysis given in the Appendix to this chapter for a specific application an be generalized as follows. Consider what happens when an arbitrary change is made in the input. Suppose that at the k^{th} iteration, the input $g_k(x)$ results in the output $g'_k(x)$. Further, suppose that the input is then changed by adding $\Delta g(x)$:

$$g_{k+1}(x) = g_k(x) + \Delta g(x) \tag{19}$$

Then one would expect the new output resulting from $g_{k+1}(x)$ to be of the form

$$g'_{k+1}(x) = g'_k(x) + \alpha\Delta g(x) + \text{additional noise} \tag{20}$$

That is, the expected (or statistical mean) value of the change of the output, due to the change $\Delta g(x)$ of the input, is $\alpha \Delta g(x)$, a constant times the change of the input. The system shown in Figure 10 is not linear; nevertheless, small changes of the input tend to result in similar changes of the output. The expected value of the change of the output can be predicted, but its actual value cannot be predicted since it has a non-zero variance. In the equation above, this lack of predictability is indicated by the "additional noise" term. The constant α depends on the statistics of $G_k(u)$ and $F(u)$ and on the Fourier-domain constraints.

If the output $g_k(x)$ does not satisfy the function-domain constraints and if $g_k(x) + \Delta g_d(x)$ does, then one might try to drive the output to satisfy the constraints by changing the input in such a way as to cause the output to change by $\Delta g_d(x)$. According to the equation above, the change of the input that will, on the average, cause a change $\Delta g_d(x)$ of the output is

$$\Delta g(x) = \alpha^{-1} \Delta g_d(x) \tag{21}$$

Then a logical choice for the new input is

$$g_{k+1}(x) = g_k(x) + \beta \Delta g_d(x) \tag{22}$$

where β is a constant ideally equal to α^{-1}, and where $\Delta g_d(x)$ is a function such that $g_k(x) + \Delta g_d(x)$ satisfies the function-domain constraints. If α is unknown, then a value of β only approximately equal to α^{-1} will usually work nearly as well. The use of too small a value of β in Eq. (22) will only cause the algorithm to converge more slowly. The noise-like terms in Eq. (20) are kept to a minimum by minimizing $\beta \Delta g_d(x)$.

As mentioned earlier, for the input-output algorithm $g_k(x)$ is not necessarily an estimate of the function; it is instead the driving function for the next output. Therefore, it does not matter whether its Fourier transform, $G_k(u)$, satisfies the Fourier domain

constraints. Consequently, for the input-output algorithm, the mean-squared error, E_F^2, is unimportant; E_o^2 is the meaningful quality criterion. When computing E_o for the input-output algorithm, the $g_{k+1}(x)$ that one should use in the integrand of Eq. (8) is the one determined by the error-reduction algorithm rather than the one computed by the input-output algorithm. That is, E_o should still be a measure of the amount by which the output, $g'_k(x)$, violates the constraints.

Another interesting property of the system shown in Figure 10 is that if an output $g'(x)$ is used as an input, then its output will be itself. Since the Fourier transform of $g'(x)$ already satisfies the Fourier-domain constraints, $g'(x)$ is unaffected as it goes through the system. Therefore, no matter what input actually resulted in the output $g'(x)$, the output $g'(x)$ can always be considered to have resulted from itself as an input. From this point of view, another logical choice for the new input is

$$g_{k+1}(x) = g'_k(x) + \beta \Delta g_d(x) \tag{23}$$

Note that if $\beta = 1$ in Eq. (23), then this version of the input-output algorithm reduces to the error-reduction algorithm. Since the optimum value of β is usually not unity, the error-reduction algorithm can be looked on as a sub-optimal subset of one version of the more general input-output algorithm. Depending on the problem being solved, other variations in Eqs. (22) and (23) may be successful ways for choosing the next input.

In order to implement the input-output algorithm using Eq. (22) or (23), one chooses $\Delta g_d(x)$ according to the function-domain constraints. In general, a logical choice is the smallest value of $\Delta g_d(x)$ allowing $g'_k(x) + \Delta g_d(x)$ to satisfy the function-domain constraints. At those values of x for which $g'_k(x)$ already satisfies the function-domain constraints, one would set $\Delta g_d(x) = 0$. At those value of x for which $g'_k(x)$ violates the function-domain constraints,

examples of logical choices of $\Delta g_d(x)$ for various applications are as follows. For the astronomy problem and other applications requiring the function to be nonnegative, choose $\Delta g_d(x) = -g_k'(x)$ where $g_k'(x)$ is negative. For applications requiring the function to be of finite extent, choose $\Delta g_d(x) = -g_k'(x)$ for x outside the known region of support. For applications requiring the function to have modulus equal to $|f(x)|$, choose

$$\Delta g_d(x) = |f(x)| \frac{g_k'(x)}{|g_k'(x)|} - g_k'(x) \tag{24}$$

In addition to the values of $\Delta g_d(x)$ given above, there are other choices that are successful when used in Eqs. (22) and (23). Any $\Delta g_d(x)$ that moves $g'(x)$ in the general direction of satisfying the function-domain constraints will usually result in an algorithm that works; sub-optimum choices of $\Delta g_d(x)$ and of β in Eq. (22) or (23) result in algorithms that converge less rapidly than the optimum. Two examples of other algorithms that converge more rapidly than the "logical" ones described in the preceding paragraph are as follows. For applications requiring the function to have modulus equal to $|f(x)|$, it was noticed that the difference in phase between $g_k'(x)$ and $g_k(x)$ tends to have the same sign as the change of phase of $g_k'(x)$ from one iteration to the next. In order to anticipate the direction that the phase is changing, one could choose a $\Delta g_d(x)$ that tends to rotate the phase angle of the new input toward that of the last output. That is, a good choice for the desired change in the output is

$$\Delta g_d(x) = \left[|f(x)| \frac{g_k'(x)}{|g_k'(x)|} - g_k'(x)\right] + \left[|f(x)| \frac{g_k'(x)}{|g_k'(x)|} - |f(x)| \frac{g_k(x)}{|g_k(x)|}\right] \tag{25}$$

in which the first component boosts (or shrinks) the magnitude of the output to match $|f(x)|$ and the second component rotates the phase angle of the input toward the phase angle of the output. For the

astronomy problem, it was found that a particularly successful algorithm was to use Eq. (23) at those points where the constraints were satisfied and use Eq. (22) at those points where the constraints were violated, i.e.,

$$g_{k+1}(x) = \begin{cases} g_k'(x), & \text{where constraints satisfied} \\ g_k(x) - \beta g_k'(x), & \text{where constraints violated} \end{cases} \tag{26}$$

Furthermore, it was found that even faster convergence was obtained by alternating between the above equation and the error-reduction algorithm every few iterations.

From the paragraphs above, it is seen that the "input-output algorithm" is really a family of algorithms. The input-output approach is one that can lead to a number of different algorithms based on the manner in which the nonlinear system of Figure 10 behaves. One would hope that the principles of control theory and possibly other disciplines could be used to shed further light on this system and help to arrive at algorithms with still more rapid convergence.

It should also be noted that, unlike the error-reduction algorithm, the input-output algorithm does not treat the two domains in a symmetric manner. By reversing the roles of the two domains, one can arrive at a different and possibly more advantageous algorithm.

4.3 Relaxation-Parameter Algorithm

A second method of improved convergence is the use of a relaxation parameter. In solving the problem of reconstructing the magnitude of a band-limited function from its phase (or, equivalently, reconstructing a function of finite extent from the phase of its Fourier transform), Oppenheim, Hayes, and Lim[57] modified the error-reduction algorithm (Figure 1) by adding a relaxation step, as shown in Figure 11. Here the band-limited function is taken to be in the

Fourier domain. The function g(x) then must be of finite extent according to the bandwidth of the Fourier-domain function. In the relaxation step, $g_k''(x)$ is formed from $g_k'(x)$ according to

$$g_k''(x) = (1 - \eta_k)g_{k-1}''(x) + \eta_k g_k'(x) \tag{27}$$

and then the new estimate $g_{k+1}(x)$ is formed from $g_k''(x)$ by making it satisfy the function-domain constraints. The parameter η_k, which is a constant which may vary from one iteration to the next, is the relaxation parameter. For $\eta_k = 1$, $g_k''(x) = g_k'(x)$ and this reduces to the error-reduction approach. For $\eta_k = 0$, $g_k''(x) = g_{k-1}''(x)$, that is, the result from the previous iteration is used. Other values of η_k give a linear combination of $g_{k-1}''(x)$ and $g_k'(x)$. For the reconstruction of a function of finite extent from the phase of its Fourier transform or from a segment of its Fourier transform (i.e., the superresolution problem), if $g_1'(x)$ and $g_2'(x)$ both satisfy the Fourier-domain constraint, then the linear combination $\eta g_1'(x) + (1 - \eta)g_2'(x)$ also satisfies the constraint in the Fourier domain. It follows from this that $g_k''(x)$ given by Eq. (27) also satisfies the Fourier-domain constraint. In those cases, it can be shown that the algorithm converges for $0 < \eta_k < 1$. However, for other sets of constraints, for example, given the modulus of the Fourier transform, $g_k''(x)$ given by the equation above does not generally satisfy the Fourier-domain constraints and so the relaxation method does not strictly apply.

The optimum value of η_k can be determined as follows. Define the function-domain squared error after the relaxation step as

$$e_o^2 = \int_\gamma |g_k''(x)|^2 \, dx \tag{28}$$

where the region of integration, γ, is the region over which the function is known to be zero. Setting equal to zero the derivative of e_o^2 with respect to η_k, and solving for η_k, one finds the optimum value of η_k to be given by

$$\eta_k = \frac{-\mathrm{Re}\left\{\int_\gamma g''_{k-1}(x)[g'_k(x) - g''_{k-1}(x)]^* \, dx\right\}}{\int_\gamma |g'_k(x) - g''_{k-1}(x)|^2 \, dx} \tag{29}$$

Use of the relaxation step for the problem of reconstructing a band-limited function from its phase resulted in an order of magnitude improvement in the speed of convergence of the algorithm over that of the error-reduction algorithm.[57]

The relaxation step described above incorporates the optimum combination of the current output with the previous output. It is also possible to extend this concept to include a number of previous outputs,[57] which may result in still more rapid convergence.

It should be noted that the majority of the work referenced in Section 3 made use of only the error-reduction algorithm. Improved speed of convergence could be expected if one of the two accelerated algorithms discussed above were employed.

5. SUMMARY AND COMMENTS

The iterative error-reduction algorithm, an extension of the Gerchberg-Saxton algorithm to include various types of constraints, has been found to be capable of solving a wide range of difficult problems in optics and other fields. It can be applied to the reconstruction of a function (an object, wavefront, signal, etc.) when only partial information is available in each of two domains, or to the synthesis of a function (wavefront, signal, etc.) having desired properties in each of two domains. The iterative algorithm is reasonably fast for most applications, since the major computational burden, two Fourier transforms per iteration, can be accomplished using the fast Fourier transform (FFT) algorithm. The iterative algorithm has been shown to outperform alternative methods of solving these classes of problems both because of its speed and its tolerance of noise.[4,9] For some applications, a large number of iterations is required for convergence of the error-reduction algorithm. This situation can be remedied by using an algorithm with accelerated convergence, such as the input-output algorithm or an algorithm employing a relaxation step.

The iterative algorithm has been in use for only a few years and yet already it has already found numerous applications; and methods of improving the algorithm have been devised. Nevertheless, it is safe to predict that it will be used in the future to solve new problems not discussed here, and it is hoped that further improvements of the algorithm will be discovered.

ACKNOWLEDGEMENT

This work was supported by the Air Force Office of Scientific Research under Contract No. F49620-80-C-0006.

APPENDIX

Consider the synthesis problem for kinoforms, for which the Fourier modulus is set equal to a constant. Suppose that the input $g(x)$ to a kinoform system results in the output $g'(x)$. The kinoform has a transmittance $G'(u) = K \exp[i\phi(u)]$ where $\phi(u)$ is the phase of $G(u) = |G(u)| \exp[i\phi(u)] = \mathcal{F}[g(x)]$, and K is a constant. The resulting image is $g'(x) = \mathcal{F}^{-1}[G'(u)]$. Now consider what happens when a change $\Delta g(x)$ is made in the input. As illustrated in the phasor diagrams in Figure A1, the change $\Delta g(x)$ of the input causes a change $\Delta G(u)$ of its Fourier transform, which causes a change $\Delta G'(u)$ of the kinoform and a corresponding change $\Delta g'(x) = \mathcal{F}^{-1}[\Delta G'(u)]$ of the output image. The goal here is to determine the relationship between the change $\Delta g'(x)$ of the output and the change $\Delta g(x)$ of the input. Figure A2 shows the relationship between $\Delta G'(u)$ and two orthogonal components of $\Delta G(u)$. By similar triangles, for $|\Delta G| \ll |G|$,

$$\Delta G'(u) \simeq \Delta G^t(u) \frac{K}{|G(u)|} \tag{A1}$$

where the two orthogonal components of $\Delta G(u)$ are

$$\Delta G^r(u) = |\Delta G(u)| \cos \beta(u)\, e^{i\phi(u)} \tag{A2}$$

parallel to $G(u)$, and

$$\Delta G^t(u) = |\Delta G(u)| \sin \beta(u)\, e^{i[\phi(u)+\pi/2]}; \tag{A3}$$

orthogonal to $G(u)$; and

$$\Delta G(u) = \Delta G^r(u) + \Delta G^t(u) = |\Delta G(u)|\, e^{i[\phi(u)+\beta(u)]} \tag{A4}$$

where $\beta(u)$ is the angle between $\Delta G(u)$ and $G(u)$. Only one of the two orthogonal components of $\Delta G(u)$, namely $\Delta G^t(u)$, contributes to $\Delta G'(u)$.

In order to compute the expected change of the output, $E[\Delta g'(x)]$, treat the phase angles $\beta(u)$ and the magnitudes $|G(u)|$ as random variables. Inserting $|\Delta G(u)|$ from Eq. (A4) into Eq. (A3), one gets

$$\Delta G^t(u) = \Delta G(u)\, e^{-i[\phi(u)+\beta(u)]} \cos \beta(u)\, e^{i\phi(u)}$$

$$= \Delta G(u)[\sin^2 \beta(u) + i \sin \beta(u) \cos \beta(u)] \qquad \text{(A5)}$$

For $\beta(u)$ uniformly distributed over $[0, 2\pi)$,[19] the expected value of $\Delta G^t(u)$ is

$$E[\Delta G^t(u)] = \Delta G(u)\left(\frac{1}{2} + i \cdot 0\right) = \frac{1}{2}\Delta G(u) \qquad \text{(A6)}$$

Therefore, the expected value of the change of the output is, using Eqs. (A1) and (A6) and assuming that the magnitudes $|G(u)|$ are identically distributed random variables[19] independent of $\beta(u)$,

$$E[\Delta g'(x)] = E\,[\mathcal{F}(\Delta G')] = \mathcal{F}[E(\Delta G')] \approx \mathcal{F}\left[E(\Delta G^t)\; E\left(\frac{K}{|G|}\right)\right]$$

$$\approx \mathcal{F}\left[\frac{1}{2}\Delta G(u)\right] E\left(\frac{K}{|G|}\right) = \frac{1}{2}\Delta g(x) E\left(\frac{K}{|G|}\right) \qquad \text{(A7)}$$

That is, the expected change of the output is α times the change of the input, giving us the second term in Eq. (20), where $\alpha = (1/2)E(K/|G|)$. After a few iterations, $|G(u)|$ will not differ greatly from K; then $\alpha \approx 1/2$.

Similarly, the variance of the change of the output can be shown to be[58]

$$E[\,|\Delta g'(x)|^2 - |E[\Delta g'(x)]|^2]$$

$$\approx \frac{1}{4}\left\{2E\left(\frac{K^2}{|G|^2}\right) - \left[E\left(\frac{K}{|G|}\right)\right]^2\right\} \cdot \frac{1}{A}\int_{-\infty}^{\infty} |\Delta g(x')|^2\, dx' \qquad \text{(A8)}$$

where A is the area of the image. That is, the variance of the change of the output $\Delta g'(x)$ at any given x is proportional to the integrated squared change of the entire input. The predictability of $\Delta g'(x)$, and the degree of control with which one can manipulate it, decreases as one makes larger changes of the input. The difference between the actual change of the output and the expected change of the output given by Eq. (A7) is what is meant by the additional

noise term in Eq. (20). If, after a few iterations, $|G(u)| = K$, then in Eq. (A8) the factor $(1/4)\{2E(K^2/|G|^2) - [E(K/|G|)]^2\} = 1/4$.

Equations (A7) and (A8) are a justification for the input-output concept: small changes of the input result in similar changes of the output, and so the output can be driven to satisfy the constraints by appropriate changes of the input, as in Eqs. (22) and (23).

REFERENCES

1. R.W. Gerchberg and W.O. Saxton, "A Practical Algorithm for the Determination of Phase from Image and Diffraction Plane Pictures," Optik 35, pp. 237-46 (1972).

2. P.M. Hirsch, J.A. Jordan, Jr., and L.B. Lesem, "Method of Making an Object-Dependent Diffuser," U.S. Patent No. 3,619,022 (Nov. 9, 1971; filed Sept. 17, 1970).

3. N.C. Gallagher and B. Liu, "Method for Computing Kinoforms that Reduces Image Reconstruction Error," Appl. Opt. 12, pp. 2328-35 (1973).

4. W.O. Saxton, Computer Techniques for Image Processing in Electron Microscopy (Academic Press, 1978).

5. W.T. Cochran, J.W. Cooley et al., "What is the Fast Fourier Transform?," Proc. IEEE 55, pp. 1664-74 (1967).

6. B. Liu and N.C. Gallagher, "Convergence of a Spectrum Shaping Algorithm," Appl. Opt. 13, pp. 2470-71 (1974).

7. J.R. Fienup, "Iterative Method Applied to Image Reconstruction and to Computer-Generated Holograms," Opt. Eng. 19, pp. 297-305 (1980).

8. D.L. Misell, "A Method for the Solution of the Phase Problem in Electron Microscopy," J. Phys. D.: Appl. Phys. 6, pp. L6-L9 (1973); D.L. Misell, "An Examination of an Iterative Method for the Solution of the Phase Problem in Optics and Electron Optics," J. Phys. D.: Appl. Phys. 6, pp. 2200-25 (1973).

9. R. Boucher, "Convergence of Algorithms for Phase Retrieval from Two Intensity Distributions," 1980 International Optical Computing Conference, Proc. Soc. Photo-Opt. Instr. Eng. 231, pp. 130-41 (1980).

10. R.W. Schafer, R.M. Mersereau, and M.A. Richards, "Constrained Iterative Restoration Algorithms," Proc. IEEE 69, pp. 432-50 (1981).

11. G. Dahlquist and A. Björck (translated by N. Anderson), Numerical Methods (Prentice-Hall, Englewood Cliffs, N.J., 1974) pp. 2-4.

12. D.C. Youla, "Generalized Image Restoration by Method of Alternating Orthogonal Projections," IEEE Trans. Circuits and Systems CAS-25, pp. 694-702 (1978).

13. M.S. Sabri and W. Steenaart, "An Approach to Band-Limited Signal Extrapolation: The Extrapolation Matrix," IEEE Trans. Circuits and Systems CAS-25, pp. 74-78 (1978).

14. A.M.J. Huiser, P. Van Toorn, and H.A. Ferwerda, "On the Problem of Phase Retrieval in Electron Microscopy from Image and Diffraction Pattern I-IV," Optik 47, pp. 123-34 (1977); J. Gassmann, "Optimal Iterative Phase Retrieval from Image and Diffraction Intensities," Optik 48, pp. 347-56 (1977).

15. A.M.J. Huiser, A.J.J. Drenth, and H.A. Ferwerda, "On Phase Retrieval in Electron Microscopy from Image and Diffraction Pattern," Optik 45, pp. 303-316 (1976); A.M.J. Huiser and H.A. Ferwerda, "On the Problem of Phase Retrieval in Electron Microscopy from Image and Diffraction Pattern II: On the Uniqueness and Stability," Optik 46, pp. 407-20 (1976); A.J. Devaney and R. Chidlaw, "On the Uniqueness Question in the Problem of Phase Retrieval from Intensity Measurements," J. Opt. Soc. Am. 68, pp. 1352-54 (1978).

16. T.S. Huang, "Digital Holography," Proc. IEEE 59, pp. 1335-46 (1971); W.-H. Lee, "Computer-Generated Holograms: Techniques and Applications," in E. Wolf, ed., Progress in Optics, Vol. 16 (North-Holland, 1978) pp. 121-232.

17. L.B. Lesem, P.M. Hirsch, and J.A. Jordan, Jr., "The Kinoform: A New Wavefront Reconstruction Device," IBM J. Res. Develop. 13, pp. 150-55 (1969).

18. H. Akahori, "Comparison of Deterministic Phase Coding with Random Phase Coding in Terms of Dynamic Range," Appl. Opt. 12, pp. 2336-43 (1973).

19. R.S. Powers and J.W. Goodman, "Error Rates in Computer-Generated Holographic Memories," Appl. Opt. 14, pp. 1690-1701 (1975).

20. W.-H. Lee, "Method for Converting a Gaussian Laser Beam into a Uniform Beam," Opt. Commun. 36, pp. 469-71 (1981).

21. R.A. Gonsalves, "Phase Retrieval from Modulus Data," J. Opt. Soc. Am. 66, pp. 961-64 (1976).

22. J. Maeda and K. Murata, "Retrieval of Wave Aberration from Point Spread Function or Optical Transfer Function Data," Appl. Opt. 20, pp. 274-79 (1981).

23. R.N. Bracewell, The Fourier Transform and Its Applications, 2nd Edition (McGraw-Hill, New York, 1978).

24. E. Wolf, "Is a Complete Determination of the Energy Spectrum of Light Possible from Measurements of the Degree of Coherence?," Proc. Phys. Soc. (London) 80, pp. 1269-72 (1962).

25. G.H. Stout and L.H. Jensen, X-Ray Structure Determination (Macmillan, London, 1968).

26. A. Walther, "The Question of Phase Retrieval in Optics," Optica Acta 10, 41-49 (1963).

AD-A113 911 ENVIRONMENTAL RESEARCH INST OF MICHIGAN ANN ARBOR F/G 5/8
FINE RESOLUTION IMAGING OF SPACE OBJECTS.(U)
FEB 82 J R FIENUP F49620-80-C-0006
UNCLASSIFIED ERIM-145400-14-F AFOSR-TR-82-0289 NL

3 OF 3
AD A
113911

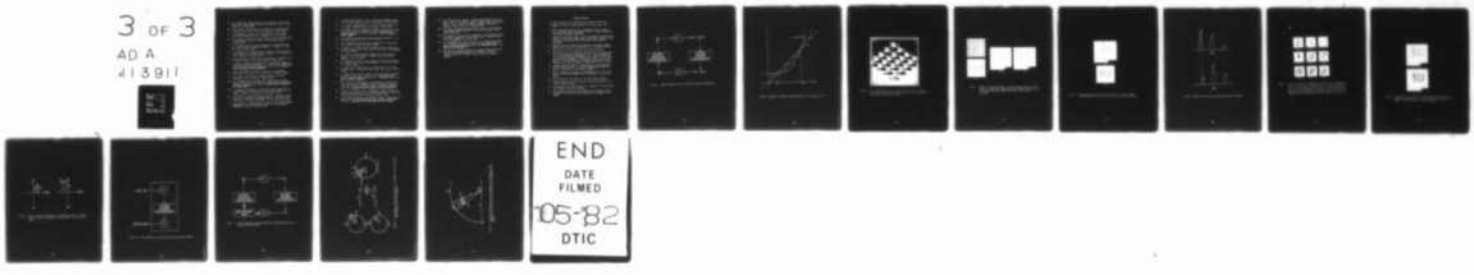

END
DATE FILMED
05-82
DTIC


A
3 9

27. E.M. Hofstetter, "Construction of Time-Limited Functions with Specified Autocorrelation Functions," IEEE Trans. Info. Theory IT-10, pp. 119-26 (1964).

28. R.H.T. Bates, "Contributions to the Theory of Intensity Interferometry," Mon. Not. R. Astr. Soc. 142, pp. 413-28 (1969).

29. A.H. Greenaway, "Proposal for Phase Recovery from a Single Intensity Distribution," Opt. Letters 1, pp. 10-12 (1977).

30. R.H.T. Bates, "Fringe Visibility Intensities May Uniquely Define Brightness Distributions," Astron. and Astrophys. 70, pp. L27-L29 (1978).

31. T.R. Crimmins and J.R. Fienup, "Ambiguity of Phase Retrieval for Functions with Disconnected Support," to appear in J. Opt. Soc. Am. 71 (August 1981).

32. J.R. Fienup, T.R. Crimmins, and W. Holstynski, "Reconstruction of the Support of an Object from the Support of Its Autocorrelation," submitted for publication.

33. Y.M. Bruck and L.G. Sodin, "On the Ambiguity of the Image Reconstruction Problem," Opt. Commun. 30, pp. 304-08 (1979).

34. W. Lawton, "A Numerical Algorithm for 2-D Wavefront Reconstruction from Intensity Measurements in a Single Plane," 1980 International Optial Computing Conference, Proc. Soc. Photo-Opt. Instr. Eng. 231, pp. 94-98 (1980).

35. A.M.J. Huiser and P. Van Toorn, "Ambiguity of the Phase-Reconstruction Problem," Opt. Letters 5, pp. 499-501 (1980).

36. J.R. Fienup, "Space Object Imaging through the Turbulent Atmosphere," Opt. Eng. 18, pp. 529-34 (1979).

37. G.B. Feldkamp and J.R. Fienup, "Noise Properties of Images Reconstructed from Fourier Modulus," 1980 International Optical Computing Conference, Proc. Soc. Photo-Opt. Instr. Eng. 231, pp. 84-93 (1980).

38. A. Labeyrie, "Attainment of Diffraction Limited Resolution in Large Telescopes by Fourier Analysing Speckle Patterns in Star Images," Astron. and Astrophys. 6, pp. 85-87 (1970).

39. D.Y. Gezari, A. Labeyrie, and R.V. Stachnik, "Speckle Interferometry: Diffraction-Limited Measurements of Nine Stars with the 200-inch Telescope," Astrophys. J. Lett. 173, L1-L5 (1972).

40. D.G. Currie, S.L. Knapp, and K.M. Liewer, "Four Stellar-Diameter Measurements by a New Technique: Amplitude Interferometry," Astrophys. J. 187, pp. 131-44 (1974).

41. R. Hanbury Brown and R.Q. Twiss, "Correlation Between Photons in Two Coherent Beams of Light," Nature 177, pp. 27-29 (1956).

42. J.R. Fienup, "Reconstruction of an Object from the Modulus of Its Fourier Transform," Opt. Lett. 3, pp. 27-29 (1978).

43. J.R. Fienup and G.B. Feldkamp, "Astronomial Imaging by Processing Stellar Speckle Interferometry Data," Applications of Speckle Phenomena, Proc. Soc. Photo-Opt. Instr. Eng. 243, pp. 95-102 (1980).

44. J.W. Goodman, Introduction to Fourier Optics (McGraw-Hill, San Francisco, 1968).

45. R.W. Gerchberg, "Super-Resolution through Error Energy Reduction," Optica Acta 21, pp. 709-20 (1974).

46. A. Papoulis, "A New Algorithm in Spectral Analysis and Band-Limited Extrapolation," IEEE Trans. Circuits and Systems CAS-22, pp. 735-42 (1975).

47. J.A. Cadzow, "An Extrapolation Procedure for Band-Limited Signals," IEEE Trans. Acoust., Speech, Signal Processing ASSP-27, pp. 4-12 (1978).

48. C.K. Rushforth and R.L. Frost, "Comparison of Some Algorithms for Reconstructing Space-Limited Images," J. Opt. Soc. Am. 70, pp. 1539-44 (1980).

49. R.J. Marks II, "Coherent Optical Extrapolation of 2-D Band-Limited Signals: Processor Theory," Appl. Opt. 19, pp. 1670-72 (1980).

50. R.J. Marks II and David K. Smith, "Iterative Coherent Processor for Band-Limited Signal Extrapolation," 1980 International Optical Computing Conference, Proc. Soc. Photo-Opt. Instr. Eng. 231, pp. 106-111 (1980).

51. K.-C. Tam and V. Perez-Mendez, "Limited-Angle 3-D Reconstructions Using Fourier Transform Iterations and Radon Transform Iterations," 1980 International Optical Computing Conference, Proc. Soc. Photo-Opt. Instr. Eng. 231, pp. 142-48 (1980).

52. T. Sato, S.J. Norton et al., "Tomographic Image Reconstruction from Limited Projections Using Iterative Revisions in Image and Transform Spaces," Appl. Opt. 20, pp. 395-99 (1981).

53. A.E.E. Rogers, "Method of Using Closure Phases in Radio Aperture Synthesis," 1980 International Optical Computing Conference, Proc. Soc. Photo-Opt. Instr. Eng. 231, pp. 10-17 (1980).

54. B.R. Brown and A.W. Lohmann, "Computer-Generated Binary Holograms," IBM J. Res. Develop. 13, pp. 160-68 (1969); A.W. Lohmann and D.P. Paris, "Binary Fraunhofer Holograms, Generated by Computer," Appl. Opt. 6, pp. 1739-48 (1967).

55. J.R. Fienup, "Reduction of Quantization Noise in Kinoforms and Computer-Generated Holograms," J. Opt. Soc. Am. 64, p. 1395 (1974) (Abstract).

56. M.H. Hayes, J.S. Lim, and A.V. Oppenheim, "Signal Reconstruction from Phase or Magnitude," IEEE Trans. Acoust., Speech, Signal Processing ASSP-28, pp. 672-80 (1980).

57. A.V. Oppenheim, M.H. Hayes, and J.S. Lim, "Iterative Procedure for Signal Reconstruction from Phase," 1980 International Optical Computing Conference, Proc. Soc. Photo-Opt. Instr. Eng. 231, pp. 121-29 (1980).

58. J.R. Fienup, "Improved Synthesis and Computational Methods for Computer-Generated Holograms," Ph.D. Thesis, Stanford University, May 1975 (University Microfilms No. 75-25523), Chapter 5.

FIGURE CAPTIONS

1. Block diagram of the iterative error-reduction algorithm.
2. Method of successive approximations for solving $4y^4 - 4y + 1 = 0$.
3. Bird transforms into fish ("Sky and Water" by M.C. Escher). This reproduction was authorized by the M.C. Escher Foundation, The Hague, Holland/G.W. Breughel.
4. Example of spectrum shaping. (a) Bird hologram and desired fish image; (b) fish output image after random phase coding of input; (c) output image after seven iterations of the iterative algorithm.
5. Computer-simulated images from kinoform. (a) object random phase coded; (b) after 8 iterations of the iterative algorithm.
6. Functions (a) and (b) having the same Fourier modulus.
7. Reconstruction of a nonnegative function from its Fourier modulus. (a) Test object; (b) modulus of its Fourier transform; (c) initial estimate of the object (first test); (d)-(f) reconstruction results—number of iterations; (d) 20, (e) 230, (f) 600; (g) initial estimate of the object (second test); (h)-(i) reconstruction results—number of iterations; (h) 2, (i) 215.
8. Computer-simulated images from hologram with 4 magnitude and 4 phase quantized levels. (a) object random phased coded; (b) after 13 iterations of the iterative method.
9. Phasor diagram of functions for convergence proof. (a) At one point in the function domain; (b) At one point in the Fourier domain.
10. Block diagram of the system for the input-output concept.
11. Block diagram of the error-reduction algorithm modified to include a relaxation step.

A1. A change Δg of the input results in a change $\Delta G'$ of the kinoform and a change of $\Delta g'$ of the output.

A2 Relationship between $\Delta G'$, the change of the kinoform, and two components of ΔG, the Fourier transform of the change of the input.

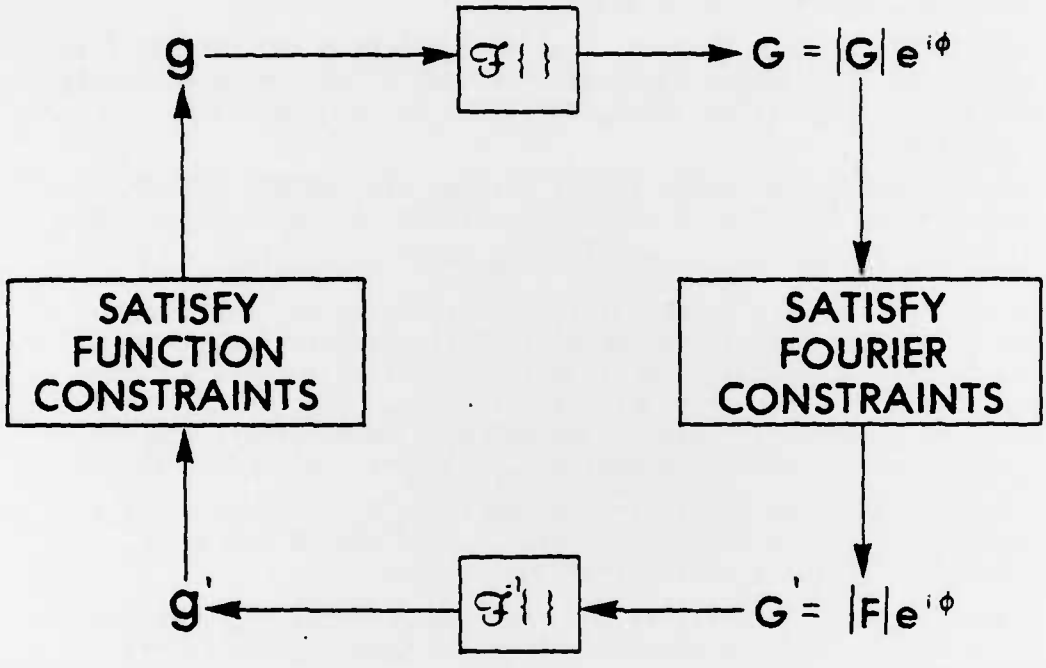

Figure 1. Block diagram of the iterative error-reduction algorithm.

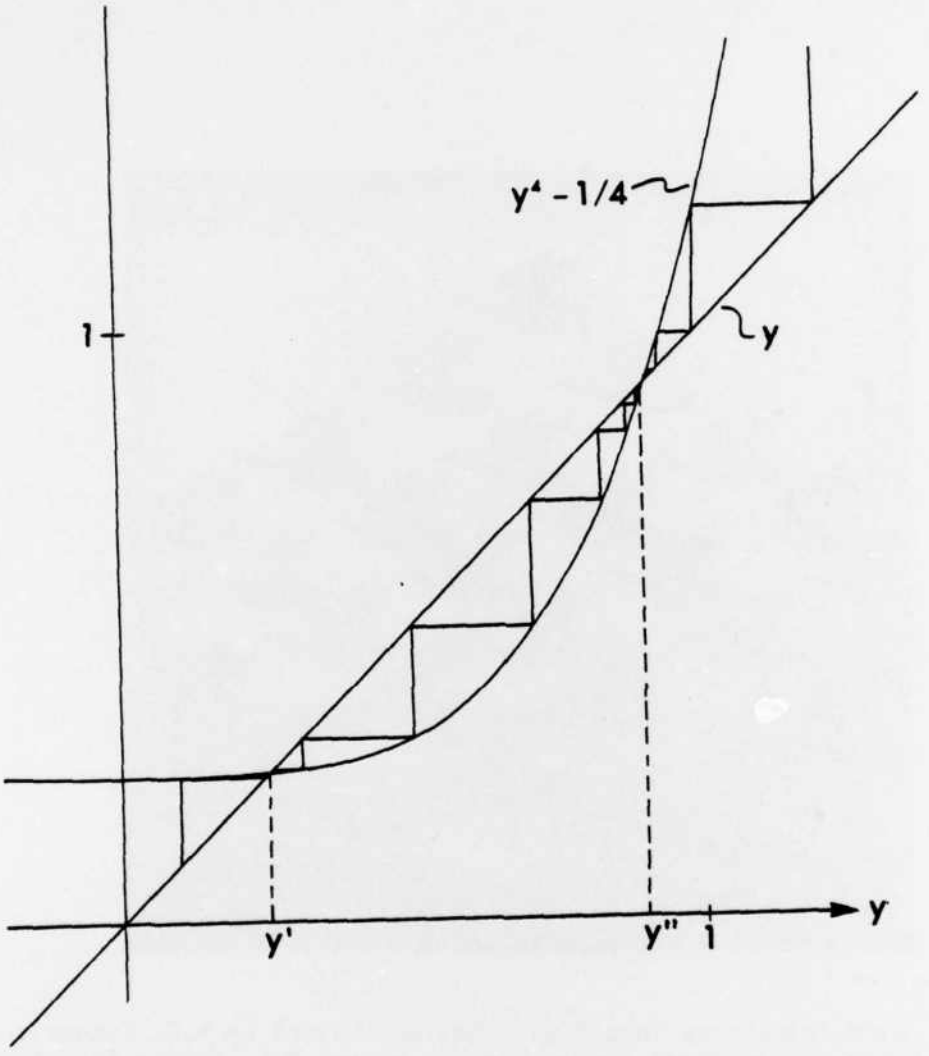

Figure 2. Method of successive approximations for solving $4y^4 - 4y + 1 = 0$.

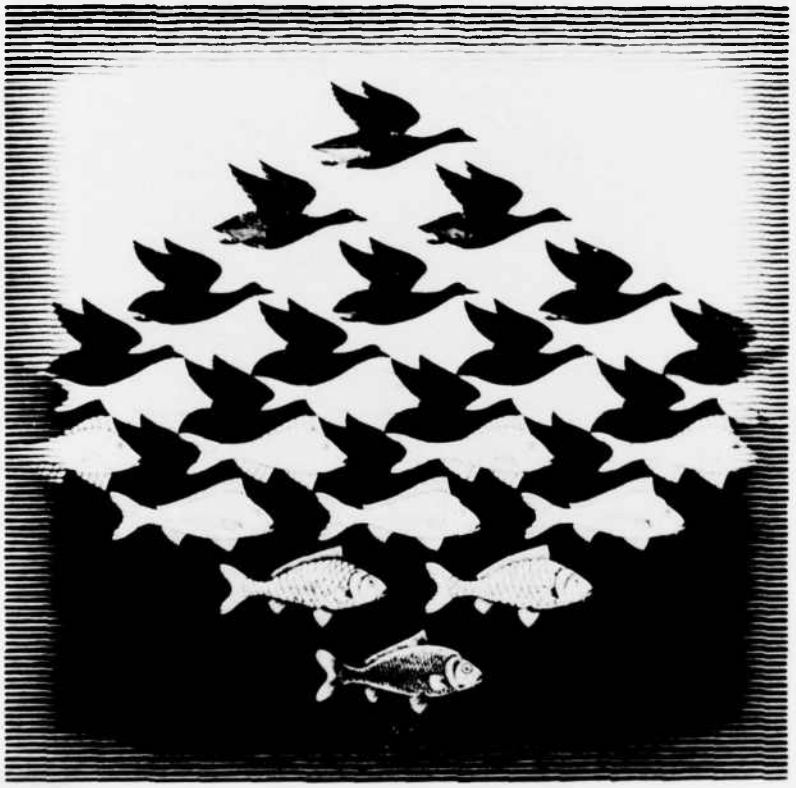

Figure 3. Bird transforms into fish ("Sky and Water" by M.C. Escher). This reproduction was authorized by the M.C. Escher Foundation, The Hague, Holland/G.W. Breughel.

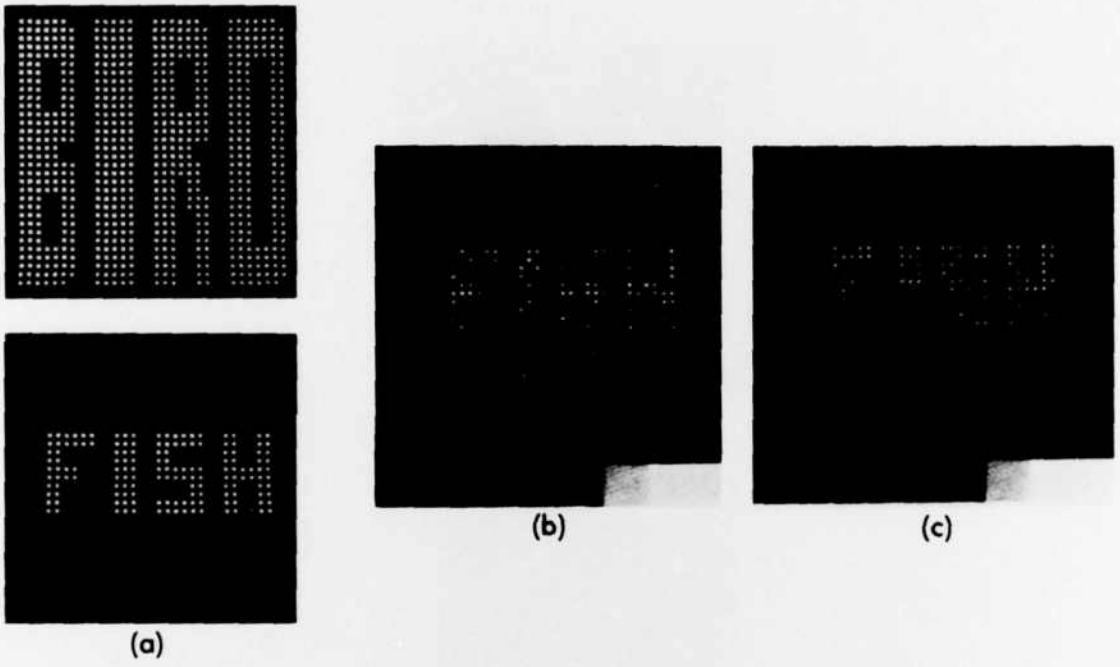

Figure 4. Example of spectrum shaping. (a) Bird hologram and desired fish image; (b) fish output image after random phase coding of input; (c) output image after seven iterations of the iterative algorithm.

Figure 5. Computer-simulated images from kinoform. (a) object random phase coded; (b) after 8 iterations of the iterative algorithm.

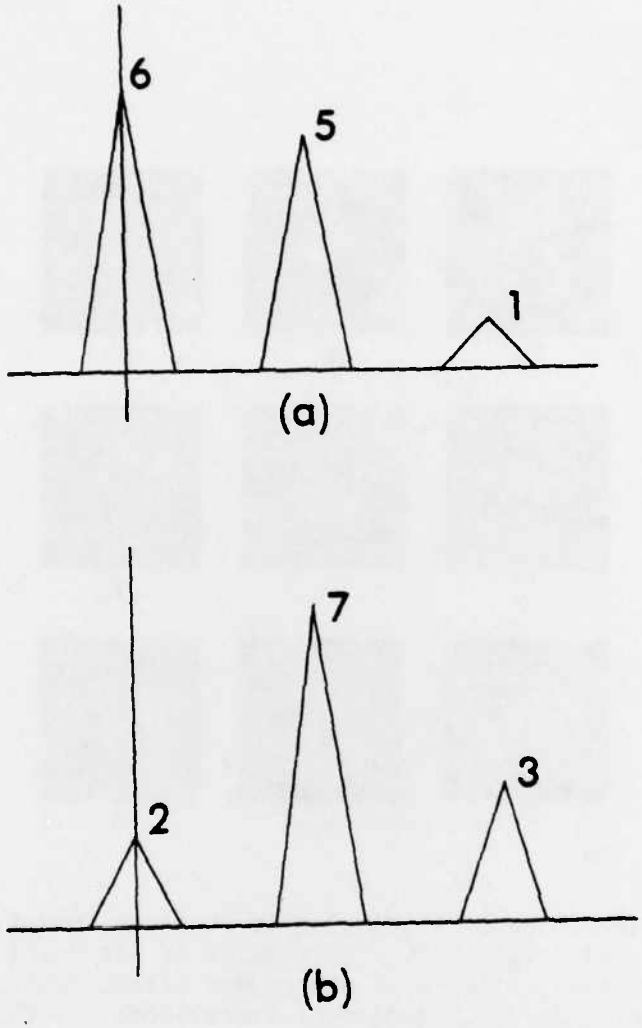

Figure 6. Functions (a) and (b) having the same Fourier modulus.

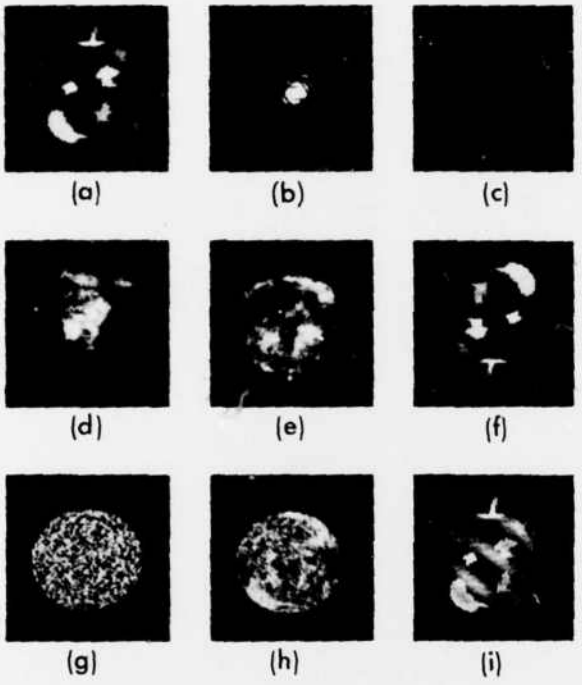

Figure 7. Reconstruction of a nonnegative function from its Fourier modulus. (a) Test object; (b) modulus of its Fourier transform; (c) initial estimate of the object (first test); (d)-(f) reconstruction results--number of iterations; (d) 20, (e) 230, (f) 600; (g) initial estimate of the object (second test); (h)-(i) reconstruction results—number of iterations; (h) 2, (i) 215.

(a)

(b)

Figure 8. Computer-simulated images from hologram with 4 magnitude and 4 phase quantized levels. (a) object random phased coded; (b) after 13 iterations of the iterative method.

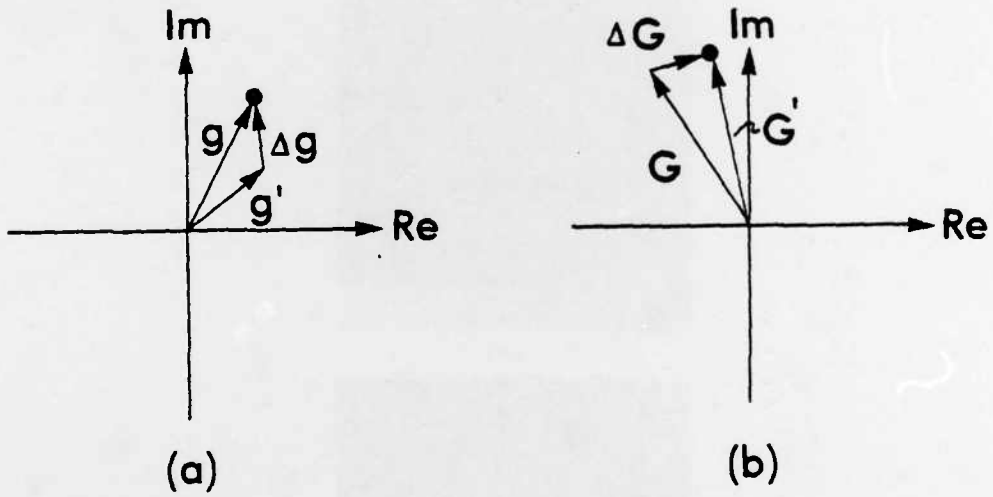

Figure 9. Phasor diagram of functions for convergence proof. (a) At one point in the function domain; (b) At one point in the Fourier domain.

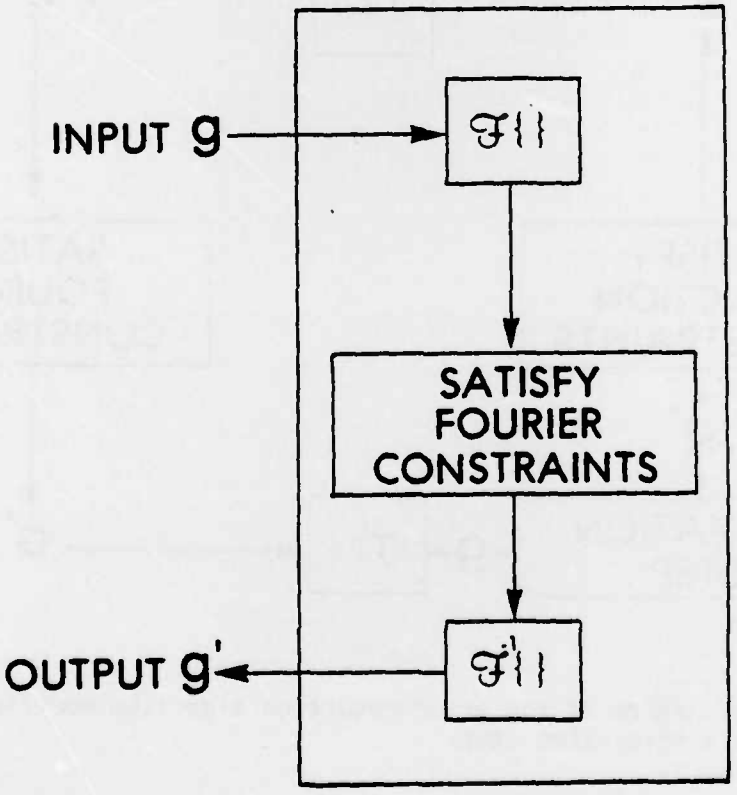

Figure 10. Block diagram of the system for the input-output concept.

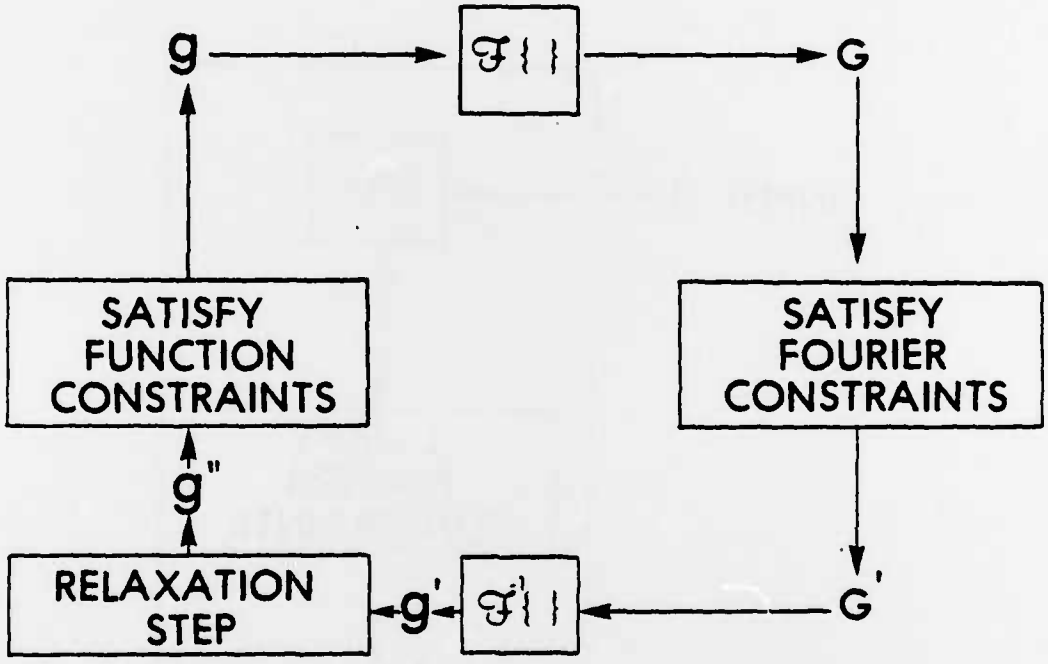

Figure 11. Block diagram of the error-reduction algorithm modified to include a relaxation step.

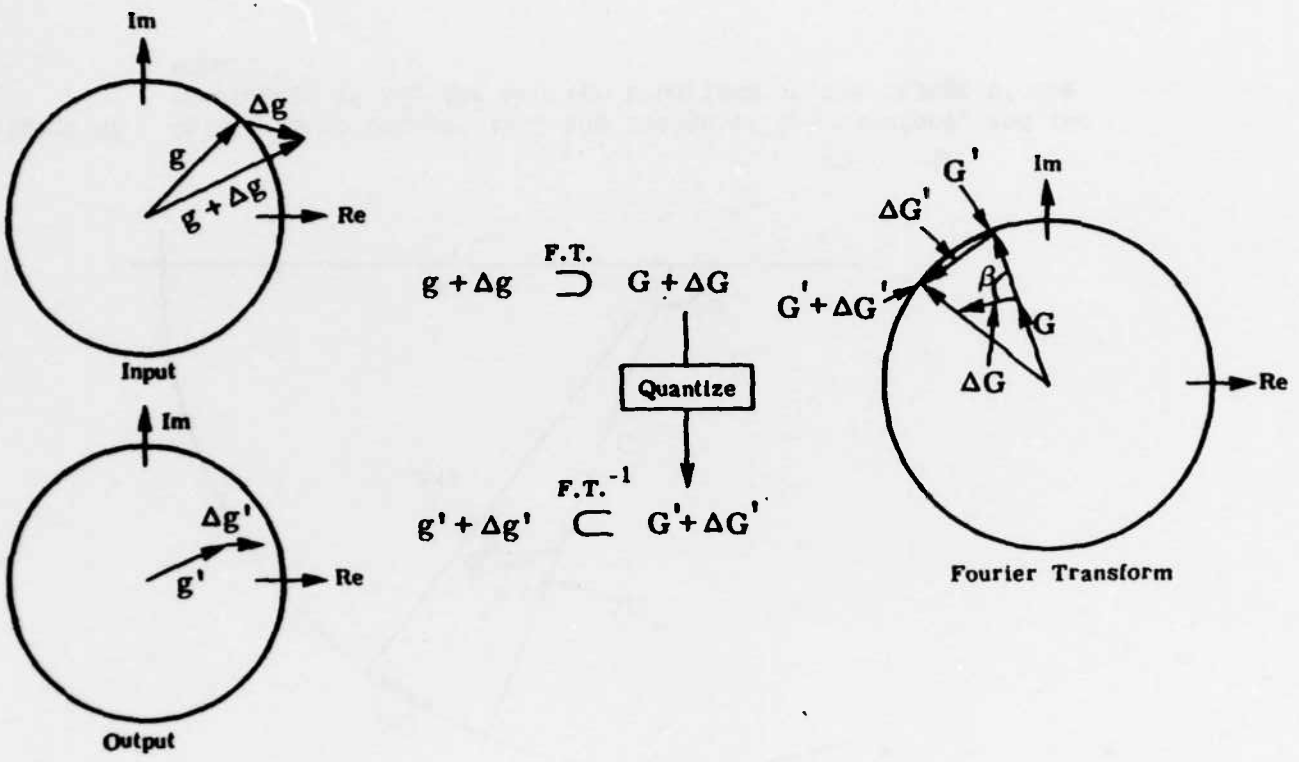

Figure A1. A change Δg of the input results in a change ΔG' of the kinoform and a change of Δg' of the output.

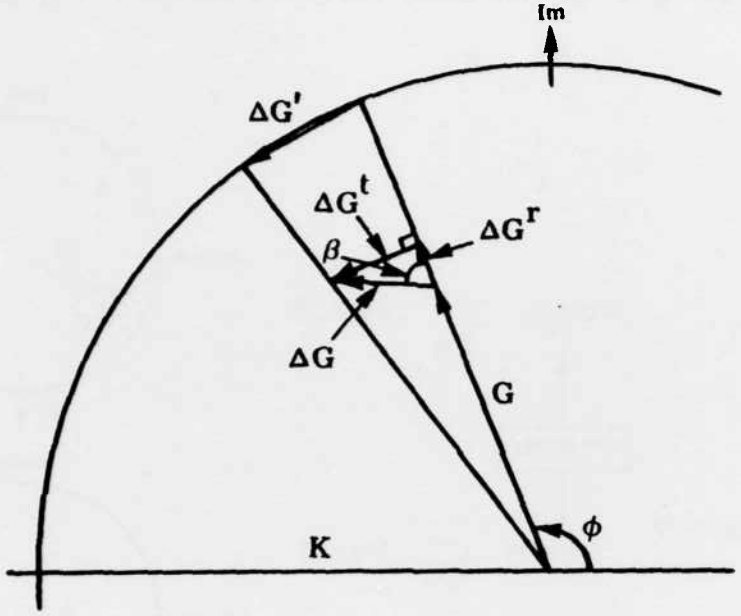

Figure A2 Relationship between ΔG', the change of the kinoform, and two components of ΔG, the Fourier transform of the change of the input.


DATE
ILME

Figure 10. Block diagram of the system for the input-output